INFORMATION TO USERS

This dissertation was produced from a microfilm copy of the original document. While the most advanced technological means to photograph and reproduce this document have been used, the quality is heavily dependent upon the quality of the original submitted.

The following explanation of techniques is provided to help you understand markings or patterns which may appear on this reproduction.

1. The sign or "target" for pages apparently lacking from the document photographed is "Missing Page(s)". If it was possible to obtain the missing page(s) or section, they are spliced into the film along with adjacent pages. This may have necessitated cutting thru an image and duplicating adjacent pages to insure you complete continuity.

2. When an image on the film is obliterated with a large round black mark, it is an indication that the photographer suspected that the copy may have moved during exposure and thus cause a blurred image. You will find a good image of the page in the adjacent frame.

3. When a map, drawing or chart, etc., was part of the material being photographed the photographer followed a definite method in "sectioning" the material. It is customary to begin photoing at the upper left hand corner of a large sheet and to continue photoing from left to right in equal sections with a small overlap. If necessary, sectioning is continued again – beginning below the first row and continuing on until complete.

4. The majority of users indicate that the textual content is of greatest value, however, a somewhat higher quality reproduction could be made from "photographs" if essential to the understanding of the dissertation. Silver prints of "photographs" may be ordered at additional charge by writing the Order Department, giving the catalog number, title, author and specific pages you wish reproduced.

University Microfilms

300 North Zeeb Road
Ann Arbor, Michigan 48106

A Xerox Education Company

Reproduced with permission of the copyright owner. Further reproduction prohibited without permission.

72-29,184

ROSS, Seymour L., 1940-
MEASUREMENTS AND MODELS OF THE DISPERSED PHASE MIXING PROCESS.

The University of Michigan, Ph.D., 1971
Engineering, chemical

University Microfilms, A XEROX Company, Ann Arbor, Michigan

THIS DISSERTATION HAS BEEN MICROFILMED EXACTLY AS RECEIVED

Reproduced with permission of the copyright owner. Further reproduction prohibited without permission.

MEASUREMENTS AND MODELS OF THE DISPERSED PHASE MIXING PROCESS

by
Seymour L. Ross

A dissertation submitted in partial fulfillment
of the requirements for the degree of
Doctor of Philosophy
(Chemical Engineering)
in The University of Michigan
1971

Doctoral Committee:

Professor Rane L. Curl, Chairman
Associate Professor Joe D. Goddard
Assistant Professor James H. Hand
Assistant Professor Norman F. Ho
Professor M. Rasin Tek

Reproduced with permission of the copyright owner. Further reproduction prohibited without permission.

PLEASE NOTE:

Some pages may have

indistinct print.

Filmed as received.

University Microfilms, A Xerox Education Company

Reproduced with permission of the copyright owner. Further reproduction prohibited without permission.

ACKNOWLEDGEMENTS

I sincerely thank Professor Rane L. Curl for his advice and support throughout this research. His encouragement and numerous ideas were always greatly appreciated.

The financial support received from the Department of Chemical Engineering and the American Petroleum Institute are gratefully acknowledged.

I thank the Cooley Laboratories for allowing me to freely use their analogue-to-digital converter.

I thank Marcia Myers for her diligence in typing this thesis.

Finally, I warmly thank my wife, Nancy, for her love and sympathy.

Reproduced with permission of the copyright owner. Further reproduction prohibited without permission.

TABLE OF CONTENTS

		Page
ACKNOWLEDGEMENTS		ii
LIST OF TABLES		vii
LIST OF FIGURES		viii
NOMENCLATURE		xii
TEXT		
CHAPTER 1	INTRODUCTION	1
CHAPTER 2	LITERATURE REVIEW	5
2.1	Introduction	5
2.2	Characteristics of Mixing Vessel	5
2.3	A Description of Turbulence	6
2.4	Description of Mixing Processes in Turbulence	7
	(a) Break-up	7
	(b) Coalescence	8
2.5	Experimental Determination of Coalescence Frequencies	11
2.6	Coalescence of Single Drops on a Liquid-Liquid Surface	12
2.7	Collision and Coalescence of Spheres and Drops	14
2.8	Simplified Theories of Mixing	16
2.9	General Mixing Model	17
CHAPTER 3	EXPERIMENTAL APPARATUS AND PROCEDURE	18

Reproduced with permission of the copyright owner. Further reproduction prohibited without permission.

Page

3.1 Introduction 18

3.2 Description of Flow System 19

3.3 Description of Sampling System 19

3.4 Preparations 27

3.5 Description of Experimental Procedure 28

CHAPTER 4 EXPERIMENTAL RESULTS 31

4.1 Calculation of Data and Distributions 31

4.2 Typical Experiment 33

4.3 Scope of Experiments 40

4.4 Reproducibility 41

(a) Component Samples 42

(b) Two Similar Experiments 42

(c) Comparison with Verhoff's Results 42

(d) Two Experiments with Low Mixing Rates 51

(e) Average Concentration 51

4.5 Matrix of Results 51

4.6 Discussion of the Experimental Results 76

(a) Dramatic Mixing Effects 76

(b) Drop-Size Effects 77

(c) Importance of Low Mixing Rates 81

(d) Power Inputs 81

(e) Implications of Results 82

CHAPTER 5 GENERAL MIXING EQUATION 85

5.1 General Mixing Equation 85

5.2 Numerical Solution of Equation 90

5.3 Mixing Rates 93

CHAPTER 6 MODELING PROCEDURE 96

Reproduced with permission of the copyright owner. Further reproduction prohibited without permission.

Page

CHAPTER 7 THEORY AND MODEL BUILDING. 102

7.1 Description of Turbulent Field 102

7.2 Regions of Breakage and Coalescence 104

7.3 Breakage Model 105

7.4 Coalescence Model 110

(a) Derivation of τ/t' Model. 111

(b) Model for Approach of Two Drops 115

(c) Coalescence Efficiency. 119

(d) Coalescence Rate 120

(e) The Case for Rigid Drops. 123

(f) Effect of Phase Fraction. 124

CHAPTER 8 OPERATION OF FUNCTIONS IN MIXING EQUATION. 127

8.1 Description of Functions 127

(a) Breakage and Coalescence Frequency Functions. . 128

(b) Breakage Distribution Function. 129

(c) Effluent Frequency and Feed Distribution Functions 130

8.2 Numerical Techniques 131

8.3 Behavior of Functions 132

(a) Breakage Effects 132

(b) Coalescence Effects 140

CHAPTER 9 CORRELATION OF THEORETICAL AND EXPERIMENTAL RESULTS. 147

9.1 Procedure. 147

9.2 Results 149

9.3 Discussion of Results. 169

9.4 Comparison with Other Work 170

CHAPTER 10 SUMMARY 173

Reproduced with permission of the copyright owner. Further reproduction prohibited without permission.

Page

APPENDICES 177

APPENDIX I DATA REDUCTION PROGRAM 178

APPENDIX II DETERMINATION OF CONCENTRATION VARIANCE 192

APPENDIX III PROGRAM FOR SOLUTION OF MIXING EQUATION 201

APPENDIX IV COMPARISON OF MIXING FREQUENCIES 211

APPENDIX V SUGGESTIONS FOR FUTURE WORK 213

BIBLIOGRAPHY 215

Reproduced with permission of the copyright owner. Further reproduction prohibited without permission.

LIST OF TABLES

Table		Page
4.1	Mixing Frequency and Concentration Variance Ratio as a Function of Agitator Speed and Dispersed Phase Fraction	74
I	Data Reduction Program Parameters.	181
IV-1	Comparison of Mixing Frequencies	212

Reproduced with permission of the copyright owner. Further reproduction prohibited without permission.

LIST OF FIGURES

Figure		Page
2.1	Turbulence-Stabilized Dispersions: logd vs logN	9
3.1	Flow System (after Verhoff)	20
3.2	Drop Generators (after Verhoff)	21
3.3	Mixing Vessel (after Verhoff)	22
3.4	Cross Section of Sampler (after Verhoff)	24
3.5	Surfactant Feed System for Sampler (after Verhoff)	25
3.6	Sampler Drive Assembly (after Verhoff)	25
3.7	Sample Handling Section (after Verhoff)	26
3.8	Microscope Assembly (after Verhoff)	26
4.1	Volume Distribution in a Volume-Concentration Space at N = 174 rpm, θ = 0.10	35
4.2	Volume Distribution in a Diameter-Concentration Space at N = 174 rpm, θ = 0.10	36
4.3	Marginal Volume Distribution at N = 174 rpm, θ = 0.10	37
4.4	Marginal Diameter Distribution at N = 174 rpm, θ = 0.10	38
4.5	Marginal Concentration Distribution at N = 174 rpm, θ = 0.10	39
4.6	Diameter Distributions of Component Samples at N = 160 rpm, θ = 0.05	43
4.7	Diameter Distributions of Component Samples at N = 210 rpm, θ = 0.05	44
4.8	Comparison of Two Experiments at N = 210 rpm, θ = 0.05	45
4.9	Comparison of Two Experiments at N = 210 rpm, θ = 0.10	46

Reproduced with permission of the copyright owner. Further reproduction prohibited without permission.

Figure		Page
4.10	Comparison of Two Experiments at N = 210 rpm, θ = 0.15	47
4.11	Comparison of Two Experiments at N = 210 rpm, θ = 0.20	48
4.12	Comparison with Verhoff's Results	49
4.13	Comparison of Two Experiments with Low Mixing Rates. N = 160 rpm, θ = 0.025 and 0.050	50
4.14	Marginal Diameter Distribution at N = 160 rpm, θ = 0.05	52
4.15	Marginal Diameter Distribution at N = 160 rpm, θ = 0.10	53
4.16	Marginal Diameter Distribution at N = 160 rpm, θ = 0.15	54
4.17	Marginal Diameter Distribution at N = 160 rpm, θ = 0.20	55
4.18	Marginal Concentration Distributions at N = 160 rpm	56
4.19	Marginal Diameter Distribution at N = 174 rpm, θ = 0.05	57
4.20	Marginal Diameter Distribution at N = 174 rpm, θ = 0.10	58
4.21	Marginal Diameter Distribution at N = 174 rpm, θ = 0.15	59
4.22	Marginal Diameter Distribution at N = 174 rpm, θ = 0.20	60
4.23	Marginal Concentration Distributions at N = 174 rpm	61
4.24	Marginal Diameter Distribution at N = 227 rpm, θ = 0.05	62
4.25	Marginal Diameter Distribution at N = 227 rpm, θ = 0.10	63
4.26	Marginal Diameter Distribution at N = 227 rpm, θ = 0.15	64
4.27	Marginal Diameter Distribution at N = 227 rpm, θ = 0.20	65
4.28	Marginal Concentration Distributions at N = 227 rpm	66
4.29	Marginal Diameter Distribution at N = 278 rpm, θ = 0.05	67
4.30	Marginal Diameter Distribution at N = 278 rpm, θ = 0.10	68
4.31	Marginal Diameter Distribution at N = 278 rpm, θ = 0.15	69
4.32	Marginal Diameter Distribution at N = 278 rpm, θ = 0.20	70

Reproduced with permission of the copyright owner. Further reproduction prohibited without permission.

LIST OF FIGURES (Continued)

Figure		Page
4.33	Marginal Concentration Distributions at N = 278 rpm	71
4.34	Sauter-Mean Diameter versus Agitator Speed	72
4.35	Sauter-Mean Diameter versus Dispersed Phase Fraction	73
4.36	Concentration Variance Ratio, C_r, versus Agitator Speed	75
4.37	Volume - Percentile Diameters versus N^2 at $\theta = 0.05$	78
4.38	Diameter Distributions at N = 174 rpm, $\theta = 0.05 - 0.20$	79
4.39	Diameter Distributions at N = 278 rpm, $\theta = 0.05 - 0.20$	80
7.1	alescence Models	116
8.1	ume Probability and Breakage Frequency versus Volume for Breakage Only	134
8.2	Theoretical Diameter Distribution for Breakage Only, a = 2 and a = 8	136
8.3	Theoretical Drop Size Distributions for Breakage Only	138
8.4	Theoretical Sauter-Mean Diameter versus N for Breakage Only	139
8.5	Theoretical Volume Distributions and Frequencies at N = 160 rpm, $\theta = 0.05$	141
8.6	Theoretical Volume Distributions and Frequencies at N = 278 rpm, $\theta = 0.05$	142
8.7	Coalescence Frequency versus Volume	143
9.1	Beta Distribution, a = 10	150
9.2	Experimental and Theoretical Diameter Distributions, N = 160 rpm, $\theta = 0.05$	151
9.3	Experimental and Theoretical Diameter Distributions, N = 174 rpm, $\theta = 0.05$	152
9.4	Experimental and Theoretical Diameter Distributions, N = 210 rpm, $\theta = 0.05$	153

Reproduced with permission of the copyright owner. Further reproduction prohibited without permission.

Figure		Page
9.5	Experimental and Theoretical Diameter Distributions, N = 227 rpm, θ = 0.05	154
9.6	Experimental and Theoretical Diameter Distributions, N = 278 rpm, θ = 0.05	155
9.7	Experimental and Theoretical Diameter Distributions, N = 160 rpm, θ = 0.15	156
9.8	Experimental and Theoretical Diameter Distributions, N = 174 rpm, θ = 0.15	157
9.9	Experimental and Theoretical Diameter Distributions, N = 210 rpm, θ = 0.15	158
9.10	Experimental and Theoretical Diameter Distributions, N = 227 rpm, θ = 0.15	159
9.11	Experimental and Theoretical Diameter Distributions, N = 278 rpm, θ = 0.15	160
9.12	Experimental and Theoretical Sauter-Mean Diameters, θ = 0.05	161
9.13	Experimental and Theoretical Sauter-Mean Diameters, θ = 0.10	162
9.14	Experimental and Theoretical Sauter-Mean Diameters, θ = 0.15	163
9.15	Experimental and Theoretical Sauter-Mean Diameters, θ = 0.20	164
9.16	Experimental and Theoretical Mixing Frequencies, θ = 0.05	165
9.17	Experimental and Theoretical Mixing Frequencies, θ = 0.10	166
9.18	Experimental and Theoretical Mixing Frequencies, θ = 0.15	167
9.19	Experimental and Theoretical Mixing Frequencies, θ = 0.20	168
9.20	Comparison of Mixing Frequencies with Other Work	171
Figure II	Histograms for Lower and Upper Concentration Zones, N = 174 rpm, θ = 0.10	193

Reproduced with permission of the copyright owner. Further reproduction prohibited without permission.

NOMENCLATURE

English Alphabet

A	Shinnar's coalescence parameter
A(v)	Number probability density function of vessel drops
a(v)	Number probability density function of feed drops
a, a'	Constants in beta function
b	Drop radius
b(v)	Number probability density function of effluent drops
c	Disc radius of circle of contact between colliding drops or a drop on a flat surface
C, C'	Dye concentration in drops (0 to 1) and (C_L to C_H)
C_L, C_H	Low and high concentrations of input droplets
C_r	Dye concentration variance ratio, vessel drops to feed drops
$\overline{C}$	Average dye concentration (0-1) on a volume basis
c_1, c_2	Constants in g(v)
c_3, c_4	Constants in $h(v, v') \cdot \lambda (v,v')$
d	Drop diameter
d_{32}	Sauter-Mean diameter, $\sum n_i d_i^3 \Big/ \sum n_i d_i^2$
d_{max}, d_{min}	"Maximum" and "minimum" drop diameters

Reproduced with permission of the copyright owner. Further reproduction prohibited without permission.

English Alphabet

D	Impeller diameter
E(k)	Turbulent energy spectrum, k = wave number
E	$\int_{1/d}^{\infty} E(k)\, dk$
f(v)	Number effluent frequency of drops of volume v
F	Force
$f(h_o, h_c)$	$1/h_c^2 - 1/h_o^2$
F(v,v')dvdv'	Number coalescence rate between drops of volume v and v'
g(v), g(d)	Number breakage rate for drops of volume v, or diameter d
h(v, v')	Symmetric function where $h(v, v')\, n_{v'}$ = collision frequency of a drop of volume v with $n_{v'}$ drops of volume v'
h	Thickness of intervening continuous fluid between a drop and a flat surface or between two colliding drops
h_c	Film thickness at coalescence
i,j	Integers
k	Wave number in E (k)
$k^{\dagger}$, $k^{\dagger\dagger}$, k'''	Dimensionless constants
K, K', K'_b , K'_c	Dimensionless constants
k_1, k_2	Constants in g(d)
k_3, k_4	Constants in $h(d, d') \cdot \lambda (d, d')$
K*	Equilibrium constant for "normal-activated" drop exchange
L	Impeller width
L'	Upper volume limit in numerical integrations
n	Number of drops in vessel
n_o	Number feed rate of droplets

Reproduced with permission of the copyright owner. Further reproduction prohibited without permission.

n_x	Number of drops in vessel of species x
n_d	Number of drops in vessel of diameter d
n_b	Number of drops of diameter d in breakage region
n'	Number of integration intervals
N	Agitator speed
N_{Re}	Reynolds number, $ND^2\rho / \mu$
N_{We}	Weber number, $N^2 D^3 \rho / \sigma$
P	Power
p	Pressure
p(t'), P(t')	p . d . f and cumulative distribution function of contact time, t'
p(coal)	Probability of a coalescence (given a collision)$= \lambda$
$r_b(v)$, $r_b(d)$	Number breakage rate of drops of volume v, or diameter d
$r_c(v,v')$, $r_c(d,d')$	Number coalescence rate between drops of volume v and v', or diameters d and d'
R_n, R_v, R_m	Number, volume and entropy mixing rates
t	Time
t', $\overline{t'}$	Contact time, average contact time
u	Velocity
$\overline{u^2(x)}$	Mean square of the relative velocity between two points separated by a distance x in the inertial subrange
v	Volume
v_o	Average input drop size
v_{10}	Number-average drop volume, $\sum n_i v_i / \sum n_i$
v_{21}	Volume-average drop volume, $\sum n_i v_i^2 / \sum n_i v_i$
V_T	Tank volume
w(v)	Number coalescence frequency out of region v to v + dv

Reproduced with permission of the copyright owner. Further reproduction prohibited without permission.

English Alphabet

Y_i	n A (v)

Greek Alphabet

α	Numerical constant in integration formulae
β (v|v')	Breakage kernel, eq. 5.8
γ	Numerical constant in integration formulae
δ	Numerical constant in integration formulae
ε	Local rate of energy dissipation per unit mass
$\bar{\varepsilon}$	Power input of the mixing impeller per unit mass of vessel contents
ε_b, ε_c	Energy dissipation rates in breakage and coalescence regions
ζ	Constant in $E(k) = \zeta \varepsilon^{2/3} k^{-5/3}$
η	Dissipation microscale
θ	Dispersed phase fraction
λ (v,v')	Coalescence efficiency of colliding drops of volumes v and v'.
μ	Continuous phase viscosity
ν (v)	Average number of drops formed on the breakage of drops of volume v
ξ	Defined by equation 5.25
ρ , ρ_d	Density of continuous phase, of dispersed phase
σ	Interfacial tension
σ_o	Standard deviation of feed volume
σ_β	Standard deviation of beta distribution
σ_τ	Standard deviation of coalescence time

Reproduced with permission of the copyright owner. Further reproduction prohibited without permission.

Greek Alphabet

Φ	Cumulative normal distribution
ω	Mixing frequency (for experimental values, calculated from equation 4.3)
ω_n, ω_v, ω_m	Theoretical mixing frequencies on a number, volume, and entropy basis

Reproduced with permission of the copyright owner. Further reproduction prohibited without permission.

CHAPTER 1

INTRODUCTION

1.1 General Issue

The complexity of mixing phenomena has led to the use of two simplified approaches in research studies. One approach has been the fundamental study of the coalescence behavior of a single drop at a liquid-liquid surface. The other more practical approach has been the study of some limited aspects associated with dispersed-phase mixing vessels. Because of the inherent probabilistic nature of both the breakage and coalescence processes, this latter approach has the advantage of considering the average behavior of thousands and even millions of drops at one time.

This thesis has reference to both of these approaches.

1.2 Specific Problem

If a mixture of two immiscible liquids of certain phase fraction is agitated in a batch or continuous flow tank, a dispersion of droplets is formed in which both breakage and coalescence are occurring. After a sufficiently long time, a steady-state balance between coalescence and break-up is established. The characteristics of the resulting dispersion are a function of such variables as the geometry and size of the mixer, the intensity of agitation, phase fraction and fluid properties such as density,

Reproduced with permission of the copyright owner. Further reproduction prohibited without permission.

viscosity, and interfacial tension. Due to the statistical nature of mixing, the mixing dependence on drop size and the particular flow conditions of the system, a relatively broad distribution of droplet sizes is produced.

In many industrially important operations such as liquid-liquid extraction, gas absorption and dispersion polymerization where mass transport across liquid-liquid interfaces is occurring, a knowledge of this drop-size distribution is essential for reactor design. Ideally it is desirable to be able to predict drop-size distributions on the basis of a knowledge of the breakage and coalescence phenomena. Unfortunately these phenomena are poorly understood.

Until very recently no research had been done in which drop-size distributions and coalescence rates are considered simultaneously. Within the last five years, however, two important studies have been performed: one by Valentas and Amundson at the University of Minnesota (49) and the other by Verhoff and Curl at this University (52). In both of these studies integro-differential equations which relate the distribution of drop sizes to the breakage and coalescence mechanisms are derived from conservation principles. Valentas and Amundson used assumed mixing functions to describe the breakage and coalescence processes and obtained numerical results for the drop-size distributions. No attempt was made to compare these distributions to experimentally-determined ones.

Verhoff and Curl, on the other hand, tried to obtain a numerical description of the mixing functions by inverting the integro-differential equation using detailed experimentally-determined

Reproduced with permission of the copyright owner. Further reproduction prohibited without permission.

information, namely a bivariate distribution of drop size and dye concentration. Although Verhoff developed an experimental method which yields more detailed information about the mixing process than any previous technique, he was unsuccessful in obtaining a numerical description of the mixing functions.

This work is a continuation of Verhoff's research. The experimental method and equipment developed and constructed by Verhoff and Curl have been used with minor modifications. Also the general purpose of this research is similar to that of Verhoff; namely, to obtain a quantitative description of the coalescence and breakage processes taking place in a continuous flow mixer by making use of the experimental data. The approach to this problem, however, is quite different in both studies. Verhoff made no assumptions regarding the mixing processes and essentially used a "black-box" method of solution. In contrast, this work opened this "black-box" by postulating a variety of possible mixing models and using these to best-fit the data. The following chronological steps were carried out in the solution of the problem:

(1) A matrix of experiments were performed with the continuous flow mixer in which stirring speed and phase fraction were varied. For each experiment a bivariate drop size-dye concentration distribution was obtained.

(2) The results of these experiments and the experimental findings of other researchers were investigated.

(3) Simple coalescence and breakage models were derived on the basis of the above investigation.

(4) These models were used to generate drop-size distri-

Reproduced with permission of the copyright owner. Further reproduction prohibited without permission.

butions and coalescence frequencies by means of the integro-differential equations.

(5) These distributions and frequencies were checked against the actual experimental values. The derived models were then modified or revised according to their ability to fit the data, their simplicity, and their generality.

Reproduced with permission of the copyright owner. Further reproduction prohibited without permission.

CHAPTER 2

LITERATURE REVIEW

2.1 Introduction

There is a fairly extensive body of literature concerning the general behavior of dispersions in an agitated mixing vessel. Unfortunately there is very little known about how single drops behave in an agitated tank. This knowledge is necessary in this study because, in the general mixing equation, one must ascribe to drops of certain size an explicit mathematical expression describing their breakage and coalescence behavior. Fortunately much research has been carried out in related fields such as (1) single drop coalescence on a liquid-liquid surface, (2) collision of spheres in Couette flow, (3) breakage of drops in pipe flow, etc. Hopefully reasonable parallels can be drawn from these studies in describing the mixing processes in an agitated vessel.

2.2 Characteristics of Mixing Vessel

The mixer used in this study is geometrically similar to those used by several other researchers and has wide industrial application. The vessel is baffled and stirred with a flat six-blade turbine. It has been shown experimentally by Rushton et al. (40), that for sufficiently high Reynolds number, the power input of the mixing impeller per unit mass of vessel contents, $\bar{\epsilon}$, is independent

Reproduced with permission of the copyright owner. Further reproduction prohibited without permission.

of the properties of the liquid and a function only of the geometry of the vessel and its speed. It has also been shown that the distribution of the main flow velocity in the tank is universal above a sufficiently high Reynold's number (12, 41, 43). Cutter (12) has described the flow of water in the tank with emphasis on the local rates of energy dissipation per unit mass, ε . He found that the flow is far from homogeneous. Most of the energy supplied to the impeller is dissipated in the impeller and the impeller stream, only about 30% being dissipated in the rest of the tank. The ratio of local energy dissipation rates, ε , to the average value, $\bar{\varepsilon}$, varies tremendously; from 0.25 outside the impeller stream to 70 in the immediate neighborhood of the impeller.

2.3 A Description of Turbulence

Kolmogoroff's theory of local isotropy has been used extensively in explaining dispersion phenomena, although it has yet to be proven experimentally (24, 5, 10, 18, 19, 44, 47). The theory assumes that at sufficiently high Reynolds numbers the small-scale eddies in the turbulent flow are isotropic and that their intensity is dependent only on the local rate of energy dissipation and the viscosity of the fluid. Furthermore, at higher Reynold's numbers there is a subrange of eddies whose intensity is a function only of their size and of the local rate of energy dissipation, ε . It is in this inertial subrange where several researchers believe drops are being broken up.

Reproduced with permission of the copyright owner. Further reproduction prohibited without permission.

2.4 Description of Mixing Processes in Turbulence

(a) Break-up

Several investigators have considered the mechanism of droplet breakup in turbulent fields (10, 18, 44, 47). Hinze has suggested that in dispersions where drops are much larger than the microscale of turbulence, dynamic forces rather than viscous shear forces control the breakage process which is characterized by a critical value of the Weber number (a dimensionless ratio relating external forces to drop surface forces). By dimensional reasoning and an invocation of the theory of local isotropy a relationship between the critical drop size and the system variables is obtained.

$$d = k^{\dagger} \sigma^{3/5} \rho_c^{-3/5} N^{-6/5} D^{-4/5} \qquad 2.1$$

where d is the "maximum" drop size in the turbulence. Equation 2.1 has also been confirmed with d being taken as the Sauter-Mean diameter, d_{32} . Equation 2.1 can also be rearranged to give:

$$\frac{d}{D} = k^{\dagger} (Nwe)^{-0.6} \qquad 2.2$$

where Nwe is the Weber number.

Several authors have found equation 2.1 or 2.2 to be in excellent accord with experimental data. Indeed Sprow (47) and Chen and Middleman (10) working independently found identical values for the dimensionless constant $k^{\dagger}$ in equation 2.1 or 2.2. Both experimental studies were performed in coalescence free systems with the dis-

Reproduced with permission of the copyright owner. Further reproduction prohibited without permission.

persed-phase concentration being lower than 1 1/2 %.

No work has been done with agitated dispersions to determine either the breakage rates or the distribution of droplet sizes resulting from the breakup of a larger drop. Rumscheidt and Mason (39) working mostly with couette flow indicate that binary breakage does not always occur and droplets often break into several droplets. Sleicher (46) investigating breakup in turbulent pipe flow observed "marginally unstable" drops breaking up into two approximately equal parts.

(b) Coalescence

The phenomenon of coalescence of liquid drops in a turbulent field is even more poorly understood than the breakup process. Shinnar (44), in an interesting and much referred to examination of the coalescence process in an agitated tank, has presented a theory of coalescence based on local isotropy concepts and the idea of an energy of adhesion between droplet pairs. This researcher dispersed a molten wax in hot water to which a protective colloid had been added. By siphoning off small samples and freezing these rapidly, drop-size distributions were obtained by microscopic inspection. He was able to obtain a stable dispersion (no coalescence) at a certain high agitator speed. Whenever the speed was reduced, coalescence immediately took place and proceeded until a new stable equilibrium was established. When this procedure was performed for various final agitator speeds a correlation was obtained, $d_{32} \propto N^{-3/4}$. Shinnar explained this -3/4 in terms of an adhesion phenomenon similar to that found in emulsion theory where particles

Reproduced with permission of the copyright owner. Further reproduction prohibited without permission.

are orders of magnitude smaller than the drops found in dispersions. Shinnar claims that drops in a dispersion adhere to each other and they will eventually coalesce except for the turbulent forces which are tending to separate them. By comparing these two opposing, drop-size dependent forces, Shinnar was able to derive an expression for the diameter above which he assumed no coalescence is possible:

$$d = k^{\dagger\dagger} A^{3/8} \rho_c^{-3/8} N^{-3/4} D^{-1/2} \qquad 2.3$$

where A is a coalescence parameter related to the energy of adhesion between drops. With reference to equation 2.1 and equation 2.3 Shinnar was able to give a unified theory of mixing behavior in an agitated vessel. The theory describes droplets in the vessel coalescing "rapidly" if their diameter is less than that predicted by equation 2.3 until the diameter of the drop formed reaches either a stable size, or the unstable size for break-up as given by equation 2.1. The fragmentation into several smaller droplets becomes probable and the process restarts with coalescence. The size distribution is determined by the state of dynamic equilibrium reached. Equations 2.1 and 2.3 can be described graphically as shown in figure 2.1.

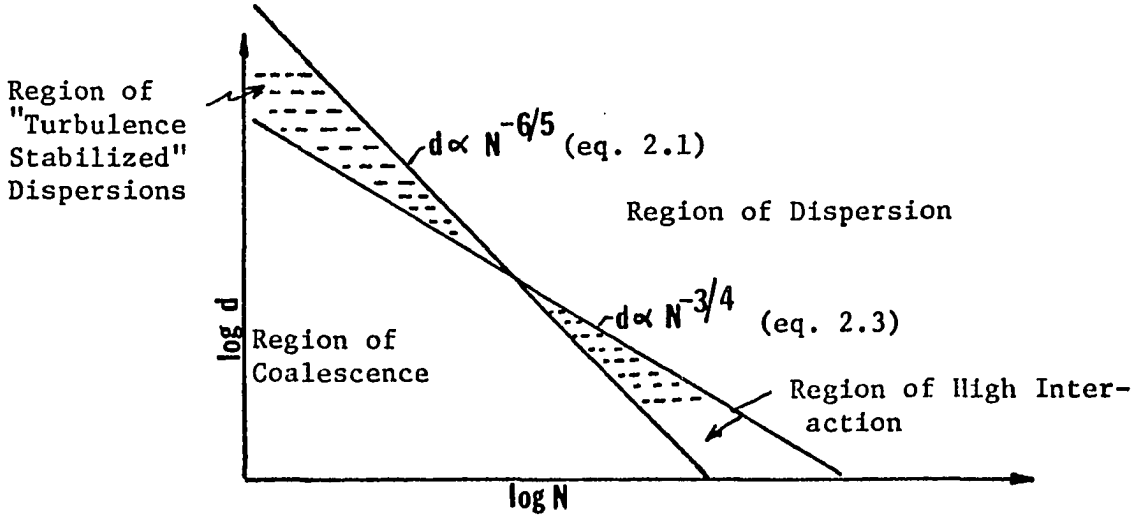

Figure 2.1 Turbulence Stabilized Dispersions

Reproduced with permission of the copyright owner. Further reproduction prohibited without permission.

As shown in the figure, there is a region in which neither breakup nor coalescence occurs. Dispersions which fall in this region are called by Church and Shinnar "turbulence-stabilized" dispersions. As stated, their experimental results seem to confirm this theory.

Rogers et al. (38) who measured drop sizes in a 50% liquid-liquid agitated dispersion found that the average diameter of the system was correlated with agitator speed, N, as $d_{32} \propto N^{-0.76}$. Shinnar took this to mean that the system was "coalescence-controlled." That is, drops were coalescing up to a certain diameter above which coalescence was prevented by the turbulence.

Sprow (48) measured drop size distributions at various locations in a turbine mixer for a strongly coalescing system. He found that drops measured near the impeller displayed a $d \propto N^{-3/2}$ dependency and those near the walls had a $d \propto N^{-3/4}$ form. Sprow, using an argument identical to Shinnar's, took this to indicate that the drop size was breakage-controlled near the impeller and coalescence-controlled away from the impeller.

Jeffreys and coworkers (22) similarly found that the drops exiting from the mixer part of a mixer-settler unit (2:1 water: kerosene and 2:1 kerosene-water) could be correlated by equation 2.3.

Thus the evidence seems quite convincing that for very concentrated, strongly coalescing systems, or for systems or regions where breakup is absent or negligible, the average drop size depends on the agitator speed as the -3/4 power. The prevalent explanation in terms of an "adhesion energy" seems unreasonable and has been disputed by Howarth (20) who developed a coalescence model based on an analogy to the simple collision theory of bimolecular gas reac-

Reproduced with permission of the copyright owner. Further reproduction prohibited without permission.

tions. His model indicates that coalescence can only occur when the relative velocity between drops exceeds a critical value. This model is in contradiction to Shinnar's theory and cannot be used to explain the latter's experimental results or the -3/4 power found by others.

2.5 Experimental Determination of Coalescence Frequencies

Several papers have been published concerning coalescence rates in agitated liquid-liquid systems (15, 21, 29, 32). In all cases coalescence frequency was found to be strongly dependent on agitator speed. Madden and Damerell (29) determined the mixing rate based on disappearance of iodine in the oil continuous phase as it reacted with sodium thiosulfate in the water dispersed phase. Using an equal drop-size homogeneous coalescence model (described later), this rate of disappearance was related to a mixing rate. It was found that the mixing frequency varied with agitator speed to the 2.40 power and with phase fraction to the 0.504 power.

Miller et al. (32) employed a light transmission technique for following the spread of dye due to coalescence. By using a homogeneous coalescence model developed by Curl (11) they were able to estimate mixing rates for a variety of vessels, impellers, phase fractions, phase properties and power inputs. The coalescence frequency varied with agitator speed to the 1.5 - 3.3 power depending on the system used and with phase fraction to the 0.6 - 1.1 power.

Groothius and Zuiderweg (15) performed experiments in a continuous flow system. Two streams of dispersed phase of different densities (0.990 g/ml and 1.030 g/ml) were fed into the water continuous phase. The output stream consisted of a light phase made

Reproduced with permission of the copyright owner. Further reproduction prohibited without permission.

up of non-coalesced heavy-phase drops and coalesced drops. The mixing rate was deduced by a simple material balance. Their results compared favorably to those of Miller et. al. with the mixing rate varying with agitator speed to about the 3.0 power. The addition of 1.5% by weight acetic acid to the dispersed phase increased the coalescence rate by about twenty fold.

Howarth (21) determined coalescence frequencies by measuring the rate of change of interfacial area on quickly decreasing the agitator speed. An equal drop size model was employed in developing a relationship between mixing rate, the average drop size in the vessel and the instantaneous rate of change in interfacial area. By assuming that the mixing rate varies inversely as the average drop size and by determining that the average drop size varies as $N^{-0.6}$ he found that the coalescence frequency depends on agitator speed to the 1.9 - 2.25 power.

2.6 Coalescence of Single Drops on a Liquid-Liquid Surface

When a drop of liquid falls through a lighter, immiscible liquid onto a flat interface separating two phases, it rests on the interface for a time until the liquid film of continuous phase retained between the drop and the interface drains and ruptures. The rate of film thinning, the critical film thickness and the location of the rupture may be affected by drop size, temperature, temperature gradients, presence of surfactants, concentration of dissolved components, vibrational and electrostatic effects and fluid properties such as density, viscosity, and interfacial tension. All of these effects have been investigated to some extent by numerous researchers

Reproduced with permission of the copyright owner. Further reproduction prohibited without permission.

(9, 16, 17, 25, 28, 34). Most workers have found that for a given system, the coalescence time is roughly Gaussian in distribution (9, 34). Several researchers have attempted to mathematically model the drainage process (8, 9, 27, 28, 34, 35). Charles and Mason, in a classic paper (9), discuss two models for the rate of thinning of the intervening film. These are the spherical-planar approach where neither the drop nor the plane deforms, and the parallel disc approach where the drop flattens until its weight is supported by its internal pressure. The resulting mathematical description of this latter, uniform film model is identical to that of another model: the approach of a sphere to a deformable interface where the deformation is small. Chappelear has considered the more general and realistic case where both drop and interface are deformable (8). These uniform film models predict the approach time or coalescence time to increase as the diameter, d, to the 5th power. Charles and Mason, however, using ultra-pure liquids found $t \propto d^{3.15}$. Hawksley* determined the exponent to be 1.02 and Lawson found it to be 1.5 (25). It is believed that the primary reason for the discrepancy is due to the movement of the interfaces (8, 9, 28, 33, 35, 42). Princen (35) set up a differential equation to describe the equilibrium shape of a drop at a liquid-liquid interface and numerically computed this shape as a function of drop size, interfacial tension and density difference between phases. His results indicate that as a limiting case, the deformable drop-and-interface model gives a correct representation of the real equilibrium case. MacKay and Mason (28) and other researchers have found that a drop on a liquid-liquid interface develops a slight reverse curvature, or dimple, on the surface

*See Lawson

Reproduced with permission of the copyright owner. Further reproduction prohibited without permission.

adjacent to the interface. Princen has theoretically considered this dimple for the cases of (1) a drop approaching a horizontal interface and (2) two approaching drops of equal size. In both cases the equation describing the approach of the closest part of the drop to the interface is similar to the undimpled case.

2.7 Collision and Coalescence of Spheres and Drops

Almost nothing is known about the collision of droplets in agitated dispersions. Summaries are available for the prediction of collision frequencies for colloidal and aerosol systems in turbulent flows, these being valid only for particles less than about 10^{-3} cm (13, 26). Nevertheless, Howarth (20) has attempted to extend this analysis to agitated systems containing larger drops.

Mason and coworkers have carried out extensive work on particle motion of spheres and liquid drops in sheared suspension (1, 4, 30, 31, 39). Manley and Mason (30) measured collision frequencies of glass spheres in couette flow and found them to be in excellent accord with a theory based on simple geometrical considerations. In a standard collision where the spheres are of equal size, the doublet rotates as a rigid dumbell at a known angular velocity and separates at a point which is a mirror image of the initial point of contact. A head-on collision would cause the doublet to rotate indefinitely without separating. For the case of spheres of unequal size, standard collisions were similar to those of equal-sized spheres when the ratio of diameters was less than 2; when the ratio was greater than 2 the smaller sphere would describe a zig-zag type of motion around the larger (31). Bartok and Mason (4)

Reproduced with permission of the copyright owner. Further reproduction prohibited without permission.

studied the case of fluid spheres in similar conditions. They found that the standard and head-on collision doublets of equal-sized liquid spheres behaved similarly to those of rigid spheres. Head on collision of doublets of fluid spheres coalesced into single droplets after a number of doublet rotations. This number varied between wide limits and depended upon the geometry of the collision doublet and the presence of surface-active impurities. Standard collisions resulted in coalescence only when sufficient contact time was allowed for film drainage. The effect of electric fields and electric charges on the coalescence of collision doublets in similar flow fields was studied by Allan and Mason (1). It was found that coalescing doublets showed a variation in coalescing time similar to the variation in rest times observed for liquid drops coalescing at flat interfaces.

McAvoy and Kintner (27) considered the case of two equal-sized rigid spheres in a liquid field and derived an equation identical to that describing a rigid drop approaching a rigid interface except for a numerical constant.

Scheele and Lang (42) studied binary collisions of drops in two phase immiscible liquid systems. Collisions were brought about by the simultaneous launching of two drops from opposing nozzles submerged in water. High speed movies of 23 collisions (7 coalescences and 16 bounces) were recorded and analyzed. In these experiments nozzle separation and approach velocity were varied. The drops were observed to undergo oscillations during their travel, the maximum amplitude being about 20% of the drop diameter (0.34 cm). These

Reproduced with permission of the copyright owner. Further reproduction prohibited without permission.

oscillations originated from the initial impulse necessary to detach the drop from the nozzle tip. Coalescence phenomena were found to be very sensitive to the phase of oscillation at point of contact: if the area of contact on collision was small enough, a coalescence occurred. Drop contact times were dependent on collision velocities. It was found that the classical parallel disc, rigid interface model for describing film thinning was insufficient in predicting fast enough rates of thinning to enable rupture to occur within the apparent time of contact. Murdoch and Leng (33) show that complete mobility of the interfaces can explain the difference.

2.8 Simplified Theories of Mixing

There are several basic mixing models for agitated vessels (37). The circulation model is based on a circular flow pattern of breakage near the impeller and coalescence in other parts of the vessel. The dead-corner model has most of the coalescing occurring between drops in the vessel and large masses of dispersed phase stagnated in dead corners. Large drops break from this unstable mass and return into the drop system. The homogeneous, equal drop-size model is the one most amenable to mathematical analysis. The basic assumptions of this model are that all drops are the same size and that coalescences are considered to occur randomly between two drops in the vessel. Redispersion of the coalesced drop is assumed to occur instantaneously into two equal-sized drops. Curl (11) developed a mixing equation based on this model, representing the transient spreading by coalescence and redispersion, of a solute among the drops in a batch reactor. He was able to relate the solute concentration variance to the coalescence frequency and time. The effect of chemical reaction

Reproduced with permission of the copyright owner. Further reproduction prohibited without permission.

was also investigated.

2.9 General Mixing Model

Valentas and Amundson (49, 50, 51) developed an integro-differential equation which describes the processes involved in a dispersed phase, continuous flow, agitated vessel. Their equation was obtained from a number balance in a differential mass range. This equation will be discussed in detail in Chapter 5. In the equation there are six general, defining functions describing: (1) the breakage frequency, (2) the average number of drops formed per breakage, (3) the distribution of drops formed on breakage, (4) the coalescence efficiency, (5) the collision frequency and (6) an escape frequency. Using many assumed forms for the above functions, Valentas and Amundson obtained numerical results for the drop-size distributions. These results indicated the relationship of the resulting drop-size distribution to the mixing functions.

Verhoff and Curl (52) similarly developed a series of integro-differential equations based on several different space balances in which the above functions were combined into a single mixing kernel or function. This kernel was then employed in a balance using a two-dimensional differential area (drop size and dye concentration). An experimental method was developed to measure the input and output bivariate distributions. Three methods of kernel approximation were developed and applied to several measured distributions. In all methods the researchers found singularity problems in the numerical inversion of the integral equation. The resulting kernels appear unreasonable and it is doubtful that they have any physical significance.

Reproduced with permission of the copyright owner. Further reproduction prohibited without permission.

CHAPTER 3

EXPERIMENTAL APPARATUS AND PROCEDURE

3.1 Introduction

The experimental apparatus and procedures used in this work are essentially identical to those used by Verhoff and are described in detail in his dissertation (52). These will be briefly discussed here along with the few modifications added.

The experimental apparatus herein described has the purpose of providing the necessary information for the analysis of the dispersed phase mixing occurring in a turbine-agitated baffled vessel. Since the three independent processes of breakage, coalescence, and flow can yield the same drop-size distribution in various ways, this necessary information requires the addition of some variable other than drop size to the system. This added variant was chosen to be dye concentration in the dispersed drops.

The basic experiment involves the baffled agitated vessel, geometrically identical to most of those described in the literature, to which is fed 2 streams of dispersed phase (oil phase) and one stream of continuous phase (water phase). Each of the two dispersed streams has a different concentration of light-absorbing dye. The drops of oil are mixed by the agitator and leave through the exit. A representative sample of these drops is collected and analyzed for size and dye concentration.

Reproduced with permission of the copyright owner. Further reproduction prohibited without permission.

3.2 Description of Flow System

The basic flow system is shown in figure 3.1. It consists of three streams from the storage tanks, each pumped by a one-sixth H.P. explosion proof reversible motor. These streams flow through Schutte-Koerting rotameters which contain their own needle valves. From the rotameters the flow continues to drop generators which are capable of producing drops of approximately equal size. One of these is shown in figure 3.2. Electrical probes inserted into the glass tube count the rate of production of the drops.

The mixing vessel is shown in figure 3.3. The vessel is cylindrical with an inside diameter of about 4 3/8 inches and a height of 5 1/2 inches, (Volume = 1.37 litres). Two of the six available ports in the center ring are used for inputs from the drop generators, two for output to the sampling probe and the waste storage tank. The remaining two are plugged. The vessel is equipped with four equally spaced baffles which extend into the vessel .437 inches (1/10 tank diameter). The agitator contains six flat stainless steel blades equally spaced around the diameter. The diameter of the agitator is two inches and each blade is 0.4 inches wide and 0.5 inches long. The agitator is driven by a 1/4 horsepower variable-drive motor. Vessel contents are maintained under a slight positive pressure by means of a back-pressure valve.

3.3 Description of Sampling System

The steps involved in the sampling system are (a) removing a sample from the vessel and stabilizing it, (b) collecting it in a reservoir, (c) forcing it at a constant volumetric rate through a thin capillary, (d) determining the size and dye concentration of

Reproduced with permission of the copyright owner. Further reproduction prohibited without permission.

Reproduced with permission of the copyright owner. Further reproduction prohibited without permission.

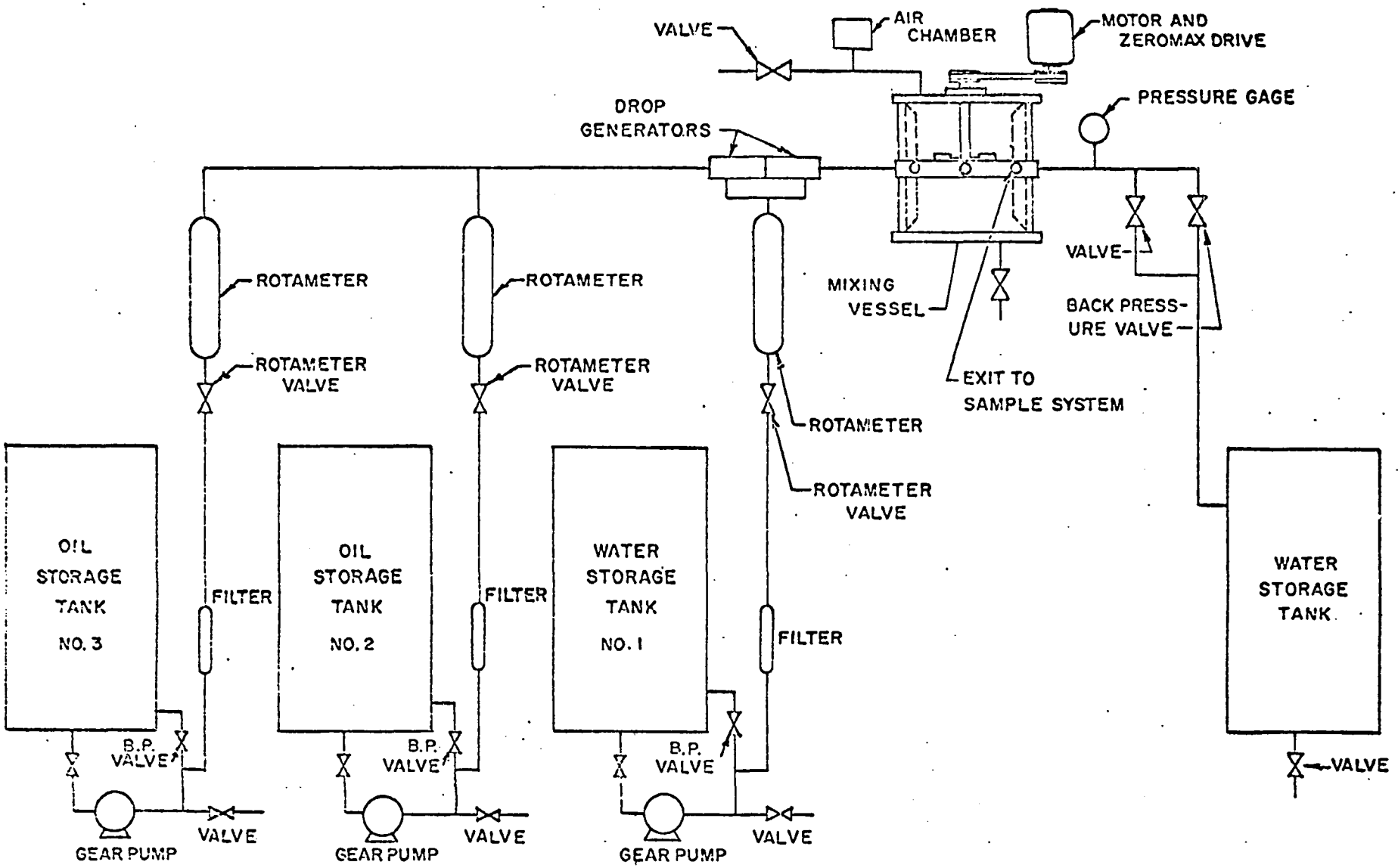

FLOW SYSTEM

FIGURE **3.1** (after Verhoff)

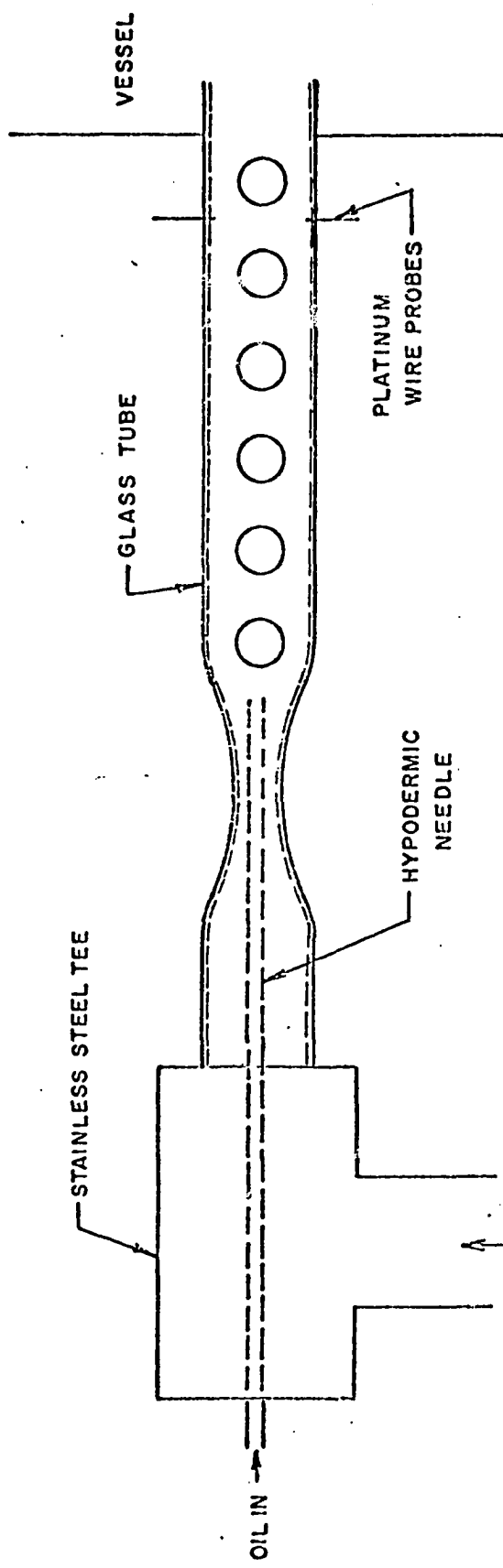

DROP GENERATORS

FIGURE 3.2 (after Verhoff)

Reproduced with permission of the copyright owner. Further reproduction prohibited without permission.

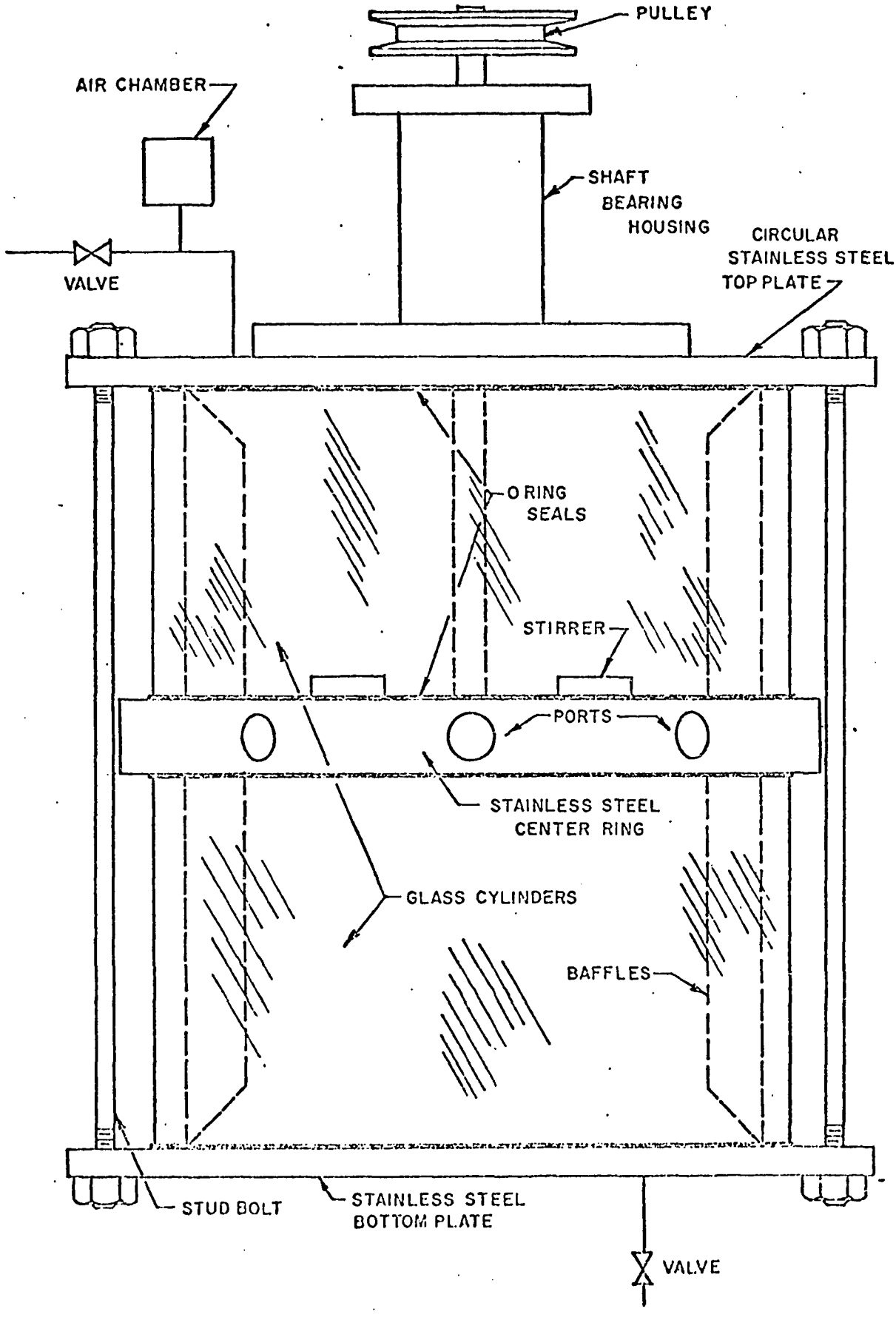

MIXING VESSEL

FIGURE **3.3** (after Verhoff)

Reproduced with permission of the copyright owner. Further reproduction prohibited without permission.

the drops passing through the capillary by means of recording the signal from a microscope-photometer-amplifier arrangement. The cross-section of the sampler is shown in figure 3.4. The surfactant feed system and the drive assembly are shown in figures 3.5 and 3.6 respectively. The operation and reliability of this system has been discussed in detail by Verhoff. The sampler is capable of withdrawing a sample from the vessel at any constant rate and simultaneously injecting a surfactant into this sample to prevent coalescence. The sampler is powered as shown in figure 3.6, by means of oil from oil-pressure air tanks. After the sample is withdrawn it is routed to a sample reservoir (about 2000 mm^3 compared to Verhoff's 200 mm^3 reservoir) shown in figure 3.7. The stabilized drops are allowed to settle toward the top. The two in-line stopcocks are then adjusted to allow the sample to be forced through a 0.220 mm capillary imbedded in plastic. A Compact Infusion Pump (Verhoff used a less versatile Sage Pump) coupled with a syringe produces a constant volumetric flow rate, which can, if desired, be varied. Verhoff has shown that the possible flow variations caused by viscosity and interfacial area changes can be considered negligible.

As a drop passes through the capillary, a microscope is focussed on it as shown in figure 3.8. The light from a 6 volt DC lamp is used, with a concave mirror focusing additional light on the pinhole. Through a 455 $m\mu$ optical filter, the coupled photometer sees only the light of wavelength near the maximum absorption for the dye used. The photometer is coupled to a photo-multiplier in such a way as to produce an output proportional to dye concentration.

The output signal is then put through an analogue computer

Reproduced with permission of the copyright owner. Further reproduction prohibited without permission.

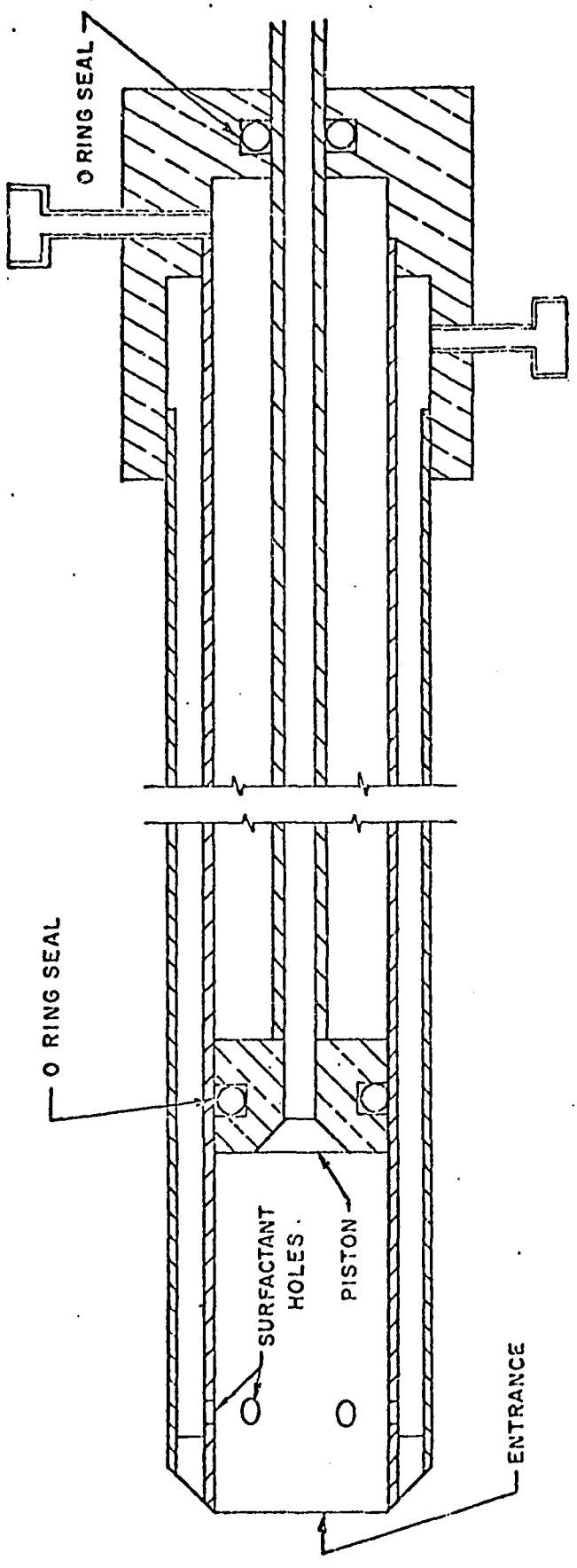

CROSS SECTION OF SAMPLER

FIGURE **3.4** (after Verhoff)

Reproduced with permission of the copyright owner. Further reproduction prohibited without permission.

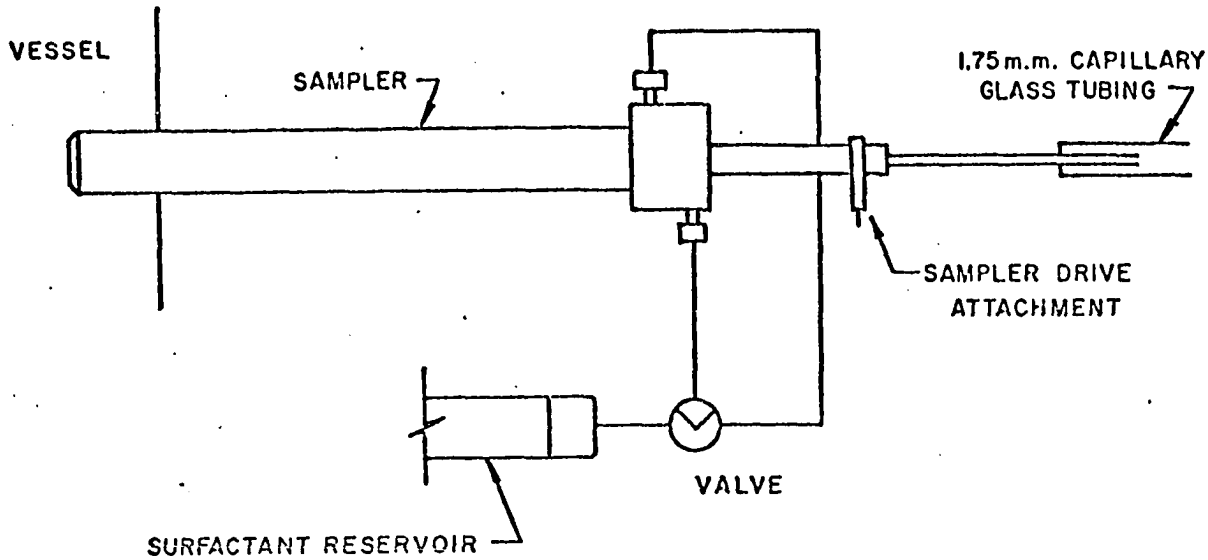

SURFACTANT FEED SYSTEM FOR SAMPLER
FIGURE **3.5** (after Verhoff)

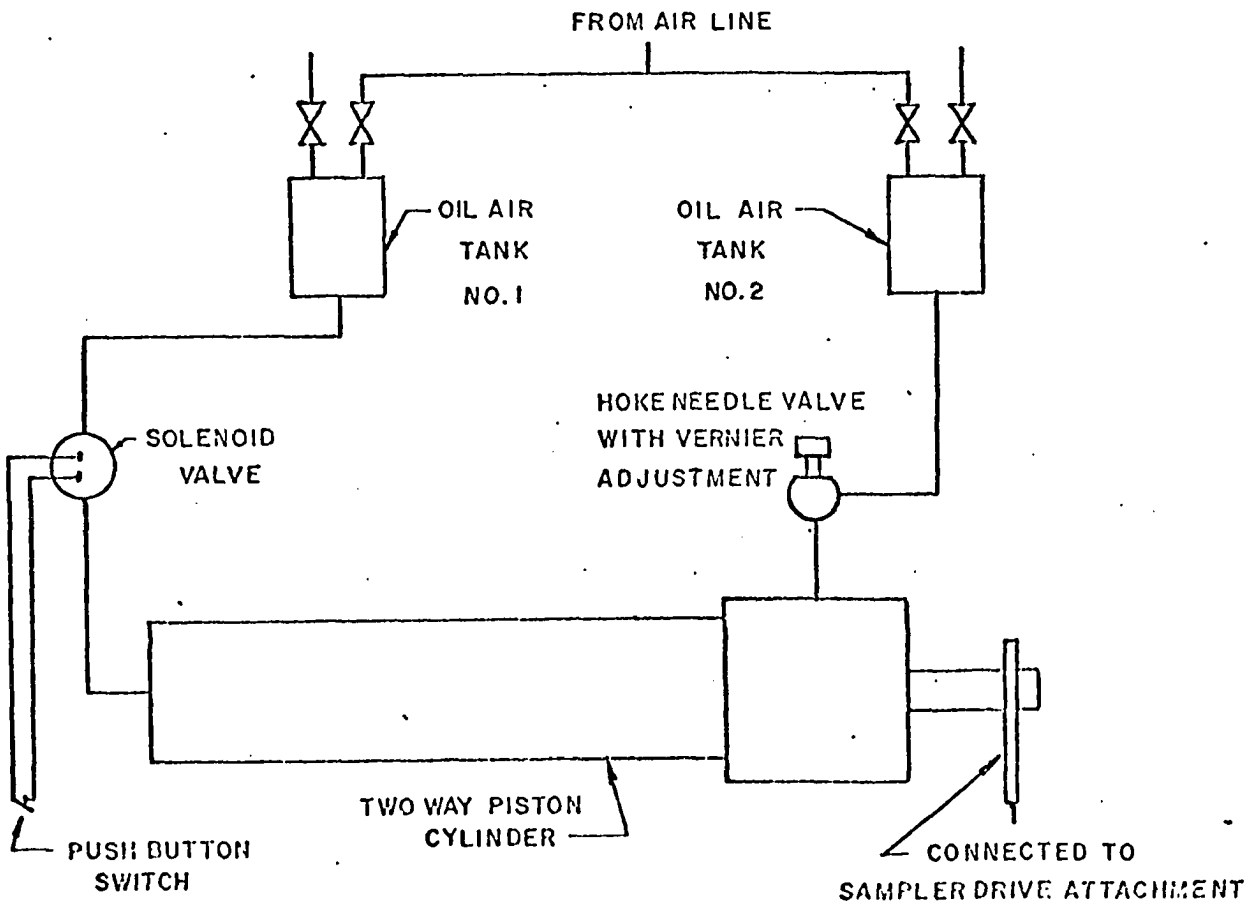

SAMPLER DRIVE ASSEMBLY
FIGURE **3.6** (after Verhoff)

Reproduced with permission of the copyright owner. Further reproduction prohibited without permission.

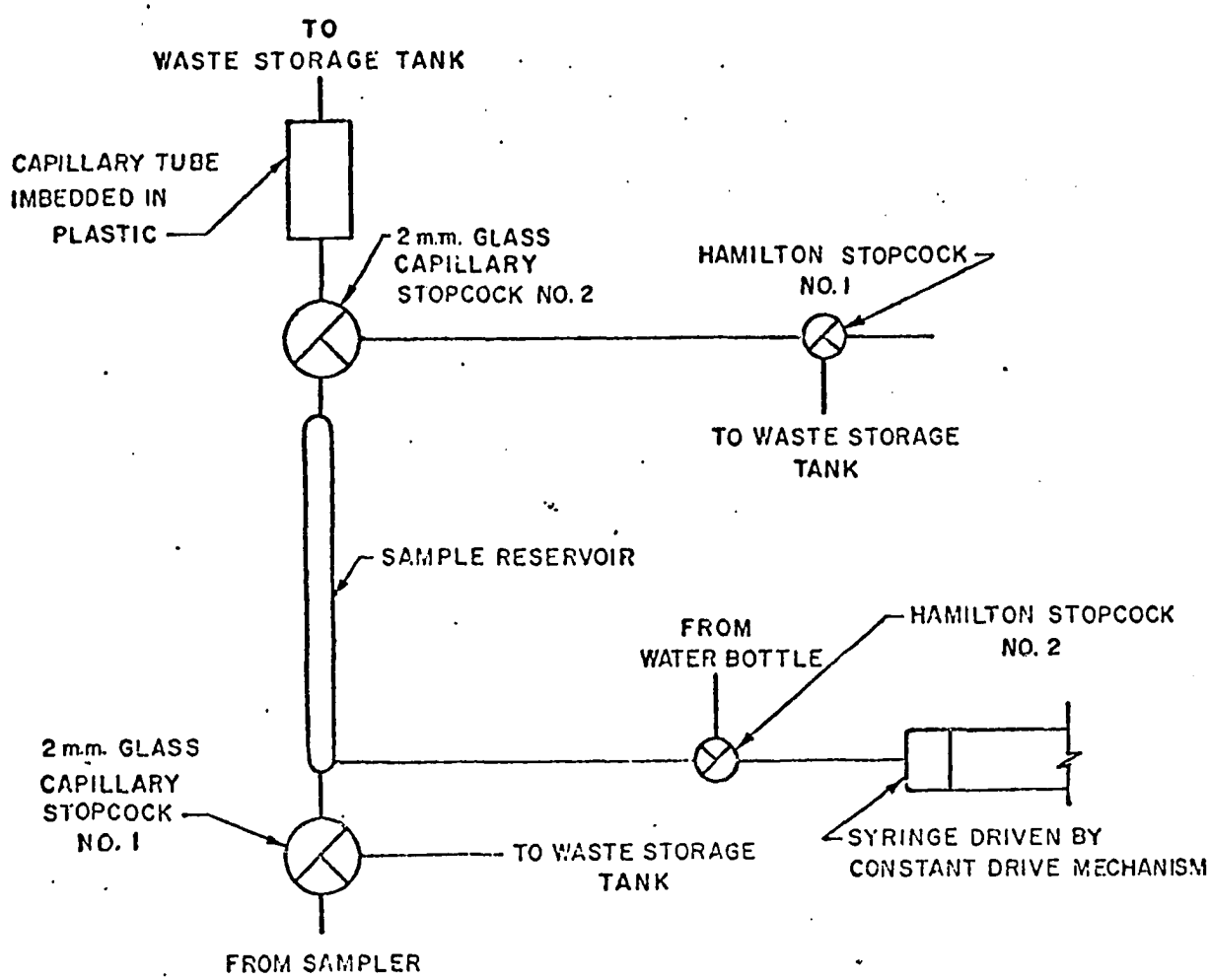

SAMPLE HANDLING SECTION
FIGURE **3.7** (after Verhoff)

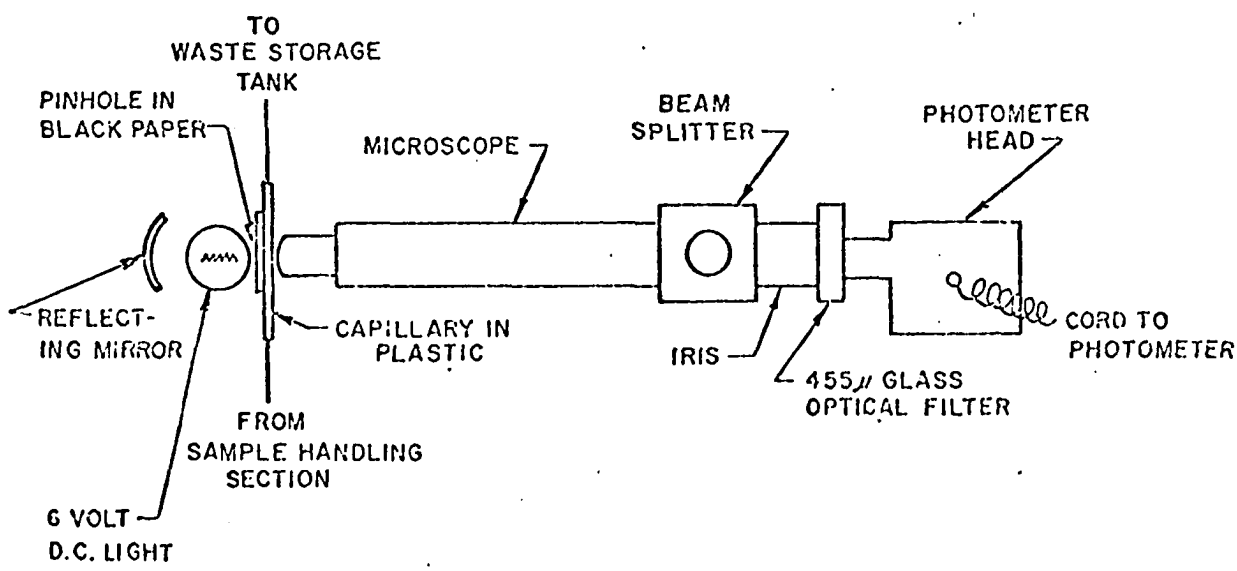

MICROSCOPE ASSEMBLY
FIGURE **3.8** (after Verhoff)

Reproduced with permission of the copyright owner. Further reproduction prohibited without permission.

to multiply the signal, balance it to zero and filter out the high frequency noise. A feed-back capacitance in the circuit allows adjustment to reduce the high frequency noise but it also reduces frequency response for measuring the smaller drops. The signal received as a drop passes through the capillary is rectangular with the height being a measure of the drop dye-concentration and the length being a measure of the drop volume.

The analogue output signal in operation varies between $\pm$ 1.0 volts and is recorded on an Ampex Sp 300 tape recorder in the FM mode. The tape speed was 1 7/8 inches per second (frequency response: 321 cps). In parallel with the tape recorder is an oscilloscope which allows one to view the voltage pulses being recorded.

The analog tape is then replayed at a speed of 15 inches per second and the data converted to digital data on an analog-to-digital converter. The A-to-D converter has two levels of accuracy, 6 and 10 bit information and two densities of recording (40,000 or 15,000 samples per second in the 6 bit mode and half these in the 10 bit mode). The 10 bit, low density combination was used in this work. The data from three to five experiments were recorded on one digital tape.

3.4 Preparations

The oil used as the dispersed phase is a mixture of Dowtherm-E and Shell # 3747 Base Oil. The mixture used in the experiments is approximately 39% Dowtherm-E and 61% by volume base oil. The density was checked with an hydrometer and was made just slightly lighter

Reproduced with permission of the copyright owner. Further reproduction prohibited without permission.

than the water phase which was a 0.001 N solution of Na_3PO_4. The interfacial tension was measured to be 35 dyne/cm. The salt provided an electrolyte for the drop-counter and also kept the glass and stainless steel reasonably clean. Verhoff claimed to have found no difference in coalescence rate with or without the Na_3PO_4.

The dye, Δ 9-9' bifluorene, was recrystallized from a 95% alcohol and 5% toluene mixture to remove possible impurities as suggested by Miller et. al. (32). Verhoff calculated the extinction coefficient of the dye to be 2.5×10^4 litres/ cm./ mole. As suggested by Verhoff, the dye concentration in both oil streams was doubled, 1 mg./ml. in one tank and 0.2 mg./ml. in the other. This was done to eliminate the problem Verhoff had in differentiating between the low concentration drops and the inherent system noise.

A solution of Tween 40 (3 wt %) was used as the surfactant in the surfactant feed reservoir (figure 3.5). A similar solution of Tween 60 was also found to be satisfactory in preventing coalescing. A small amount of methylene blue was added to the Tween 40 solution. This provided a coloured marking for the stabilized sample as it flowed into the sample reservoir.

The water that was used to pump the sample through the capillary was made 0.05 N of Na_3PO_4 to insure clean walls with no drop sticking.

3.5 Description of Experimental Procedure

It was discovered after several experimental runs that, if the inside of the mixing vessel was not absolutely clean, oil drops tended to stick to the sides of the glass and on the stainless steel

Reproduced with permission of the copyright owner. Further reproduction prohibited without permission.

baffles. These drops, even one or two of them, had a marked effect on the measured bivariate distribution and on the reproducibility of the experiment. The tank was thoroughly cleaned first with pure acetone and then with a saturated solution of Na_3PO_4.

After cleaning, the mixing vessel was filled with the water phase and all air pockets were purged. The agitator speed was set with the use of a tachometer. It was checked periodically during the experiment and was found to vary not at all. The oil and water phase flows were then started and the back pressure valve was adjusted to maintain the tank under a slight positive pressure. The input flows had a tendency to fluctuate usually within $\pm$ 10% and the rotameter valves had to be continually adjusted. The oil flows were maintained at identical rotameter readings. Because the calibration curves for these meters were different, the dark oil flow was slightly greater than the light, (0.525 vs 0.475). These fluctuations in flow, although having little effect on the average phase ratio in the vessel, did cause a variation in the input drop size. While the system was approaching steady-state, stabilized samples were withdrawn and used to calibrate the sampling system. This was done by first forcing a sample through the capillary at a given infusion rate. The voltage pulses produced by the drops were viewed on the oscilloscope. If the pulses were not sufficiently rectangular (poor frequency response) and/or the high frequency noise was unsatisfactory, the infusion rate and/or the analogue circuitry was changed. The infusion rate selected was the largest possible to measure satisfactorily the "smallest" drop size in the sample. In this way the number of drops analyzed per length of analogue or digital tape was maximized. This

Reproduced with permission of the copyright owner. Further reproduction prohibited without permission.

"smallest" drop size in any given distribution was selected to be that size below which the volume contribution to the whole sample was considered negligible.

About 30 minutes to one hour after the flows were started, a time sufficient for steady-state to be reached, and after the sampling system was calibrated, a stabilized sample was withdrawn and collected in the sample reservoir. The sample size was about 200-1000 drops, depending on the phase fraction of dispersed phase in the tank and the agitator speed. These drops were allowed to settle to the top of the reservoir and then studied with a flashlight to check for the "sparkling" that accompanies coalescences. If the sample was deemed stable, a signal was placed on the analogue tape to indicate the start of a sample; the sample was then forced through the capillary. The recording time was logged with a stopwatch. The taping was stopped when all but a few small drops had passed through the capillary. This procedure was repeated until sufficient samples had been collected to make up about 1000-3000 drops. A signal was then put on the tape to indicate the end of the last sample.

The experiment was ended by closing the input and output valves to the vessel and then stopping the input flows and agitator. The vessel contents were collected in a 2000 ml. vessel, and allowed to settle. The phase fraction was then measured. It was always within 5% of the estimated input value.

Reproduced with permission of the copyright owner. Further reproduction prohibited without permission.

CHAPTER 4

EXPERIMENTAL RESULTS

4.1 Calculation of Data and Distributions

The data from an experiment were on a digital tape which contained the digitized output signal of the photometer for several experimental samples. Those data were interpreted using the IBM 360 computer to give the dye concentration and volume of each drop in the sample. This required reading the numbers from the tape, converting them into integers and measuring the height and length of each of the pulses in the digitized sample. The data were read from the tape using an Assembly Language subroutine written, described and discussed in detail by Verhoff (52). The program works as follows:

(1) The base line is established by averaging the signals received while water was flowing through the capillary.

(2) The digitized signals are read in succession and if the signals have not deviated from the base line by a prescribed amount, they are averaged into the base line.

(3) If such a deviation is detected (i.e., a drop is starting to pass through the capillary), the computer counts the number of digital signals and accumulates the sum of the values until the signal is again within the prescribed band of the base line (i.e., the drop is leaving the capillary).

Reproduced with permission of the copyright owner. Further reproduction prohibited without permission.

(4) The "concentration" of the drop is calculated by dividing this accumulated sum by the total number of signals. The "volume" of the drop is the total number of signals.

(5) These values are stored if the "volume"* is larger than a particular value. In all cases this value is taken to be larger than the inside diameter of the capillary.

The associated volume and concentration of each drop measured is therefore available for further analysis. This information is used in the calculation of (1) the bivariate distributions of volume-concentration, log volume-concentration and diameter-concentration, (2) the marginal distributions of volume, log-volume, diameter and concentration, (3) various properties of the sample such as Sauter-mean diameter, volume-and number-average drop sizes, maximum and minimum volumes and concentrations, and second and crossmoments of the distribution.†

Because of the high frequency noise, there is a small error associated with the measurement of the dye concentration in each drop. This noise tends to slightly increase the measured variance of the drops (while, of course, mixing decreases the variance). Although this effect can be considered negligible where there is substantial mixing, it is important where there is only a very small amount of mixing. On measuring drops containing only the high and low feed concentrations, it is found that the concentrations are distributed

---

*The actual volume can easily be derived by knowing this number, the volumetric flow rate through the capillary, and the recording information of the analogue and digital tapes.

†A detailed discussion of the computer program used to calculate these quantities is presented in Appendix I.

Reproduced with permission of the copyright owner. Further reproduction prohibited without permission.

approximately normally about these high and low concentrations. Each distribution curve is contained within about 5% of the average or peak values (i.e., the feed concentrations). Two methods are used for accounting for this noise: (1) All drops in this normally distributed region are assumed to have the average, peak value. This is equivalent to having the concentration variance be a function of the mixing effects only. (2) A computer program is used to filter out the zero-mean noise associated with each concentration measurement. These techniques are discussed in detail in Appendix II.

4.2 Typical Experiment

Consider a typical experiment carried out at an agitator speed of 174 rpm, a residence time of 19.6 minutes and a phase fraction of 0.10.

Statistics:

Agitator speed = 174 rpm

Residence Time = 19.6 min.

Phase Fraction = 0.10

Number of Drops in Sample = 1693

Smallest Drop Size Measured = 0.0269 mm^3

Largest Drop Size Found = 1.92 mm^3

Sauter-Mean Diameter, d_{32} , = 0.836 mm

Number-Average Drop Volume, v_{10} , = 0.236 mm^3

Volume-Average Drop Volume, v_{21} , = 0.462 mm^3

Ratio of Concentration Variance, Vessel-to-Feed, C_r = 0.6644

Measured Average Concentration = 0.517

Reproduced with permission of the copyright owner. Further reproduction prohibited without permission.

The bivariate volume distribution in a concentration-volume space is given in figure 4.1; that in a concentration-diameter space is given in figure 4.2. Each number refers to the fraction of the total volume contained in a (C, C+ ΔC : v, v+ Δv) interval and (C, C+ ΔC : d, d+ Δd) interval respectively. The marginal distributions of volume, diameter, and concentration are given in figures 4.3, 4.4, and 4.5 respectively.

It is noted in the volume and diameter distributions that the curves do not "smooth" down to zero density at small drop sizes. The reason is that the smallest drop measured was 0.0269 mm^3. Drops smaller than this did not produce a rectangular pulse as they passed through the capillary and were rejected.

Also note the concentration distribution (figure 4.5). The first and last intervals of the 20 interval space essentially contain the volume fraction of drops that have the low and high feed concentrations, respectively. If there were no mixing at all, all the volume would be contained in these first and last intervals. On the other hand, if mixing were substantial, all the volume would be contained in the interval at C = 0.516. It may be seen, then, that the variance of concentration in the vessel as compared to the concentration variance of the feed streams can be taken as some measure of mixing. This concentration variance ratio is calculated to be:

$$C_r = \frac{\sum_{i=1}^{n} x_i C_i^2 - \bar{C}^2}{\bar{C} - \bar{C}^2} \qquad 4.1$$

where x_i = volume fraction

Reproduced with permission of the copyright owner. Further reproduction prohibited without permission.

Reproduced with permission of the copyright owner. Further reproduction prohibited without permission.

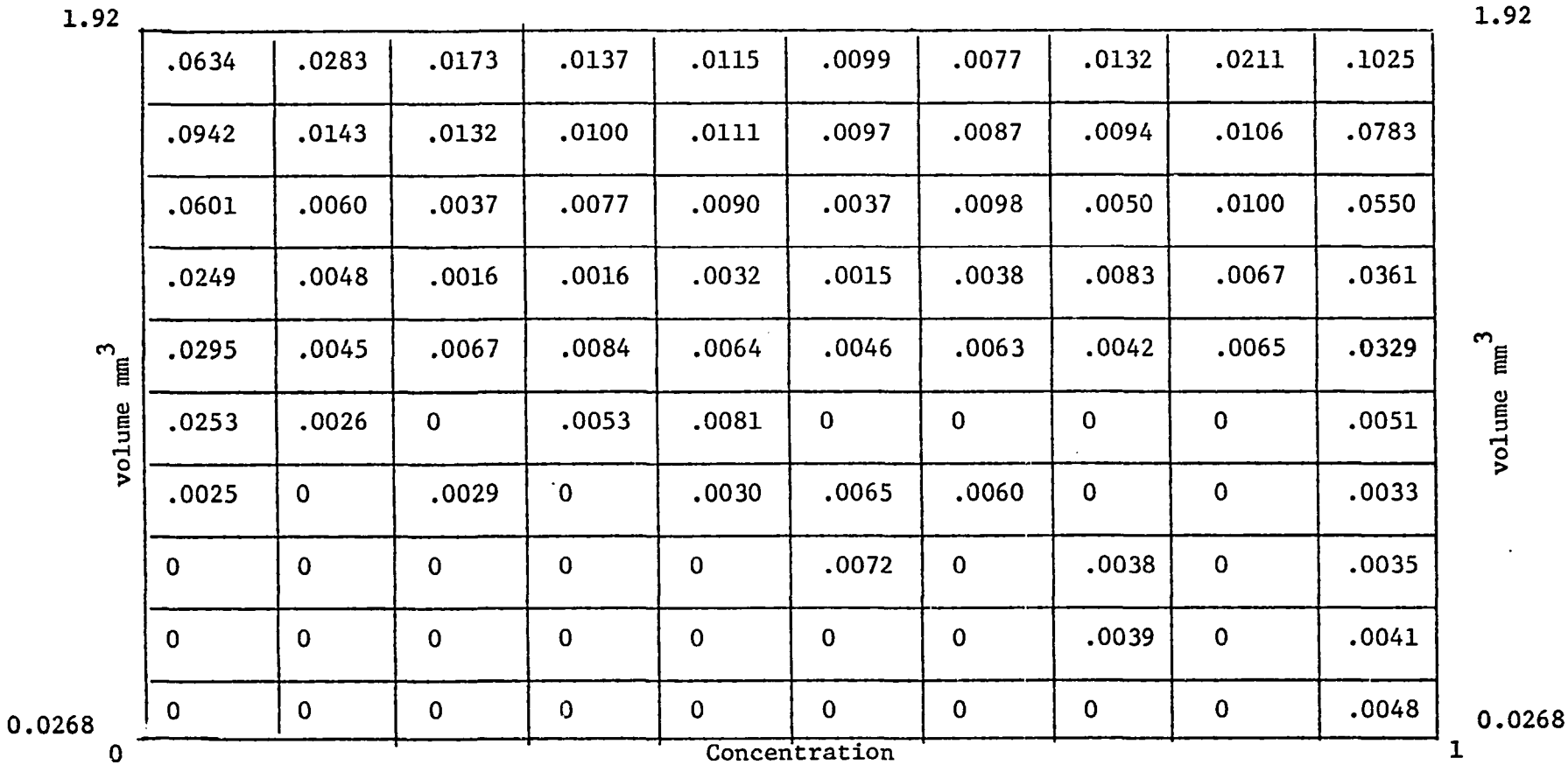

Figure 4.1 Volume Distribution in a Volume-Concentration Space; N = 174 rpm, θ = 0.10

Reproduced with permission of the copyright owner. Further reproduction prohibited without permission.

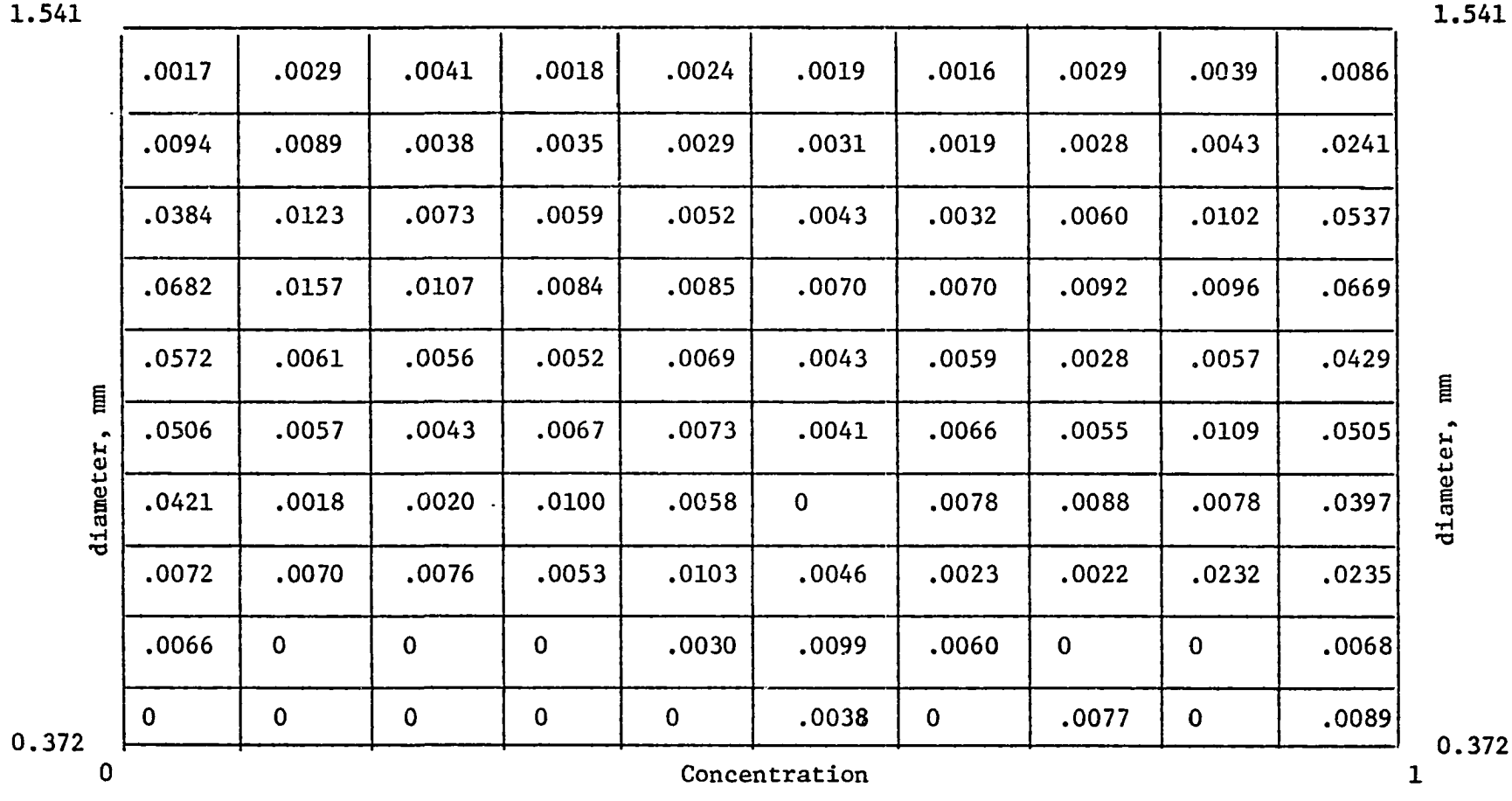

Figure 4.2 Volume Distribution in a Diameter-Concentration Space; N = 174 rpm, $\theta = 0.10$

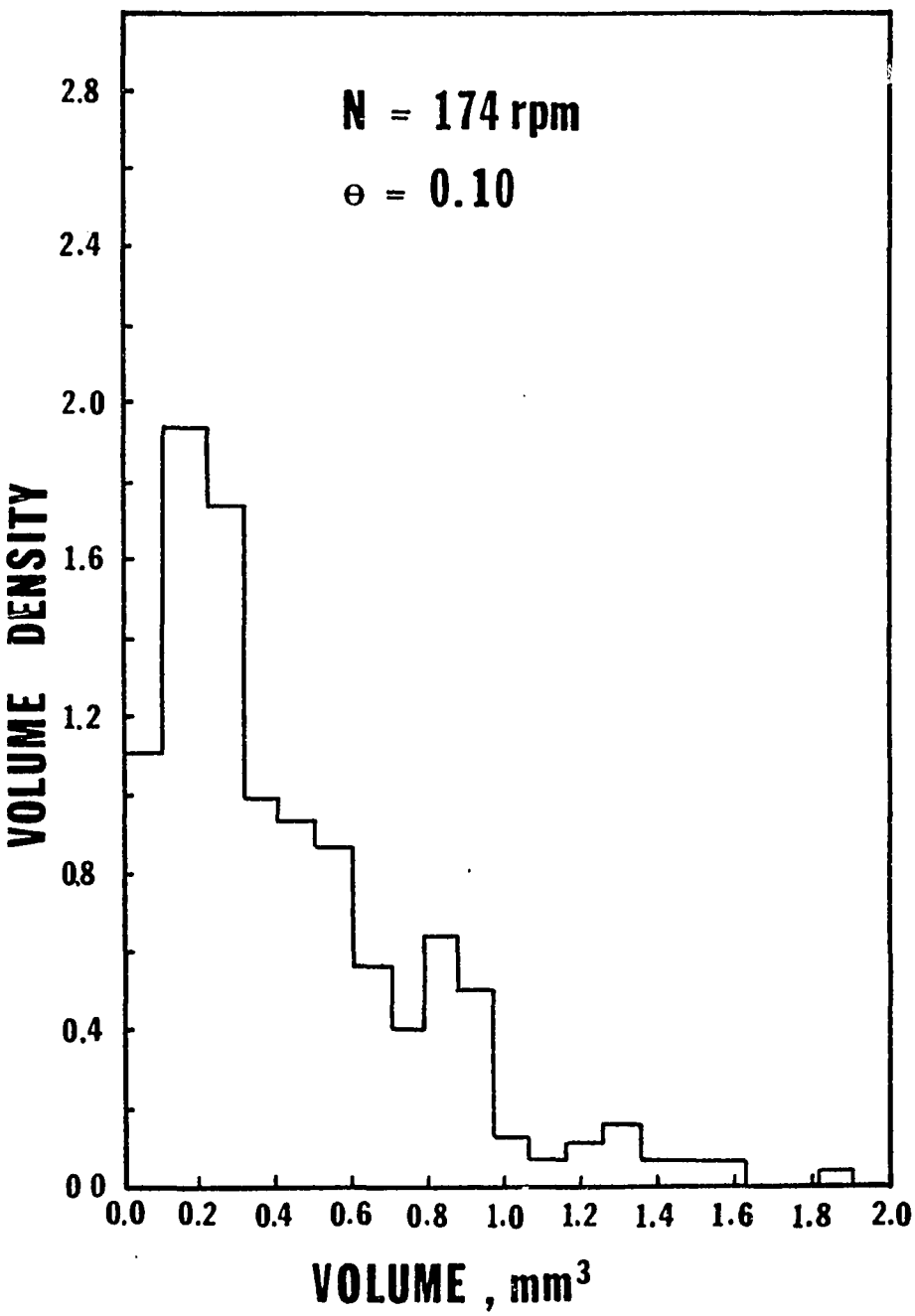

Fig. 4.3 Marginal Volume Distribution at N = 174 rpm, $\theta = 0.10$

Reproduced with permission of the copyright owner. Further reproduction prohibited without permission.

Reproduced with permission of the copyright owner. Further reproduction prohibited without permission.

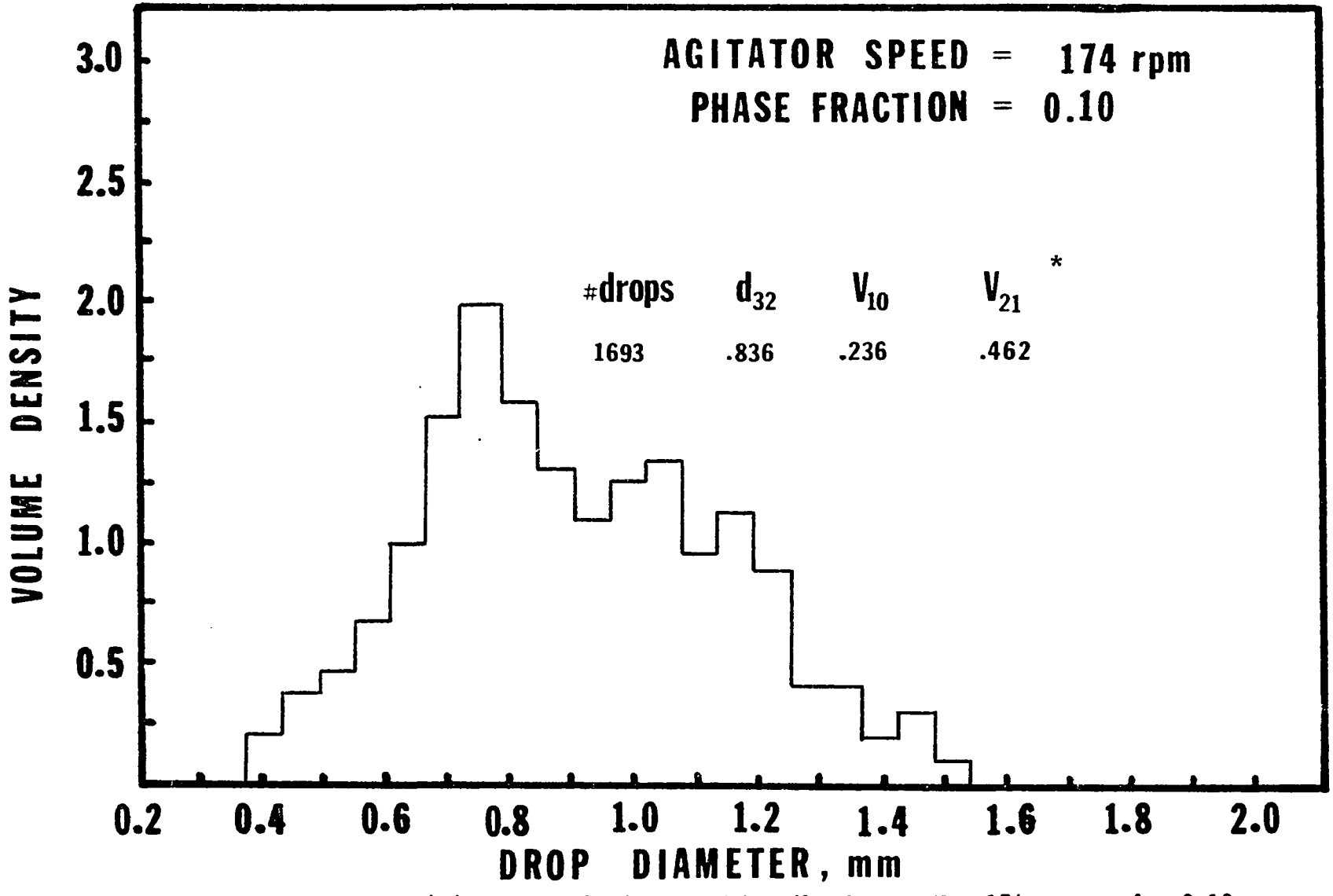

Fig. 4.4 Marginal Diameter Distribution at N = 174 rpm, θ = 0.10

*(the units here, and in all other figures are d_{32}: mm, v_{10}, v_{21}: mm^3)

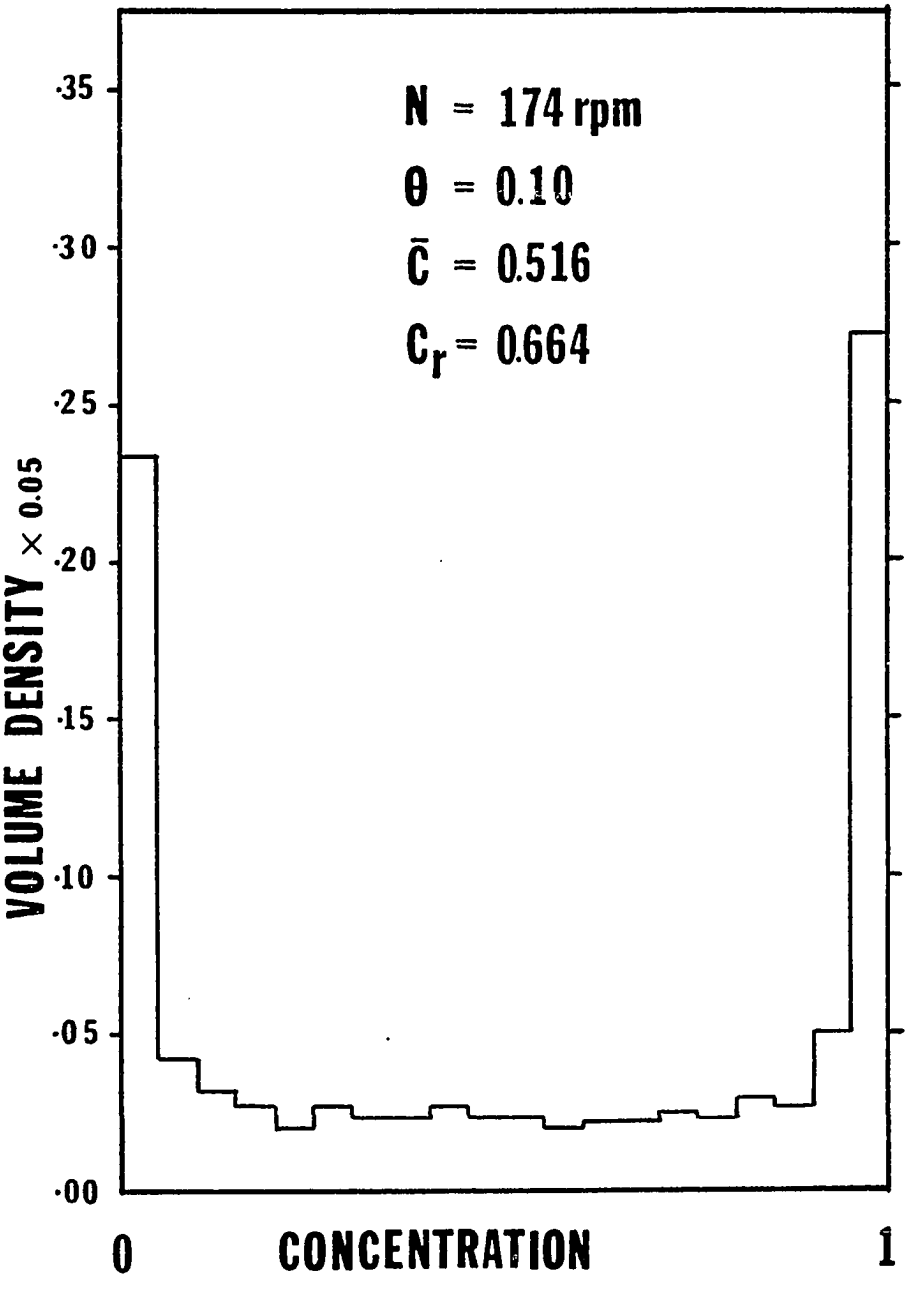

Fig. 4.5 Marginal Concentration Distribution at N = 174 rpm, θ = 0.10

Reproduced with permission of the copyright owner. Further reproduction prohibited without permission.

and $$C_i = \frac{C_i' - C_L}{C_H - C_L} \quad 4.2$$

for feed concentrations of C_L and C_H (thus the feed concentration are normalized and have values of 0 and 1.) It may be shown from Curl's theoretical work (11) for the case of the homogeneous equal-drop-size model that the coalescence frequency is related to this concentration variance ratio as:

$$C_r = \frac{1}{1 + \frac{1}{2}\omega T} \quad 4.3$$

where ω is the coalescence or mixing frequency and T = the residence time. Verhoff has shown that equation 4.3 can be used to approximately relate the concentration variance ratio to the mixing frequency in the range of mixing times studied. Since the drops in the mixing vessel are far from being of equal size, equation 4.3 must be considered an approximation only.

4.3 Scope of Experiments

The design of the equipment and the liquid properties are such that the experimental operation is only satisfactory in the agitator speed range of about 150-300 rpm. At higher speeds the drops in the vessel become too small to analyze accurately; at lower speeds the drops are relatively large and display a buoyant effect in the vessel.

Reproduced with permission of the copyright owner. Further reproduction prohibited without permission.

A total of 88 experiments was performed.* Unfortunately, many of the first experiments carried out had associated with them a wall-mixing effect and were not reproducible. It was found that one or two small clumps of dispersed phase always became attached to the baffles. These drops would be seen to grow in size, become unstable and break off. The cycle was repeated every minute or so. These baffle-drops had a remarkable effect on the resulting bivariate distribution. The results of these experiments are available but no attempt has been made, at this time, to analyze them thoroughly.

When the walls and baffles were thoroughly cleaned, these wall-effects were avoided and the experiments could be satisfactorily reproduced. The scope of these acceptable experiments is:

Agitator Speed: 160, 174, 185, 195, 210, 227, 278 rpm

Phase Fraction: 0.025, 0.05, 0.10, 0.20

Residence Time: 19.6 minutes

4.4 Reproducibility

The experimental results were found to be remarkably reproducible. The appealing aspect of the experimental technique is that it is just as easy to analyze 10,000 drops as it is 1000, except for the computer cost. It is felt that the good reproducibility is due to the large number of drops that were analyzed per experiment (1000-3000). The reliability and reproducibility of the results are considered as follows:

---

*The concentration and size of every drop of these experiments are available on computer cards. Appendix I discusses how to use these cards and the computer program to obtain the distributions and other statistics of each experiment.

Reproduced with permission of the copyright owner. Further reproduction prohibited without permission.

(a) Component Samples

As mentioned, a few samples of about 500 drops each were withdrawn from the vessel per experiment. The time between withdrawals was about 10 minutes. All the results shown in this study are based on a combination of these samples. Figures 4.6 and 4.7 however, describe the component samples withdrawn for two particular experiments. In figure 4.6 the four distributions and C_R values described are based on each of the four samples withdrawn (compare this with figure 4.14). Note that the distributions, the concentration variance values and the size statistics are very similar. The same can be said of the results shown in figure 4.7.

(b) Two Similar Experiments

Consider the two experiments that were carried out at an agitator speed of 210 rpm and a residence time of 19.6 minutes, with varying phase fraction. These experiments were performed about two months apart during which time parts of the sampling system were changed (mostly the analogue circuitry).* Figures 4.8 - 4.11 compare these two experiments. It is shown that the experiments yielded practically identical distributions including the slight bimodality which seems to appear in each curve.

(c) Comparison with Verhoff's Results

Verhoff carried out experiments at an agitator speed of 195 rpm and at various residence times. Figure 4.12 compares one such experiment with two similar experiments performed in this work. Note that the residence time and phase fraction are dissimilar.

*The results for the experiments carried out first are shown as solid curves in the figures.

Reproduced with permission of the copyright owner. Further reproduction prohibited without permission.

Reproduced with permission of the copyright owner. Further reproduction prohibited without permission.

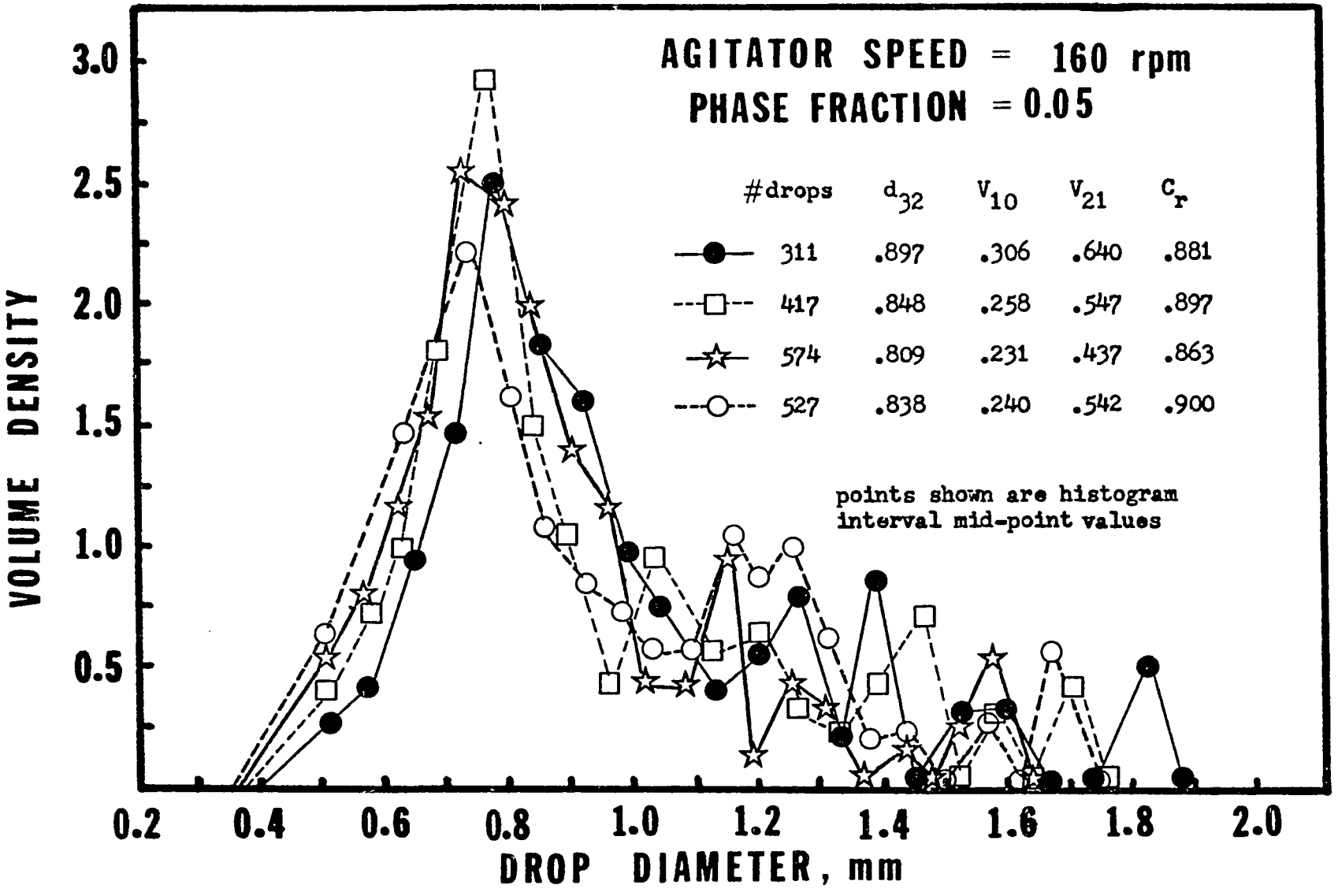

Fig. 4.6 Diameter Distributions of Component Samples at N = 160 rpm, θ = 0.05

Reproduced with permission of the copyright owner. Further reproduction prohibited without permission.

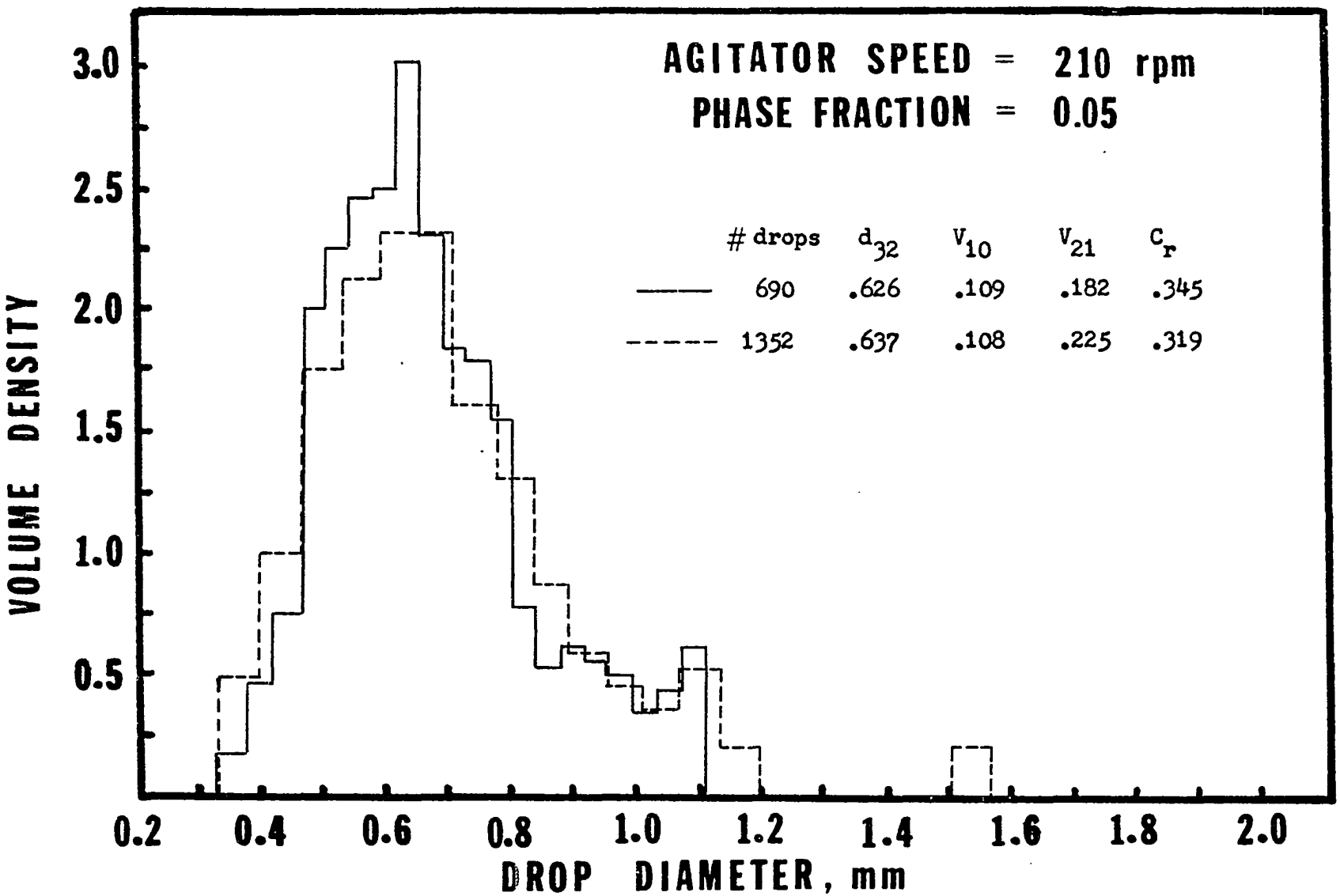

Fig. 4.7 Diameter Distributions of Component Samples at N = 210 rpm, θ = 0.05

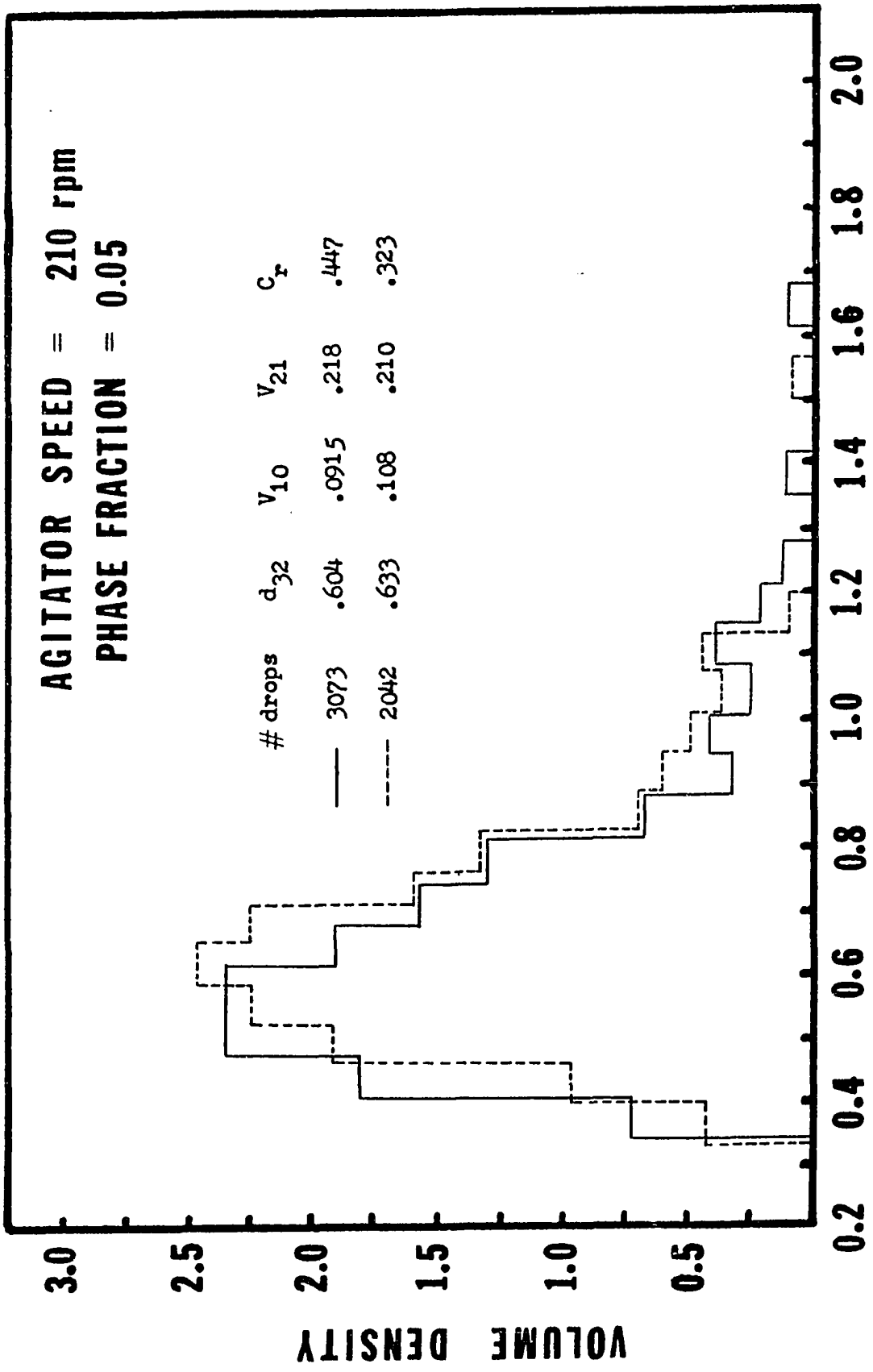

Fig. 4.8 Comparison of Two Experiments at N = 210 rpm, θ = 0.05

Reproduced with permission of the copyright owner. Further reproduction prohibited without permission.

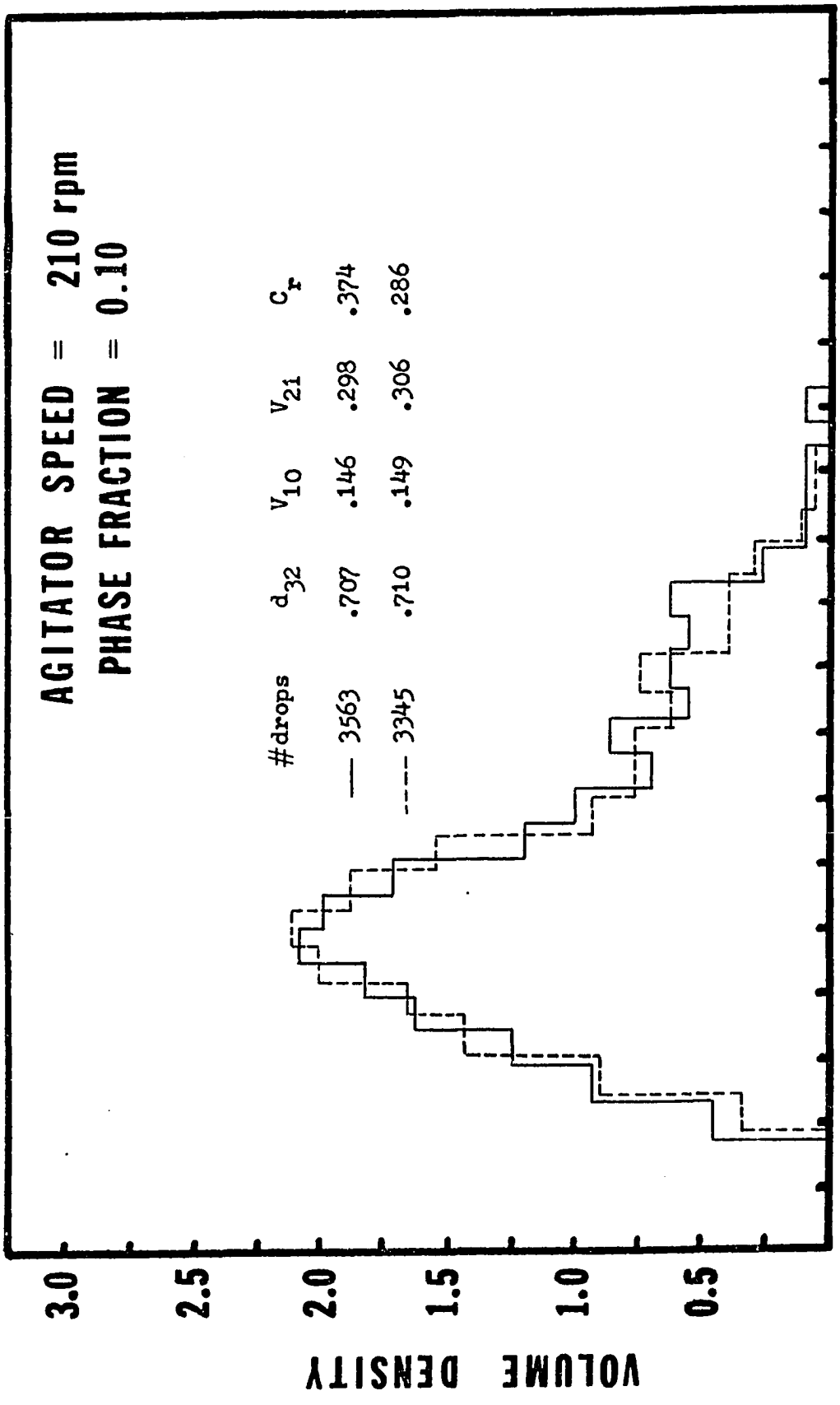

Fig. 4.9 Comparison of Two Experiments at N = 210 rpm, θ = 0.10

Reproduced with permission of the copyright owner. Further reproduction prohibited without permission.

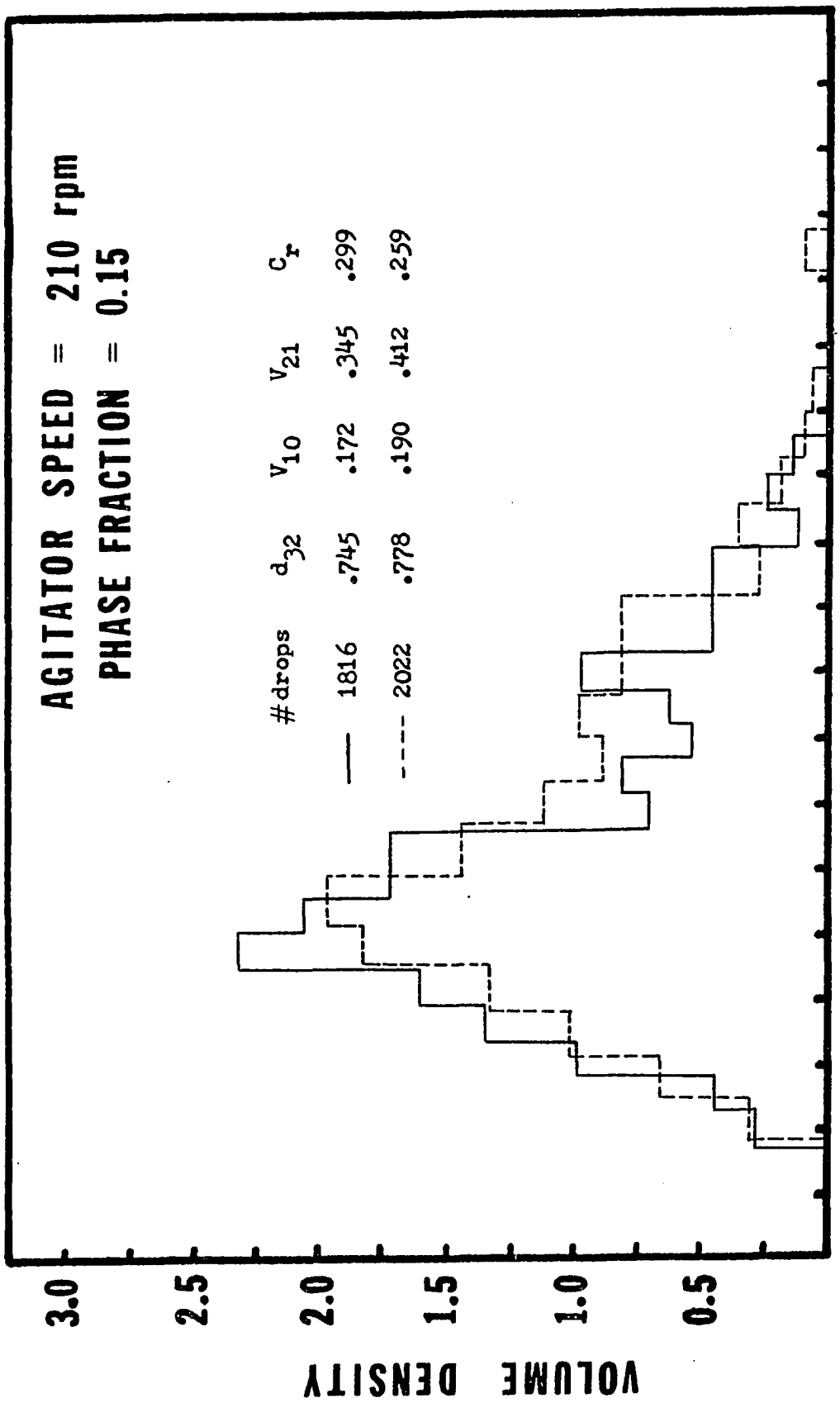

Fig. 4.10 Comparison of Two Experiments at N = 210 rpm, θ = 0.15

Reproduced with permission of the copyright owner. Further reproduction prohibited without permission.

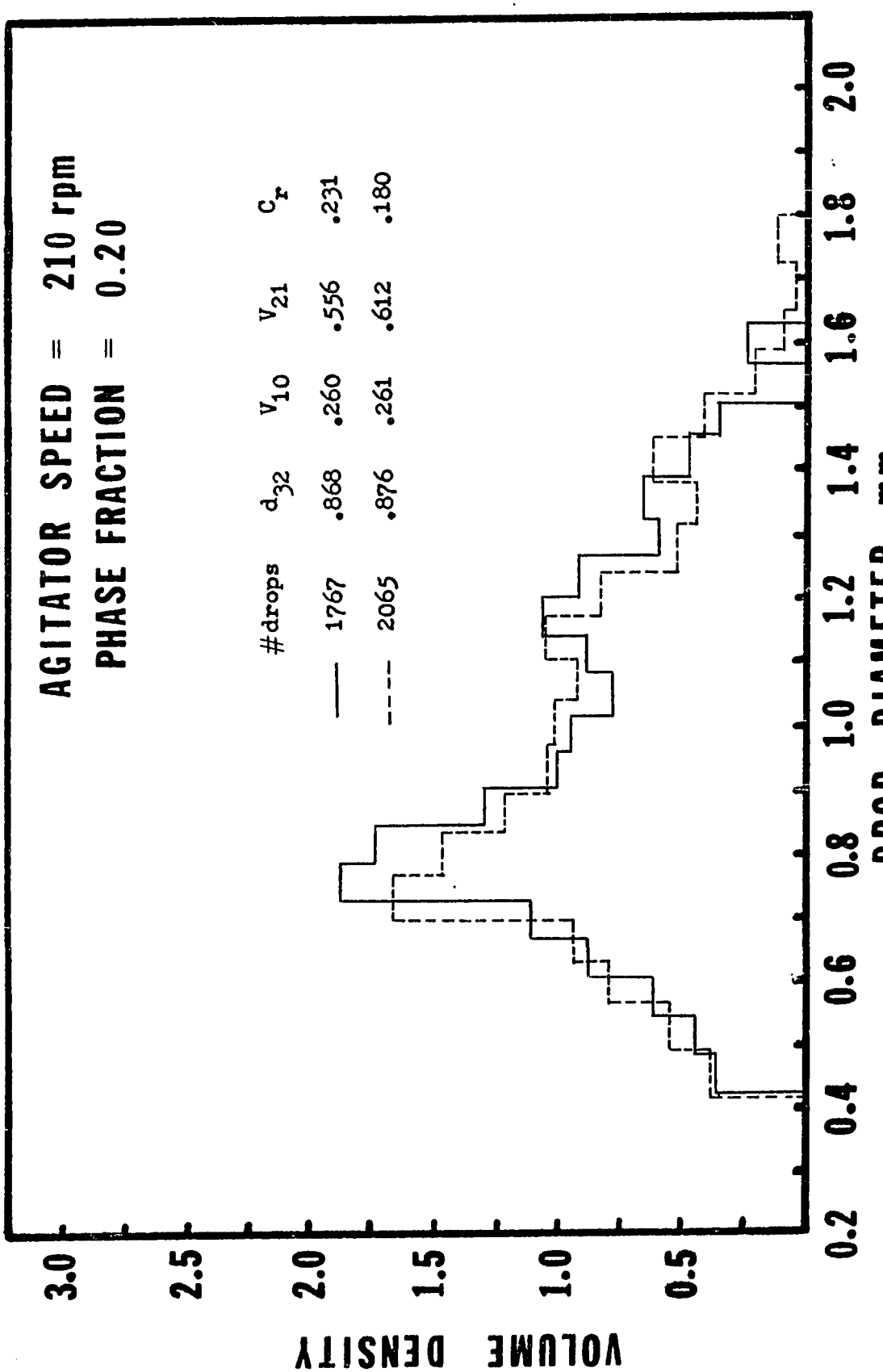

Fig. 4.11 Comparison of Two Experiments at N = 210 rpm, θ = 0.20

Reproduced with permission of the copyright owner. Further reproduction prohibited without permission.

Reproduced with permission of the copyright owner. Further reproduction prohibited without permission.

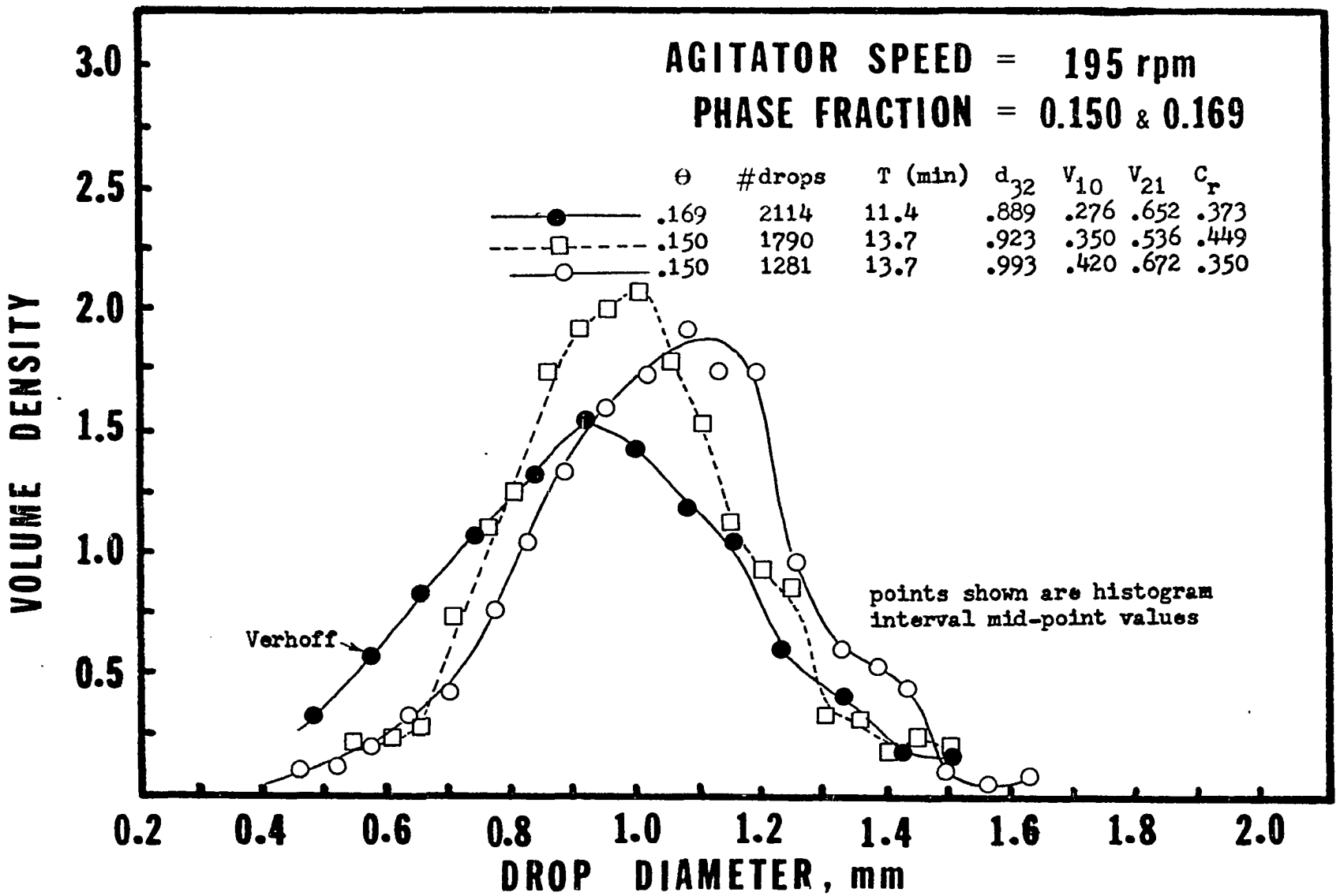

Fig. 4.12 Comparison with Verhoff's Results

Reproduced with permission of the copyright owner. Further reproduction prohibited without permission.

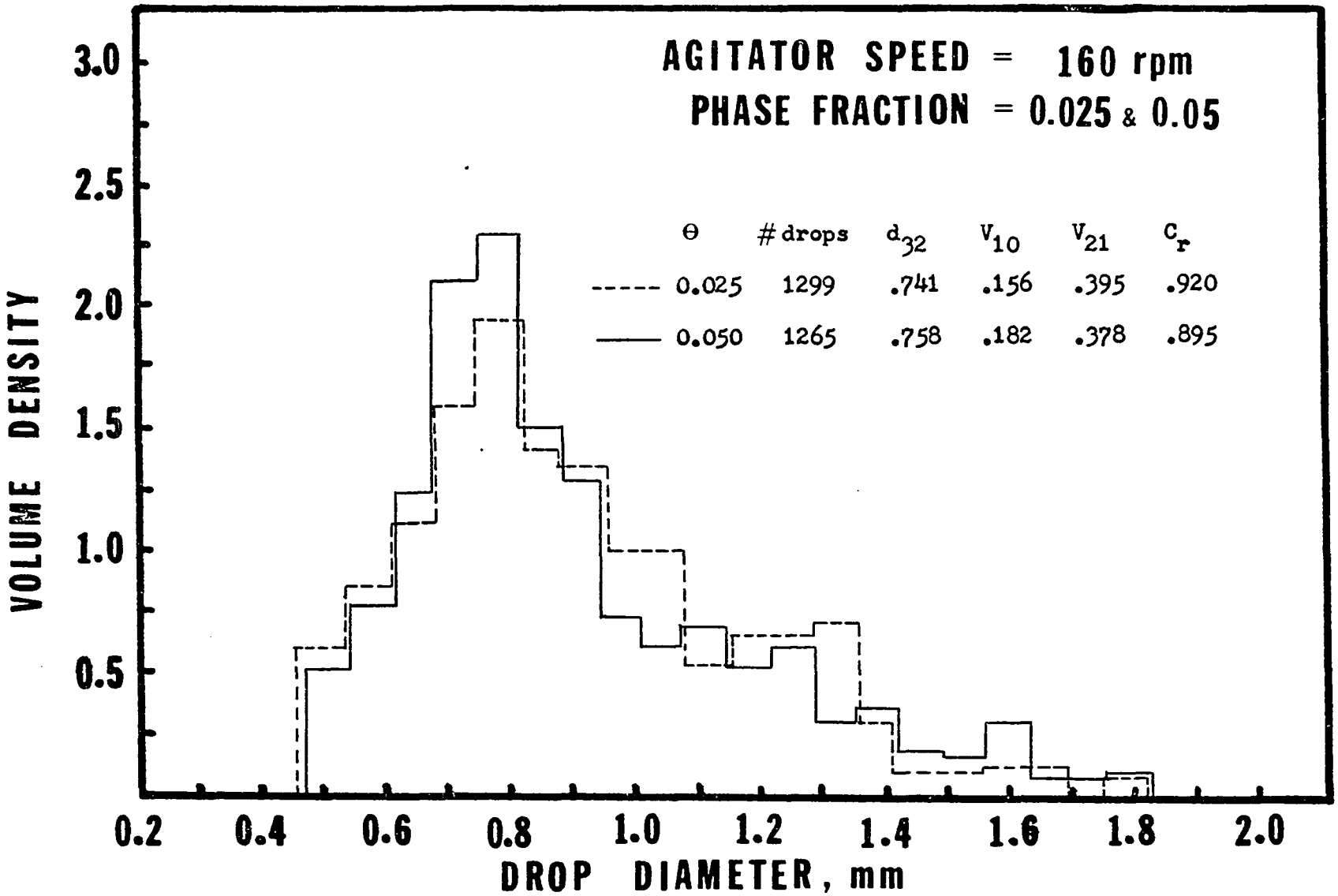

Fig. 4.13 Comparison of Two Experiments with Low Mixing Rates. N = 160 rpm, θ = 0.025 and 0.050

Notwithstanding this, and the fact that the equipment has been modified, the comparison can be considered good.

(d) Two Experiments with Low Mixing Rates

At low phase fraction and low mixing rates the bivariate distributions should be independent of phase fraction because the breakage mechanism predominates. Two such experiments that were performed at an agitator speed of 160 rpm and phase fraction of 0.025 and 0.05 are compared in figure 4.13. Again the comparison is favorable.

(e) Average Concentration

The experimentally determined average concentration, $\bar{C}$, of the feed normalized at 0 (low concentration) and 1 (high concentration, see equation 4.2) is measured to be 0. 525 - 0. 530. All average concentration (except one) calculated on the basis of the drops in the vessel samples were independently calculated to be within 5% of this value. Precisely, $\bar{C} = 0.528 \pm .017$ at 95% confidence.

4.5 Matrix of Results

Some of the results in the form of marginal size and concentration distributions are shown in figures 4.14 to 4.33. A general comparison of all the experiments is given in figures 4.34 - 4.36, and Table 4.1 based on Sauter-mean diameters and C_R values. The average input drop sizes for a residence time of 19.6 minutes were measured and found to be in the range of 4.5 to 7.5 mm^3 depending on

Reproduced with permission of the copyright owner. Further reproduction prohibited without permission.

Reproduced with permission of the copyright owner. Further reproduction prohibited without permission.

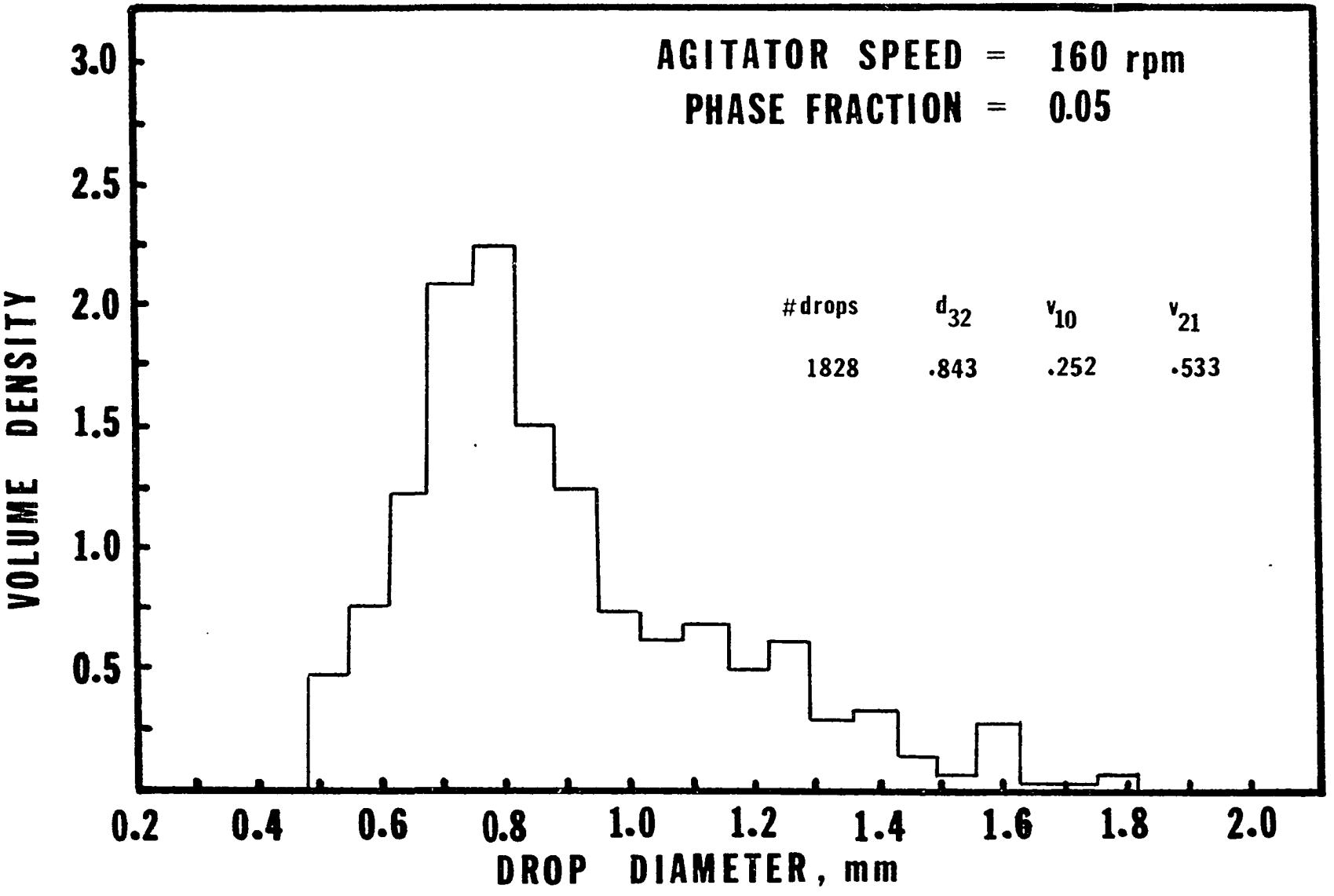

Fig. 4.14 Marginal Diameter Distribution at N = 160 rpm, θ = 0.05

Reproduced with permission of the copyright owner. Further reproduction prohibited without permission.

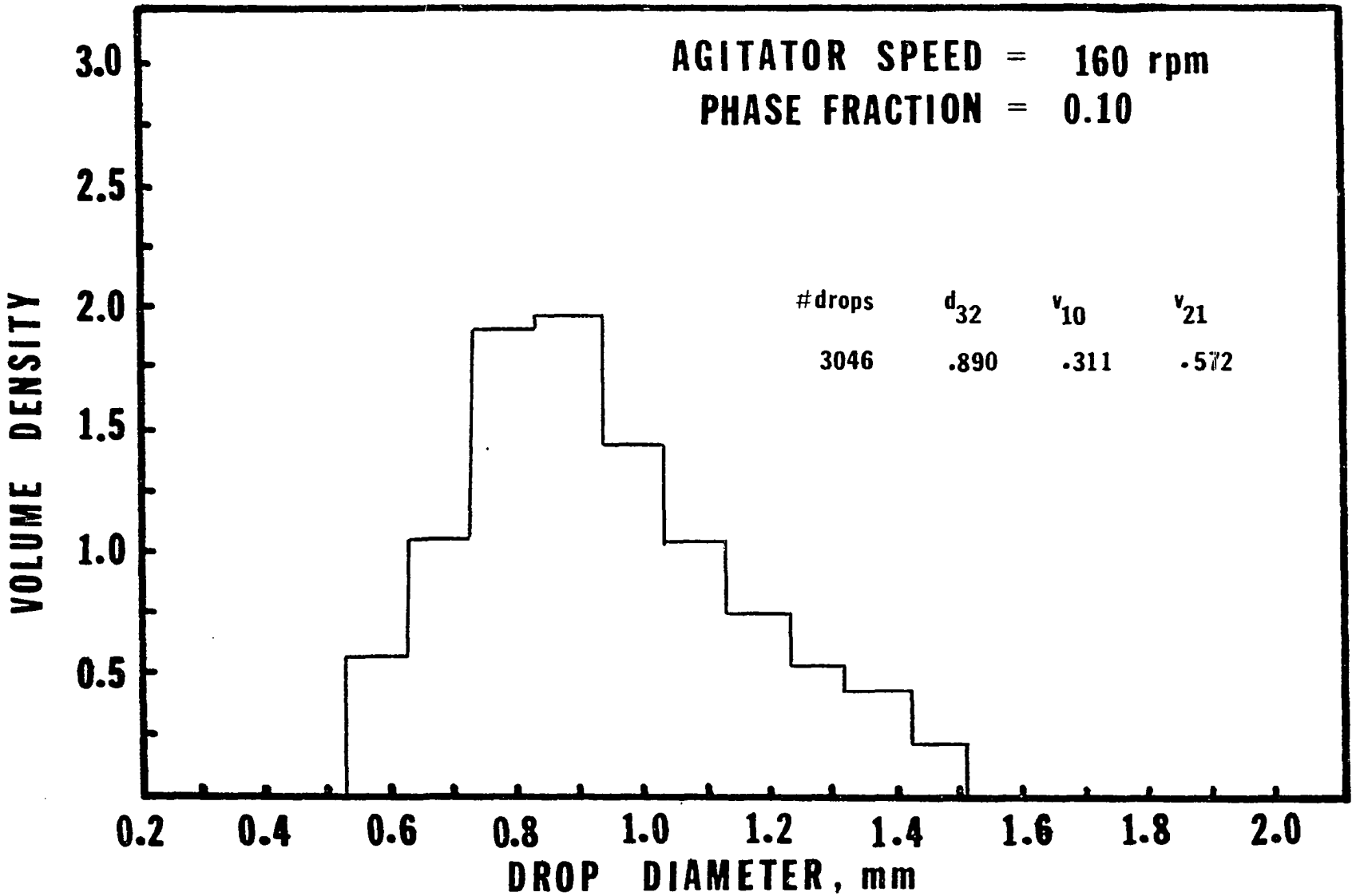

Fig. 4.15 Marginal Diameter Distribution at N = 160 rpm, θ = 0.10

Reproduced with permission of the copyright owner. Further reproduction prohibited without permission.

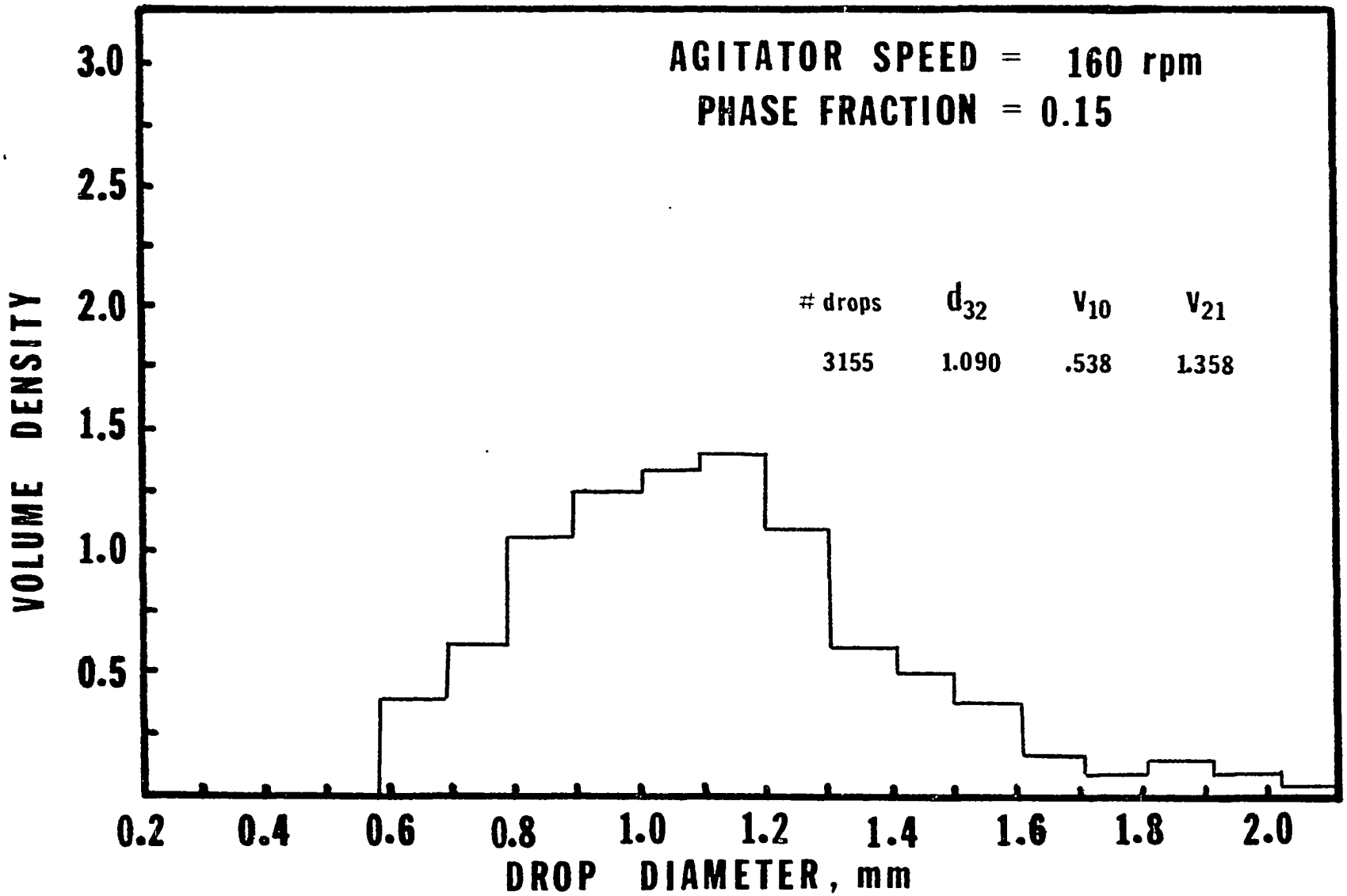

Fig. 4.16 Marginal Diameter Distribution at N = 160 rpm, θ = 0.15

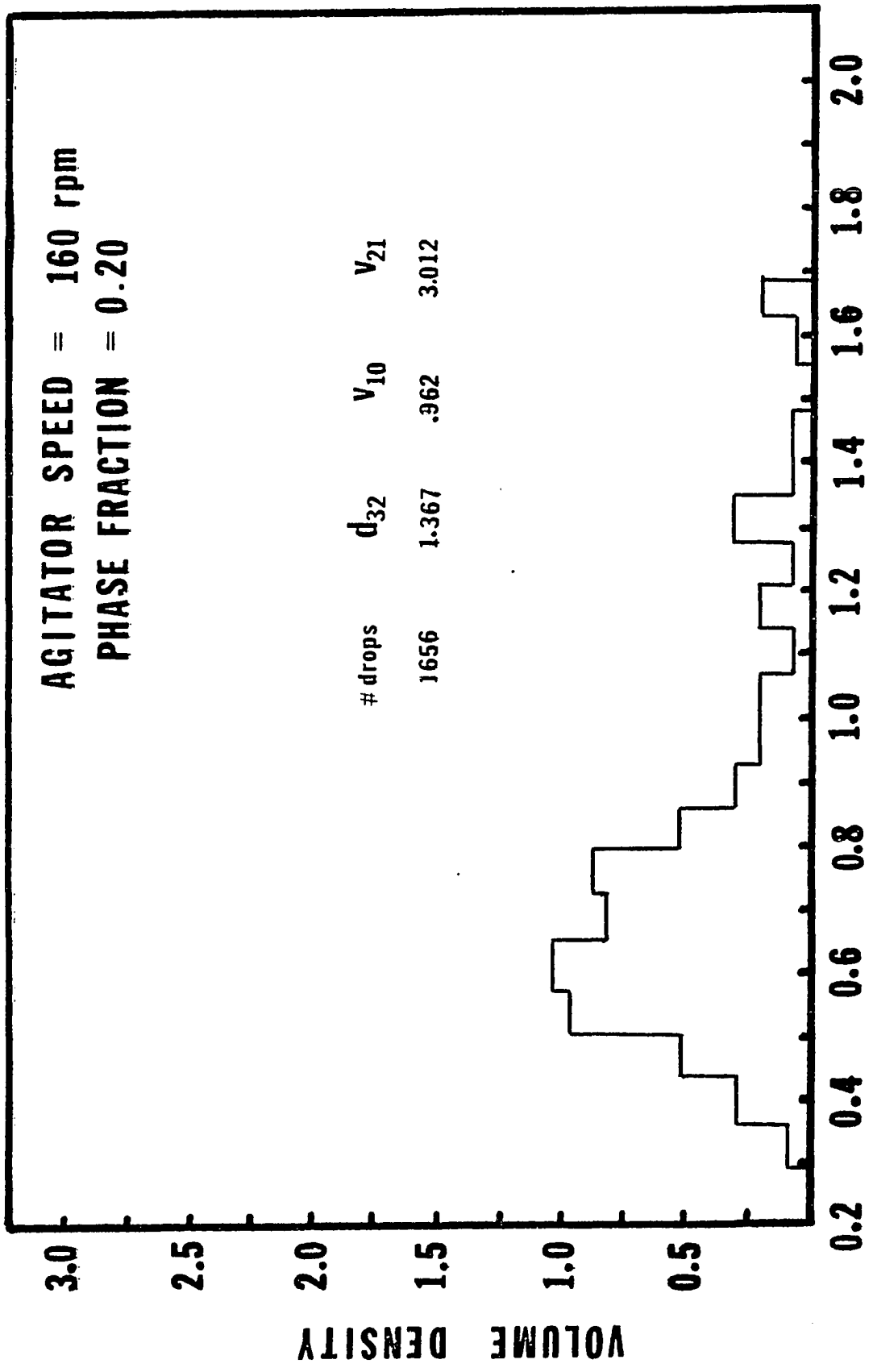

Fig. 4.17 Marginal Diameter Distribution at N = 160 rpm, θ = 0.20

Reproduced with permission of the copyright owner. Further reproduction prohibited without permission.

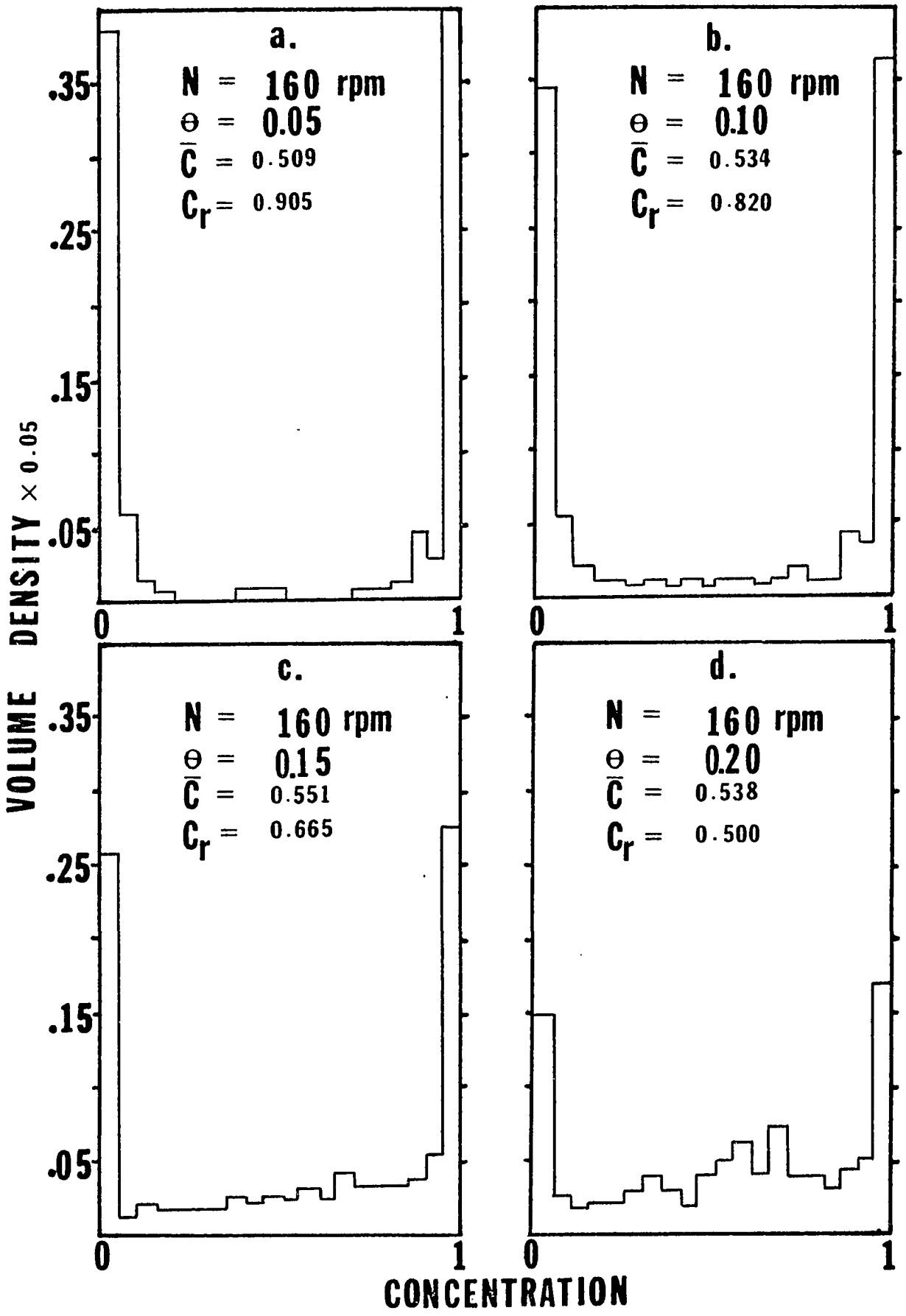

Fig. 4.18 Marginal Concentration Distributions at N = 160 rpm

Reproduced with permission of the copyright owner. Further reproduction prohibited without permission.

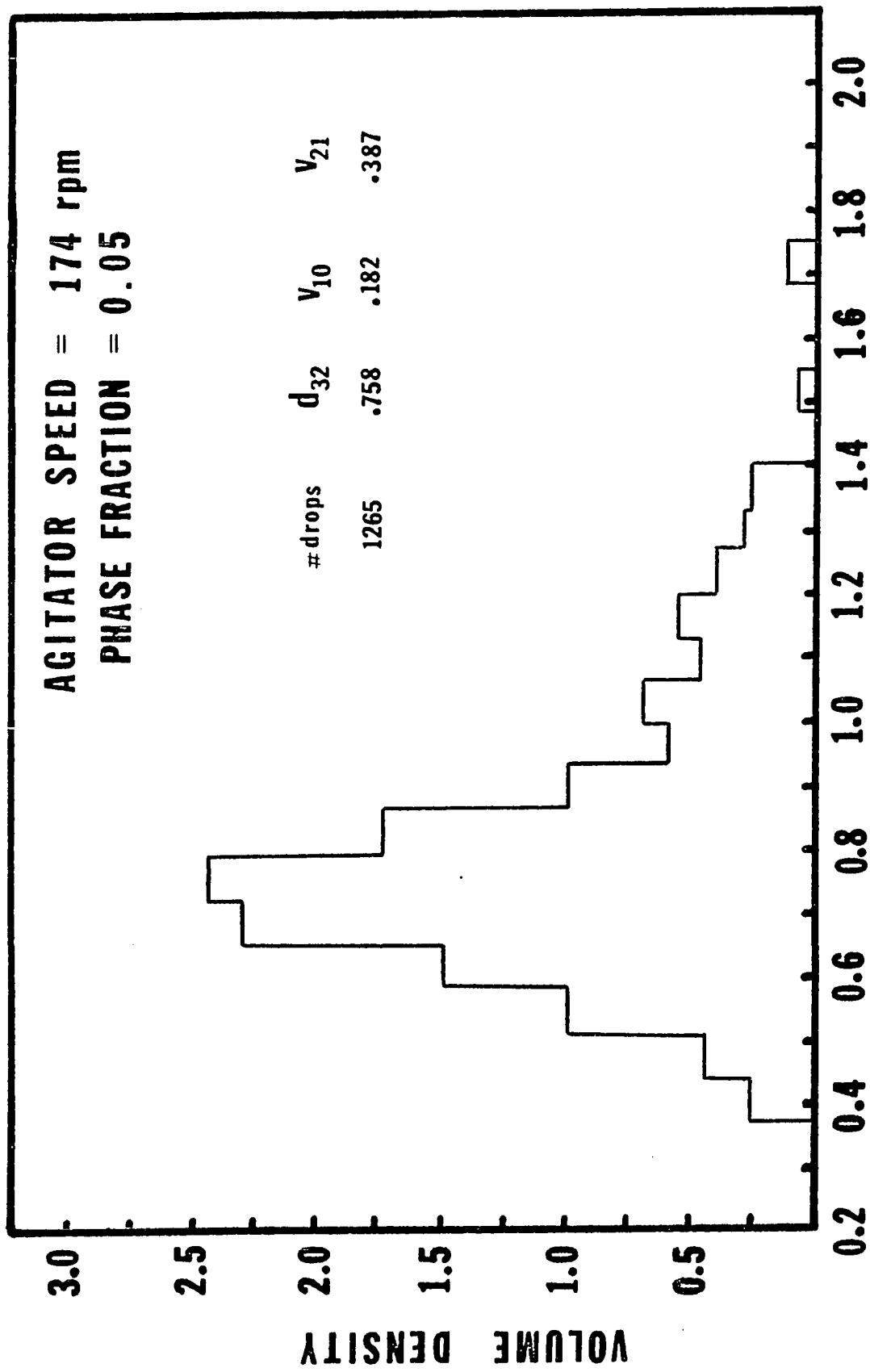

Fig. 4.19 Marginal Diameter Distribution at N = 174 rpm, θ = 0.05

Reproduced with permission of the copyright owner. Further reproduction prohibited without permission.

Reproduced with permission of the copyright owner. Further reproduction prohibited without permission.

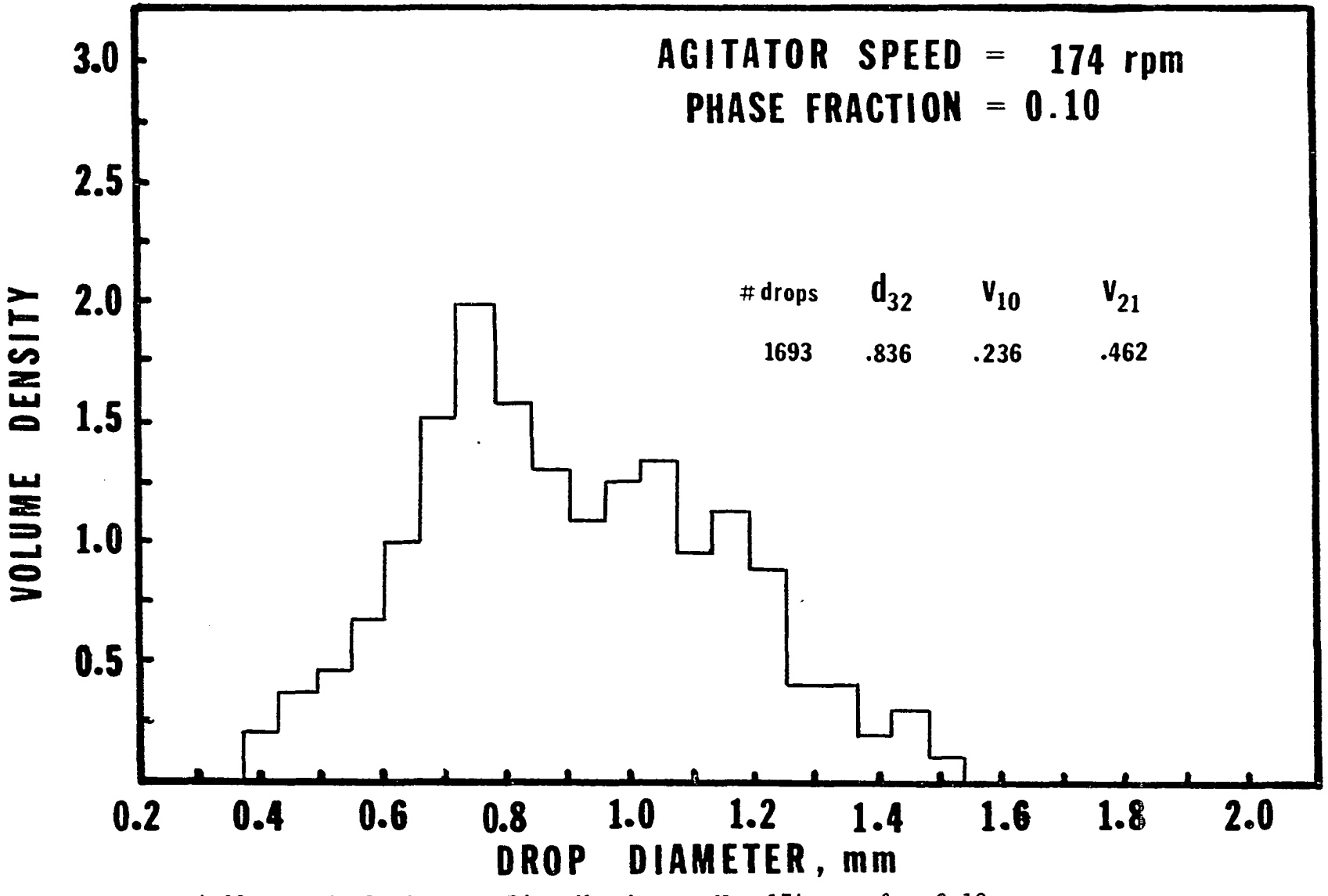

Fig. 4.20 Marginal Diameter Distribution at N = 174 rpm, θ = 0.10

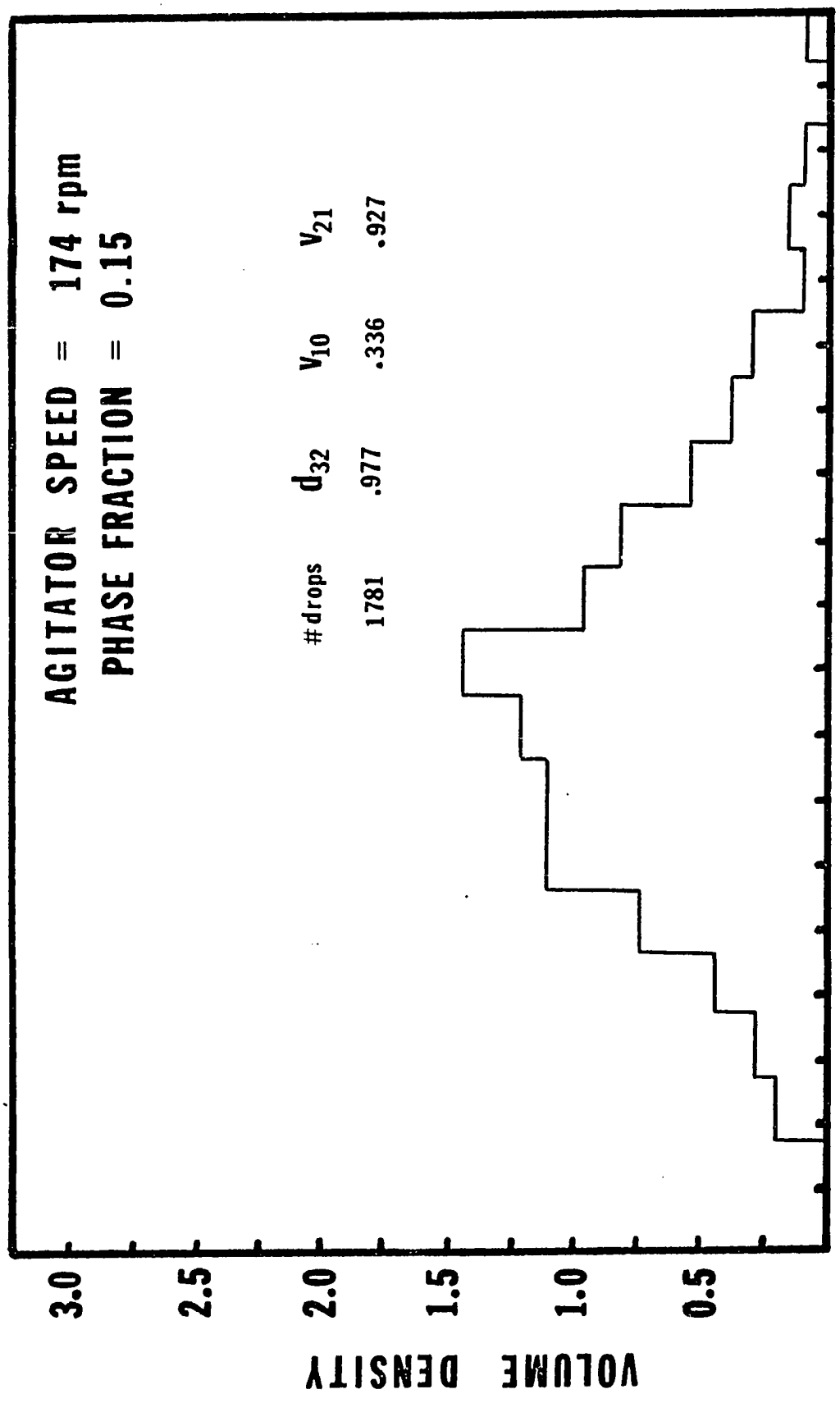

Fig. 4.21 Marginal Diameter Distribution at N = 174 rpm, θ = 0.15

Reproduced with permission of the copyright owner. Further reproduction prohibited without permission.

Reproduced with permission of the copyright owner. Further reproduction prohibited without permission.

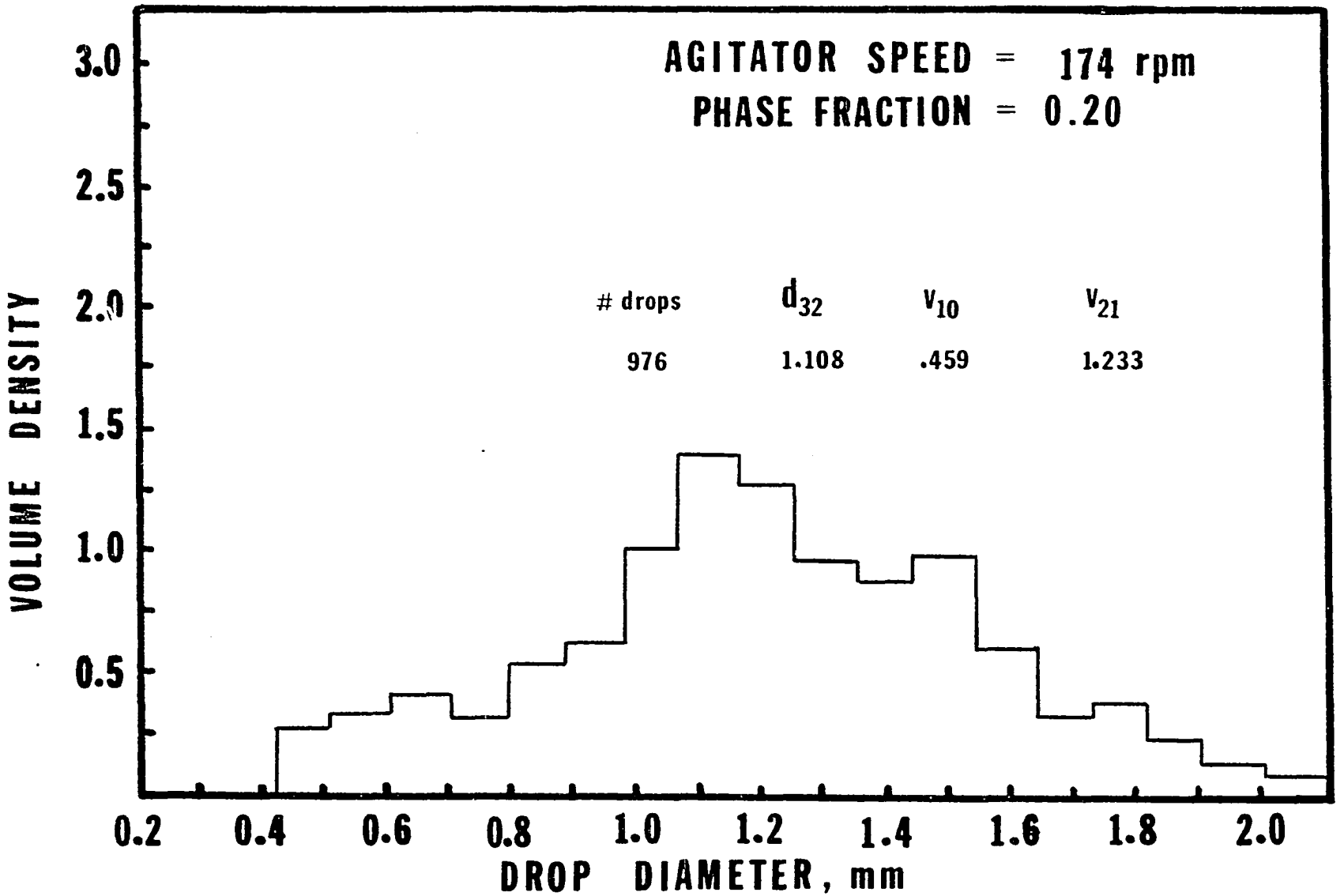

Fig. 4.22 Marginal Diameter Distribution at N = 174 rpm, θ = 0.20

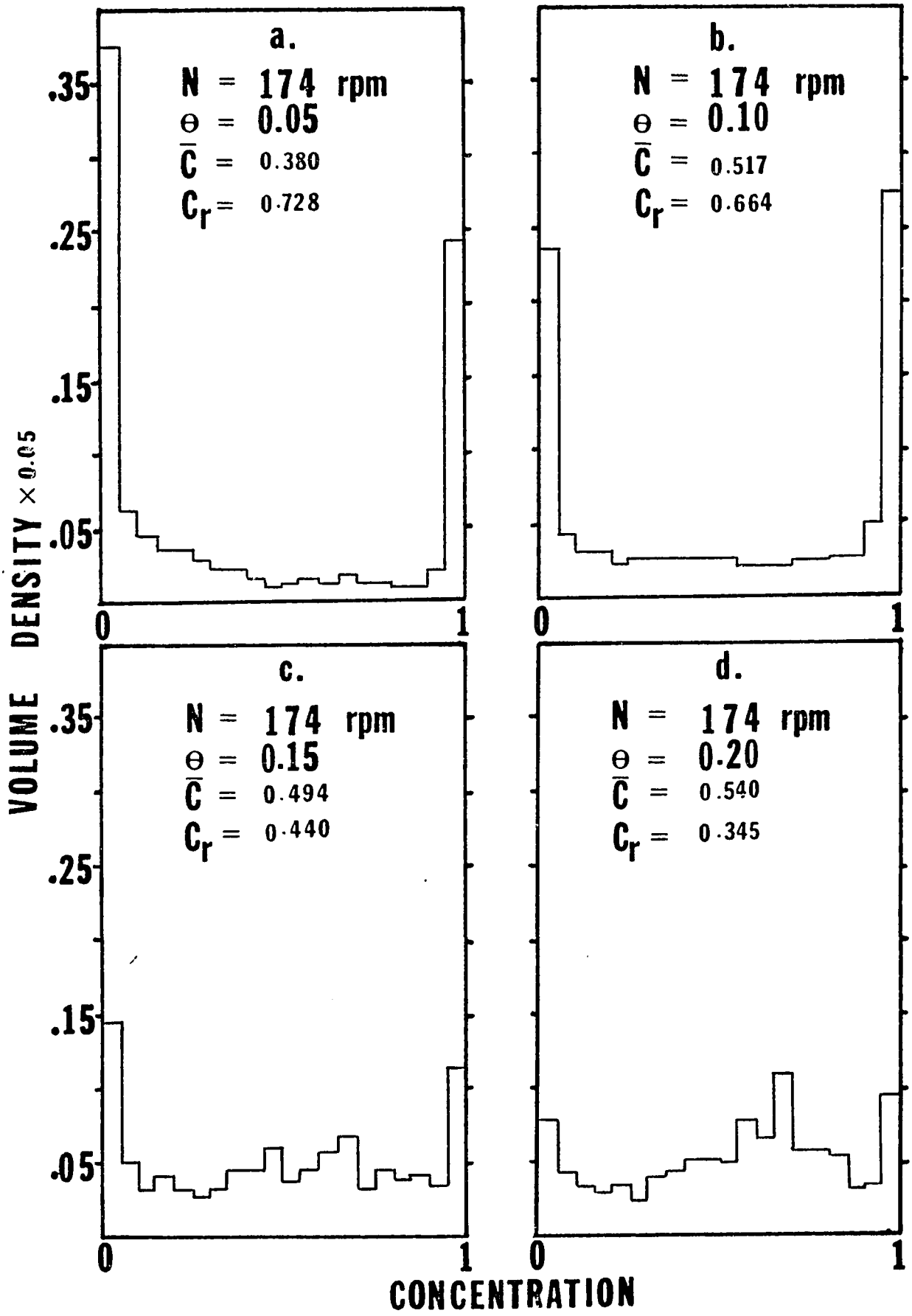

Fig. 4.23 Marginal Concentration Distributions at N = 174 rpm

Reproduced with permission of the copyright owner. Further reproduction prohibited without permission.

Reproduced with permission of the copyright owner. Further reproduction prohibited without permission.

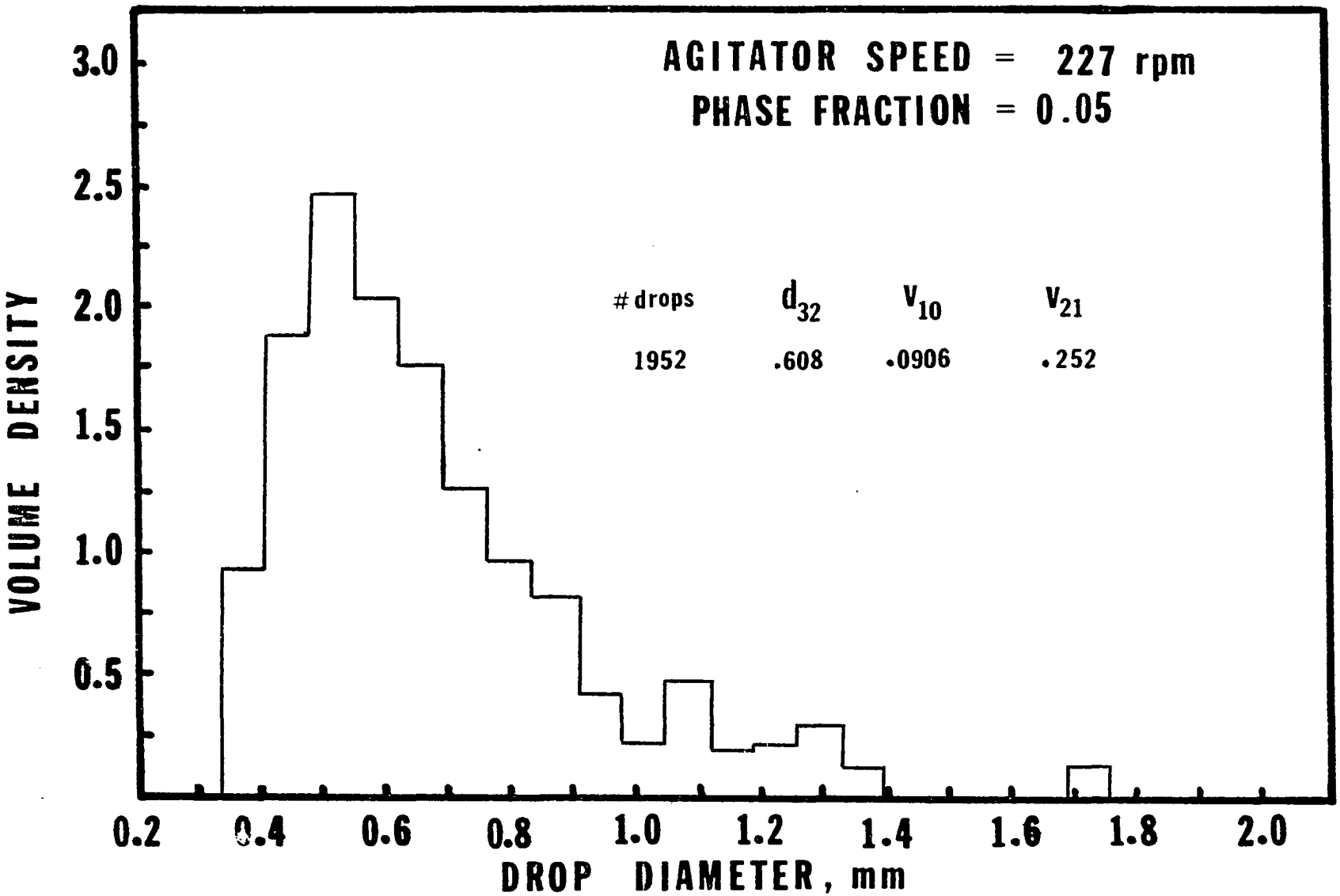

Fig. 4.24 Marginal Diameter Distribution at N = 227 rpm, θ = 0.05

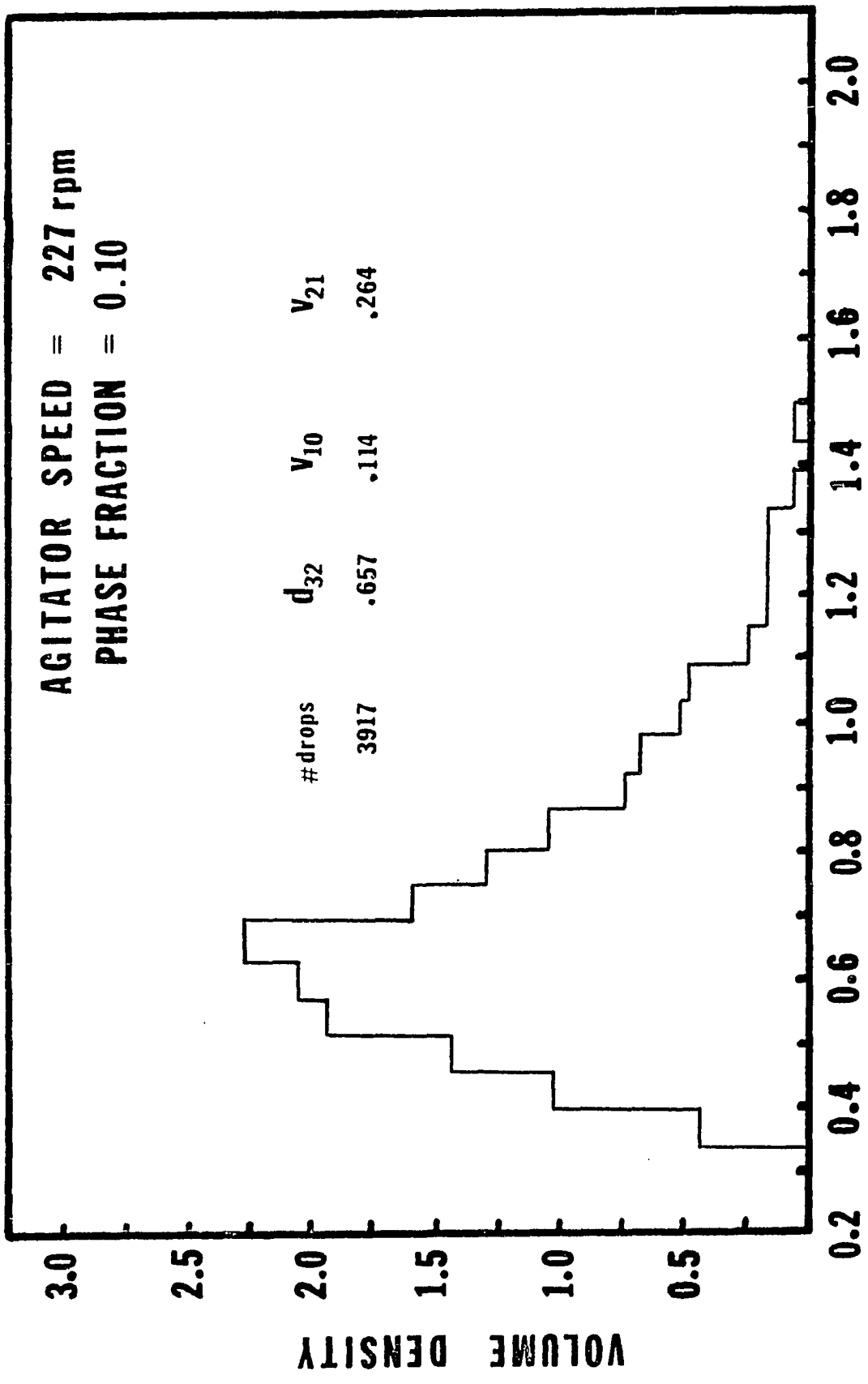

Fig. 4.25 Marginal Diameter Distribution at N = 227, θ = 0.10

Reproduced with permission of the copyright owner. Further reproduction prohibited without permission.

Reproduced with permission of the copyright owner. Further reproduction prohibited without permission.

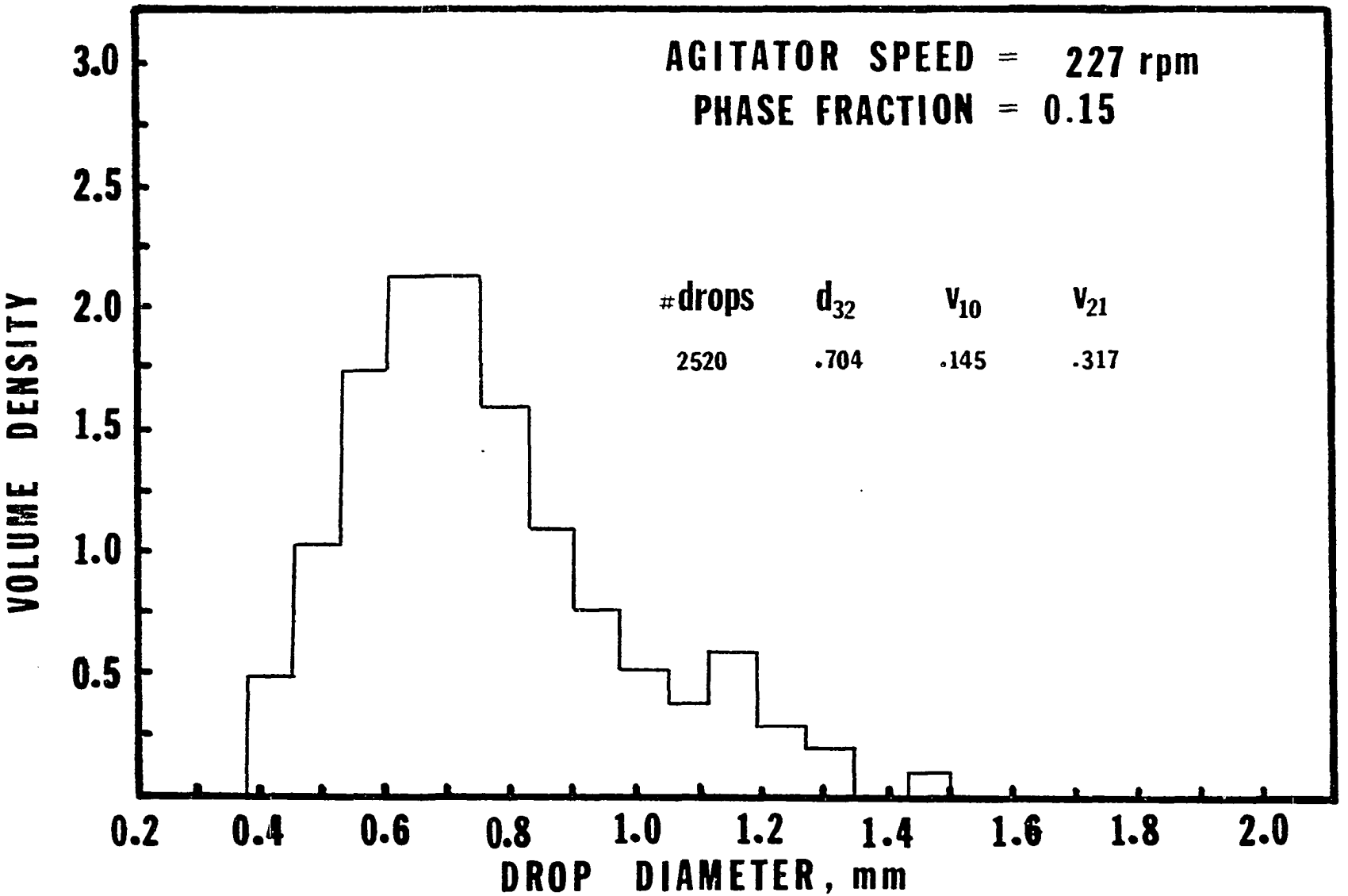

Fig. 4.26 Marginal Diameter Distribution at N = 227 rpm, θ = 0.15

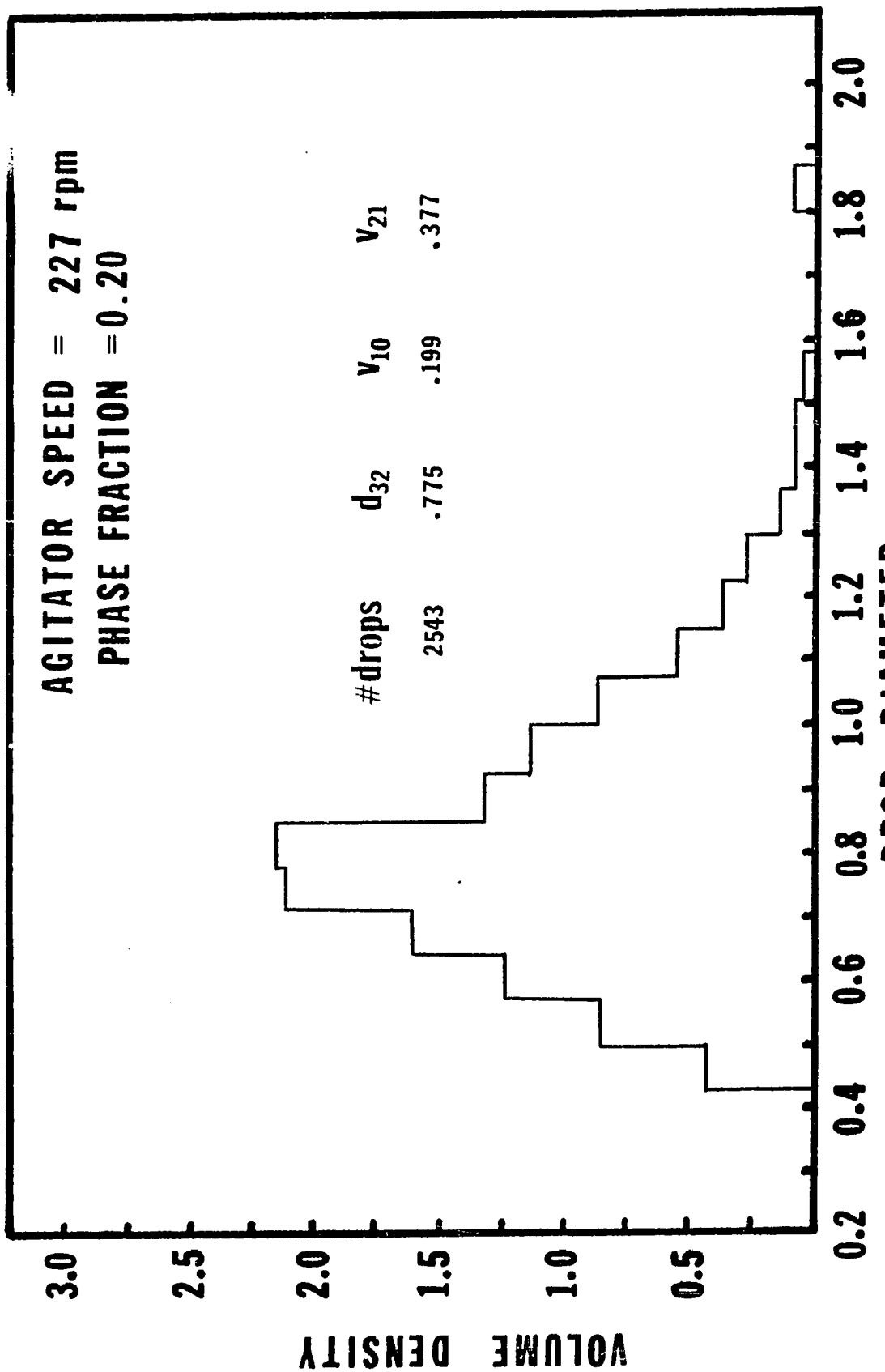

Fig. 4.27 Marginal Diameter Distribution at N = 227 rpm, θ = 0.20

Reproduced with permission of the copyright owner. Further reproduction prohibited without permission.

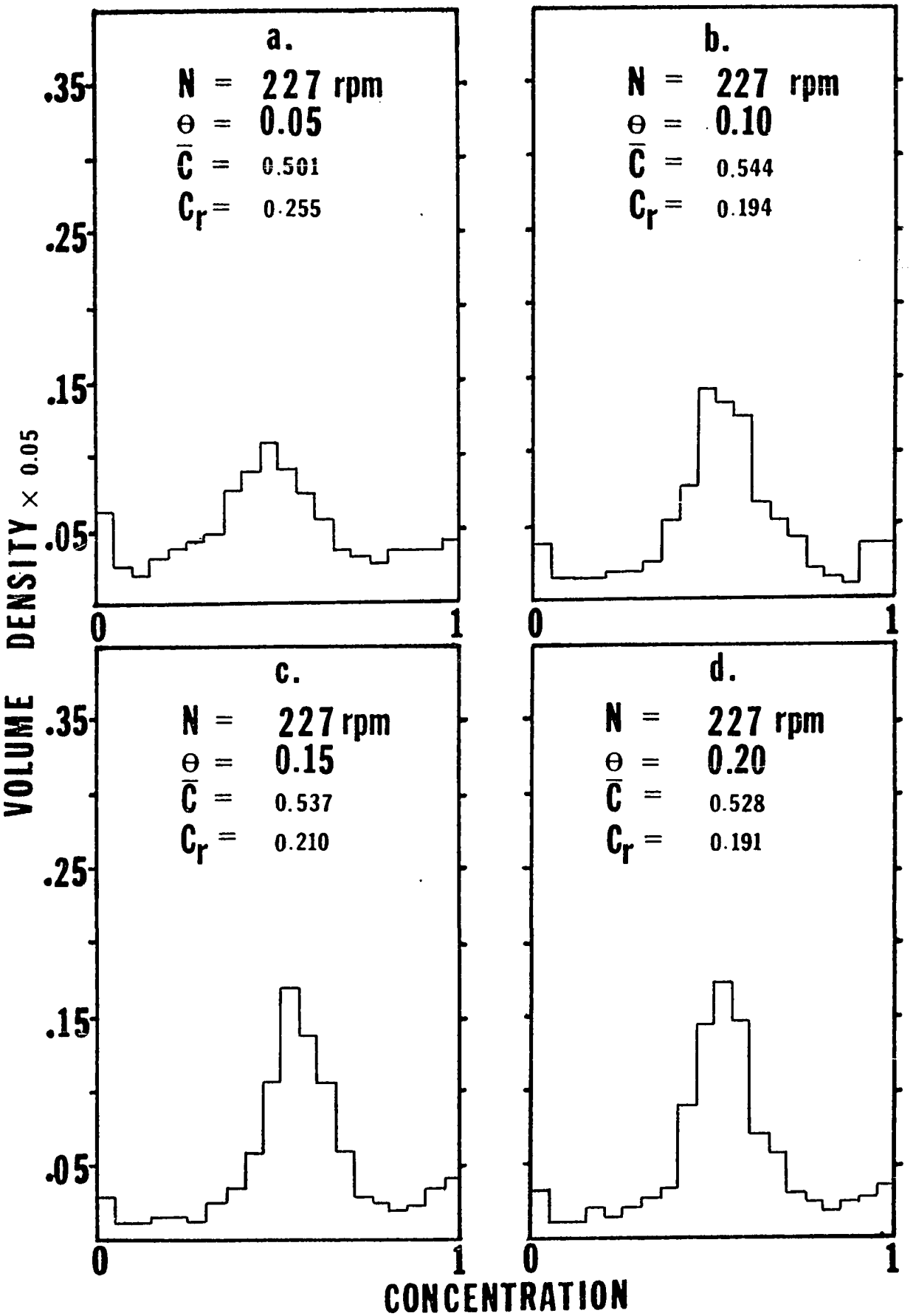

Fig. 4.28 Marginal Concentration Distributions at N = 227 rpm

Reproduced with permission of the copyright owner. Further reproduction prohibited without permission.

Reproduced with permission of the copyright owner. Further reproduction prohibited without permission.

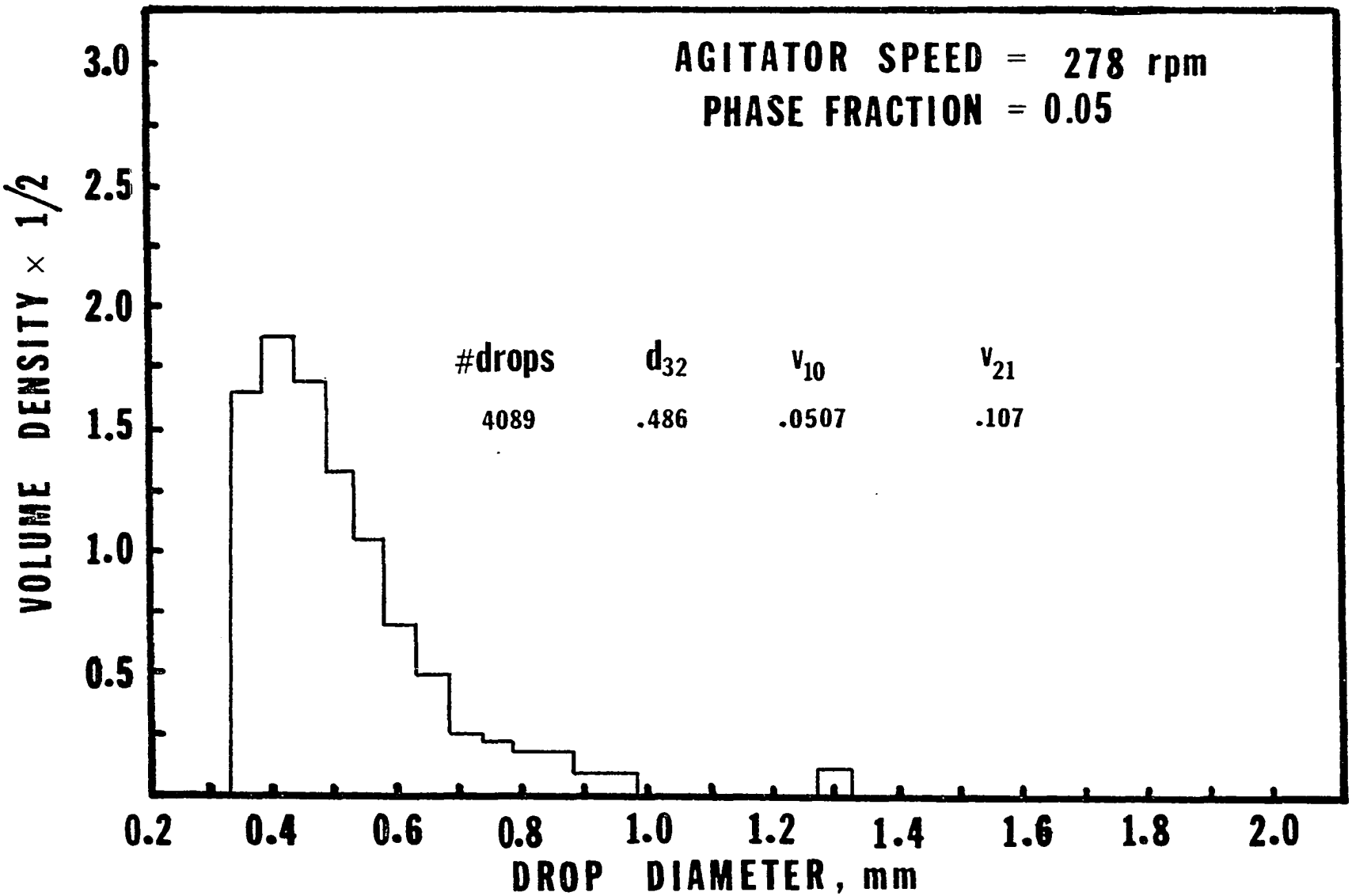

Fig. 4.29 Marginal Diameter Distribution at N = 278 rpm, θ = 0.05

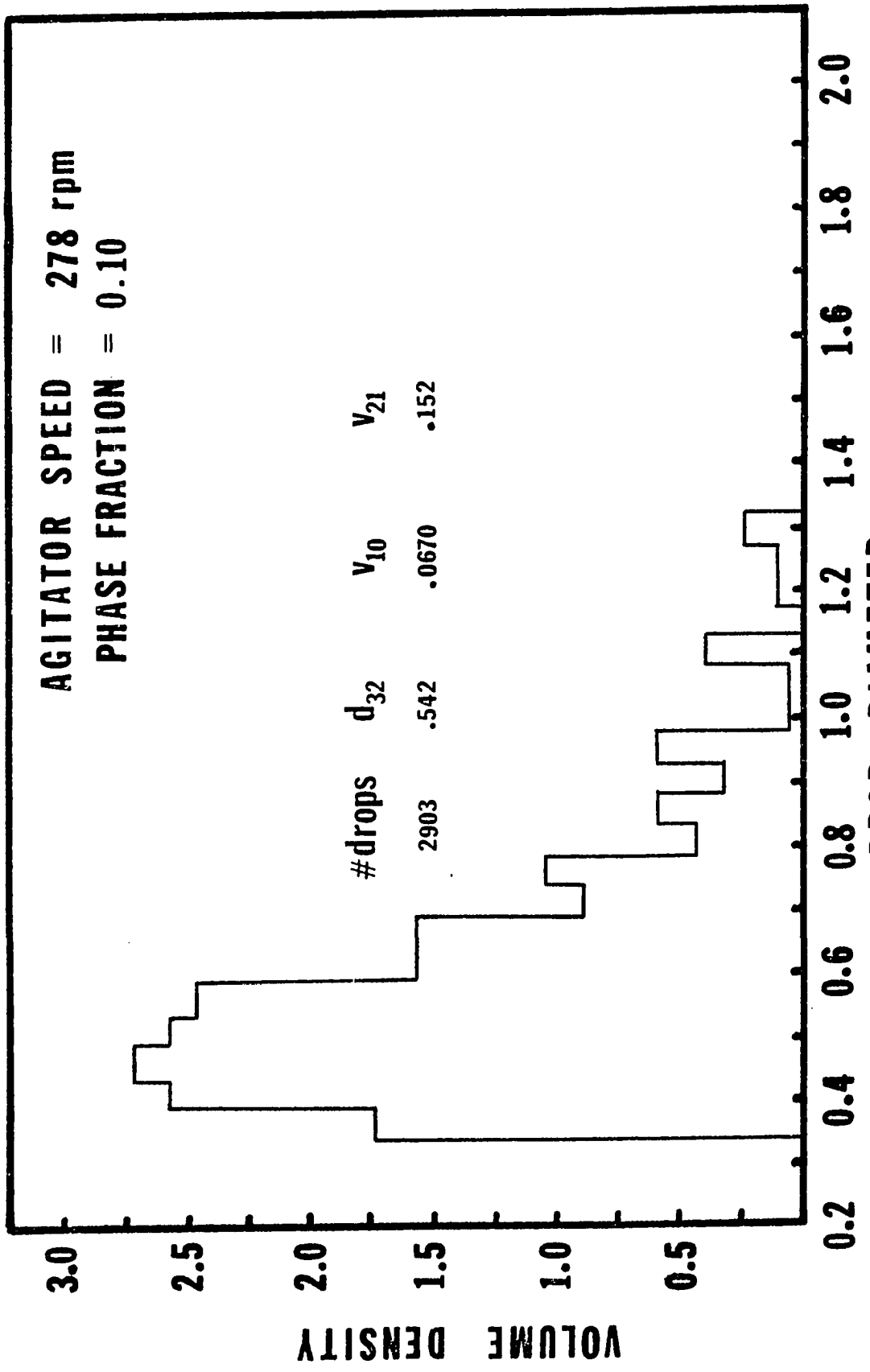

Fig. 4.30 Marginal Diameter Distribution at N = 278 rpm, θ = 0.10

Reproduced with permission of the copyright owner. Further reproduction prohibited without permission.

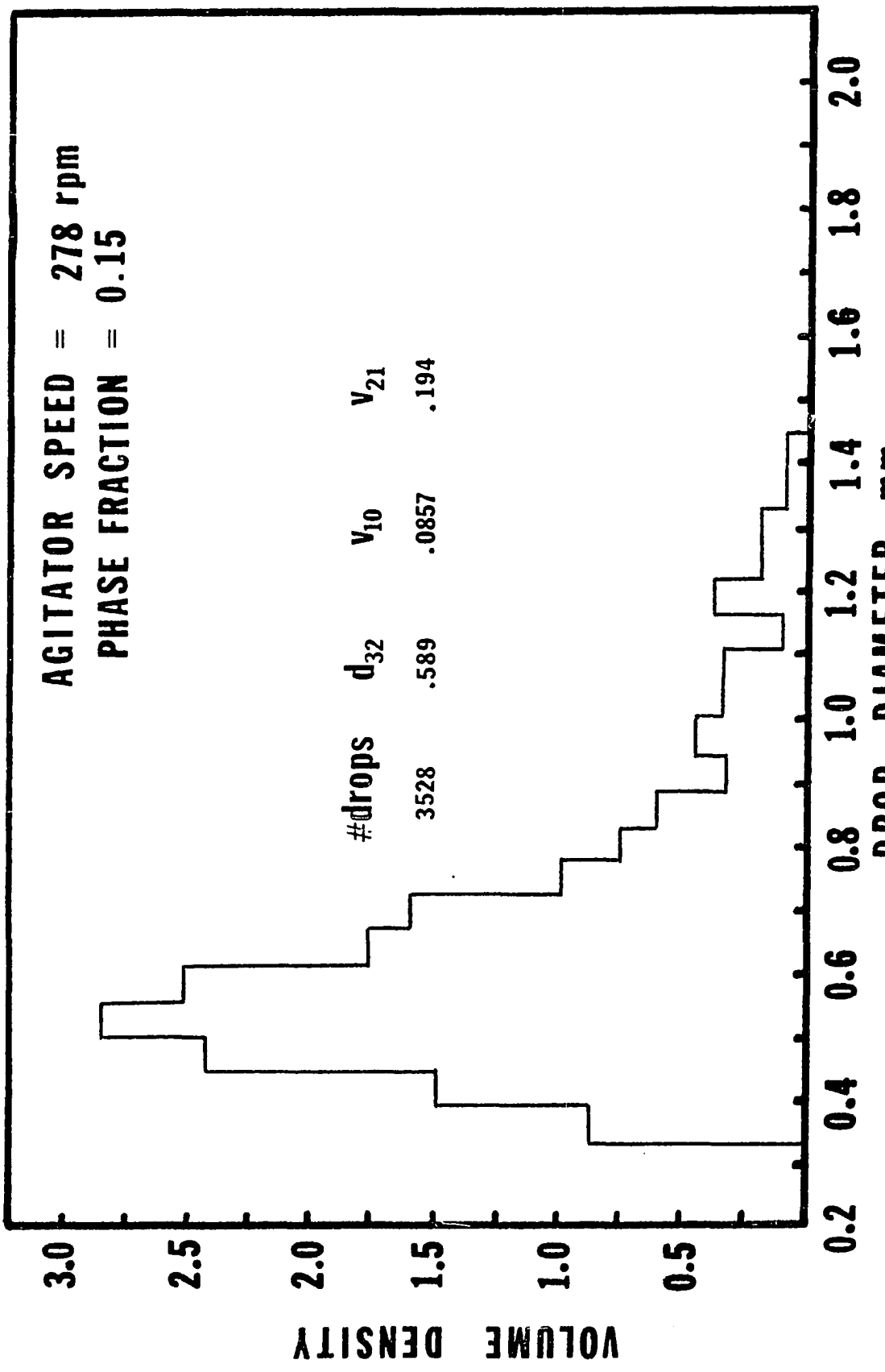

Fig. 4.31 Marginal Diameter Distribution at N = 278 rpm, θ = 0.15

Reproduced with permission of the copyright owner. Further reproduction prohibited without permission.

Reproduced with permission of the copyright owner. Further reproduction prohibited without permission.

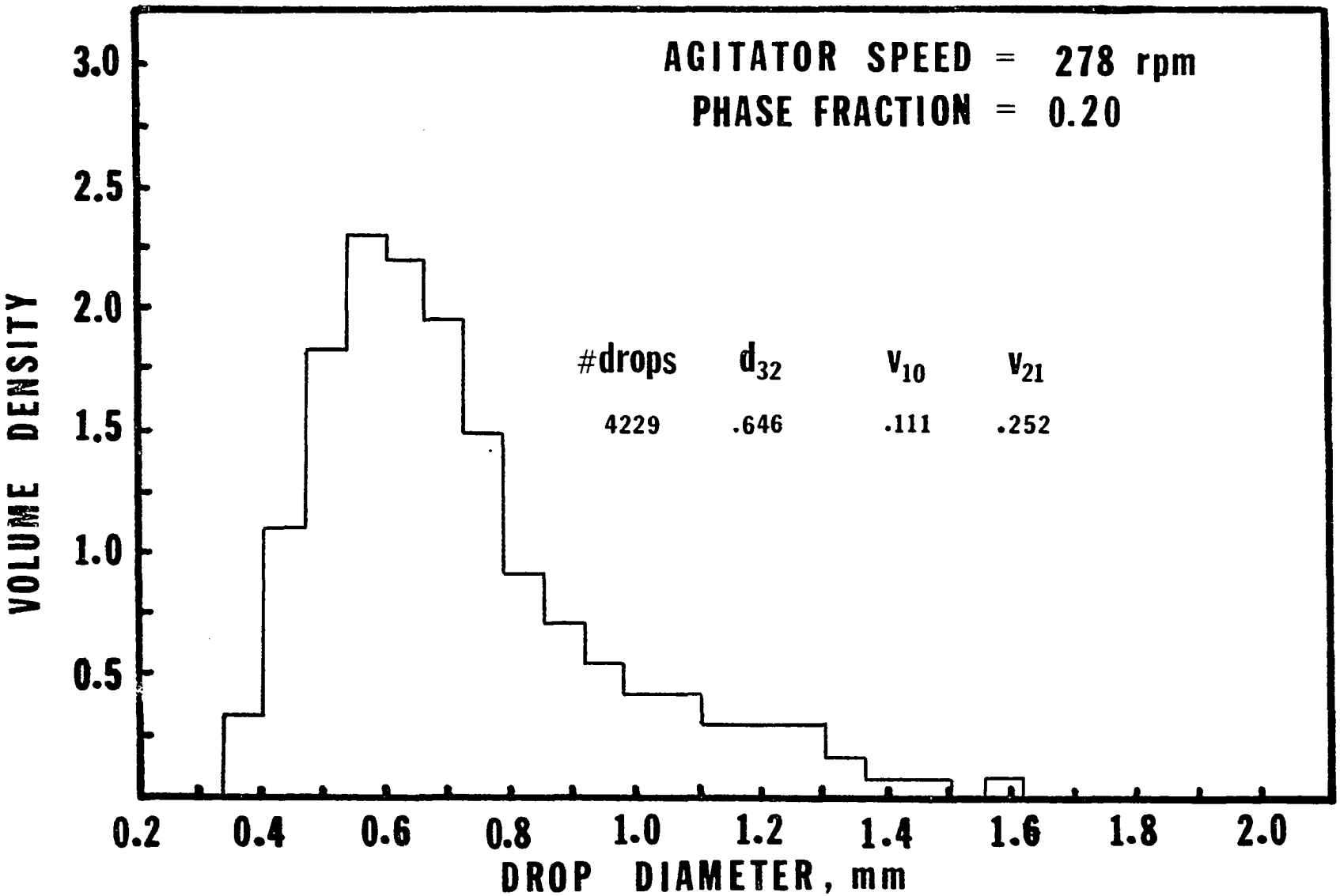

Fig. 4.32 Marginal Diameter Distribution at N = 278 rpm, θ = 0.20

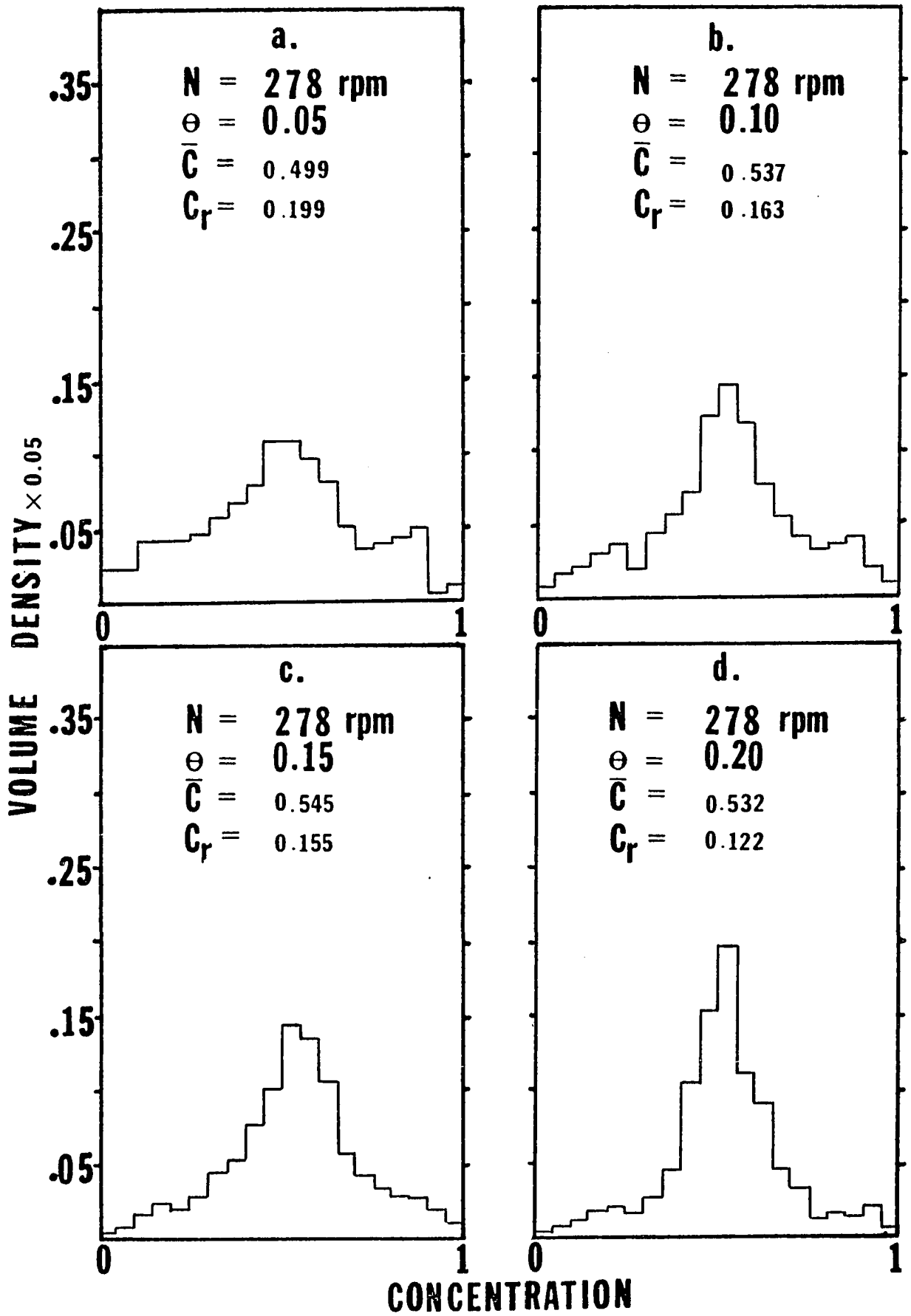

Fig. 4.33 Marginal Concentration Distributions at N = 278 rpm

Reproduced with permission of the copyright owner. Further reproduction prohibited without permission.

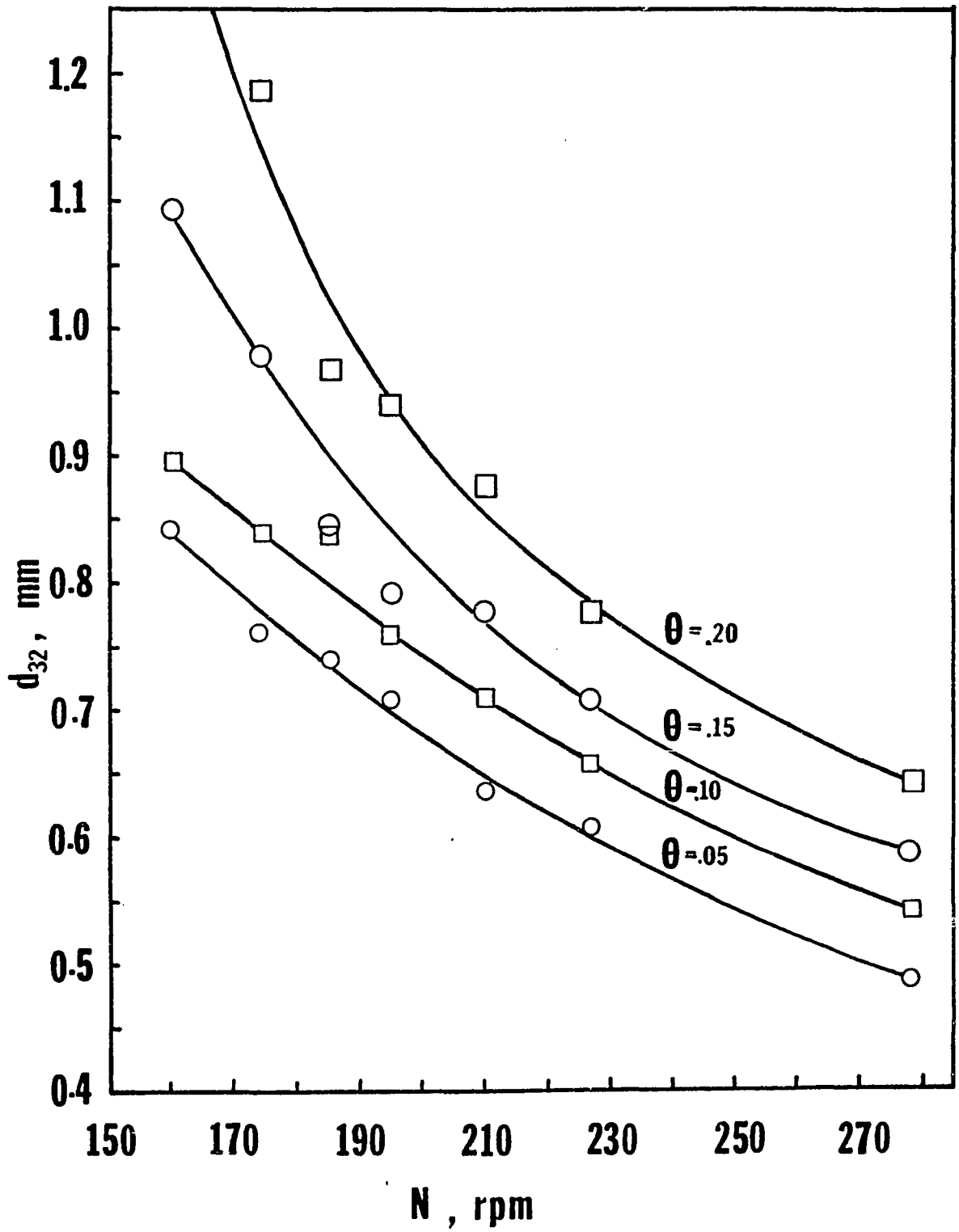

Fig. 4.34 Sauter-Mean Diameter versus Agitator Speed

Reproduced with permission of the copyright owner. Further reproduction prohibited without permission.

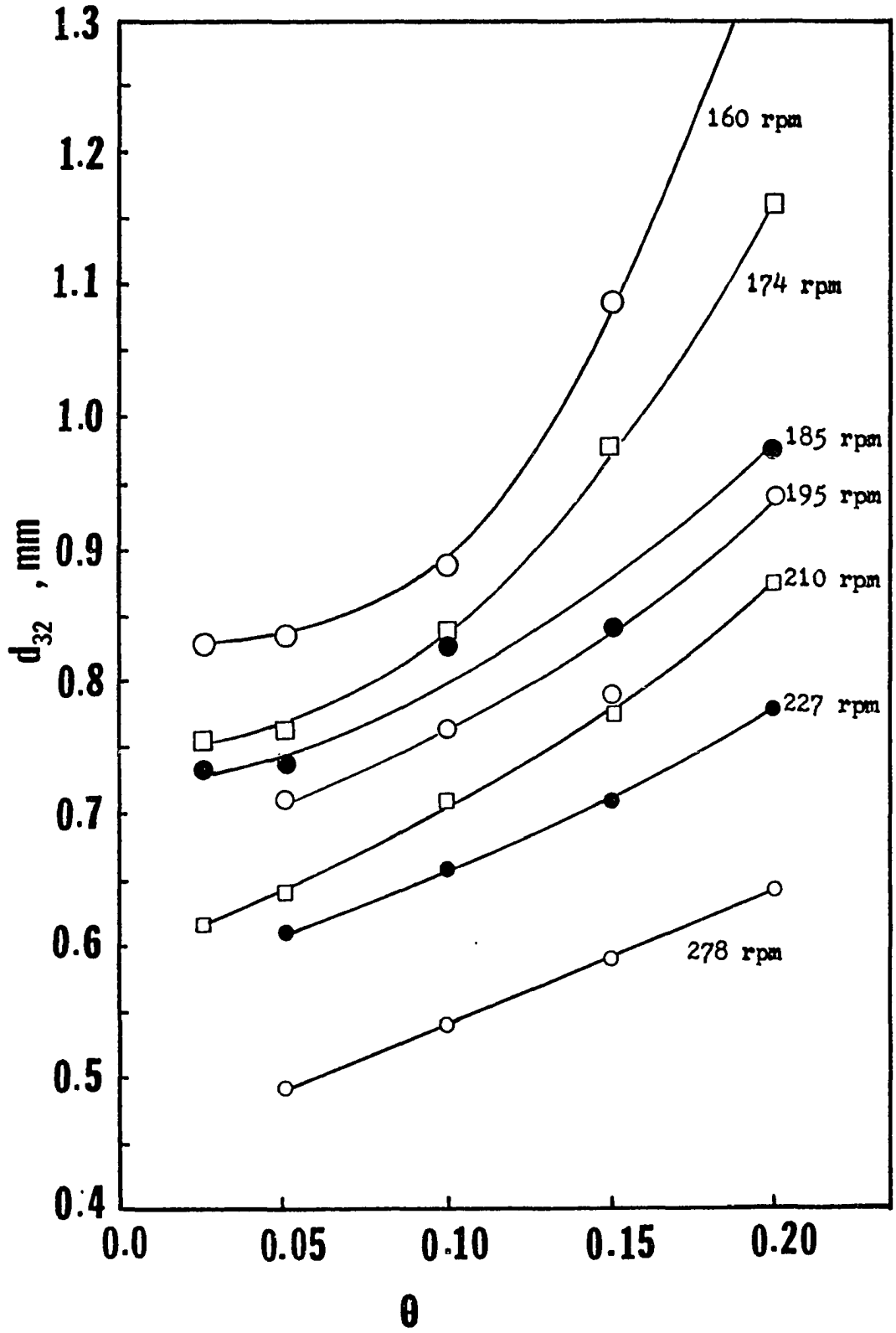

Fig. 4.35 Sauter-Mean Diameter versus Dispersed Phase Fraction

Reproduced with permission of the copyright owner. Further reproduction prohibited without permission.

TABLE 4.1

MIXING FREQUENCY AND CONCENTRATION VARIANCE RATIO
AS A FUNCTION OF AGITATOR SPEED AND PHASE FRACTION

AGITATOR SPEED r.p.m.	PHASE FRACTION θ	C_r	ω^* minutes^{-1}
160	0.05	0.905	0.0102
	0.10	0.820	0.0225
	0.15	0.665	0.0475
	0.20	0.500	0.102
174	0.05	0.728	0.0386
	0.10	0.664	0.0524
	0.15	0.440	0.132
	0.20	0.345	0.196
185	0.05	0.548	0.0874
	0.10	0.415	0.146
	0.15	0.267	0.284
	0.20	0.191	0.440
195	0.05	0.351	0.191
	0.10	0.307	0.234
	0.15	0.225	0.358
	0.20	0.132	0.682
210	0.05	0.323	0.216
	0.10	0.286	0.260
	0.15	0.259	0.296
	0.20	0.180	0.472
227	0.05	0.255	0.298
	0.10	0.194	0.423
	0.15	0.210	0.385
	0.20	0.191	0.433
278	0.05	0.199	0.410
	0.10	0.163	0.525
	0.15	0.155	0.555
	0.20	0.122	0.735

*From equation 4.3

Reproduced with permission of the copyright owner. Further reproduction prohibited without permission.

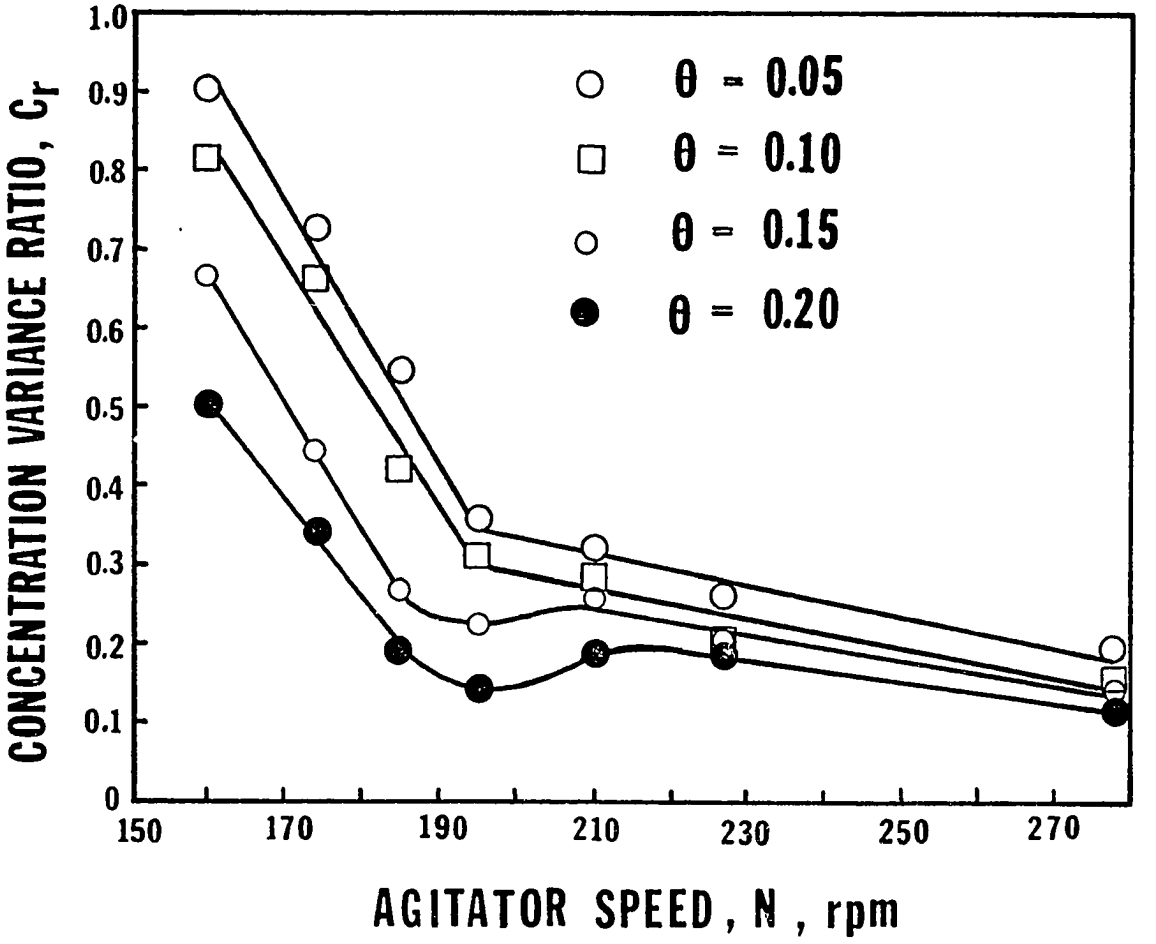

Fig. 4.36 Concentration Variance Ratio, C_r, versus Agitator Speed

Reproduced with permission of the copyright owner. Further reproduction prohibited without permission.

the phase fraction of the flows. There is a wide variation of this quantity due to the fluctuations of the flows. It is believed, however, that the steady-state distributions are not very dependent on this input drop size which is generally more than ten times the average size in the vessel. This will be shown later. Note that for the high agitator-speed experiments the lower end of the diameter distribution is somewhat abrupt. This is due to the inability to measure accurately (and subsequent rejection of) the very tiny drops which nevertheless contribute perhaps as much as 10% of the total volume. Also note the slight bimodality which seems to be consistently evident in several of the curves.

4.6 Discussion of the Experimental Results

(a) Dramatic Mixing Effects

The experimental work was begun by using an agitator speed of 195 rpm, primarily for the purpose of comparing these results to those of Verhoff who confined almost all of his experiments to this speed. Verhoff's results, of course, gave no intimation of the dramatic effects that would ensue on varying this parameter. It was found immediately that when the agitator speed was lowered by 10%, the mixing frequency decreased by more than 100%. It was decided to pursue this effect to its natural limits and the agitator speed was lowered about 10% in steps down to N = 160 rpm where the mixing rate was near to being negligible. In order to search for the region where the mixing rate has the more gradual effect noted by other researchers, experiments were performed on the high side of 195 rpm up to 278 rpm. The concentration variance ratio, C_r , and the mixing

Reproduced with permission of the copyright owner. Further reproduction prohibited without permission.

frequency for the entire agitator speed range is shown in figure 4.36 and Table 4.1. The mixing or coalescence frequency value is the one calculated from equation 4.3; it is considered to be a reasonable approximation for the mixing frequency in the real system.

Note the enormous agitator-speed effect. At the lower phase fraction, .05, the 15% increase from 160 rpm to 185 rpm results in more than a 800% increase in mixing frequency (.01 to .087). At higher agitator speeds this effect is much less, with ω varying as N^{2-3}. Also note how the mixing frequency varies with phase fraction. At the lower agitator speeds, as the phase fraction is increased 4-fold from .05 to 0.20, the mixing frequency increases 5 to 10-fold. At the higher stirring speeds this same increase in phase fraction produces less than a 2-fold increase in ω .

(b) Drop-Size Effects

In contrast to the dramatic mixing effects, the drop sizes in the vessel were observed to be only moderately dependent on the agitator speed and phase fraction. This is shown generally in figures 4.34 and 4.35. A plot of diameter distribution versus N^2 has also been made (figure 4.37) for the experiments carried out at $\theta = 0.05$. The $d_{X\%}$ values represent the diameter in each distribution below which X % of the total volume is contained. As shown, the Sauter-mean diameter, d_{32} , varies as N^{-1}.

In order to show more clearly the changes in the drop size distribution resulting from phase fraction changes, the smoothed curves of figures 4.19 - 4.22 and figures 4.29 - 4.33 are combined in two figures, figure 4.38 and figure 4.39 respectively. It is seen that, as one might expect, the drops become larger and the spread in

Reproduced with permission of the copyright owner. Further reproduction prohibited without permission.

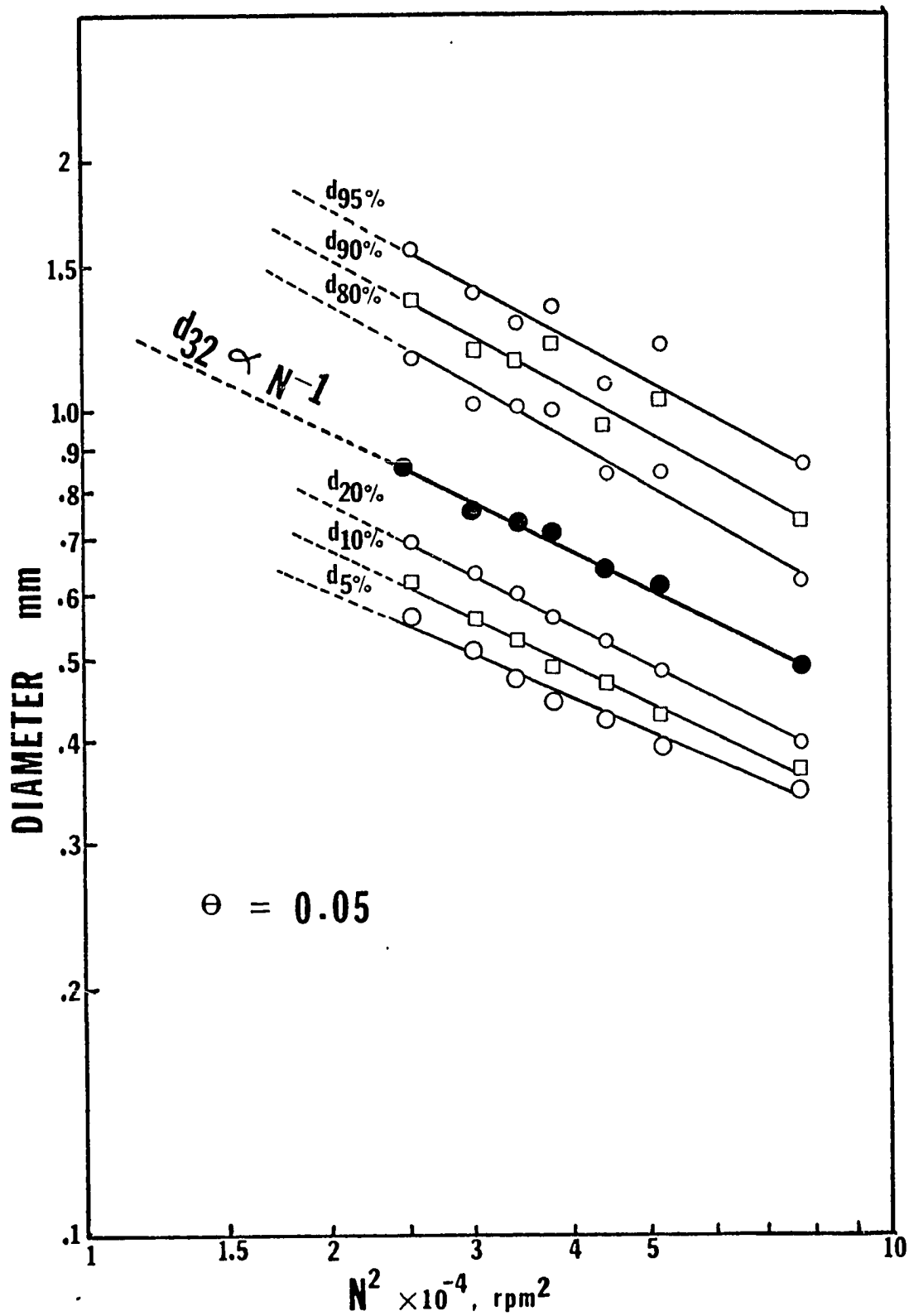

Fig. 4.37 Volume - Percentile Diameters versus N^2 at $\theta = 0.05$

Reproduced with permission of the copyright owner. Further reproduction prohibited without permission.

Reproduced with permission of the copyright owner. Further reproduction prohibited without permission.

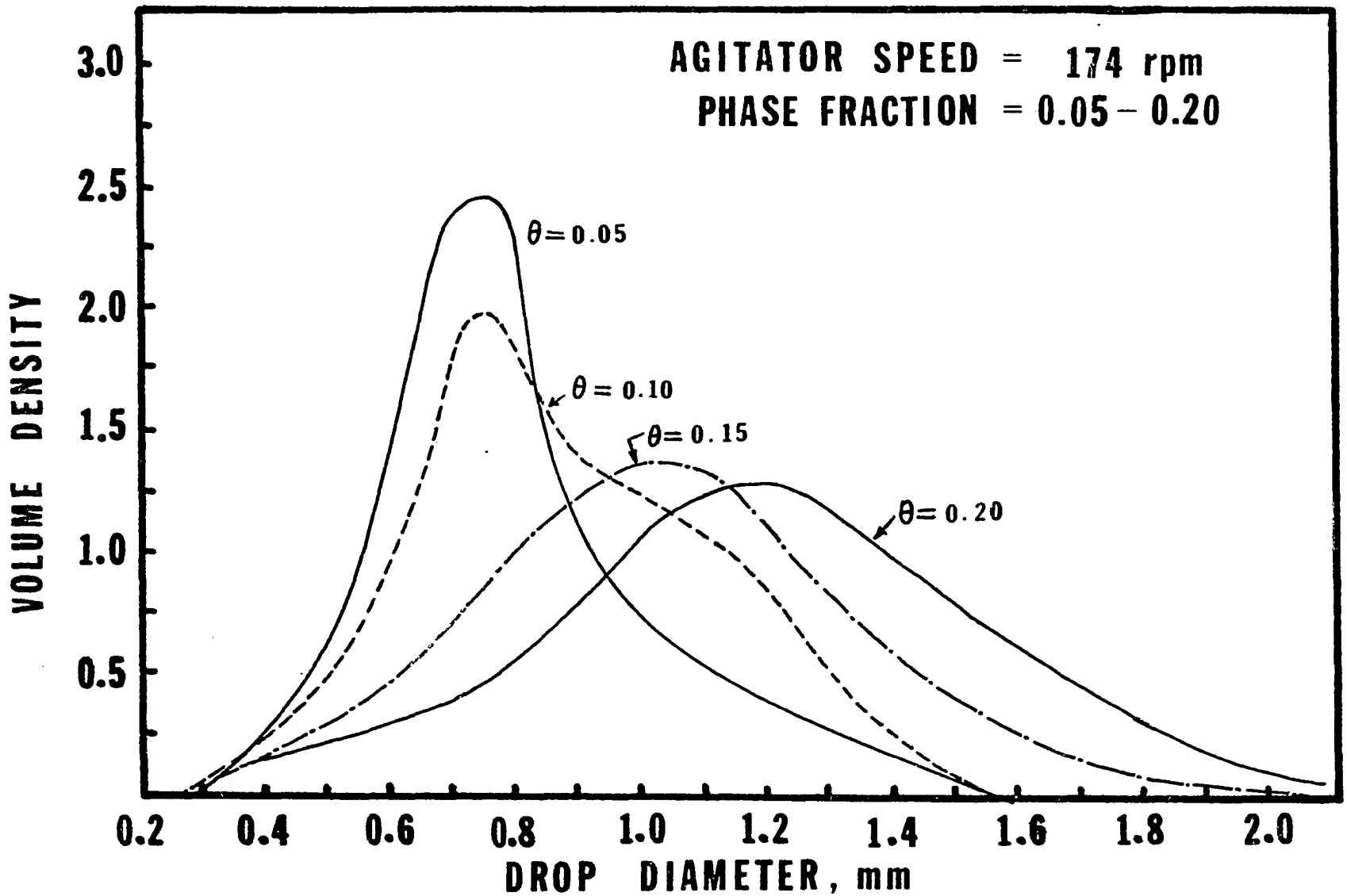

Fig. 4.38 Diameter Distributions at N = 174 rpm, θ = 0.05 - 0.20

Reproduced with permission of the copyright owner. Further reproduction prohibited without permission.

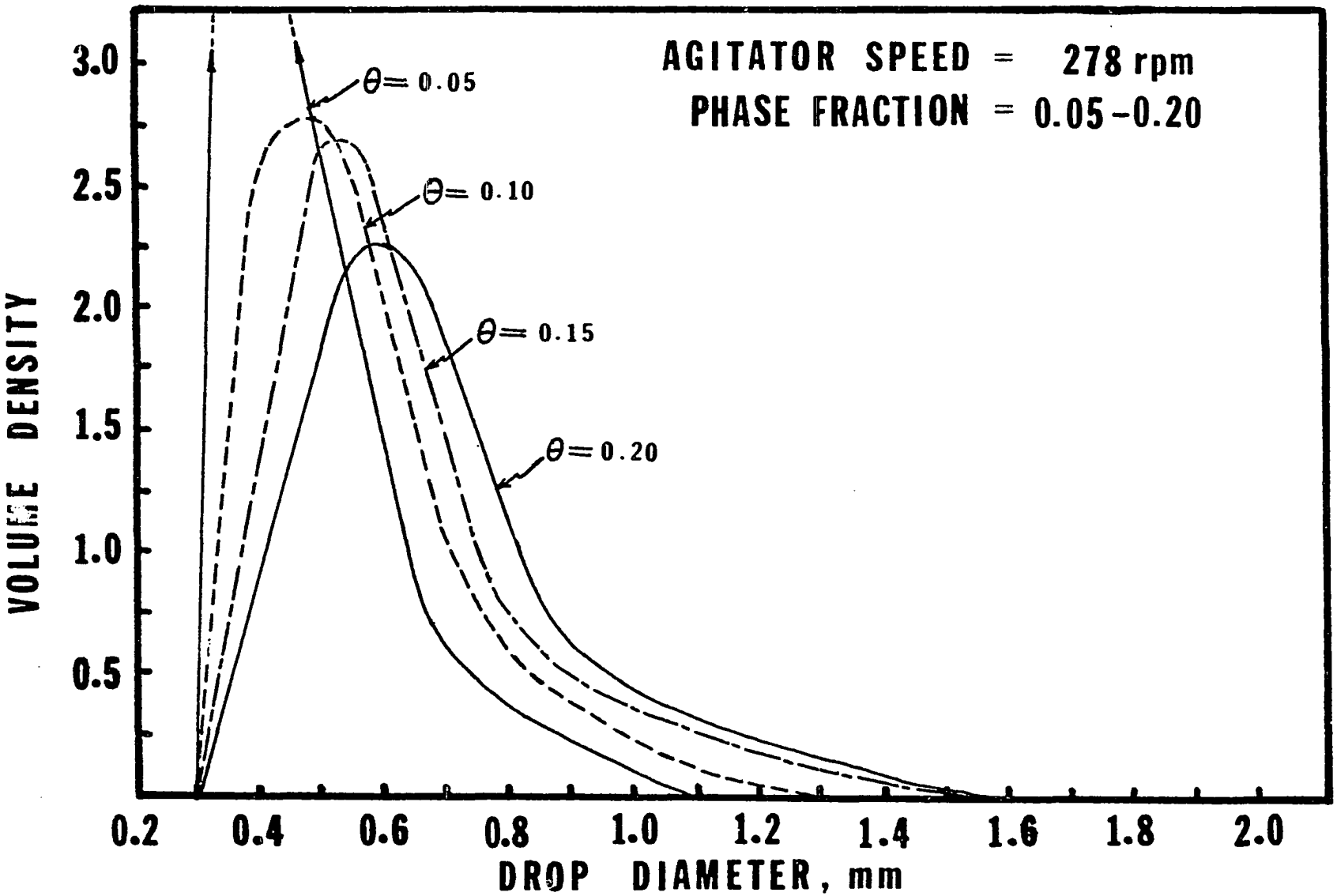

Fig. 4.39 Diameter Distributions at N = 278 rpm, θ = 0.05 - 0.20

the distributions increases as the phase fraction is increased. This effect is more pronounced at the lower agitator speed than at the higher.

(c) Importance of Low Mixing Rates

The mixing frequencies in the vessel range from 0.01 min^{-1} to 0.735 min^{-1}. This implies that the average time between coalescences ranges from about 3 minutes to 200 minutes. Since an average drop will then make several cycles within the vessel before coalescing, the dispersion can thus be considered approximately statistically homogeneous, i.e., the time average distribution of drops is the same everywhere in the vessel. This is discussed in more detail in the next chapter.

(d) Power Inputs

Rushton has shown that for Reynold's numbers greater than about 5×10^3, the power input for a flat, six-blade turbine in a 4-baffle mixing vessel is:

$$P = \frac{6 \rho N^3 D^5}{g_c 550} \qquad 4.4$$

where ρ is density, N, agitator speed and D, diameter of the blades.

The Reynold's number for our system is:

$$N_{Re} = \frac{N D^2 \rho}{\mu} \qquad 4.5$$

or

$$N_{Re} = 43.0\ N \qquad 4.6$$

Reproduced with permission of the copyright owner. Further reproduction prohibited without permission.

for N in rpm. Thus for N = 160 rpm, N_{Re} = 6890, and equation 4.4 applies for our range of agitator speeds.

The power input per unit mass of vessel content (0.362 gallons) is:

$$\bar{\varepsilon} = 7.64 \times 10^{-3} \cdot \left(\frac{N}{60}\right)^3 \qquad 4.7$$

where N is rpm, and $\bar{\varepsilon}$ is HP/1000 gallons.

The range of power inputs from N = 160 rpm to 278 rpm is 0.145 - 0.760 HP/gallons.

(e) Implications of Results:

(i) Agitator Speed Effect

Consider the experiments carried out at θ = 0.05 and at various agitator speeds (figure 4.34, 4.35, and 4.37). At the lowest speed of 160 rpm it is evident that very little mixing is taking place. This is shown graphically in figure 4.18a. The average drop size is d_{32} = 0.843 mm. When the agitator speed is increased to 174 rpm the average size decreases to 0.758 mm and the mixing rate increases more than 300%. It can be assumed that the drops in the vessel are smaller at the higher N because the overall breakage rate is higher.

If one were to assume that all the drops in the vessel behaved similarly with respect to coalescence, then he would be hard-pressed to explain the 300% increase in coalescence rate. The only aspects that are different between the case at N = 160 rpm and that at N = 174 rpm are (1) the relative velocity between drops is 10% larger and (2) the drops are 10% smaller. If, on the other hand,

Reproduced with permission of the copyright owner. Further reproduction prohibited without permission.

one were to assume that there is a strong drop-size dependency for both the breakage and coalescence mechanisms, he could present a reasonable explanation for the dramatic results. For argument's sake, let us say that the coalescence frequency of drops in the vessel is described by a strong function (perhaps exponential) by which very small drops have a much greater coalescing frequency than large drops. In addition, let us say that the breakage frequency of drops is similarly described by a strong function whereby large drops have a much greater breakage frequency than small drops. By exaggerating the argument, we can then say that at lower agitator speeds (e.g., N = 160) there are no "small" drops available for coalescence. At higher speeds (e.g., N = 174) where the breakage rate is much higher, these "small" drops are formed and will coalesce. As agitator speed is increased, more and more "small" drops will be formed and will coalesce. Ultimately the whole system will be composed of "small" drops, all having similar coalescence frequencies.

This simplified argument is essentially the same as that used by Shinnar to explain "turbulence-stabilized" dispersions (refer to figure 2.1). According to Shinnar there is a maximum drop size, d_{max} below which the breakage rate is zero. This diameter is correlated with N as $d_{max} \propto N^{-6/5}$. Similarly there is a minimum drop size, d_{min}, above which the coalescence rate is zero. This diameter is correlated with N as $d_{min} \propto N^{-3/4}$. Any drops between d_{max} and d_{min} are stable, neither breaking up nor coalescing. As applied to our system (although it is not a batch system) his theory would say that the drops formed at N = 160 rpm are all between d_{max} and d_{min}. At N = 174 rpm, there are drops formed below d_{min}; thus coalescence

Reproduced with permission of the copyright owner. Further reproduction prohibited without permission.

is probable. As N increases the "stabilized" region decreases in size as shown in figure 2.1 until some point is reached where all drops are coalescing and none is considered "stable."

Although Shinnar's derivation of the $d_{min} \propto N^{-3/4}$ dependency is highly questionable and although the idea of a minimum and maximum drop size is an unnecessary and unwarranted concept, his theory provides a general basis for explaining the experimental result. Later it will be shown that the experimental observations can be explained by the use of rate equations, comprising exponential functions in which d varies as $N^{-6/5}$ for breakage and d varies as $N^{-3/4}$ for coalescence.

(ii) Phase Fraction Effect

The results seem to suggest that as phase fraction is increased within a given agitator speed, the small and the large drops within the system coalesce and form much larger drops. For example, at N = 160 rpm, the drops at θ = 0.20 are four or five times larger in volume than those found at θ = 0.05. This observation seems to be in direct contradiction to the postulation presented in (a) above, where coalescence was attributed to the smaller drops. The matter can be resolved by considering a "packing" phenomenon which affects both the breakage and coalescence rates. This will be discussed later.

Reproduced with permission of the copyright owner. Further reproduction prohibited without permission.

CHAPTER 5

GENERAL MIXING EQUATION

5.1 General Mixing Equation

The general mixing equation described here has been derived and discussed in detail by Valentas and Amundson (49 - 51). Rather than using a number-over-mass balance we will consider the equivalent number-over-volume balance.

The physical model considered is a continuous flow agitated vessel which is fed with two streams of immiscible liquids. The droplet size distributions in the feed, effluent and vessel are described by the probability density functions (p · d · f), a(v, t), b(v, t), and A(v, t) as:

$a(v,t)dv$ = number fraction of the droplets in the feed with volume between v and $\dot{v}$ + dv at time t 5.1

$b(v,t)dv$ = number fraction of the droplets in the exit stream with volume between v and v + dv at time t 5.2

$A(v,t)dv$ = number fraction of the droplets in the vessel with volume between v and v + dv at time t 5.3

Perfect macroscopic mixing will be assumed. That is, the effluent is a representative sample of the vessel contents. Thus:

$$b\ (v,\ t) = A\ (v,\ t) \qquad 5.4$$

Reproduced with permission of the copyright owner. Further reproduction prohibited without permission.

The application of perfect macroscopic mixing in a heterogeneous system implies only this and not that the drops are of anequal size. Also, the use of the general mixing equation implies homogeneity of the vessel contents. In our system, as mentioned, we may assume approximate statistical homogeneity due to the fact that the coalescence rate is small. Here statistical homogeneity means that the time-average position distributions of drops in any two small volumes in the vessel are approximately the same. It does not mean that the flow or energy conditions are distributed homogeneously in the vessel, or that the breakage, coalescence, or escape rates are identical in space. Obviously Sprow's strongly coalescing system, where the drop sizes near the walls were much larger than those near the impeller, cannot be considered statistically homogeneous (48).

The basis of the general mixing equation is a mass or volume balance over any size range v to v + dv. Droplets enter this region by means of the breakage of drops larger than v, the coalescence of drops smaller than v and the feed flow of drops of the same size. Drops of size v to v + dv leave this region through breakage, coalescence or by flow out of the vessel. The balance can be expressed mathematically by first considering the following definitions:

n_o = number feed rate of droplets 5.5

$n(t)$ = number of droplets in vessel at time t 5.6

$g(v)$ = fraction of drops in vessel with volume between v and v + dv , disappearing through breakage per unit time. 5.7

$\beta(v \mid v')dv$ = number fraction of droplets with volume between v and v + dv formed by the breakup of a drop of volume v'. 5.8

Reproduced with permission of the copyright owner. Further reproduction prohibited without permission.

$\nu(v)$ = average number of drops formed per breakage of drops of size v . 5.9

$F(v, v')\,dvdv'$ = number rate at which drops of volume v to $v + dv$ are coalescing with drops of volume v' to $v' + dv'$. 5.10

$f(v)$ = number fraction of drops in the vessel with volume between v and $v + dv$ flowing out per unit time. 5.11

As an example, consider the droplets that are entering drop region v to $v + dv$ by breakage of drops larger than v, at time t:

$n(t)\,A(v', t)\,dv'$ = no. of drops in vessel with volume between v' and $v' + dv'$.

$g(v)\,n(t)\,A(v', t)\,dv'$ = no. of drops in vessel with volume between v' and $v' + dv'$ disappearing through breakage per unit time.

$\nu(v)\,g(v')\,n(t)\,A(v', t)\,dv'$ = no. of daughter droplets formed per unit time from the breaking drops of volume between v' and $v' + dv'$.

$\beta(v|v')\,\nu(v')\,g(v')\,n(t)\,A(v', t)\,dv'dv$ = number of drops with volume between v and $v + dv$ formed by the breakage of drops with volume between v' and $v' + dv'$, per unit time.

$\int_v^\infty \beta(v|v')\,\nu(v')\,g(v')\,n(t)\,A(v', t)\,dv'dv$ = number of droplets with volume between v and $v + dv$ formed by the breakage of drops of size greater than v, per unit time.

Similarly other terms can be obtained to give the number

Reproduced with permission of the copyright owner. Further reproduction prohibited without permission.

balance in volume region v to v + dv

$$\frac{d}{dt}\left[\, n(t)\, A\,(v,t)\, dv \right] \;=\; n_o\, a(v,t)\, dv$$

accumulation in dv — flow into dv

$$+ \int_v^\infty \beta(v|v')\, \nu(v')\, g(v')\, n(t)\, A(v',t)\, dv'dv$$

breakage into dv

$$+ \int_o^{v/2} F\,(v - v',\, v')\, dv'dv$$

coalescence into dv

$$- f(v)\, n(t)\, A\,(v,t)\, dv \quad - \quad g(v)\, n(t)\, A(v,t)\, dv$$

flow out of dv — breakage out of dv

$$- \int_o^\infty F\,(v,\, v')\, dv'dv \qquad 5.12$$

coalescence out of dv

Reproduced with permission of the copyright owner. Further reproduction prohibited without permission.

Notice in the "coalescence into" term the integration is taken from 0 to v/2 in order not to count each coalescence twice. (F (v', v) is a symmetric function). At steady state equation 5.12 reduces to:

$$0 = n_o\, a(v)\, dv + \int_v^\infty \nu(v')\, g\,(v')\, \beta\,(v|v')\, n\, A(v')\, dv'dv$$

$$+ \int_o^{v/2} F\,(v-v',\, v')\, dv'dv \qquad - f(v)\, n\, A\,(v)\, dv$$

$$- g\,(v)\, n\, A\,(v)\, dv \quad - \int_o^\infty F\,(v,\, v')\, dv'dv \qquad 5.13$$

The coalescence rate can be further refined by considering it to be made up of a collision rate and a coalescence efficiency. With regard to the drops in the vessel with size v and v', the number of collisions per unit time suffered by a drop of size v with drops of size v' is $h\,(v\,,\, v')\, nA\,(v')dv$ where $h\,(v\,,\, v')$ is the collision frequency. Thus the number of collisions per unit time between drops of volume v and drops of volume v' is:

$$h\,(v'_j\, v)\, nA\,(v')\, nA\,(v)\, dv'dv$$

The coalescence rate is obtained by multiplying this by the coalescence efficiency or the probability of coalescence given a collision, $\lambda(v'_j\, v)$. Then:

$$F\,(v,\, v')\, dvdv' = \lambda\,(v,v')\, h\,(v,v')\, n\, A\,(v)\, dvdv' \qquad 5.14$$

Reproduced with permission of the copyright owner. Further reproduction prohibited without permission.

By substituting equation 5.14 into equation 5.13, and rearranging we get:

$$n\,A(v) = \left\{ n_o\, a(v) + \int_v^{\infty} \nu(v')\, g\,(v')\, \beta\,(v|v')\, n\, A\,(v')\, dv' \right.$$

$$\left. + \int_o^{v/2} \lambda(v - v',\, v')\, h\,(v - v',\, v')\, n\, A\,(v - v')\, n\, A\,(v')\, dv' \right\} \Big/ \left\{ f\,(v) + g\,(v) + w(v) \right\} \qquad 5.15$$

where

$$w(v) = \int_o^{\infty} \lambda(v,\, v')\, h\,(v,\, v')\, n\, A\,(v')\, dv' \qquad 5.16$$

5.2 Numerical Solution of Equation

The numerical scheme is taken from Valentas. Analytical solutions of equation 5.15 are not known. A numerical solution is obtained by a reduction with integration formulae which leads to

$$Y_j = \left\{ n_o\, a_j + \sum_{i=j+1}^{n'} \alpha_i\, g_i\, \nu_i\, \beta_{i,j}\, Y_i \right.$$

$$\left. + \sum_{i=1}^{j/2} \gamma_i \lambda_{j-i,i}\, h_{j-i,i}\, Y_{j-i}\, Y_i \right\} \Big/ \left[f_j + g_j + w_j \right] \qquad 5.17$$

for $j = 2$ to $n' - 1$

Reproduced with permission of the copyright owner. Further reproduction prohibited without permission.

$$Y_1 = \left\{ n_o\, a_1 + \sum_{i=2}^{n'} \alpha_i\, \nu_i\ \ g_i\ \ \beta i,j\ Y_i \right\} \Big/ \left[f_1 + g_1 + w_1 \right] \qquad 5.18$$

for $j = 1$

and

$$Y_{n'} = \left\{ n_o\, a_n + \sum_{i=1}^{n'/2} \gamma_i\, \lambda_{j-i,\,i}\, h_{j-i,\,i}\, Y_{j-i}\, Y_i \right\} \Big/ \qquad 5.19$$

$$\left[f_{n'} + g_{n'} + w_{n'} \right]$$

for $j = n'$

where

$$w_j = \sum_{i=1}^{n'-j} \delta_i\, \lambda_{j,i}\, h_{j,i}\, Y_i \qquad 5.20$$

and

$$n' = \frac{jL'}{v} \quad \text{where} \qquad 5.21$$

L' is largest drop considered

Reproduced with permission of the copyright owner. Further reproduction prohibited without permission.

and $Y_j = n\ A_j$ 5.22

If breakage alone is considered equations 5.17 to 5.18 reduce to

$$Y_j = F_j + \xi_j \sum_{i=j+1}^{i=n} \alpha_i \nu_i g_i \beta_{i,j} Y_i \qquad 5.23$$

where

$$F_j = \frac{n_o a_j}{f_j + g_i} \qquad 5.24$$

and $$\xi_j = \frac{1}{f_j + g_j} \qquad 5.25$$

α , γ and δ are numerical constants whose values depend on the order of difference retained in the integration formulae. Equation 5.23 can be solved recursively by marching backwards from Y_n. Thus the case of breakage alone can be solved with one pass through the entire drop size range.

The case of breakage and coalescence (equations 5.17 - 5.19) is more difficult. It is seen that an iterative technique is necessary to solve these sets of equations. The technique used is such that each new calculation of Y_j is used in the next iteration. Thus for the k -th iteration on the j -th variable in an n - th order system,

$$Y_j^{(k)} = G_j\left(Y_1^{(k-1)}, \ldots Y_j^{(k-1)}, Y_{j+1}^{(k)} \ldots Y_n^{(k)} \right) \qquad 5.26$$

First order differences were retained in the itegration formula to

Reproduced with permission of the copyright owner. Further reproduction prohibited without permission.

maintain the simplicity of form in programming. The following scheme was used in the solution of equations 5.17 - 5.19.

1. Take the initial solution $Y_j^{(o)}$ [illegible] be that of breakage alone, equation 5.23.
2. Compute w_j from $Y_j^{(o)}$ and equation 5.20.
3. Starting at j = n and marching backwards compute $Y_j^{(1)}$ from equations 5.19, 5.17, and 5.18 using the values of w_j, computed in step 2.
4. Iterate until convergence requirements are satisfied.

5.3 Mixing Rates

The overall number coalescence rate is:

$$R_n = 2\int_o^\infty \int_o^{v/2} F\,(v - v',\, v')\, dv'dv \qquad 5.27$$

where R_n is the number of drops in the vessel coalescing per unit time. The coalescence frequency on a number basis is then:

$$\omega_n = R_n/n \qquad 5.28$$

where n is the total number of drops in the vessel.

Similarly the coalescence rate on a volume basis is:

$$R_v = \int_o^\infty \int_o^{v/2} v\, F\,(v-v',\, v')\, dv'dv \qquad 5.29$$

and the volume coalescence frequency is:

$$\omega_v = R_v / V_T \theta \qquad 5.30$$

Reproduced with permission of the copyright owner. Further reproduction prohibited without permission.

where V_T is the total vessel volume and θ is the volume fraction of dispersed phase.

If all drops coalescing are of equal size then $\omega_n = \omega_v$, and this is equal to the mixing frequency derived by Curl in equation 4.3. However, if the coalescences in the vessel are between droplet pairs of unequal size, then the above number and volume coalescence rates may not be a good measure of the "mixing" rate. For example, if the spread of dye in the dispersed phase is being measured, it is seen that a very small drop coalescing with a large drop will produce very little mixing. A measure of mixing accounting for this, but still not involving the concentration distribution actually present, is the "entropy" generation rate given by

$$R_m = \frac{1}{\ln 2} \int_o^{\infty} \int_o^{v/2} v_m F(v - v', v')\, dv'dv \qquad 5.31$$

where

$$v_m = v' \ln \frac{v'}{v} + (v - v') \ln \frac{v - v'}{v} \qquad 5.32$$

The mixing frequency is then:

$$\omega_m = R_m / V_T \theta \qquad 5.33$$

It is seen that for equal size drops coalescing:

$$\omega_m = \omega_v = \omega_n \qquad 5.34$$

Throughout the theoretical work, the above coalescence and mixing

Reproduced with permission of the copyright owner. Further reproduction prohibited without permission.

frequencies are calculated and compared to the mixing frequency, ω , calculated from the data on the basis of equation 4.3.

Reproduced with permission of the copyright owner. Further reproduction prohibited without permission.

CHAPTER 6

MODELING PROCEDURE

After completing the laboratory work, the purpose of this research was to develop mathematical models for the mixing processes that could be used in the mixing equations to explain the experimental results. The specific problem involved (1) developing models for the mixing functions, $\nu(v)$, $\beta(v\ v')$, $g(v)$, $h(v, v')$, $\lambda(v, v')$ and $f(v)$, (2) using these models in conjunction with the general mixing equation to generate drop size distributions and mixing rates, and (3) "fitting" these distributions and rates to those found experimentally. "Fitting" the data required a trial-and-error operation involving the unknown parameters associated with the developed models. A "sensitivity" analysis in a parameter space was carried out to determine whether any set of these parameters could be used to generate distributions and rates that fit the experimental data. If none could, then the models were rejected, new ones were constructed, and the operation was repeated.

It should be emphasized here that a fit of the drop-size distributions alone is not a sufficient condition for determining the parameters in the mixing functions. At a condition of constant N (agitator speed) and constant θ (dispersed phase fraction), there are various combinations of the functional parameters that can be used in the fitting of the distributions. Verhoff has shown

Reproduced with permission of the copyright owner. Further reproduction prohibited without permission.

mathematically that the mixing kernel (which describes both the breakage and coalescence processes) is indeed not uniquely determined by a knowledge of the drop-size distributions alone (52, p. 22). Thus the determination of the mixing functions in this work is based on the fitting of not only the drop-size distributions but also the mixing frequency, ω .

The basic difficulty in the modeling was trying to explain the unique experimental results, particularly the strong dependence of mixing rate on agitator speed. Throughout this work, whatever models were chosen, the problem always revolved around the ability of the models to explain the enormous increase in mixing rate at the lower agitator speeds (a 300% increase in ω for a 10% increase in N). The problem was compounded by the self-imposed requirement that the developed models be compatible with the findings of other researchers.

This chapter will serve as a necessary introduction to the last four chapters, where only the final or most satisfactory models are described and discussed. The intention here is to describe briefly and chronologically the methods and reasoning that led to the ultimately accepted models.

(1) After the experimental results were obtained, it was decided to carry out a preliminary analysis of the results using the models developed by Valentas (49). The purpose of this was twofold: (1) to become familiarized with the numerical analyses and (2) to get a sense of the types of mixing models that were required to fit the data. The functions chosen were:

$$\nu = 2, \text{binary breakage} \qquad 6.1$$

Reproduced with permission of the copyright owner. Further reproduction prohibited without permission.

$$\beta(v|v') \quad = \text{normal density function} \qquad 6.2$$

$$g(v) = \begin{cases} 0 & v < v_{max} \\ k_1' N^x (v - v_{max})^{m_1} & v > v_{max} \end{cases} \qquad 6.3$$

where

$$v_{max} = k_2' N^{-3.6}$$

and

$$h(v,v') \quad (v,v') = \begin{cases} k_3' N^y (v\, v')^{m_2} & 0 < v < v_{min} \\ k_3' N^y (v\, v')^{m_2} \exp\left(-k_4' (v-v_{min})^2\right) & v > v_{min} \end{cases} \qquad 6.4$$

where

$$v_{min} = k_5' N^{-2.25}$$

v_{max} and v_{min} are the volumes corresponding to Shinnar's "d max and d min", discussed in Chapter 2. The breakage frequency below v_{max} is zero and the coalescence efficiency is constant up to v_{min} and decreases sharply for $v > v_{min}$. Values of m_1 and m_2 were chosen to be 1, 2, or 3. Because there is a total of 11 arbitrary constants in the above functions, there is not too much difficulty in using these in the mixing equation to generate drop size distributions and mixing rates that approximately fit the experimental results at the lower agitator speed region (where there is the 300% increase in ω for the 10% increase in N). This could be only done, however, if x and y were large, that is, if g and $h\ \lambda$ were proportional to

Reproduced with permission of the copyright owner. Further reproduction prohibited without permission.

N^{4-7}.

(2) The above result suggested an "Arrhenius" type of mechanism with turbulent energy ($\propto N^2$) being analogous to RT energy in molecular reactions. Thus g (v) and h (v, v′) λ (v, v′) were made proportional to exp (- constant/ N^2). This was a better function than N^x or N^y because as N increases, g and hλ level off, as do the experimentally determined mixing frequencies, ω .

(3) Modeling was then begun on the breakage mechanism. A model was constructed that was based on an analogy to molecular decomposition. This is the model derived and discussed in the next chapter. It is

$$g(v) = c_2 N v^{-2/9} \exp\left\{ \frac{- c_1}{N^2 v^{5/9}} \right\} \qquad 6.5$$

This model, when used in the mixing equation, was able to describe very well the experimental cases at low dispersed phase fraction and low agitator speed, where coalescence was almost negligible. The attractive aspects of this function is that the breakage frequency has non-zero values for all drop sizes in the vessel (in contrast to equation 6.3) and that the $d \propto N^{-6/5}$ dependency found by other researchers is explained.

(4) Modeling was then begun on the coalescence process. The exponential behavior of the (collision frequency x coalescence efficiency) functions, h (v, v) λ (v, v), was attributed to the coalescence efficiency. In developing a model to explain this, Shinnar's "adhesion-phenomena" model, and Howarth's "big-crash" model were rejected

Reproduced with permission of the copyright owner. Further reproduction prohibited without permission.

for several reasons. After a considerable period of time, during which various models were developed and rejected, a satisfactory coalescence model was constructed. It is derived and discussed in the next chapter and is:

$$h(v_1, v_2)\,\lambda(v_1, v_2) = c_4 N (v_1^{1/3} + v_2^{1/3})^2 e^{-\left[c_3 N^3 \left(\frac{v_1^{1/3} v_2^{1/3}}{v_1^{1/3} + v_2^{1/3}}\right)^4\right]} \quad 6.6$$

This model could be used to explain the $d \propto N^{-3/4}$ results found by other researchers and the concept of "turbulence-stabilized" dispersions.

(5) The above models for breakage rate and coalescence rate were then used in the mixing equation, along with the other functions, and a parameter search was begun. This was done by first assuming that a drop breaks into two drops of about equal size ($\nu(v)$ and $\beta(v/v')$ were then accounted for) and f(v), the escape frequency was taken to be the inverse of the residence time (a reasonable assumption based on perfect macroscopic mixing). In this way the only parameters to be considered were c_1, c_2, c_3, c_4 in equations 6.5 and 6.6. At first only the experimental results at a given phase fraction were considered ($\theta = 0.05$). The difficulties involved in finding suitable values for these constants to fit both the drop-size distributions and the mixing rates are discussed in Chapter 9. In any case, these were chosen to fit some of the cases at $\theta = 0.05$.

(6) Using these constants, drop-size distributions and mixing rates were obtained numerically and compared to the experimental results at other dispersed phase fractions. Only the results at $\theta = 0.025$ and

Reproduced with permission of the copyright owner. Further reproduction prohibited without permission.

θ = 0.10 could be satisfactorily fit. The models could not explain the rather large drop sizes for large values of dispersed phase concentration (15% and 20%).

(7) It was thought that the reason for this perhaps resided in the $\nu(v)$ and $\beta(v \mid v')$ functions. It was at this point that these functions were explored. The average number of drops on breakage was varied from 2 to 8. Some numerical work was also performed with ν taken to be a function of the kinetic energy/surface energy ratio ($\propto N_{we} \cdot \frac{d}{D}^{5/3}$). Several forms were also assumed for the breakage distribution function, $\beta(v \mid v')$. It was found that none of these ν and β functions (along with new c_1, c_2, c_3, and c_4 values) could be used to explain the large increases in drop size with increasing θ.

(8) Finally it was realized that these large increases in drop size with increasing θ were probably due to a turbulence-damping effect. That is, the forces associated with the breakage and coalescence processes were being attenuated by the presence of the dispersed phase drops. This "packing" effect was expressed mathematically and two new constants were introduced into the parameter space.

(9) Using the resulting six constants, and assuming binary breakage into two drops of about equal size, the data were finally and satisfactorily fit at all N and θ levels.

Reproduced with permission of the copyright owner. Further reproduction prohibited without permission.

CHAPTER 7

THEORY AND MODEL BUILDING

7.1 Description of Turbulent Field

In turbulence, instabilities of the main flow produce eddies whose size is determined by the size of the apparatus. These large unstable primary eddies disintegrate into smaller and smaller eddies until a lower limit, η , is reached where the viscous shear effects counteract the eddying motion and prevent further cascading. The turbulent flow field may be described by an energy spectrum function E (k) such that E (k) dk is the energy per unit mass of continuous phase associated with fluctuations of wave number k to k + dk.

The diameter of droplets in strongly agitated dispersions is usually small compared with some macroscopic dimensions such as the impeller width, L, and large compared to the dissipation micro-scale, η . Kolmogoroff's theory of local isotropy predicts that at sufficiently high Reynold's number the small scale eddies in the turbulent flow are isotropic and their intensity is dependent only on the local rate of energy dissipation per unit mass, ε , and the viscosity of the fluid (5, 19, 24). For local isotropy to exist, the linear scale, L, of the energy containing eddies must be large compared to the scale of the small energy dissipating eddies, η . In this range, called the inertial subrange, it is known

Reproduced with permission of the copyright owner. Further reproduction prohibited without permission.

that (19),

$$E(k) = \zeta \varepsilon^{2/3} k^{-5/3} \qquad 7.1$$

If one wishes to view the turbulence in terms of velocity fluctuations, then by dimensional reasoning, the mean square of the relative velocity between two points separated by a distance d in the inertial subrange is:

$$\overline{u^2(d)} \propto \varepsilon^{2/3} d^{2/3} \qquad L \gg d \gg \eta \qquad 7.2$$

The dissipation rate, ε, is a local quantity which varies enormously throughout an agitated vessel. Cutter has shown that ε varies 280 fold from a region near the impeller tip to regions outside the impeller stream (12). Although the spacial variation of ε is not fully understood, it has been shown that for Reynold's numbers ($\rho ND^2/\mu$) greater than about 5×10^3 in well baffled agitated tanks the rate of energy input of the mixing impeller per unit mass of vessel contents, $\bar{\varepsilon}$, is independent of the properties of the liquid and a function only of the geometric design of the agitator and its speed (40). Thus:

$$\bar{\varepsilon} = KN^3 D^2 \qquad 7.3$$

where N is the agitator speed and D is its diameter. K is a dimensionless constant.

It has also been shown that the velocity distribution in well-

Reproduced with permission of the copyright owner. Further reproduction prohibited without permission.

baffled mixing vessels is universal (12, 41, 43). That is, the ratio of the average flow velocities at any two points is constant. Thus:

$$\epsilon = K'(r, z, \Phi)\, N^3 D^2 \qquad 7.4$$

where K'is a function of the co-ordinates, r, z , ϕ , of any point in the vessel.

7.2 Regions of Breakage and Coalescence

All drops of a certain size in our system behave differently because, (1), their coalescence and breakage processes are governed by random statistical laws, and, (2), the forces associated with these processes are distributed within the vessel, i.e., the velocity or ϵ - field is inhomogeneous as described by equation 7.4. In order to simplify the mathematics of analysis we will speak of breakage and coalescence regions in which we have spacial homogeneity. In this way the variance of a given breakage or coalescence process will be a result of random statistical behavior only. The simplest such assumption is to say that the energy dissipation is spacially homogeneous throughout the tank. With this, one is restricted to saying that breakups and coalescences are as equally likely near the impeller as near the walls. It has been described, however, that this is not the case (12, 43). Breakage most likely occurs near the impeller tip and coalescence in less intense regions. A better assumption would be to say there are two regions, one around the impeller tip where break-up is exclusively occurring and the other (the rest of the tank) where coalescences alone are happening. In each region we will say that there is a homogeneous energy dissipation field. Thus from

Reproduced with permission of the copyright owner. Further reproduction prohibited without permission.

equation 7.4:

$$\epsilon_b = K_b' (r, z, \Phi) N^3 D^2 \qquad 7.5$$

and

$$\epsilon_c = K_c' (r, z, \Phi) N^3 D^2 \qquad 7.6$$

where ϵ_b and ϵ_c are the energy dissipation rates per unit mass for the breakage and coalescence regions.

7.3 Breakage Model

Although much research has been carried out concerning the size of the maximum or average drop in an agitated tank, no work has considered the rate laws governing the breakage process. As mentioned, preliminary work with the data and the general mixing equations indicates that the breakage and coalescence rates are very strong functions of the agitator speed with the rates varying as N^{4-7} under some conditions. This observation, which suggests an "Arrhenius" type of mechanism, and the obvious parallels between a drop breaking up and a molecule decomposing makes an analogy irresistible. In both cases there is a bound energy associated with the reactant, for drops this energy being represented by the surface energy. Both types of processes are associated with an energy field responsible for reaction. In the case of molecules this is the thermal energy. For drops it is turbulent energy. The essential feature of the reaction theory is the postulation of an activated complex, which is an unstable intermediate formed from the reactant and decomposing into products. A further assumption is that this

Reproduced with permission of the copyright owner. Further reproduction prohibited without permission.

activated complex is in equilibrium with the reactant. This idea of an equilibrium activation step followed by a slow reaction is equivalent to assuming a time lag between activation and final decomposition. For the decomposition of a molecule the rate of reaction (for a first order reaction) is derived as:

$$r_A = \frac{k'T}{h} \; e^{-\frac{\Delta F^*}{RT}} \cdot n_A \qquad 7.7$$

where ΔF^* is the standard free energy of activation, R, k', h are established constants and n_A is the number of reactant molecules A.

It is proposed, as a first approximation, that the break-up of drops in a turbulent field can be described by the above reaction theory. A drop travelling in a turbulent flow is exposed to local pressure fluctuations. One can assume that the drop is oscillating with the surrounding field, to an extent depending upon the intensity of the turbulence, the size and surface energy of the drop and the density difference between drop and fluid. This "normal" drop will become unstable (or activated) if the kinetic energy is sufficient to make up the difference in surface energy between the single drop and the smaller drops formed on break-up. The unstable or "activated" drop will either be sheared to form smaller drops or by further flow and/or collision with other drops return to the "normal" state. If it is assumed that the activated drops are in equilibrium with the normal drops, then transition-state theory is applicable.

Consider drops of diameter d in the breakage region of the

Reproduced with permission of the copyright owner. Further reproduction prohibited without permission.

agitated vessel. The break-up of these drops can be described schematically as:

$$\begin{pmatrix}\text{Normal}\\ \text{Drops}\end{pmatrix} \rightleftharpoons \begin{pmatrix}\text{activated or}\\ \text{unstable drops}\end{pmatrix} \xrightarrow{k''} \begin{pmatrix}\text{breakage}\\ \text{product}\end{pmatrix} \qquad 7.8$$

where the normal drops are in equilibrium with the unstable drops and k'' is the rate constant for the decomposition or break-up process. The rate of breakage, $r_b(d)$ is:

$$r_b(d) = \begin{pmatrix}\text{number of}\\ \text{activated drops}\end{pmatrix} \cdot \begin{pmatrix}\text{rate of decomposition}\\ \text{of activated drop}\end{pmatrix} \qquad 7.9$$

or:

$$r_b(d) = k''.\ K^{*} \cdot n_b \qquad 7.10$$

where K^{*} is the equilibrium constant for the normal-activated drop exchange and n_b is the number of normal drops of diameter d in the breakage region. From the reaction theory:

$$K^{*} = \exp\left(-\frac{\text{Activation Energy}}{\text{Kinetic Turbulent Energy}}\right) \qquad 7.11$$

The kinetic turbulent energy trying to break up the drop is proportional to $\frac{\pi}{6} \cdot d^3 \cdot \rho \cdot E$ where:

$$E = \int_{1/d}^{\infty} E(k)\, d\, k \qquad 7.12$$

Reproduced with permission of the copyright owner. Further reproduction prohibited without permission.

Only energies associated with fluctuations of a scale smaller than d are considered because larger eddies would presumably only carry the droplet along with it without breaking it. Combining equations 7.12 and 7.1 and integrating we get:

$$\text{Kinetic Turbulent Energy} \propto \rho \frac{\pi}{6} d^3 \; E \propto \rho \, \varepsilon^{2/3} \, d^{11/3} \qquad 7.13$$

The same result can be obtained by considering the kinetic energy to be proportional to $\rho \overline{u^2} d^3$. The mean-square velocity across diametrically opposite points on the surface of the droplet is taken from equation 7.2.

The activation energy is related to the difference in surface energy between the normal and activated drop.

Let us assume for the time being that this energy is only proportional to the size of the drop breaking up (and not a function of the number and distribution of product drops). Then:

$$\text{Activation Energy} \propto \sigma d^2 \qquad 7.14$$

where σ is the interfacial tension.

It is reasonable to suppose that the rate of decomposition of the activated drop is a function of the rate of shear of the drop. Thus:

$$k'' \propto \frac{\text{energy input per unit time}}{\text{kinetic turbulent energy}} \qquad 7.15$$

From equation 7.13 and 7.15 we get:

Reproduced with permission of the copyright owner. Further reproduction prohibited without permission.

$$k'' \propto \frac{\rho \cdot \pi/6 \cdot d^3 \varepsilon}{\rho \cdot \pi/6 \cdot \varepsilon^{2/3} \cdot d^{11/3}} \propto \varepsilon^{1/3} d^{-2/3} \qquad 7.16$$

Combining equations 7.10, 7.11, 7.13, 7.14, and 7.16 and taking $\varepsilon = \varepsilon_b$ from equation 7.5 the breakage rate in the breakage region is:

$$r_b(d) \propto ND^{2/3} d^{-2/3} \exp\left(\frac{-k_1}{\rho N^2 D^{4/3} d^{5/3}}\right) \cdot n_b \qquad 7.17$$

and the breakage rate (drops/time) in the whole tank is:

$$r_b(d) = k_2 ND^{2/3} d^{-2/3} \exp\left(-\frac{k_1}{\rho N^2 D^{4/3} d^{5/3}}\right) \cdot n_d \qquad 7.18$$

where n_d is the number of drops of diameter d in the whole vessel and k_1 and k_2 are dimensionless constants. This may be written as:

$$r_b(d) = k_2 N \left(\frac{D}{d}\right)^{2/3} \exp\left(-k_1 N_{we}^{-1} \left[\frac{D}{d}\right]^{5/3}\right) \cdot n_d \qquad 7.19$$

where Nwe is the Weber number, $N^2 D^3 \rho / \sigma$.

It is seen that at a given agitator speed, very large drops will break up relatively quickly down to a size (d_{max}, let us say) where the breakage rate equals some arbitrarily low value close to zero. This size is a function of agitator speed or Weber number as shown in equation 7.18 and 7.19, and is dominated by the behavior of the exponential function.

Reproduced with permission of the copyright owner. Further reproduction prohibited without permission.

$$d_{max} \propto N^{-6/5} \qquad 7.20$$

and:

$$\frac{d_{max}}{D} \propto N_{we}^{-0.6} \qquad 7.21$$

7.4 Coalescence Model

Several researchers have found that in systems where the drop-size distribution is primarily a function of the coalescence process, the drop size is correlated with agitator speed as $N^{-3/4}$ (22, 38, 44, 48). Shinnar was the first to explain this dependency in terms of an adhesion process. Shinnar claimed that droplets in a dispersion adhere to each other and will coalesce in time unless turbulent fluctuations communicate sufficient energy to the droplets to cause re-separation. On this basis he has proposed the existence of a "turbulence-stabilized" dispersion where the turbulent forces, independent of the cohesive forces, predominate and coalescence is prevented. He experimentally confirmed the existence of such dispersions.

Although Shinnar had not defined what these cohesive forces are, presumably they are the forces of molecular attraction which can cause the aggregation of smoke and other colloidal-sized particles (6). Such forces are known to be of very short range and can be considered insignificant in relation to other forces acting on drops in turbulent dispersions.

It will be shown here that the $d \propto N^{-3/4}$ relationship and

Reproduced with permission of the copyright owner. Further reproduction prohibited without permission.

the concept of "turbulence-stabilized" dispersions can be derived from hydrodynamic considerations alone.

(a) Derivation of τ/t' Model

In describing coalescences in an agitated dispersion one speaks of a collision followed by a coalescence. The use of the word collision, suggesting a violent crash, may be a misnomer. This is perhaps proper for gas kinetics but to suggest that such a contact is a necessary prelude for coalescence is unjustified. In developing a theory of coalescence, Hesketh has done just that, claiming that coalescence occurs whenever the relative velocity along the centre line on collision exceeds a critical value (20). This is in total contradiction to the experimental findings of Shinnar. With this theory, in addition, one would expect coalescence to be more probable near the intense region of the impeller. This is also not the case (48).

It is reasonable to say that there is a vast range of collision types in an agitated dispersion. The collisions near the impeller (where drop breakage is probable) are undoubtedly intense and involve oscillating drops. These collisions are relatively short-lived because of this intensity. Bouncing effects are probably pronounced. Leng and coworkers have described similar collisions (42). On the other hand, the collisions near the walls and away from the impeller are less intense, involve more non-oscillating drops, have longer contact times and result in fewer bounces.

In any case, a collision can be viewed as the approach of two drops within a centre-line distance of their radii sum. These drops stay together for some time, following which they separate or

Reproduced with permission of the copyright owner. Further reproduction prohibited without permission.

coalesce. The event of a drop resting on a liquid-liquid surface is such that a coalescence is inevitable; this is not the case for the event of a collision between two drops in an agitated vessel.

Let us consider the probability of coalescence for a given collision as being a function of two independent random variables, τ , the coalescence time, the time required for coalescence upon collision, and, t' , the contact time, which is defined as the time upon collision that the drops would remain together if coalescence were prevented. One can think of t' as being the measurable time the drops would stay together if a hypothetical surfactant, which does not interfere with the system hydrodynamics, were added to the drops to prevent coalescence.

Let us say that for a given collision the coalescence time is distributed normally, as is the case for drops on a liquid-liquid surface (9). The probability density function is

$$p(\tau) = \frac{1}{\sqrt{2\pi}\cdot\sigma_\tau} \exp\left\{ -\frac{1}{2\sigma_\tau^2}\cdot(\tau - \bar{\tau})^2 \right\} \qquad 7.22$$

where σ_τ = standard deviation of coalescence time and $\bar{\tau}$ = average coalescence time.

We define the probability of coalescence, given a contact time t', as being the probability that the coalescence time, τ, is equal to or less than t', the contact time. Thus:

$$p(\text{coal}|t') = p(\tau \leq t')$$

and

Reproduced with permission of the copyright owner. Further reproduction prohibited without permission.

$$p\ (\tau \leq t') = \int_{-\infty}^{t'} N\left(\frac{t'' - \bar{\tau}}{\sigma_\tau}\right) dt'' = \Phi\left(\frac{t' - \bar{\tau}}{\sigma_\tau}\right) \qquad 7.23$$

The probability of coalescence is then,

$$p\ (\text{coal}) = \int_0^\infty p\ (\text{coal},\ t')\ dt' = \int_0^\infty p\ (\text{coal}/t')\ p(t')\ .\ dt' \qquad 7.24$$

where $p(t')$ is the contact-time distribution (p · d · f), which must be estimated.

When two drops are together in a turbulent field, the pressure or velocity fluctuations across the droplet-pair will vary in such a way as to force the drops together at one moment and separate them at the next. The time the drops stay together under the influence of these velocity fluctuations can be described as a random variable.

For a droplet-pair that has survived to time t', let the conditional probability of separation in the next interval of length, $\Delta t'$, be approximately $c' \cdot \Delta t'$ for small $\Delta t'$. Then the probability of survival until time t' and separation in the succeeding interval $\Delta t'$ is:

$$\left[1 - P\ (t')\ \right] c' \cdot \Delta t'$$

where P(t) designates the cumulative distribution function. This probability is also equal to $p(t')\ \Delta t'$. Thus:

$$c'\left[1 - P\ (t')\right] = p(t') = \frac{dP(t')}{dt'} \qquad 7.25$$

Reproduced with permission of the copyright owner. Further reproduction prohibited without permission.

Solving 7.25 with appropriate limits, we get:

$$p\ (t') = c' . e^{-ct'} \qquad 7.26$$

and for an average contact time of $\bar{t}'$ we have:

$$p\ (t') = \frac{1}{\bar{t}'} . e^{-\frac{t'}{\bar{t}'}} \qquad 7.27$$

This is the classic exponential or "waiting time" distribution.

Combining equation 7.27 with equation 7.24, the probability of coalescence for a given collision is:

$$p\ (\text{coal}) = \int_o^\infty \frac{1}{\bar{t}'} e^{-\frac{t'}{\bar{t}'}} . \Phi\left(\frac{t' - \bar{\tau}}{\sigma_\tau}\right) \ . \ dt' \qquad 7.28$$

After integration this becomes:

$$p\ (\text{coal}) = \frac{1}{2}\ e^{-\frac{\bar{\tau}}{\bar{t}'}} . e^{\frac{1}{2}\frac{\sigma_\tau^2}{\bar{t}'^2}} . \operatorname{erfc}\left(\sqrt{\frac{2}{2}}\ \frac{\sigma_\tau^2 - \bar{\tau}\bar{t}'}{\bar{t}' \cdot \sigma_\tau}\right) \qquad 7.29$$

The following is an example of the type of assumptions and simplifications made throughout this work. Equation 7.29 indicates that the probability of coalescence, for a given σ_τ , decreases as $\bar{\tau}/\bar{t}'$ increases until at $\bar{\tau}/\bar{t}' \to \infty$, it becomes negligible. Since nothing is known of σ_τ , the simplest assumption to make is that $\sigma_\tau = 0$, i.e., the coalescence time is not distributed, although contact time remains a random variable. Thus

Reproduced with permission of the copyright owner. Further reproduction prohibited without permission.

$$p\ (\text{coal}) = e^{-\bar{\tau}/\bar{t}'} \qquad 7.30$$

The assignment of randomness entirely to contact time retains the statistical character of coalescence but simplifies 7.29 into a relatively convenient form (7.30).

(b) Model for Approach of Two Drops

The event of two drops coalescing with each other is similar to that of a drop coalescing at a flat interface. Several models describing the rate of thinning of the intervening film between a liquid drop and a flat liquid-liquid interface have been derived in the literature. Chappelear (8) has discussed the following models: (1), the spherical-planar approach where neither the drop nor the plane deforms, (2), the parallel-disc approach where the drop flattens until its weight is supported by its internal pressure, (3), the rigid drop-deformable interface approach, and, (4), the approach of a deformable drop to a deformable interface. (See figures 7.1 a to d) Chappelear has shown that the equations describing Models 2, 3, and 4 are identical for small deformations except for numerical constants. The equation for Model 2 has been derived by several researchers (9, 14, 25, 28, 35).

At equilibrium the drop whose shape is that shown in figure 7.1b has an excess pressure, Δp , inside which balances the force, F, on the interface,

$$F = \Delta p \cdot \pi c^2 \qquad 7.31$$

Reproduced with permission of the copyright owner. Further reproduction prohibited without permission.

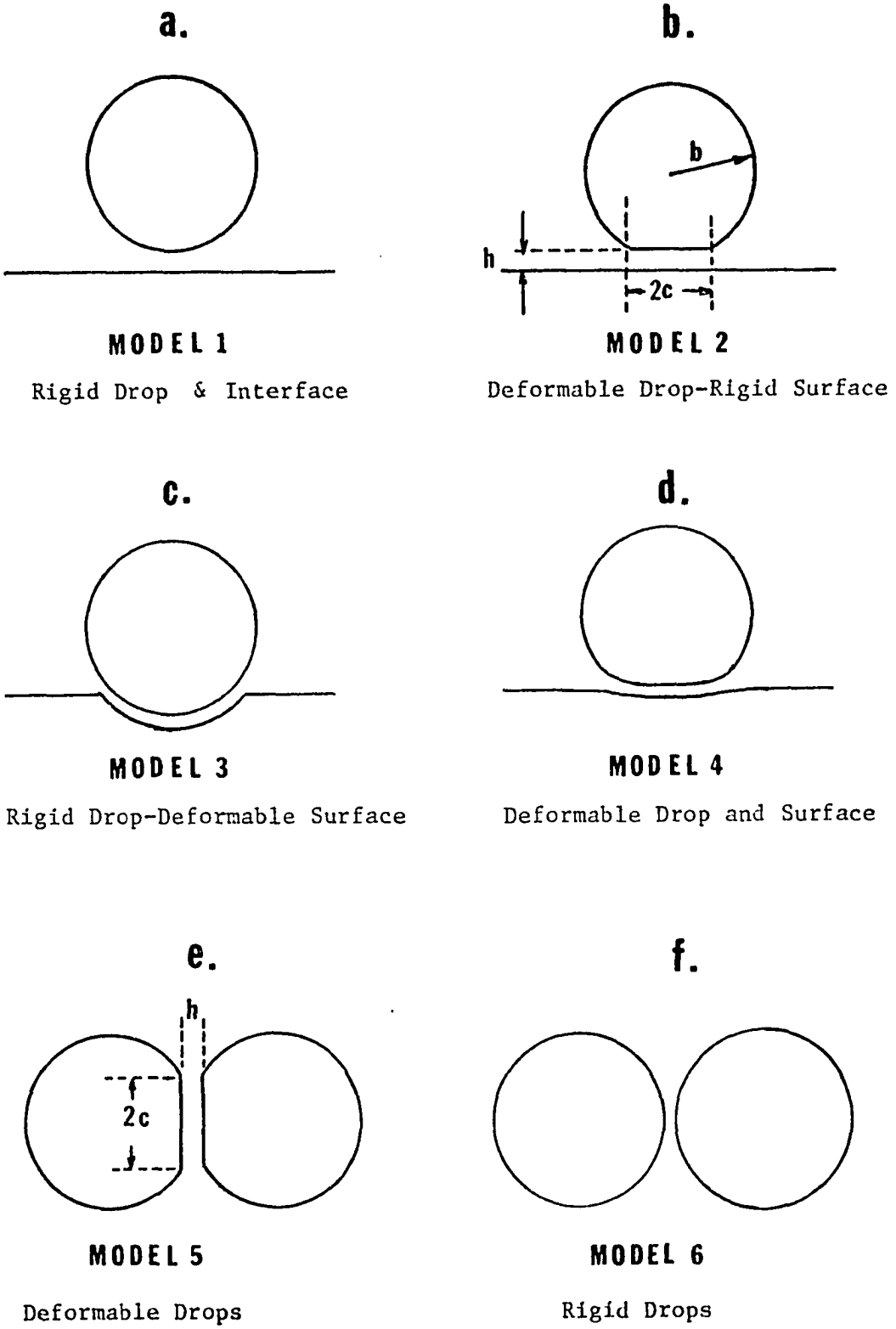

Fig. 7.1 Coalescence Models

Reproduced with permission of the copyright owner. Further reproduction prohibited without permission.

where c is the disc radius. By carrying out a volume balance before and after compression and relating the excess internal pressure to the interfacial tension and geometry of the resting drop, for small deformations the force becomes:

$$F = \frac{2\pi\sigma}{b} \cdot c^2 \qquad 7.32$$

where b is the drop radius, and σ is the interfacial tension.

As the drop rests on the interface, the continuous phase drains away from between the approaching drop and the bulk interface. Reynold's equation describing the drainage between two parallel rigid discs is generally accepted as being applicable to this process, (9, 36). This equation is:

$$-\frac{dh}{dt} = \frac{2F}{3\pi\mu c^4} \cdot h^3 \qquad 7.33$$

or, expressed in another form by substituting for c from equation 7.32:

$$-\frac{dh}{dt} = \frac{8\pi\sigma^2}{3\mu F b^2} \cdot h^3 \qquad 7.34$$

where h = the distance between discs and μ = viscosity of draining fluid.

Princen has pointed out two important complications which

Reproduced with permission of the copyright owner. Further reproduction prohibited without permission.

may arise which upset the validity of equations 7.33 or 7.34 (35):

(a) The approaching interfaces are not resistant to the normal stresses which exist in the draining film owing to the radial pressure gradient. Consequently the interfaces will not be quite parallel.

(b) The interfaces are not generally resistant to tangential stresses which also exist during drainage. This means the interfaces are moving, with a consequent increase in the drainage rate.

Factor (a) is relatively unimportant in systems with a low value of c (high interfacial tension and small density difference). Factor (b) is negligible in systems where the interfaces have high interfacial rigidity or viscosity.

Most researchers who have found their system not to be well correlated by equation 7.33 have suggested that these factors are indeed the reason for the discrepancy. In our system, because the oil and water phases are not exceptionally "clean" it is probable that there is no interfacial movement. Mason has found this for moderately impure systems (4). In addition, it is supposed that the drops colliding away from the intense impeller region do not deform appreciably. Consequently, Reynolds' equation will be used, as a first approximation, to describe the rate of approach.

From the integration of equation 7.34, the time required for the disc to approach the plane surface from a distance h_o to h_c where coalescence takes place becomes:

$$\bar{\tau} = \frac{3}{16} \cdot \frac{\mu F}{\pi \sigma^2} \cdot \left[\frac{1}{h_c^2} - \frac{1}{h_o^2} \right] b^2 \qquad 7.35$$

Reproduced with permission of the copyright owner. Further reproduction prohibited without permission.

Chappelear (8) has shown that equation 7.35 is applicable for a rigid drop approaching a deformable surface, for small deformation. He has also shown that the approach time for the more realistic case of a deformable drop and deformable surface, for small deformation, can be described by equation 7.35 except for the numerical constant (3/4 rather than 3/16). It is proposed, although it has not been formally derived, that the approach of two deformable drops in a liquid medium has the following form.

$$\bar{\tau} = \frac{3}{4} \cdot \frac{\mu F}{\sigma^2 \pi} \cdot \left[\frac{1}{h_c^2} - \frac{1}{h_o^2} \right] \left[\frac{b_1 \cdot b_2}{b_1 + b_2} \right]^2 \qquad 7.36$$

Thus for $b_1 = b_2$ equation 7.36 becomes identical to equation 7.35. For $b_1 \gg b_2$, equation 7.36 becomes identical to the case for a deformable drop - deformable surface.

The net force F compressing the drops together is taken by dimensional reasoning and assumption to be:

$$F \propto \rho_d \cdot \bar{u}^2 \cdot \left(\frac{d_1 \cdot d_2}{d_1 + d_2} \right)^2 \qquad 7.37$$

where d_1 and d_2 are the drop diameters, ρ_d is the drop density, and $\bar{u}^2$ is the mean-square relative velocity between the two drops. Note, as in 7.36, that for $d_1 \gg d_2$, $F \propto d_2^2$. Combining equation 7.37 and 7.36, the coalescence time becomes:

$$\bar{\tau} \propto \frac{f(h_o, h_c) \cdot \mu \cdot \rho_d \cdot \bar{u}^2}{\sigma^2} \left(\frac{d_1 \cdot d_2}{d_1 + d_2} \right)^4 \qquad 7.38$$

where $f(ho, hc) = \frac{1}{h_c^2} - \frac{1}{h_o^2}$

(c) Coalescence Efficiency

Reproduced with permission of the copyright owner. Further reproduction prohibited without permission.

By dimensional reasoning and assumption the average contact time can be taken to be:

$$\bar{t}' \propto \frac{d_1 + d_2}{\bar{u}} \qquad 7.39$$

and from equation 7.2 the mean-square velocity between drops of diameter d_1 and d_2 is:

$$\bar{u}^2 \propto \varepsilon^{2/3} (d_1 + d_2)^{2/3} \qquad 7.40$$

Combining equations 7.30, 7.38, 7.39, and 7.40, the probability of a coalescence for a given collision between two drops of diameter d_1 and d_2 in a constant ε - field becomes:

$$p\ (\text{coal}) = \exp\left\{ - \frac{k''' \cdot f\ (h_o, h_c) \cdot \mu \cdot \rho_d \cdot \varepsilon}{\sigma^2} \cdot \left(\frac{d_1\ d_2}{d_1 + d_2} \right)^4 \right\} \qquad 7.41$$

where k''' is a dimensionless constant.

(d) Coalescence Rate

It remains to determine the collision frequency between drops of diameters d_1 and d_2 in the agitated vessel. For lack of information regarding collision rates of dispersions in turbulence, the binary collision frequency is taken to be simply,

Reproduced with permission of the copyright owner. Further reproduction prohibited without permission.

$$h\ (d_1,\ d_2) \propto \quad \varepsilon^{1/3}\ (d_1 + d_2)^2 \qquad 7.42$$

No support can be given for the above equation except to say that drop collisions may be proportional to the collision cross-section of the drops and to the rms velocity of the drops, which Cutter has shown to be proportional to $\varepsilon^{1/3}$ (12).

Combining equations 7.41, 7.42 and 5.14, and taking $\varepsilon = \varepsilon_c$ from equation 7.6, the coalescence rate becomes:

$$r_c\ (d_1,d_2) = k_4 \cdot N \cdot (d_1+d_2)^2 \cdot e^{\left\{ - k_3 \cdot N^3 \cdot \left(\frac{d_1\ d_2}{d_1+d_2} \right)^4 \right\}} n_1 \cdot n_2 \qquad 7.43$$

where n_1 and n_2 are the numbers of drops of diameter d_1 and d_2 respectively and k_3 and k_4 are constants = f(ho, hc, μ, ρd, σ, D).

Equation 7.43 has desirable properties. For simplicity, consider the case of $d_1 = d_2$. Then:

$$r_c\ (d,d) = 4\ k_4\ N\ d^2\ e^{-\left(\frac{k_3}{16}\ N^3\ d^4\right)} \cdot n^2 \qquad 7.44$$

It is seen that if the coalescence efficiency is not unity, i.e., all collisions do not result in coalescences, then the exponential component of equation 7.44 will predominate. In words, the equation indicates that for a given drop size the coalescence rate decreases with increasing agitator speed. This is due to the paradoxical phenomenon explained in the development of the theory, i.e.,

Reproduced with permission of the copyright owner. Further reproduction prohibited without permission.

the harder the drops are forced together, the more they will deform, the larger will be the interfacial disc between the compressed drops and the longer will be the drainage time. Hence the coalescence rate decreases with an increase in agitation for a given drop size. This explains the concept of "turbulence-stabilized" dispersions. Shinnar formed a dispersion at a high agitator speed in which no coalescences were occurring. He then lowered the agitator speed and found a substantial amount of coalescing taking place. This observation can be explained as follows: the relatively intense collision at the higher agitator speed creates a large disc volume of continuous phase separating the colliding drops. This volume does not have time enough to drain sufficiently in the contact time provided to lead to coalescence. This is not the case at the lower agitator speed. Not only is the disc volume smaller but the contact time is higher; consequently, coalescences are more probable.

Equation 7.43 or 7.44 also explains another observation found by others. It is seen that at a given agitator speed, very small drops will coalesce relatively quickly up to a size (d_{min}, let us say) where the coalescence rate equals some arbitrarily low value close to zero. This size is a function of agitator speed as shown in equation 7.44:

$$d_{min} \propto N^{-3/4} \qquad 7.45$$

We will now show that equation 7.43 combined with equation 7.18 which describes the breakage rate can also explain the experimental observation that ω, the coalescence frequency, increases

Reproduced with permission of the copyright owner. Further reproduction prohibited without permission.

greatly with an increase in agitator speed.

For simplicity in this discussion, consider that the drops are of equal size, $d_1 = d_2$ (equation 7.44) and that the drops available for coalescence are those provided by the rapid breakup of drops in the vessel. This is the case for very low coalescence frequencies compared to breakage frequencies. Then from equation 7.18 the drop size available is, $d \propto N^{-6/5}$. Using this value in equation 7.44 and taking $n = \frac{V_T \theta}{\frac{\pi}{6} d^3}$ (V_T = volume of tank; θ = phase fraction), we get

$$\text{coalescence frequency} = k_4' N^{2.2} \; e^{-\frac{k_3'}{N^{9/5}}} \qquad 7.46$$

where coalescence frequency = coalescence rate/n.

Thus the coalescence frequency increases dramatically for increasing N until it levels off as $N^{2\cdot2}$. It should be emphasized, however, that the drops available for coalescence are determined by the dynamic equilibrium of the break-up and coalescence processes together.

(e) The Case for Rigid Drops

It is interesting to note briefly what the coalescence probability would be if the rigid-drop-rigid drop model (figure 7.1f) were considered. The rate of approach for two drops of diameter d_1 and d_2 is derived as:

$$-\frac{dt}{dh} = \frac{6\pi\mu}{F \cdot h} \cdot \left(\frac{b_1 b_2}{b_1 + b_2}\right)^2 \qquad 7.47$$

Reproduced with permission of the copyright owner. Further reproduction prohibited without permission.

or by integration:

$$\overline{\tau} = \frac{6\pi\mu}{F} \cdot \left(\frac{b_1 b_2}{b_1+b_2}\right)^2 \ln \frac{h_o}{h_c} \qquad 7.48$$

By making the suitable substitutions (equations 7.6, 7.30, 7.37, 7.39, 7.40) an analogue to equation 7.43 is derived as:

$$p(\text{coal})_{\text{rigid drops}} = e^{-\frac{\text{constant}}{N (d_1 + d_2)4/3}} \qquad 7.49$$

This does not have the form necessary to explain Shinnar's or the experimental results of this thesis. However, note the $d \propto N^{-3/4}$ dependency.

(f) Effect of Phase Fraction

In the development of the equations describing the breakage and coalescence processes no account was taken of the effect of "packing". It was assumed that the forces causing break-up and coalescences were not affected by the number of drops or the amount of dispersed phase in the vessel. It will be shown in later chapters, however, that a consideration of this effect helps to explain the experimental results.

The behavior of a swarm of droplets in a turbulent fluid depends largely on their concentration and on the size of the droplets with respect to the scale of turbulence of the fluid. At great concentration the relative motion of the particles with respect to the fluid undoubtedly causes, via the creation of additional turbulence, extra dissipation of the kinetic energy of the turbulent fluid. The extreme case of this occurs at the maximum packing con-

Reproduced with permission of the copyright owner. Further reproduction prohibited without permission.

centration where Bagnold has found that the turbulence motion is almost entirely damped even though the particles still exhibit appreciable normal and shear stresses (3).

It is likely that the coalescence process will be more affected by this attenuation of the turbulent fluctuations than the breakage process because the latter is taking place near the source of a constant energy supplier and the former occurs away from this source where total damping is possible.

It is proposed that the velocity fluctuations responsible for the coalescence and breakage processes are dependent on phase fraction, to a negligible extent as θ approaches zero and to a large extent as θ approaches the maximum packing concentration. We will describe this dependency as a simple function, thusly:

$$\bar{u}_{\theta} = (1 + k_c \theta)^{-1} \bar{u}_{\theta = 0} \qquad 7.50$$

for coalescence, and

$$\bar{u}_{\theta} = (1 + k_B \theta)^{-1} \bar{u}_{\theta = 0} \qquad 7.51$$

for breakage where k_c and k_B are dimensionless constants and $k_c > k_B$.

Using these values of $\bar{u}_{\theta}$ rather than $\bar{u}_{\theta = 0}$, equations 7.18 and 7.43 become:

$$r_B (d) = \frac{k_2 D^{2/3} d^{-2/3} N}{(1 + k_B \theta)} \cdot \exp \left[- \frac{k_1 (1 + k_B \theta)^2}{N^2 D^{4/3} d^{5/3}} \right] \cdot n_d \qquad 7.52$$

Reproduced with permission of the copyright owner. Further reproduction prohibited without permission.

and:

$$r_c\ (d_1,d_2) = \frac{k_4\ N\ (d_1 + d_2)^2}{(1 + k_c\theta\ )} \exp\left(- \frac{k_3\ N^3}{(1+k_c\theta\ )^3} \left[\frac{d_1\ d_2}{d_1+d_2}\right]^4 \right) \cdot n_1 n_2$$

7.53

Reproduced with permission of the copyright owner. Further reproduction prohibited without permission.

CHAPTER 8

OPERATION OF FUNCTIONS IN MIXING EQUATION

As mentioned in Chapter 6, various models and functions were examined in this study. In this chapter, only the models that were derived in the previous chapter are discussed. The purpose here is to describe the general behavior of these models in the mixing equation. Their more specific behavior, vis-a-vis their ability to fit the experimental results, is given in the next chapter.

8.1 Description of Functions

The theoretical drop-size distributions and mixing rates obtained by the use of the mixing equation are dependent not only on the form of the chosen functions but also on the parameters associated with them. Early in the study, polynomial functions were chosen which contained numerous constants that were physically meaningless. The physical models described in the previous chapter, have associated with them parameters which have physical meaning. Some of the parameters are easily measurable. These include the liquid properties of viscosity, density and interfacial tension. Others are nearly impossible to experimentally determine. These include the film thickness at coalescence, h_c, and the dimensionless constants related to the description of turbulence. For a given system, all these parameters are constant. These parameters are combined to make up the

Reproduced with permission of the copyright owner. Further reproduction prohibited without permission.

constants in the mixing functions.

(a) Breakage and Coalescence Frequency Functions

The models developed earlier to describe the breakage and coalescence rates, for the case of low phase fraction, are relatively simple. The coalescence rate equation contains two constants to be determined. One of these is related to the collision frequency and the other to the coalescence efficiency. Similarly the breakage rate equation contains two constants, one related to the fraction of droplets that are "activated" or unstable, and the other related to the rate of decomposition of the unstable drop.

The breakage frequency is taken from equation 7.18. In terms of diameter it is:

$$g(d) = k_2 \, N \, D^{2/3} \, d^{-2/3} \exp\left[\frac{-k_1}{N^2 \, D^{4/3} \, d^{5/3}}\right] \qquad 7.18$$

or in terms of volume, grouping constants, it is:

$$g(v) = c_2 \, N \, v^{-2/9} \exp\left[\frac{-c_1}{N^2 \, v^{5/9}}\right] \qquad 8.1$$

The coalescence rate is given in 7.43 as:

$$h(d_1,d_2)\,\lambda(d_1,d_2)n_1n_2 = k_4 \, N(d_1+d_2)^2 \, e^{-k_3 N^3 \left\{\frac{d_1 \, d_2}{d_1+d_2}\right\}^4} n_1n_2 \qquad 7.43$$

Reproduced with permission of the copyright owner. Further reproduction prohibited without permission.

where n_1 and n_2 are the numbers of drops of sizes d_1 and d_2. In terms of volume, this becomes:

$$h(v_1,v_2)\,\lambda(v_1,v_2)n_1n_2 = c_4 \cdot N\left[v_1^{1/3} + v_2^{1/3}\right]^2 \cdot e^{-c_3N^3\left\{\frac{v_1^{1/3}\cdot v_2^{1/3}}{v_1^{1/3}+v_2^{1/3}}\right\}^4} \cdot n_1n_2 \qquad 8.2$$

The coalescence frequency of a drop of size v_1 with drops of size v_2 is then $h(v_1, v_2) \cdot \lambda(v_1, v_2)\, n_2$.

(b) Breakage Distribution Function

In addition to the above functions one must have some knowledge of the distribution of the drops formed on the breakup of a larger drop. At one extreme it can be proposed that a droplet breaks up into two drops of about equal size. At the other extreme one can postulate that a droplet is "shattered" into numerous small droplets distributed in a uniform manner. Mathematically, these possibilities are described by $\nu(v')$ the average number of droplets formed on the breakage of a drop of volume v', and $\beta(v|v')$ the breakage kernel. This function is simply the probability density function for the distribution of drops formed on the breakup of a drop of size v' into ν (on the average) smaller drops.

Several distribution forms were assumed for the breakage kernel, β :

(1) a normal distribution, (2) a beta distribution and (3) volume and number uniform distributions. The beta distribution has the advantage over the symmetrical normal distribution in that it can be used for $\nu > 2$, and in that $\beta(v|v') = 0$ for $v < 0$ and $v > v'$.

Reproduced with permission of the copyright owner. Further reproduction prohibited without permission.

$$\beta(v|v') = \frac{\Gamma(a + a' + 2)}{\Gamma(a+1)\ \Gamma(a'+1)} \cdot \frac{1}{v'} \left[\frac{v}{v'}\right]^{a} \left[1 - \frac{v}{v'}\right]^{a'} \qquad 8.3$$

where Γ is the gamma function and a and a' are constants related to ν by:

$$a = (a' + 2 - \nu) \ / \ (\nu - 1) \qquad 8.4$$

The variance of the distribution is:

$$\sigma_{\beta}^{2} = \frac{\Gamma(a + a' + 2)\ \Gamma(a + 3)}{\Gamma(a + a' + 4)\ \Gamma(a + 1)} - \frac{1}{\nu} \qquad 8.5$$

For $\nu = 2$, it is seen then the function becomes symmetric and a = a'.

(c) Effluent Frequency and Feed Distribution Functions

The escape frequency, f (v), in all of the numerical work was assumed to be independent of drop size and simply equal to

$$f(v) = \frac{1}{T} \qquad 8.6$$

where T is the residence time. This is a reasonable assumption based on perfect macroscopic mixing.

As mentioned in Chapter 3, experimentally it was not possible to keep the input drop size constant because of the fluctuations of the input flows. To account for this, the p.d.f. of the feed

Reproduced with permission of the copyright owner. Further reproduction prohibited without permission.

drop volumes was taken to be Gaussian:

$$a(v) = \frac{1}{\sigma_o \sqrt{2\pi}} \cdot \exp \left\{ - \frac{(v - v_o)^2}{2 \sigma_o^2} \right\} \qquad 8.7$$

with v_o being the average drop size and σ_o being the standard deviation.

8.2 Numerical Techniques

Equations 5.17 - 5.19 were used to solve numerically the integro-differential equation 5.15. The computer program for doing this is available in Appendix III. The program reads into the computer the constants that are associated with the mixing functions and the characteristics of the system: the input flow and drop size, the vessel volume, the agitator speed and phase fraction. The number of integration intervals is set at 100 to 250 depending on the accuracy desired. Then the program calculates the drop size distribution for the case of breakage alone, using equation 5.23. The total volume of dispersed phase is calculated using this distribution and compared to the actual volume. If there is any volume "lost" during the integration, the calculated distribution is normalized proportionately. In most cases the difference between actual and calculated volume was not allowed to be more than 5% (the size of the integration interval determines this error). This distribution is then used as the starting case for the solution of the breakage-and-coalescence equation, which must be solved iteratively. The numerical scheme is described in Chapter 5. After each iteration the distribution is printed, nor-

Reproduced with permission of the copyright owner. Further reproduction prohibited without permission.

malized to account for "lost volume" and compared to the distribution calculated in the previous iteration. If they are the same (taken to be within one-tenth to one-half of 1%), the iterations are stopped. The computer output contains (1) a volume-volume density distribution, (2) a number-volume density distribution, (3) a diameter-volume density distribution, (4) breakage and coalescence frequency plots, (5) the "size" statistics, v_{10}, v_{21}, and d_{32}, and (6) the mixing frequencies ω_n, ω_v and ω_m.

8.3 Behavior of Functions

In trying to understand qualitatively what is happening to a droplet in a continuous flow vessel, it is helpful to refer to the three independent processes that affect its behavior. At any moment, a drop of certain size has a certain probability of breaking up, coalescing or leaving the vessel. These probabilities are expressed as frequencies, which are drop-size dependent. The relative values of these frequencies determine the action of the droplet. One can think of the mechanism which has the largest frequency as being the "controlling" mechanism, for that drop size. For our system, the controlling mechanism for very small drops is coalescence; for very large drops it is breakage.

(a) Breakage Effects

The effect of v and the parameters in the breakage functions, $g(v)$ and $\beta(v|v')$ will be first studied independently of the coalescence effect.

Reproduced with permission of the copyright owner. Further reproduction prohibited without permission.

(i) Breakage Frequency

Let us consider the example where $\nu = 2$ and $a = 8$. That is,

$$\beta(v \mid v') = \frac{2.188 \times 10^6}{v'} \left[1 - \frac{v}{v'}\right]^8 \left[\frac{v}{v'}\right]^8 \qquad 8.8$$

Thus when a drop breaks up it forms two droplets of about equal size. Consider the two cases shown in figure 8.1. In one instance $c_1 = 4.48 \times 10^4$ and $c_2 = 0.0125$ and in the other, $c_1 = 10.2 \times 10^4$ and $c_2 = 8.75$. Sauter-mean diameters for both cases are identical. It is seen that the breakage frequency for drops larger than about 0.5 mm^3 is much larger than the escape frequency, .051 min^{-1}. That is to say, drops larger than about 0.5 mm^3 would much rather break than leave the vessel. Thus the feed drops, which are about 4 mm^3 in volume, are quickly broken as they enter the vessel. The drops which are formed ($\sim$ 2 mm^3) are similarly broken very quickly. This cascading effect continues, and smaller and smaller drops are formed. At a certain drop size, the breakage frequency of the drops equals the escape frequency. At this point, the drops would just as soon leave the vessel as break. Below this point the breakage frequency is dropping rapidly and the probability of a drop exiting is greater than its probability of breaking up. The peak of the drop-size distribution occurs in a region where the (drops-in) / (drops-out) ratio is maximized. It can be seen in both cases shown in figure 8.1, because $\nu = 2$, that these peaks occur at volumes equal to one-half those volumes where the breakage frequency equals the escape

Reproduced with permission of the copyright owner. Further reproduction prohibited without permission.

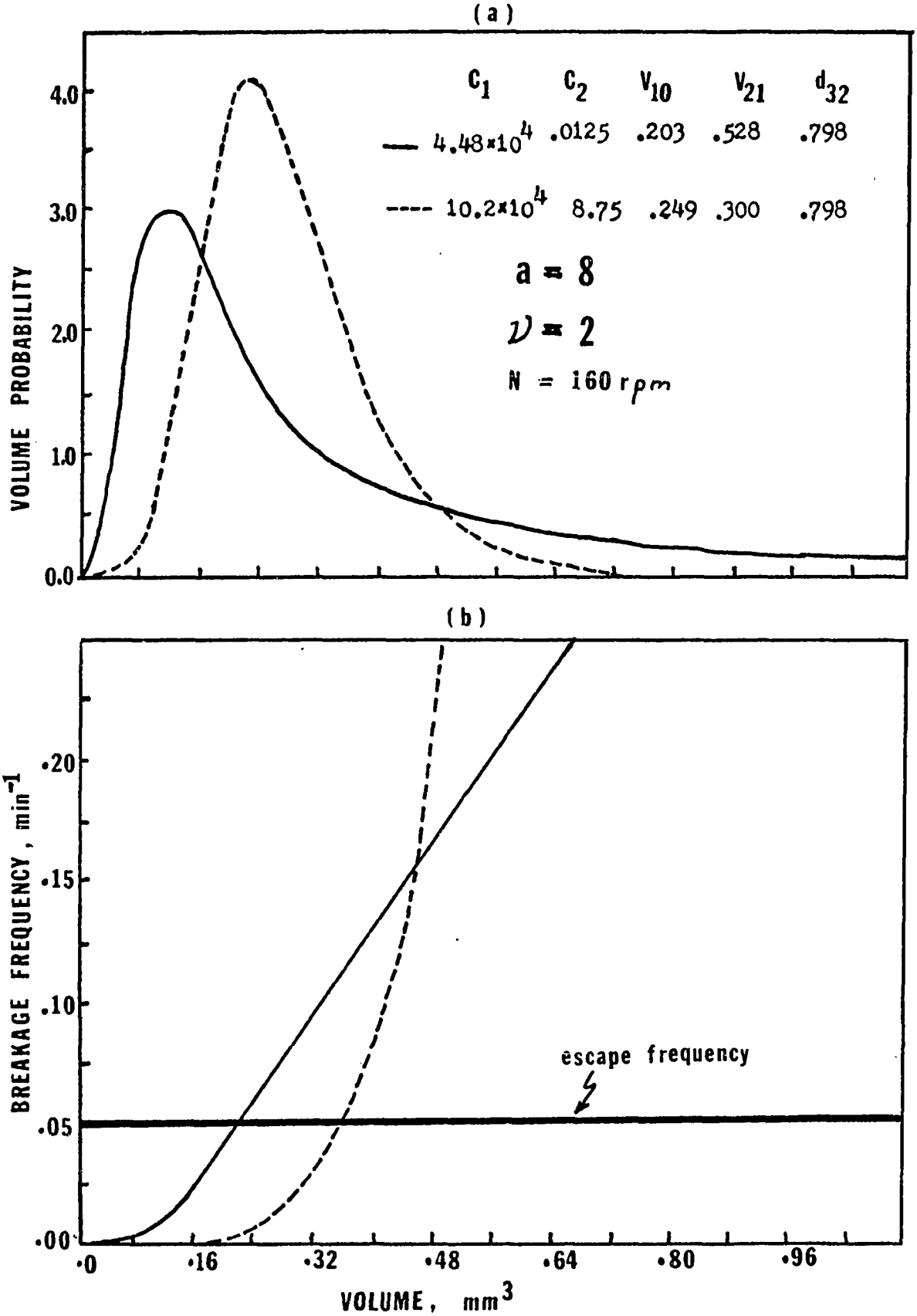

Fig. 8.1 Volume Probability and Breakage Frequency versus Volume for Breakage Only

Reproduced with permission of the copyright owner. Further reproduction prohibited without permission.

frequency.

With reference to figure 8.1, the effect of varying c_1 and c_2 is seen. For a given average drop size, the higher is the value of c_1 the more peaked is the distribution. This is due to the fact that the breakage frequency described in equation 8.1 and in figure 8.1 (b) is more sensitive to v for higher values of c_1.

The input drop size, depending on the agitator speed, can be varied within limits to yield the same distributions. The drop size distributions shown in figures 8.1 are identical for input drop volumes of 2, 4, and 6 mm^3. The reason for this is that all these sized drops are breaking relatively rapidly such that their existence is short-lived, i.e., their volume contribution to the steady-state vessel contents is negligible.

It should be noticed that there is an important difference between this continuous flow system and a batch system. In a batch system the drops will cascade down to a drop size where the breakage frequency is close to zero. In a continuous flow system it is seen that the drops break down to a size where the breakage frequency is close to the escape frequency. That is, further cascading is prevented by the removal (or flow out) of the drops in the vessel. It will be shown later that this has an important effect on the coalescence behavior in the vessel.

(ii) Breakage Kernel, $\beta(v \mid v')$

In figure 8.2 are two cases that were run under identical conditions except for the $\beta(v \mid v')$ function. In one case a = 2,

Reproduced with permission of the copyright owner. Further reproduction prohibited without permission.

Reproduced with permission of the copyright owner. Further reproduction prohibited without permission.

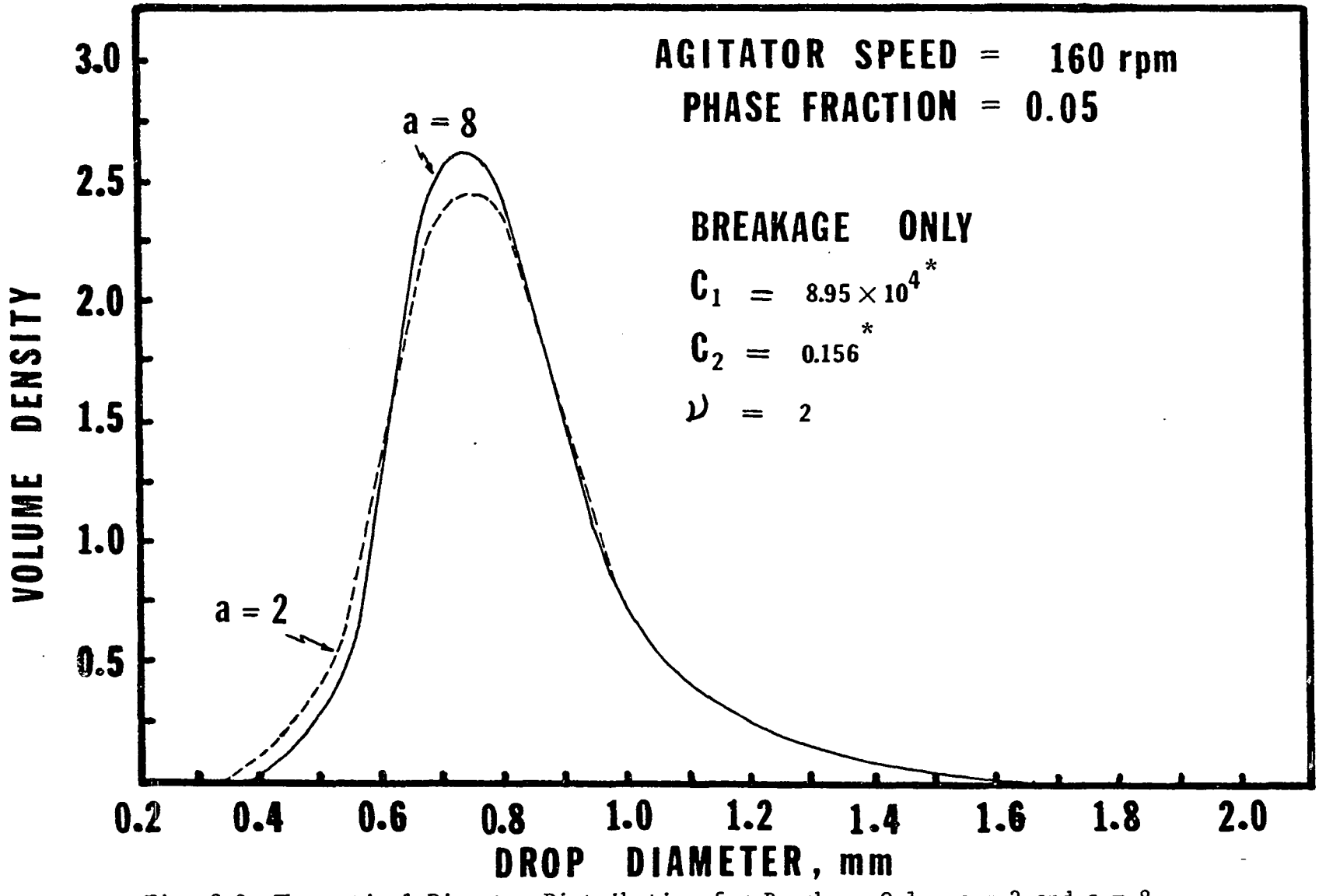

Fig. 8.2 Theoretical Diameter Distribution for Breakage Only, a = 2 and a = 8.

*Used in equation 8.1, N in rpm and v in mm^3.

$$\beta(v|v') = \frac{300}{v'}\left[1 - \frac{v}{v'}\right]^2\left[\frac{v}{v'}\right]^2 \qquad 8.9$$

and in the other, a = 8. (See equation 8.8) It is seen that there is a very small difference between the resulting drop-size distributions. For the case of a = 2, the distribution is only slightly less peaked. For the case of a = 0, i.e., a uniform distribution, this effect is more exaggerated.

(iii) Average Number of Drops Formed in Breakage, ν

It is obvious that if c_1, c_2 and a are kept constant, the drop size distribution will be shifted toward smaller drop sizes as ν is increased. However, similar drop size distributions can be obtained by properly adjusting all these constants. This is true for values of ν up to about 4. Above this value the drop size distributions, for certain values of c_1 and c_2 become bimodal. In addition, when coalescence is considered to be occurring simultaneously, these bimodal breakage-distributions become trimodal in some instances. In this work the effect of varying ν from 2 to 8 was explored extensively. With regard to fitting the data, nothing was apparently gained by considering ν to be greater than 2. This is discussed in Chapter 6. For this reason, a detailed discussion of this effect although being inherently interesting, is not relevant to this thesis and is not included here.

(iv) Effect of Agitator Speed

One might suspect, for given values of the parameters in

Reproduced with permission of the copyright owner. Further reproduction prohibited without permission.

Reproduced with permission of the copyright owner. Further reproduction prohibited without permission.

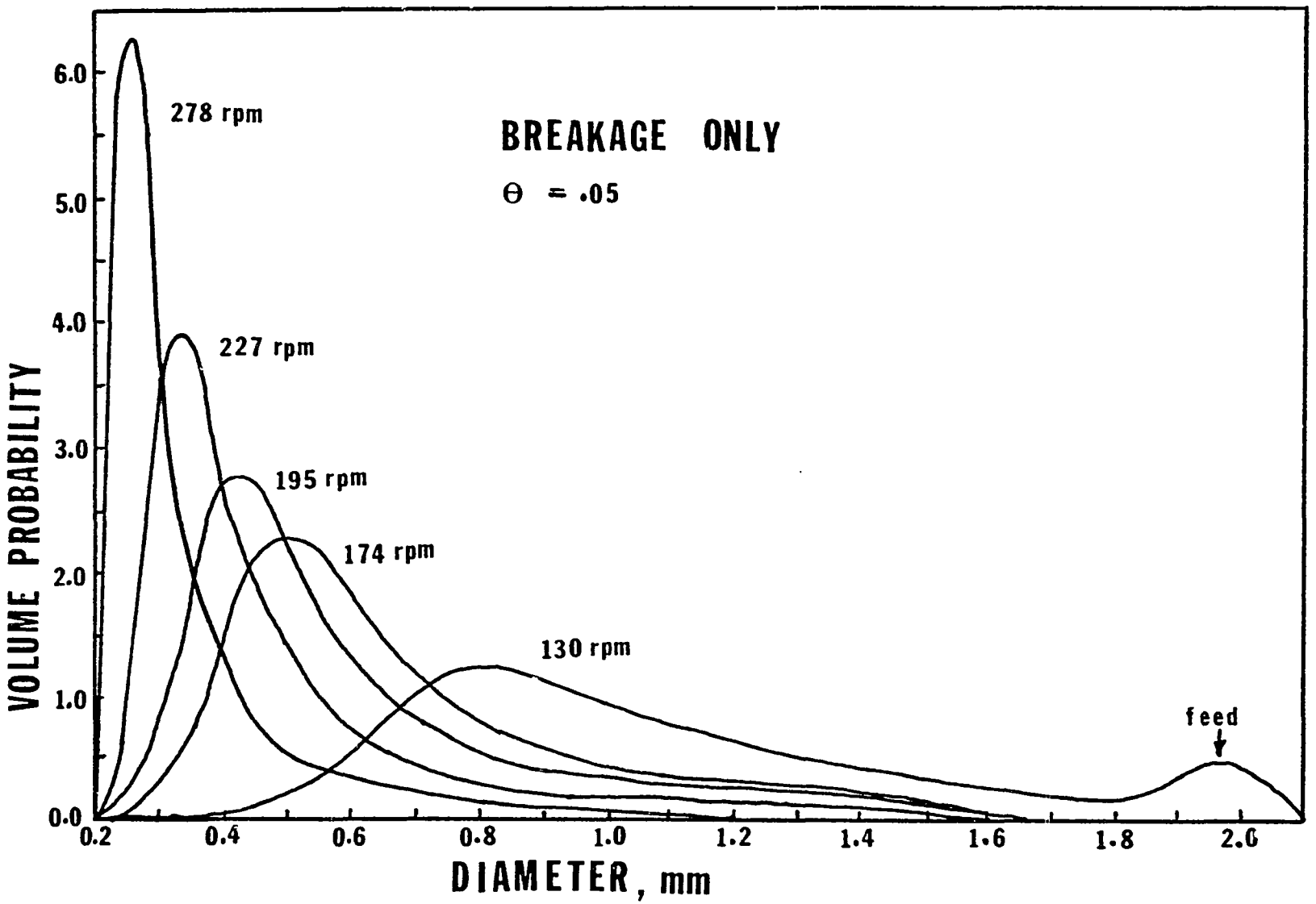

Fig. 8.3 Theoretical Drop Size Distributions for Breakage Only
(From final models, equations 9.1 - 9.4)

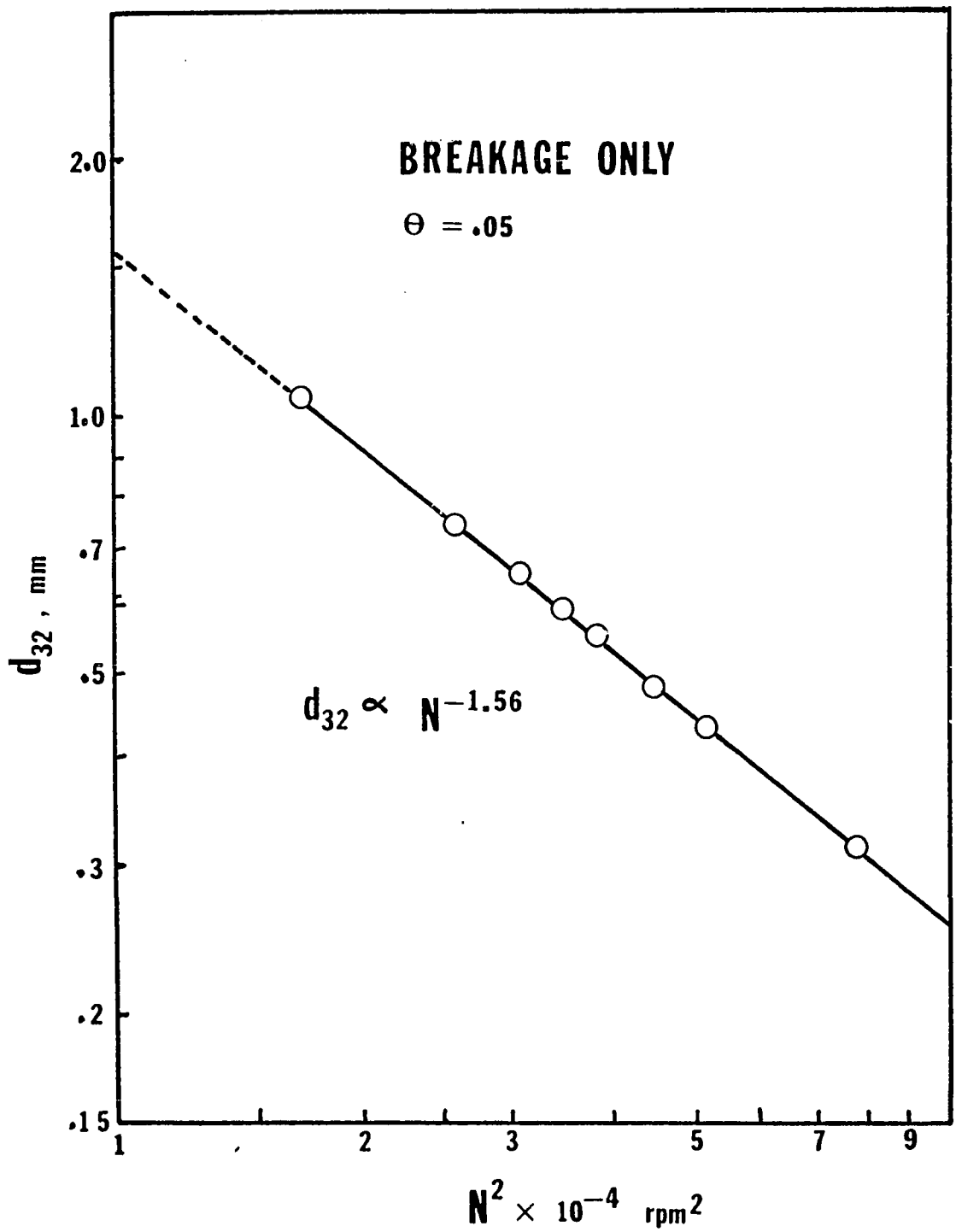

Fig. 8.4 Theoretical Sauter-Mean Diameter versus N for Breakage Only

Reproduced with permission of the copyright owner. Further reproduction prohibited without permission.

the breakage functions, that the average diameter in the vessel would vary as $N^{-6/5}$ according to equation 7.18 or equation 8.1. Although this would be the case for a batch system, it is not true for the continuous flow system. In a flow system the drop size distribution in the vessel is a function not only of the agitator speed but also of the residence time and input drop size. This is best shown in figure 8.3, which shows some mathematically generated distributions. It is seen that the distribution of N = 130 rpm is bimodal, one mode being at the feed drop size. If the input drop size were smaller or if the residence time were longer, the distribution would be shifted to smaller sizes. The overall effect is shown in figure 8.4 with $d_{32} \propto N^{-1.56}$. The flow effect tends to increase the average diameter more at N = 130 rpm than at N = 278 rpm.

(b) Coalescence Effects

The superposition of the mechanism of coalescence onto the flow and breakage processes greatly complicates the qualitative and quantitative analysis of the system.

The behavior of the coalescence function has been discussed briefly in the previous chapter. Referring to equation 8.2 it is seen that c_4 is related to the collision frequency and c_3 is related to the coalescence efficiency. For a given collision frequency, if c_3 is very large, none of the drops will coalesce; if c_3 is zero, then all collisions will result in coalescences. For intermediate values the function is such that the coalescence frequency decreases exponentially for increasing drop size. But the breakage frequency increases exponentially for increasing drop size. The combined

Reproduced with permission of the copyright owner. Further reproduction prohibited without permission.

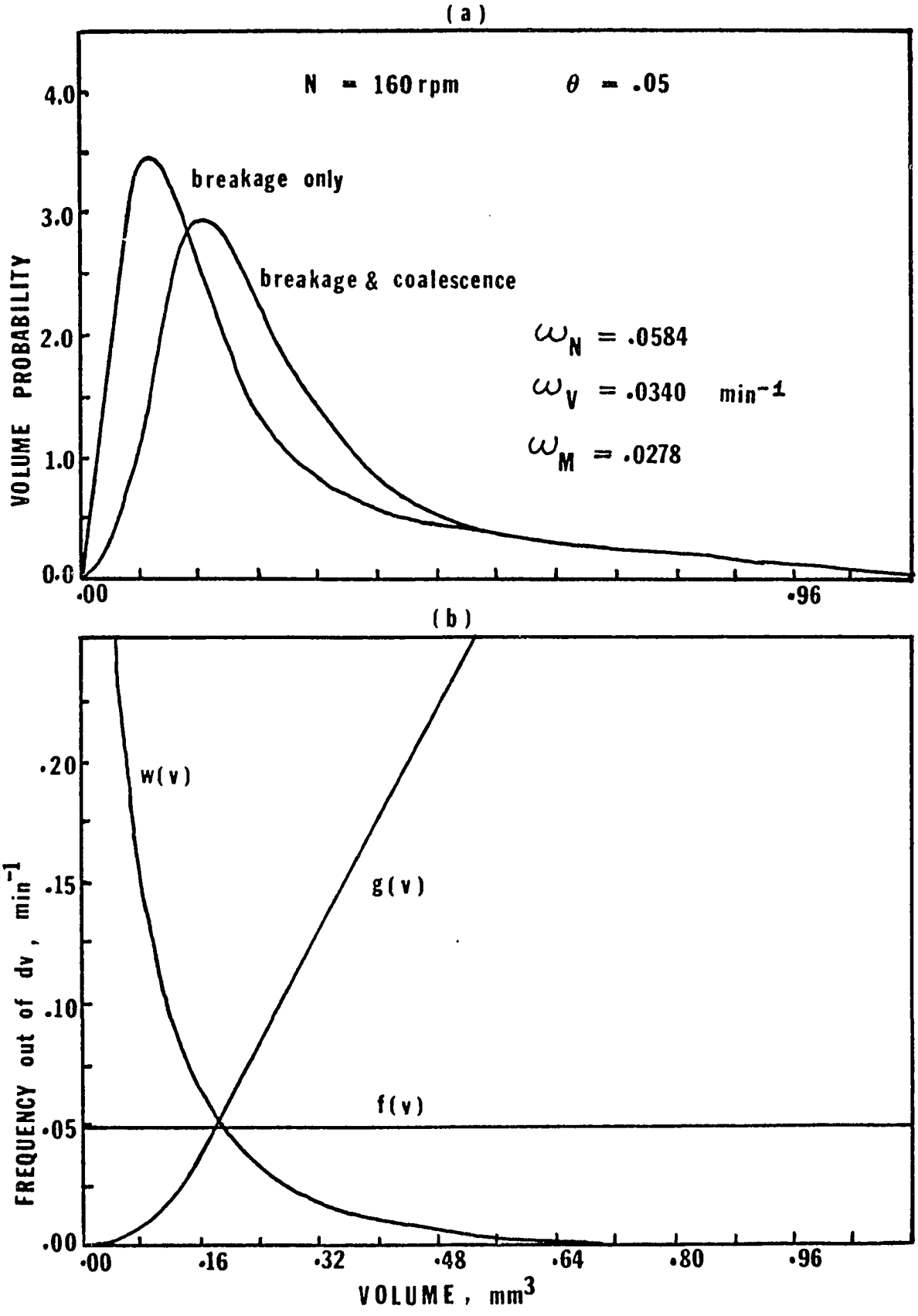

Fig. 8.5 Theoretical Volume Distributions and Frequencies at N = 160 rpm, θ = 0.05

Reproduced with permission of the copyright owner. Further reproduction prohibited without permission.

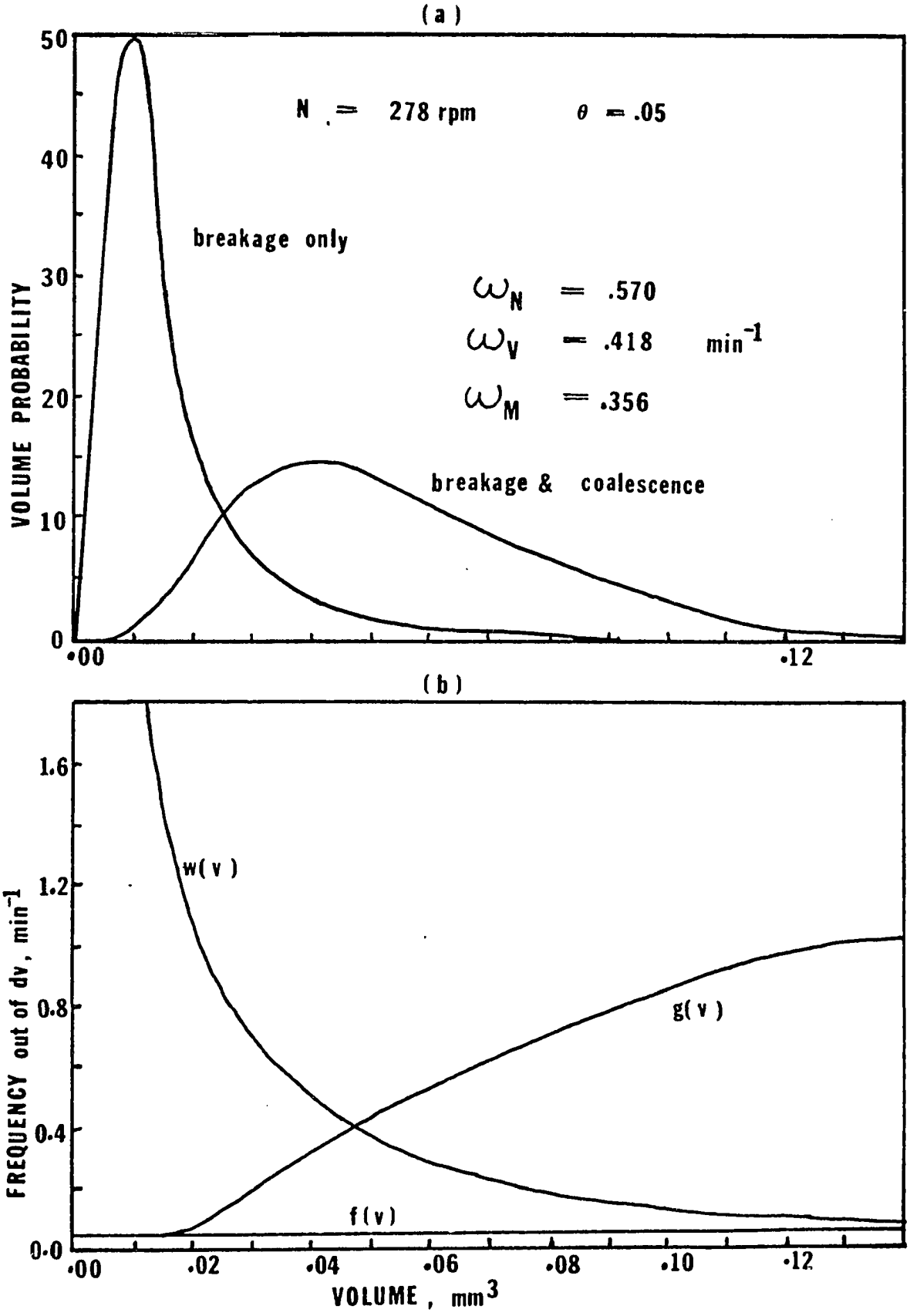

Fig. 8.6 Theoretical Volume Distributions and Frequencies at N = 278 rpm, θ = 0.05

Reproduced with permission of the copyright owner. Further reproduction prohibited without permission.

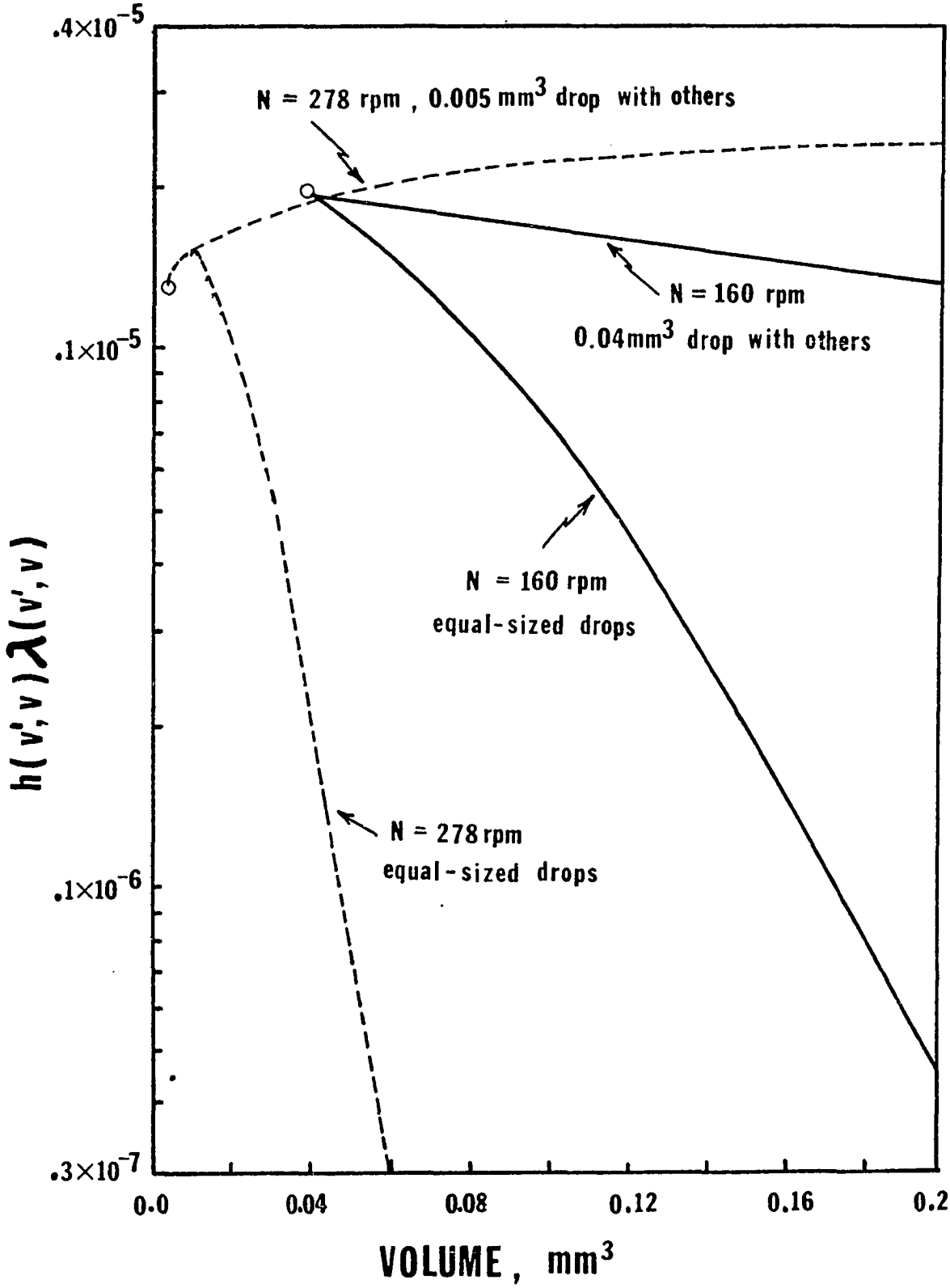

Fig. 8.7 Coalescence Frequency versus Volume

Reproduced with permission of the copyright owner. Further reproduction prohibited without permission.

effect both of these frequencies and the escape frequency have on the dispersion can best be described graphically.

Figures 8.5 and 8.6 show drop size distributions and associated frequencies for two agitator speed conditions. The parameters in the mixing functions are identical to those described in the next chapter; the volume-volume distributions shown here are equivalent to the diameter-volume distributions shown in figures 9.2 and 9.6. The number frequencies shown are those described in the denominator of equation 5.15 in the mixing equation, f(v), g(v) and w(v). The coalescence frequency described in equation 5.16 is more complex than the other frequencies because (1) it depends on the number of drops in the vessel and (2) it is bivariately dependent on drop size. The $h(v,v') \cdot \lambda(v,v')$ values of equation 5.16 are plotted in figure 8.7 for two cases: equal sized drops coalescing, and the smallest drop coalescing with other sized drops. It is seen that although the coalescence frequency rapidly decreases with increasing drop size, this effect is not as pronounced for the case of small drops with larger ones. This is a result of the $(d_1 d_2 / (d_1 + d_2))$ function in the coalescence efficiency term.

It is seen that the coalescence frequency in figure 8.5 (b) is much larger than the other frequencies for small drops, and decreases sharply as v increases. Thus the small drops formed on breakage will immediately coalesce into larger drops as shown in figure 8.5 (a). It might be expected, on the basis of equation 5.15, that the peak of the resulting drop size distribution occurs where $f(v) + g(v) + w(v)$ is near a minimum. This does happen as shown in figures 8.5 and 8.6.

Reproduced with permission of the copyright owner. Further reproduction prohibited without permission.

As agitator speed is decreased for the same system, a point is reached where the breakage-only and the breakage-coalescence distributions coincide. That is, the coalescence rates are negligible. This happens despite the fact that the coalescence frequency increases exponentially with decreasing N as shown in equation 8.2. The reason, as explained in Chapter 7, is that this increase in coalescence frequency is not large enough to cause the coalescence of the relatively large drops formed through breakage, at this lower agitator speed.

By the same argument, the coalescence rate will increase with increasing agitator speed. Once again, this occurs despite the fact that the coalescence efficiency decreases with increasing N as shown in figure 8.7. As shown in figure 8.6, almost all the drops formed on breakage are involved in coalescences.

Included in figures 8.5 and 8.6 are the three mixing frequencies: ω_n, ω_v, and ω_m. If all the coalescing drops are of equal size, then $\omega_n = \omega_v = \omega_m$. The fact that $\omega_n > \omega_v$ indicates that the coalescing drops are comprised of small drops more than large ones. The fact that $\omega_m < \omega_v$ indicates that drops of unequal size are coalescing with each other.

For the 1.74 fold increase in agitator speed from 160 rpm to 278 rpm, the overall coalescence frequency, ω_m, increases 13 fold. In explaining this increase, one may refer to the discussion in section 7.4 (d). Briefly stated, because of the $d \propto N^{-6/5}$ dependency in the exponential breakage frequency function, as opposed to the $d \propto N^{-3/4}$ dependency in the exponential coalescence frequency function, the fraction of the colliding drops in the vessel that result in coalescences sharply increases with increasing N.

Reproduced with permission of the copyright owner. Further reproduction prohibited without permission.

We can now see an important effect of flow on the dispersion. In a continuous flow system, the drops have a chance of leaving the vessel before being broken down into smaller and smaller drops. Thus the drops in the vessel can be kept at a larger enough size such that coalescences are not probable. That is essentially what is happening at the lower agitator speeds. If the residence time were increased, smaller and smaller drops would be created and these would easily coalesce. This is why it is difficult to get a "stabilized" (non-coalescing) dispersion in a batch system without adding surfactants. The ability to get a "flow-stabilized" dispersion in a continuous flow system depends on the relative values of the escape and coalescence frequencies. If the residence time is low enough, such a dispersion is possible.

Reproduced with permission of the copyright owner. Further reproduction prohibited without permission.

CHAPTER 9

CORRELATION OF THEORETICAL AND EXPERIMENTAL RESULTS

9.1 Procedure

The mixing equation described in Chapter 5 can be used in conjunction with the mixing functions developed in Chapter 7 to generate theoretical drop-size distributions and mixing rates that can be compared to the experimental results. These functions should have the following properties: (1) they should be general (that is, based on physical laws and compatible with other researchers' findings) and (2) they should be able to be used to closely fit the experimental results. The first condition has been met. It remains to show how well the theoretical and experimental results correlate.

It is recalled from Chapter 6, in the modeling procedure a point was reached where the parameter space included only the breakage and coalescence constants, c_1, c_2, c_3, and c_4. In trying to fit the data by adjusting these constants, it was found that the dramatic mixing-frequency dependence on agitator speed could be obtained if c_1 and c_3 were made relatively large. The reason for this is seen in equations 8.1 and 8.2. Having large values for these constants, makes both the breakage and coalescence rates more sensitive to changes in agitator speed. At the same time, the corresponding shape of drop-size distribution is affected because the exponential functions in

Reproduced with permission of the copyright owner. Further reproduction prohibited without permission.

equation 8.1 and 8.2 include the variables of volume as well as agitator speed. In fact, the large values of c_1 and c_3 that yield the desired mixing frequency - vs. - N results, tend to make the drop-size distributions very peaked, whereas the experimental distributions are rather broad. In fitting the data, these considerations led to a "compromise" selection of the constants, where a better fit of the drop-size distributions was favored.

In this way, c_1, c_2, c_3 and c_4 were selected to fit the distributions and mixing rates at a dispersed phase fraction of $\theta = 0.05$. The results at $\theta = 0.15$ could only be fitted well by assigning new values to c_1 and c_3. The same was true at $\theta = 0.20$. The problem was that the simple models (equations 8.1 and 8.2) could not account for the rather large drop sizes at these higher dispersed-phase concentrations. The problem was resolved by considering a "packing" effect. It was assumed that as the dispersed phase concentration is increased, the forces causing breakage and coalescence decrease due to a damping of the turbulent fluctuations. This attenuation decreases the breakage rate to some extent and increases the coalescence rate, to a greater extent. The overall result of both of these effects is an increase in drop size. This "packing" effect was expressed mathematically (see Section 7.4 (f)) and two new constants k_B and k_c were introduced into the parameter space.

Using the six constants of c_1, c_2, c_3, c_4, k_B and k_c, and assuming binary breakage into two drops of nearly equal size, the data were finally fitted at all N and θ levels.

Reproduced with permission of the copyright owner. Further reproduction prohibited without permission.

9.2 Results

As mentioned earlier, depending on the agitator speed, the input drop size could be varied within limits to yield the same distributions. In order to cut down substantially on the computer cost, the smallest possible values were chosen. These values were obtained by trial-and-error for every agitator speed. In this way consistent accuracy was obtained using integration intervals of 150 - 250.

Some of the drop size distribution fits are presented in figures 9.2 - 9.11. The theoretical mixing frequency given is ω_m.* The whole range is shown in terms of Sauter-mean diameter in figures 9.12 - 9.15. The mixing frequency comparisons are shown in figures 9.16 - 9.19. The final mixing functions are given below:

$$\nu = 2 \quad \text{Binary Breakage} \tag{9.1}$$

$$\beta(v \mid v') = \frac{0.38799 \times 10^{7}}{v'} \left[1 - \frac{v}{v'}\right]^{10} \left[\frac{v}{v'}\right]^{10} \tag{9.2}$$

This function is plotted in figure 9.1.

$$g(v) = \frac{0.0118\ N\ v^{-2/9}}{1 + \theta} \exp\left\{- \frac{3.48 \times 10^{4}\ (1+\theta)^{2}}{N^{2}\ v^{5/9}}\right\} \tag{9.3}$$

This function is plotted in figures 8.5(b) and 8.6(b) for $\theta = 0.05$ and N = 160 rpm and N = 278 rpm. (N in rpm, v in mm^3).

*A Table of all ω_n, ω_v, and ω_m values are given in Appendix IV.

Reproduced with permission of the copyright owner. Further reproduction prohibited without permission.

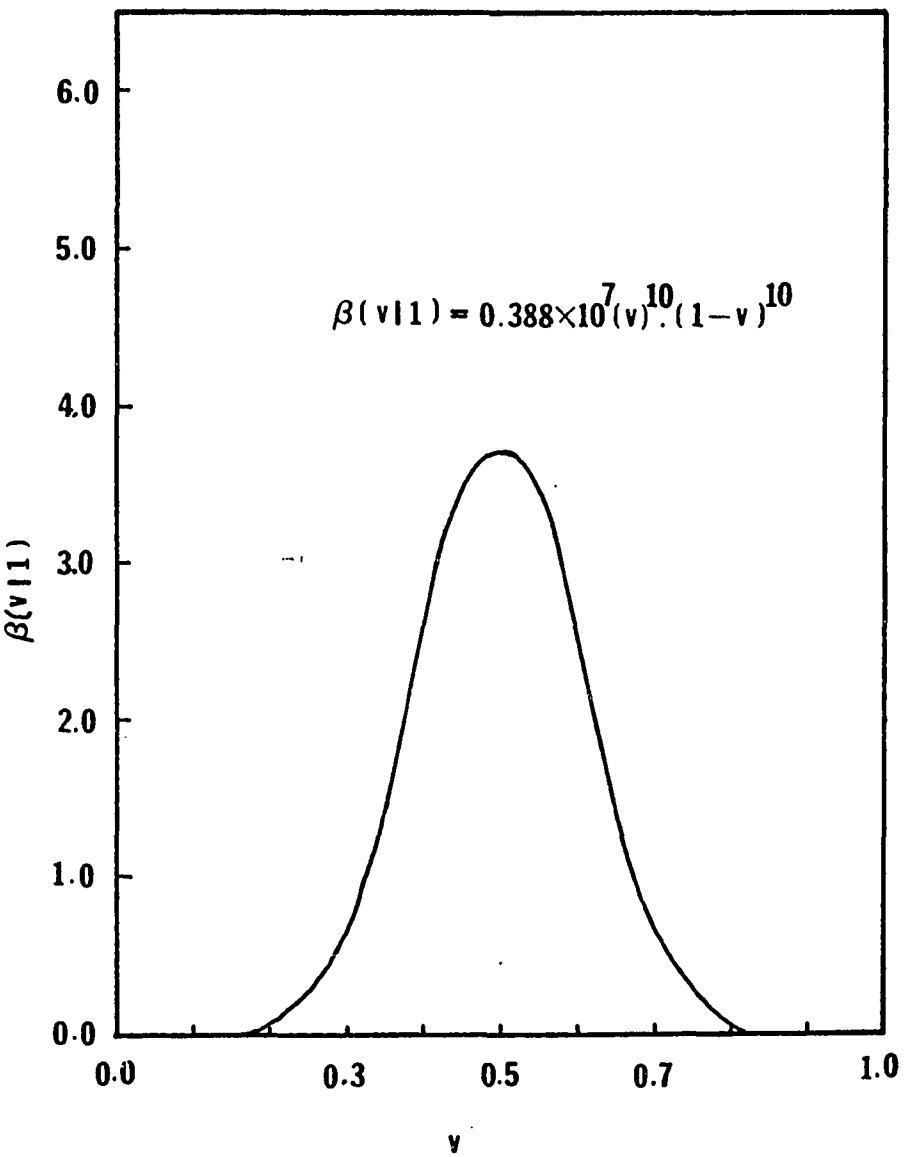

Fig. 9.1 Beta Distribution, a = 10

Reproduced with permission of the copyright owner. Further reproduction prohibited without permission.

Reproduced with permission of the copyright owner. Further reproduction prohibited without permission.

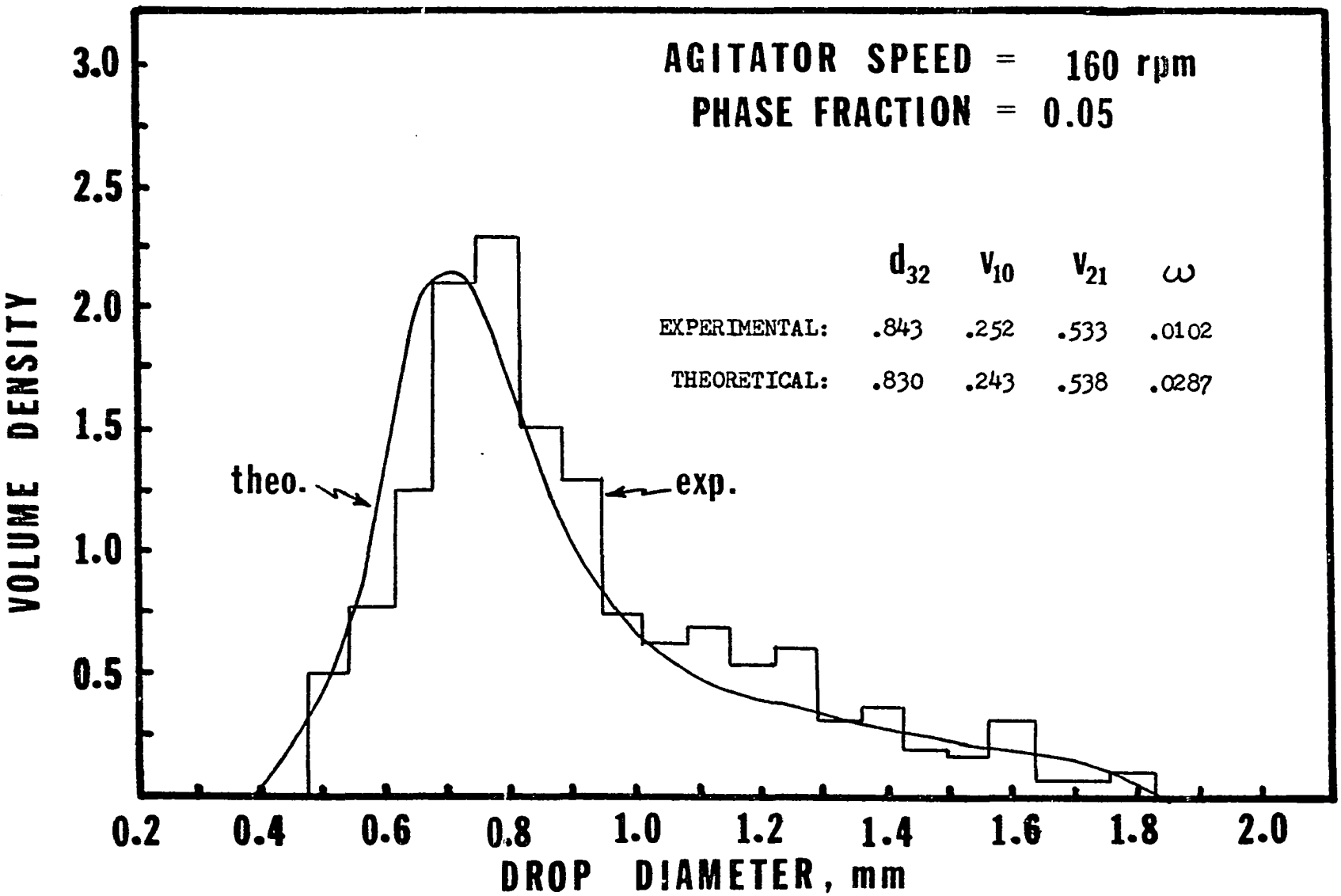

Fig. 9.2 Experimental and Theoretical Diameter Distributions, N = 160 rpm, θ = 0.05

Reproduced with permission of the copyright owner. Further reproduction prohibited without permission.

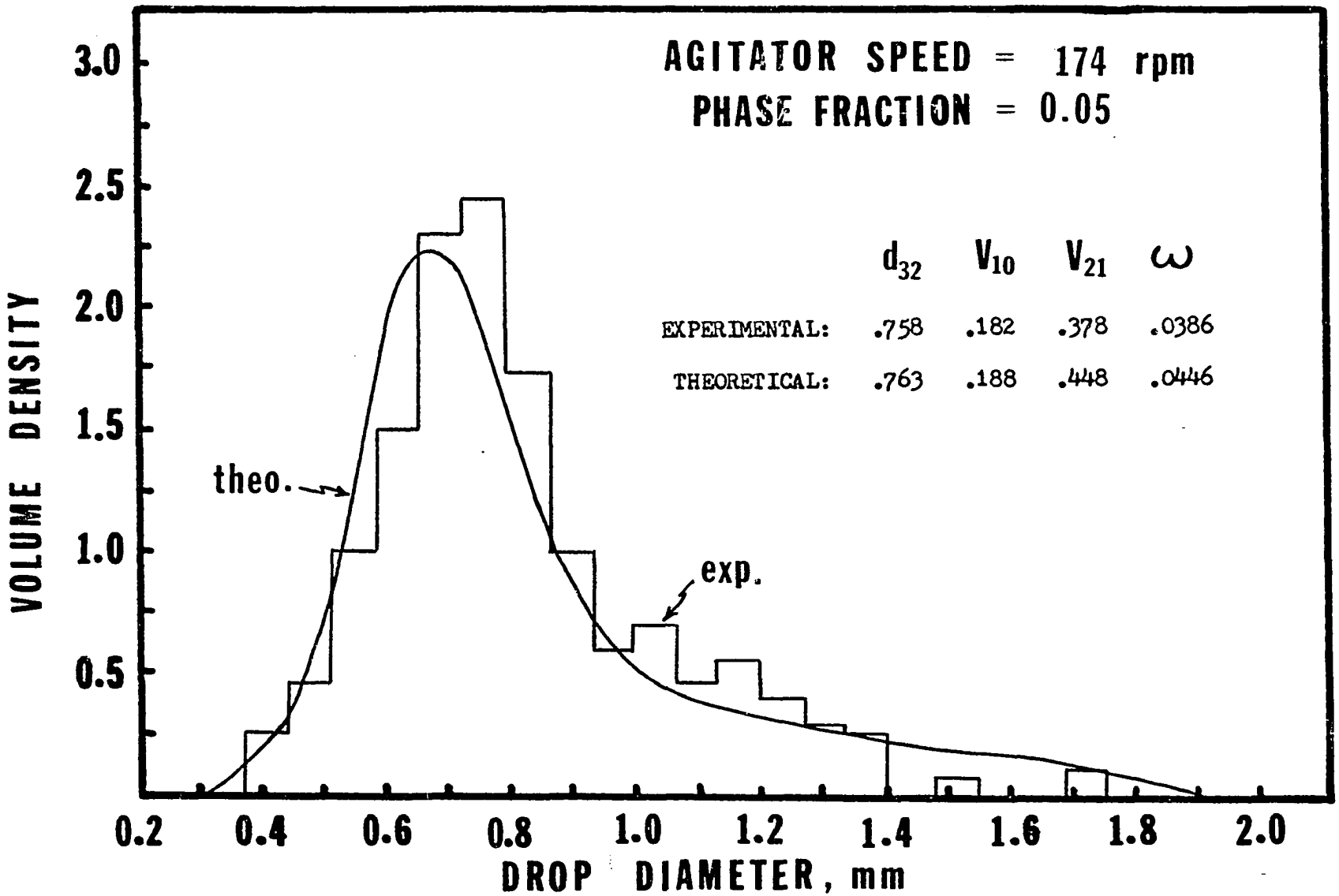

Fig. 9.3 Experimental and Theoretical Diameter Distributions, N = 174 rpm, θ = 0.05

Reproduced with permission of the copyright owner. Further reproduction prohibited without permission.

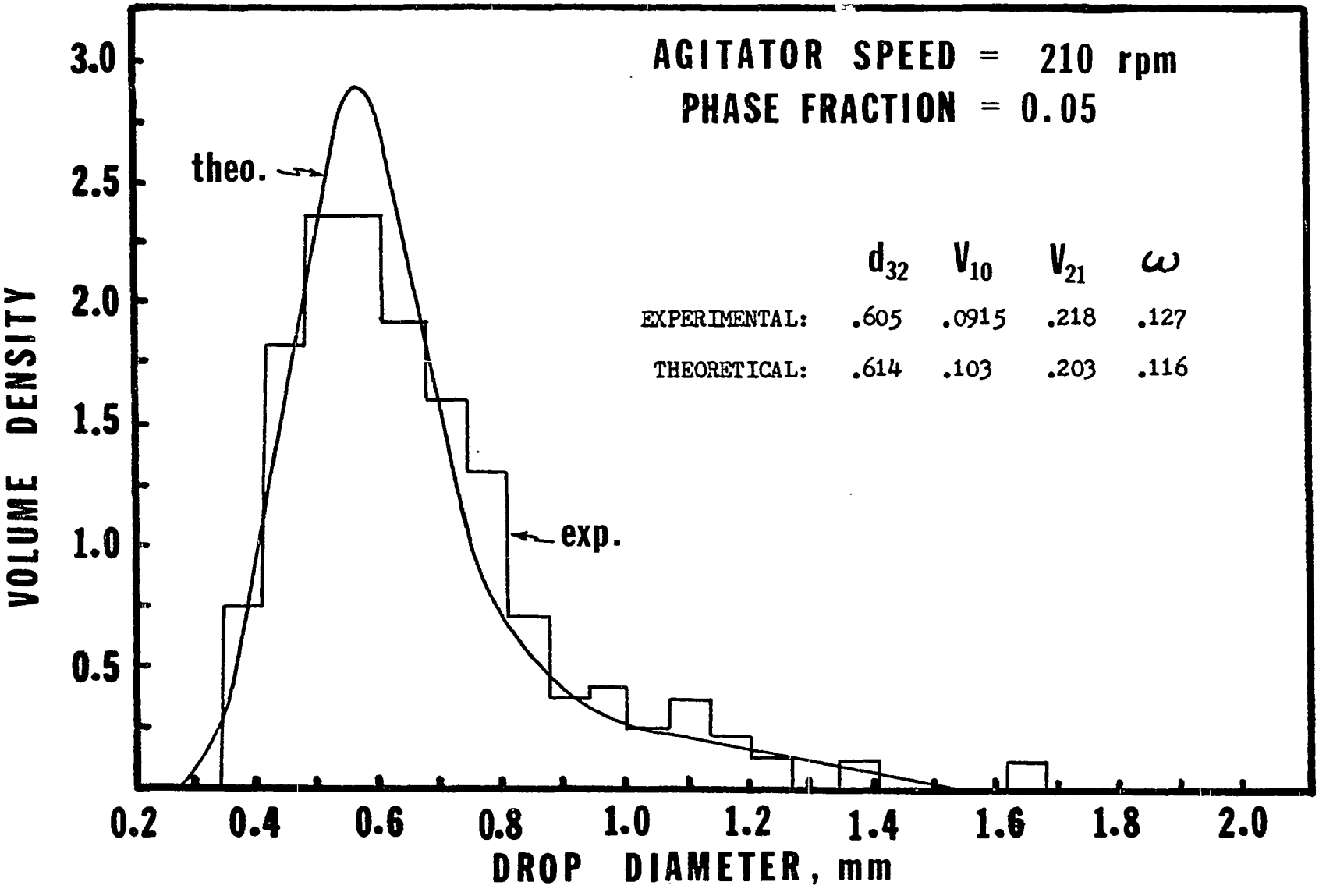

Fig. 9.4 Experimental and Theoretical Diameter Distributions, N = 210 rpm, θ = 0.05

Reproduced with permission of the copyright owner. Further reproduction prohibited without permission.

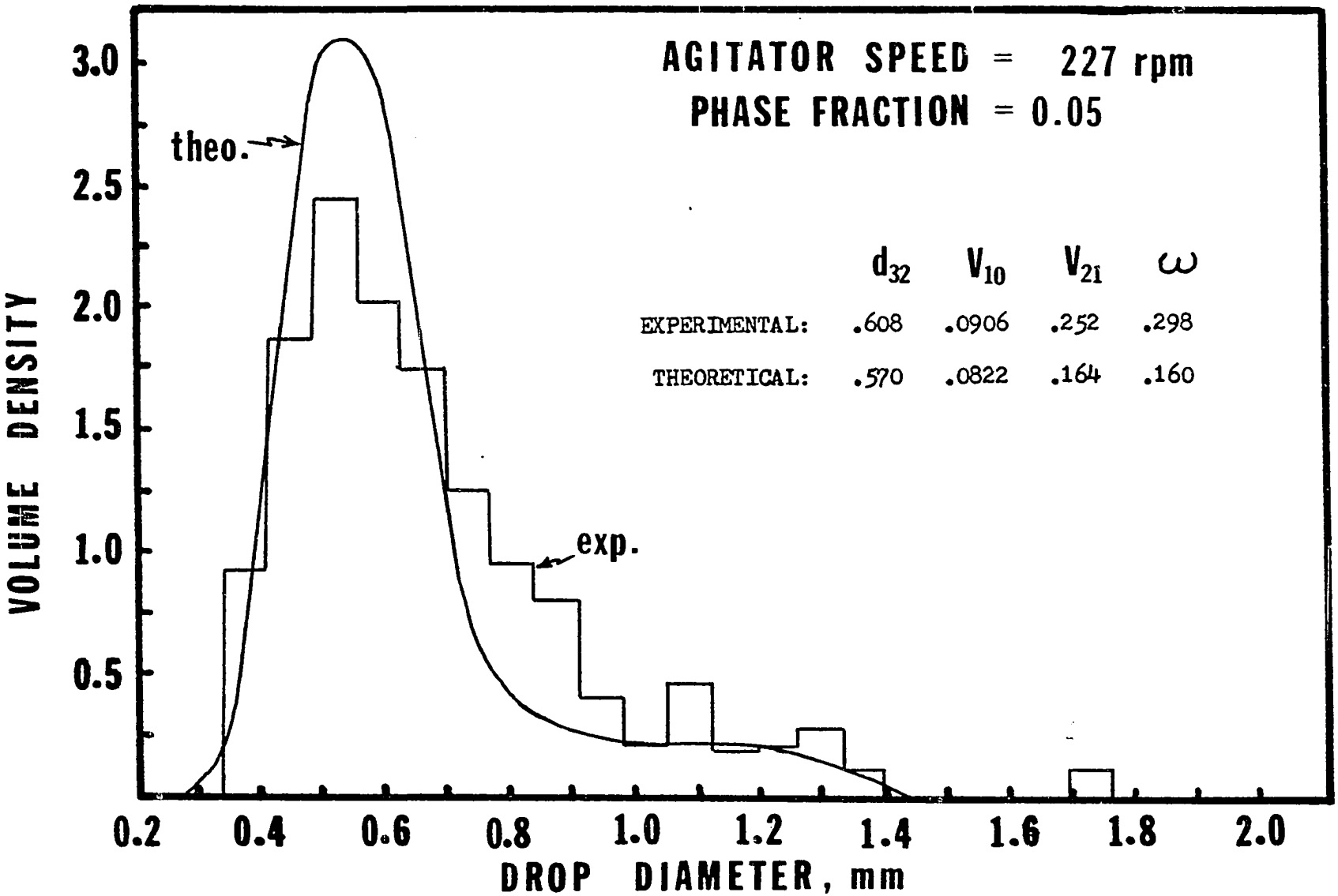

Fig. 9.5 Experimental and Theoretical Diameter Distributions, N = 227 rpm, θ = 0.05

Reproduced with permission of the copyright owner. Further reproduction prohibited without permission.

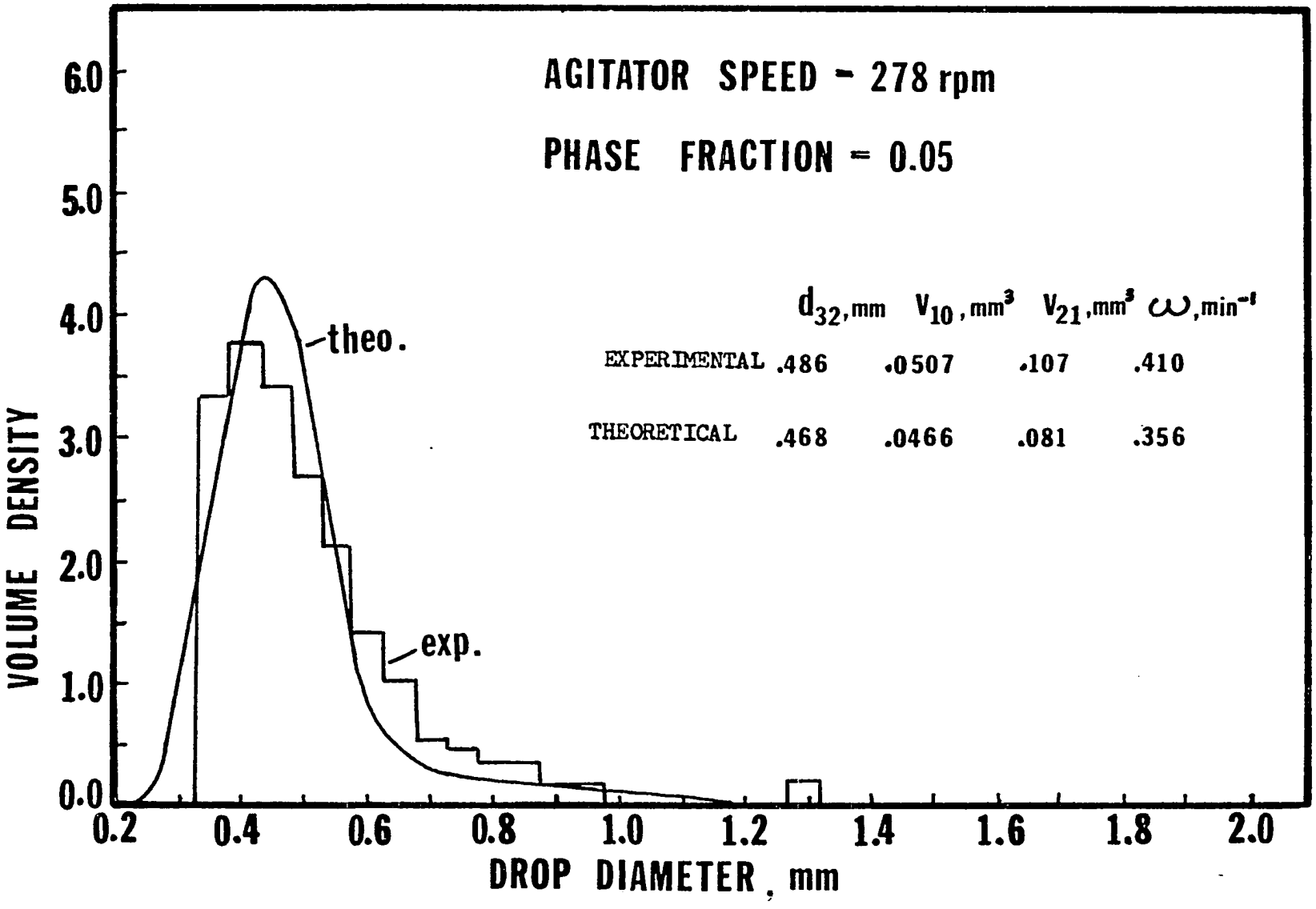

Fig. 9.6 Experimental and Theoretical Diameter Distributions, N = 278 rpm, θ = 0.05

Reproduced with permission of the copyright owner. Further reproduction prohibited without permission.

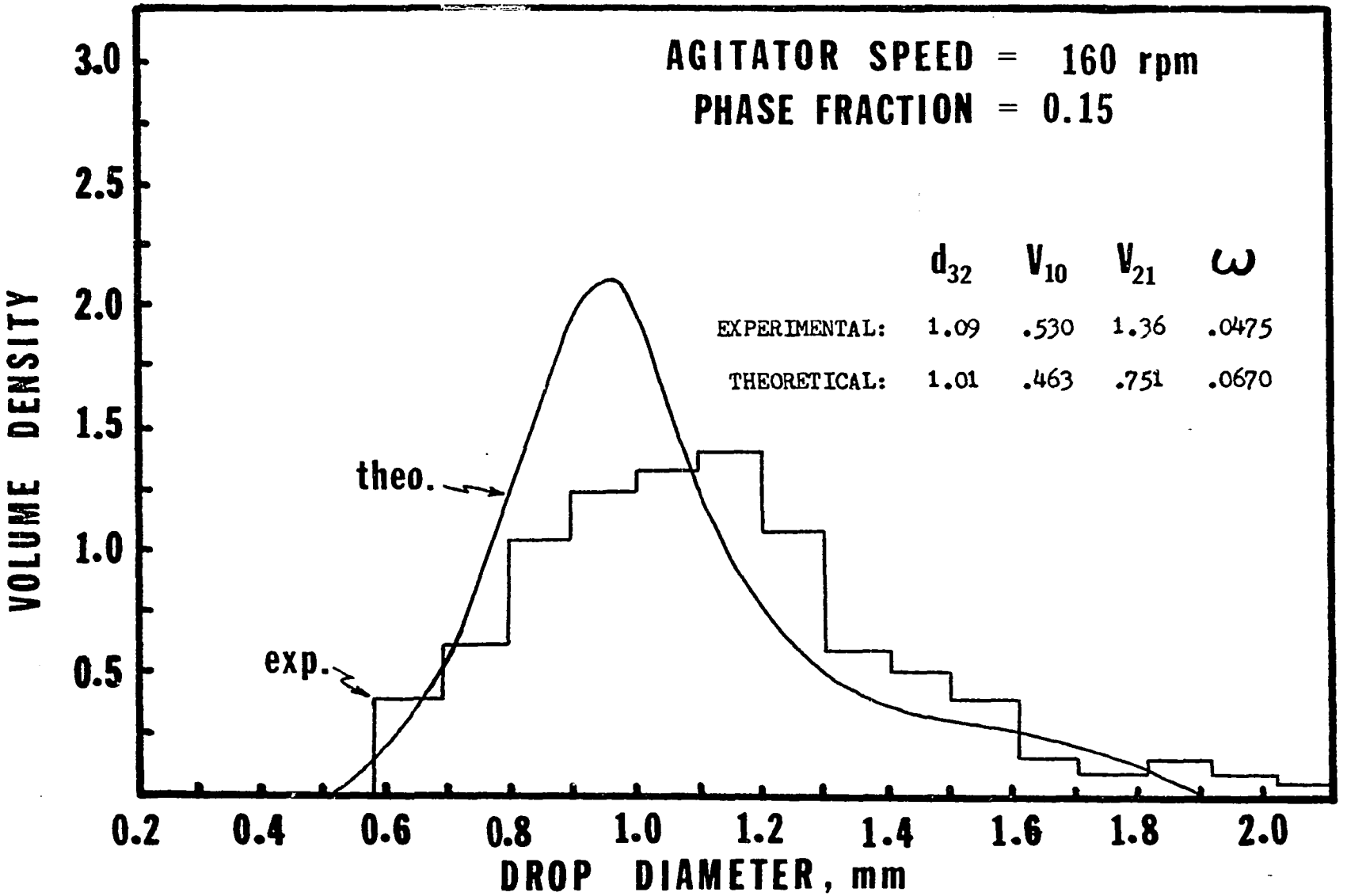

9.7 Experimental and Theoretical Diameter Distributions, N = 160 rpm, θ = 0.15

Reproduced with permission of the copyright owner. Further reproduction prohibited without permission.

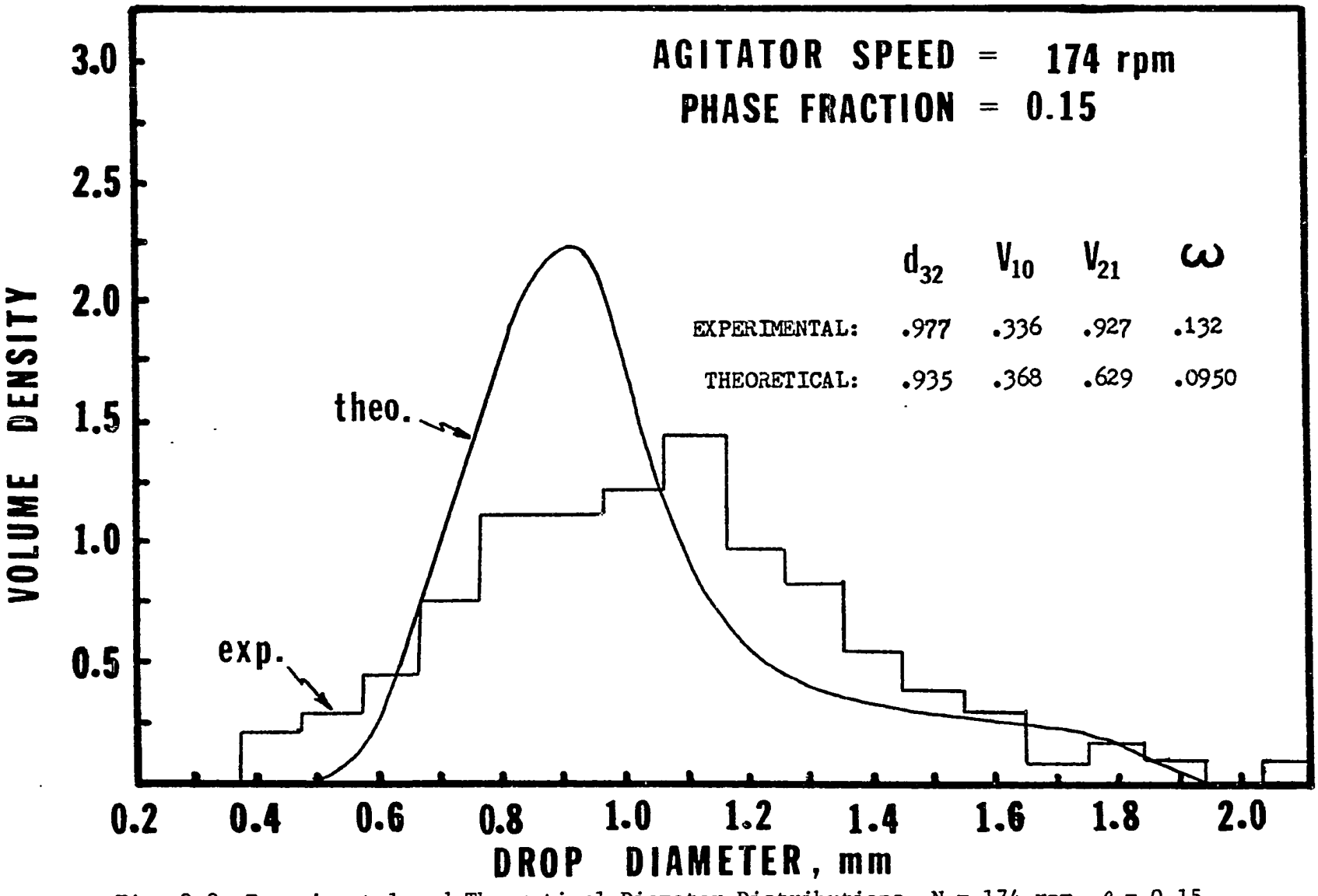

Fig. 9.8 Experimental and Theoretical Diameter Distributions, N = 174 rpm, θ = 0.15

Reproduced with permission of the copyright owner. Further reproduction prohibited without permission.

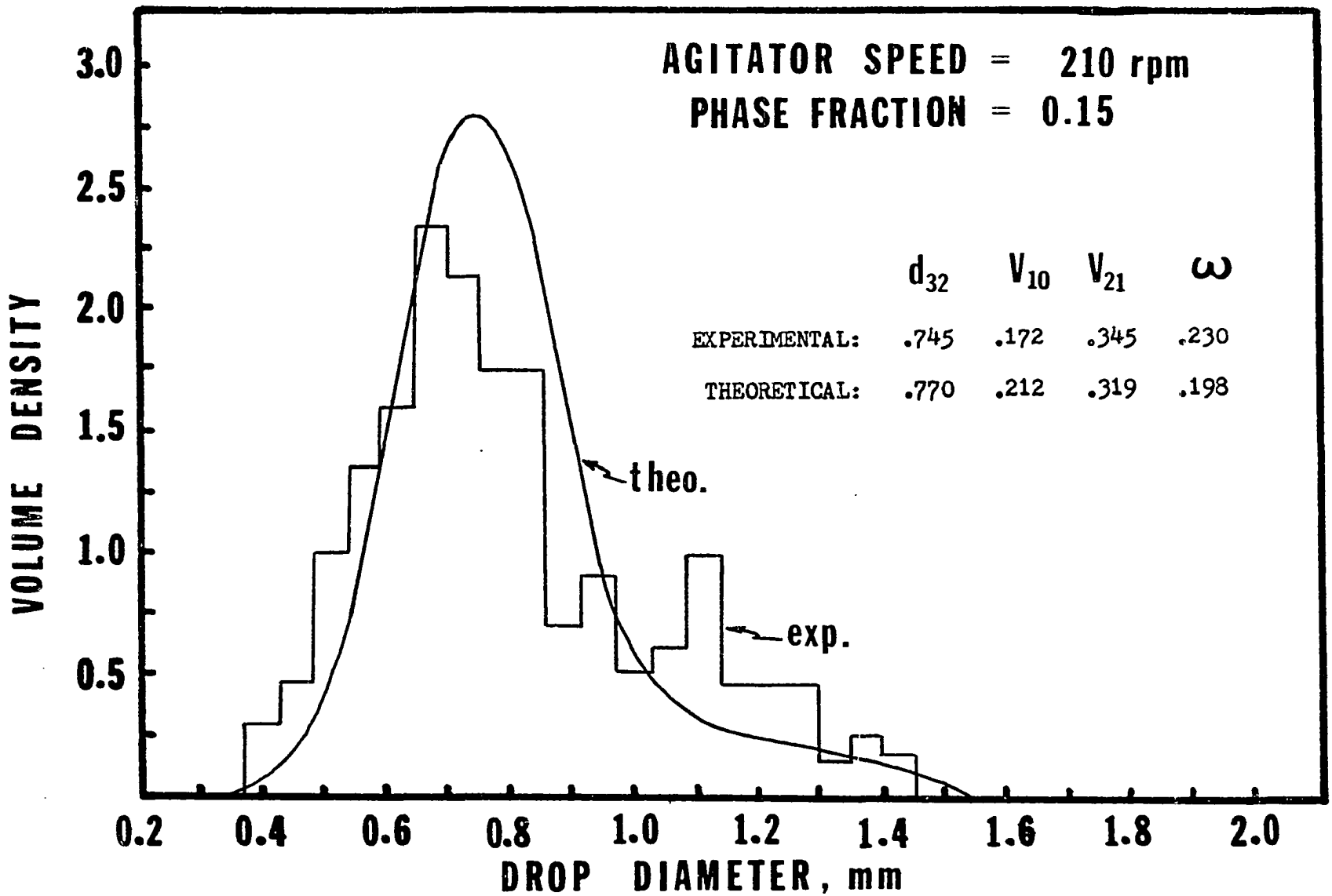

Fig. 9.9 Experimental and Theoretical Diameter Distributions, N = 210 rpm, θ = 0.15

Reproduced with permission of the copyright owner. Further reproduction prohibited without permission.

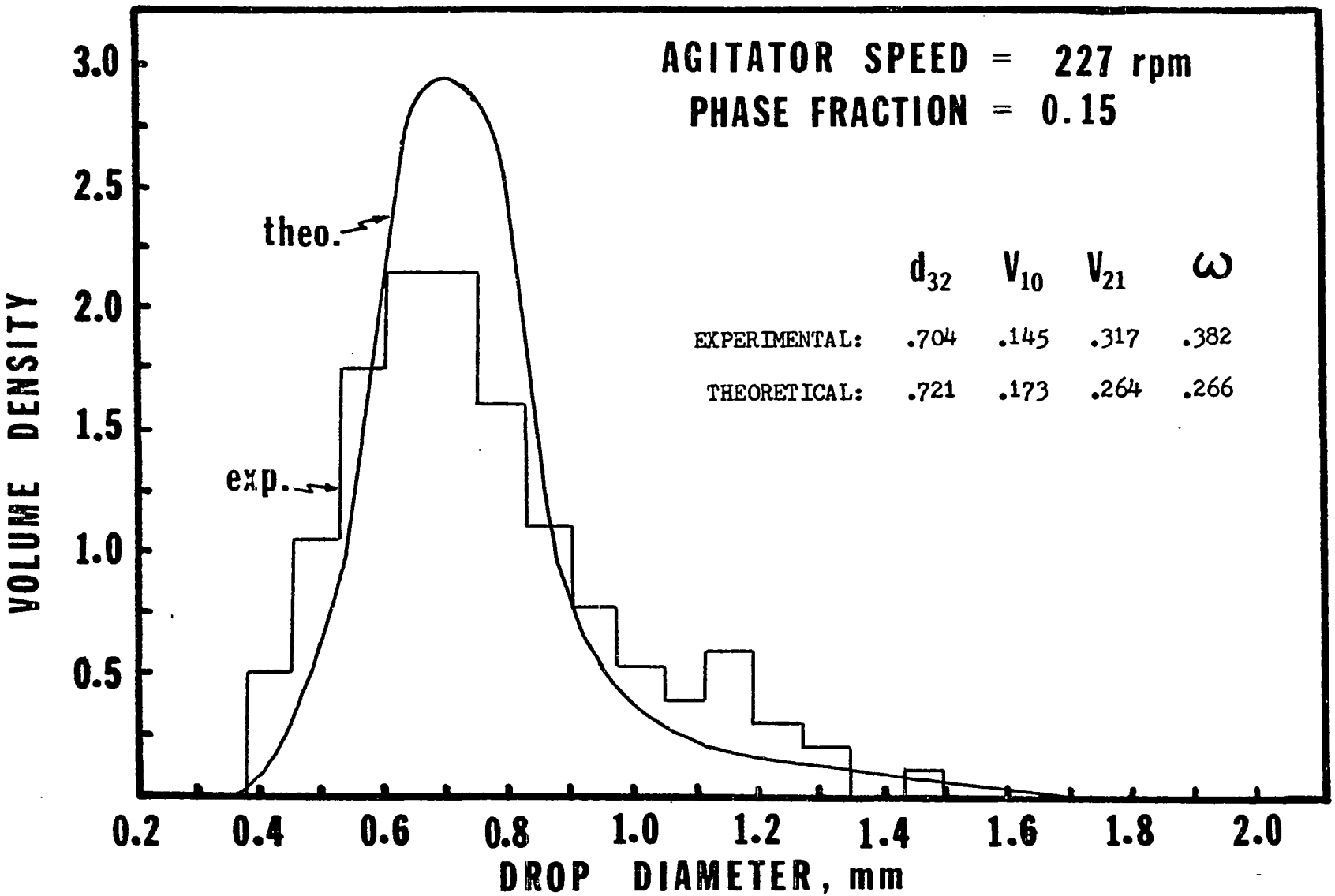

Fig. 9.10 Experimental and Theoretical Diameter Distributions, N = 227 rpm, θ = 0.15

Reproduced with permission of the copyright owner. Further reproduction prohibited without permission.

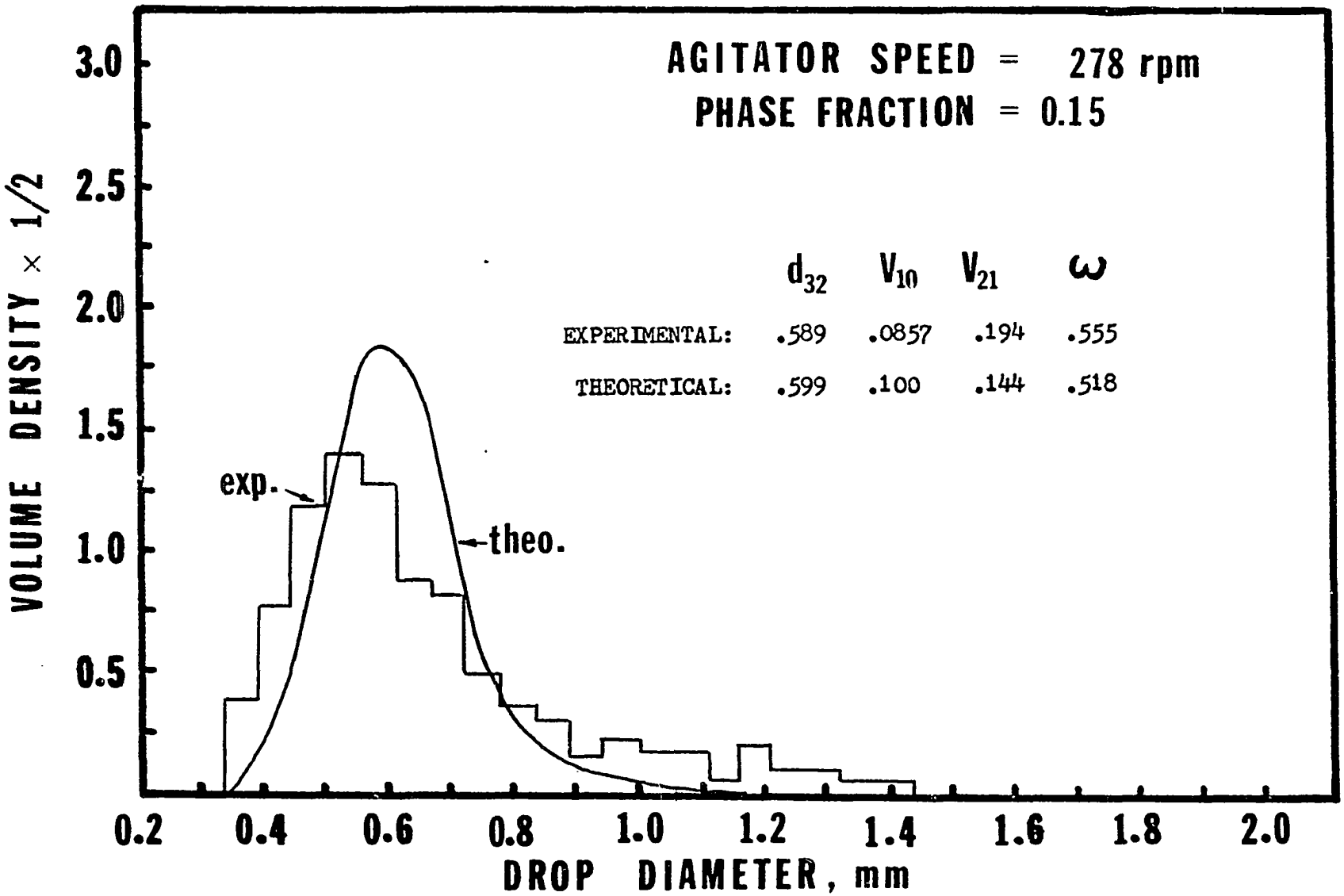

Fig. 9.11 Experimental and Theoretical Diameter Distributions, N = 278 rpm, θ = 0.15

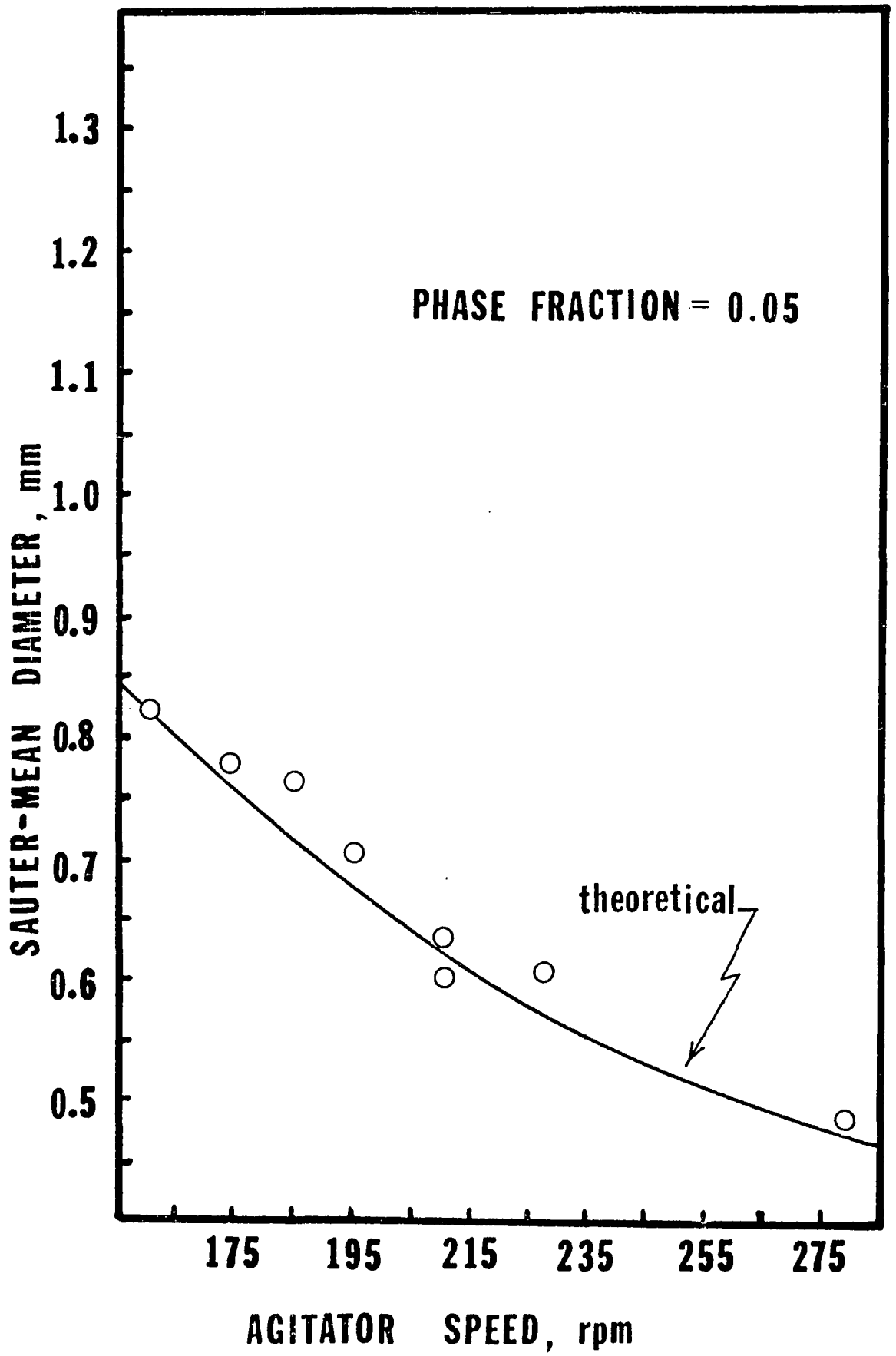

Fig. 9.12 Experimental and Theoretical Sauter-Mean Diameters, $\theta = 0.05$

Reproduced with permission of the copyright owner. Further reproduction prohibited without permission.

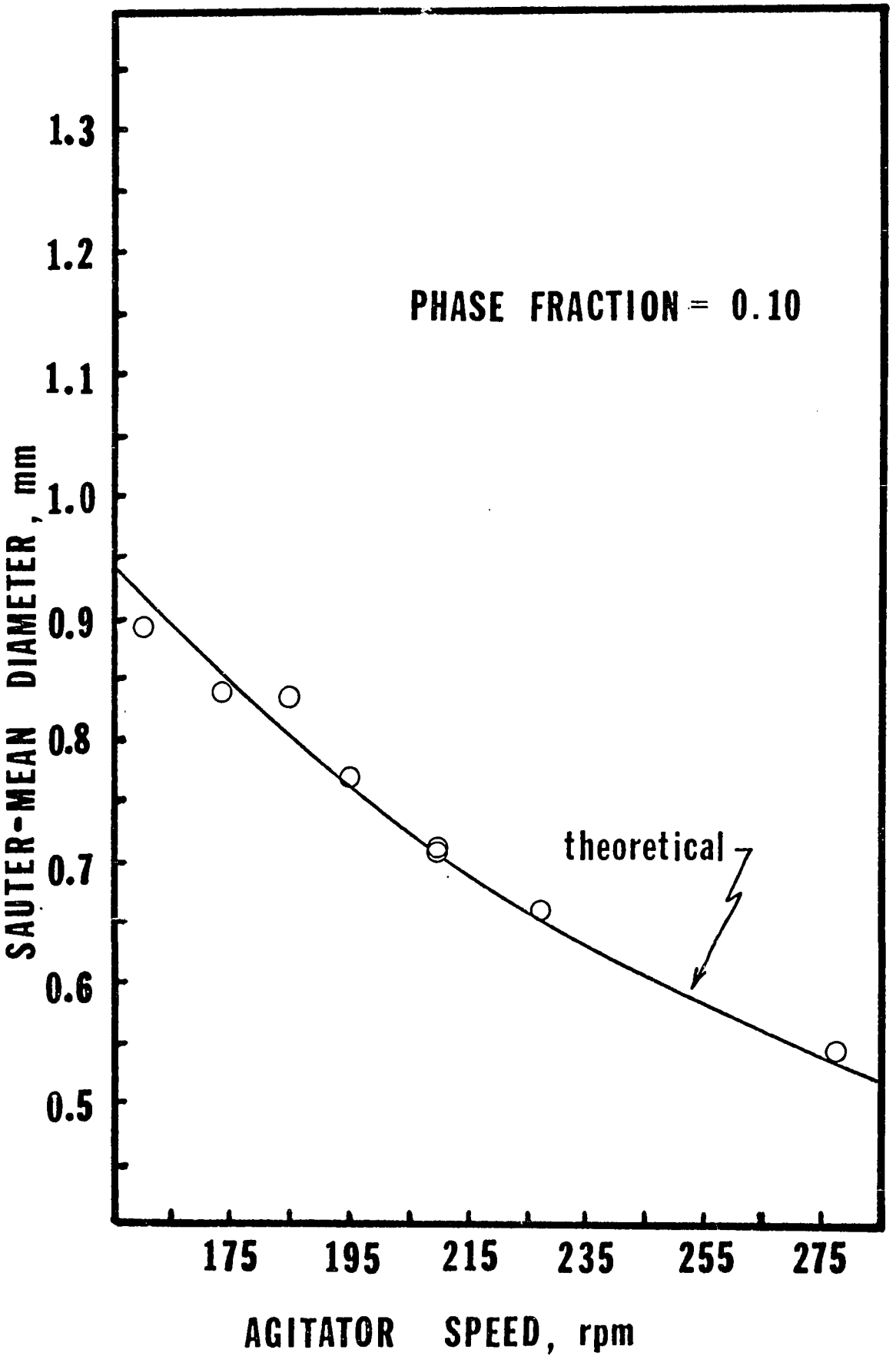

Fig. 9.13 Experimental and Theoretical Sauter-Mean Diameters, θ = 0.10

Reproduced with permission of the copyright owner. Further reproduction prohibited without permission.

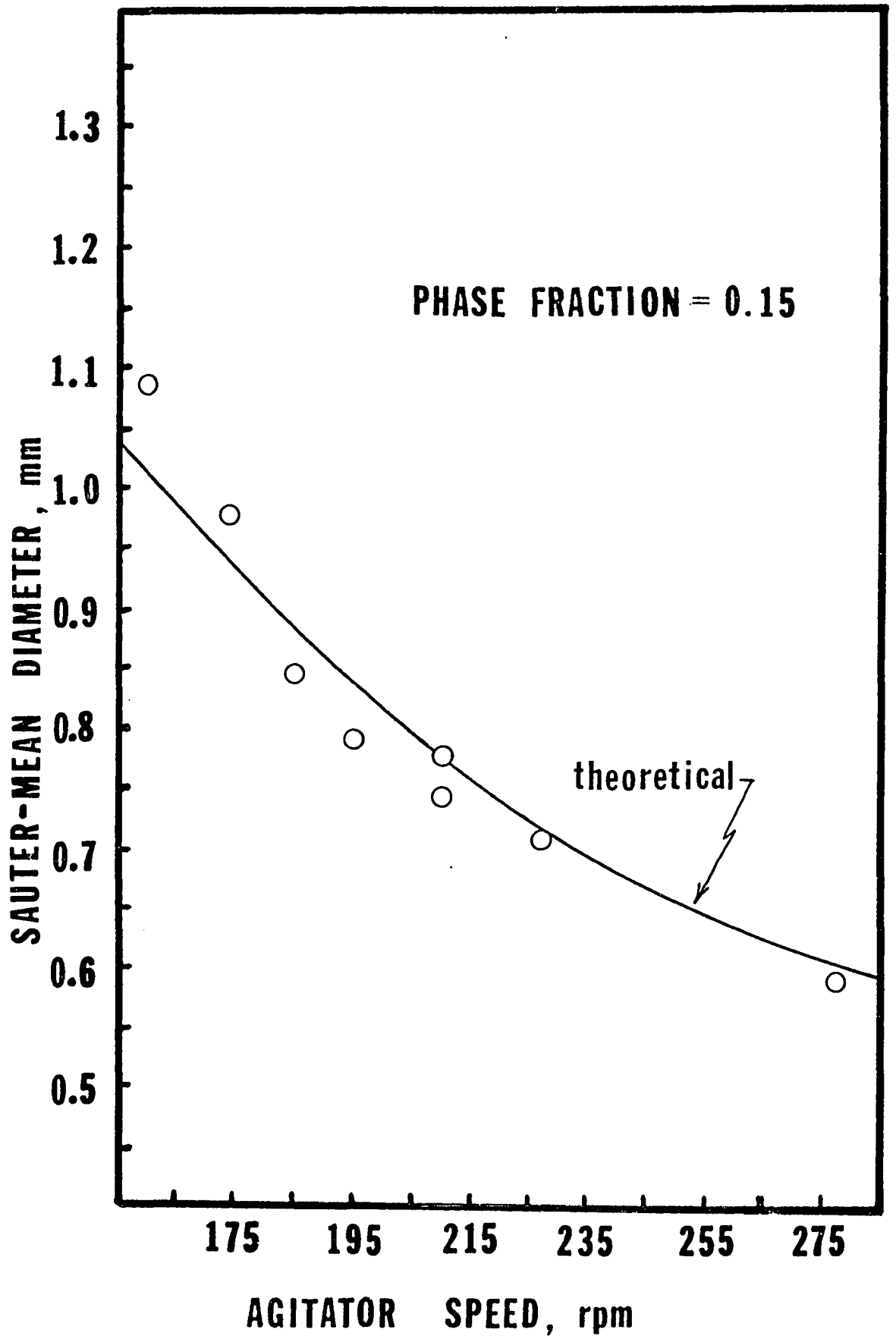

Fig. 9.14 Experimental and Theoretical Sauter-Mean Diameters, θ = 0.15

Reproduced with permission of the copyright owner. Further reproduction prohibited without permission.

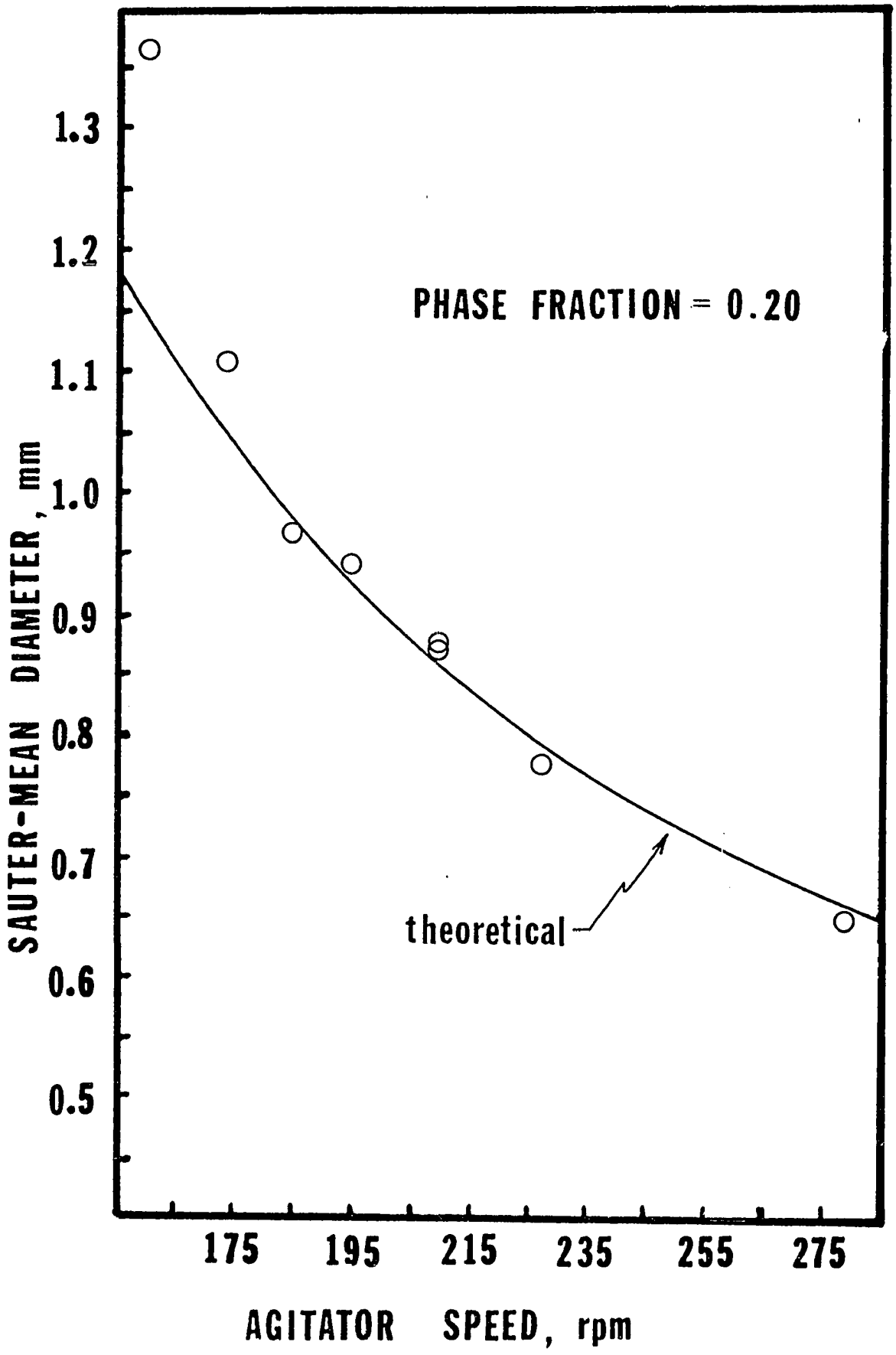

Fig. 9.15 Experimental and Theoretical Sauter-Mean Diameters, θ = 0.20

Reproduced with permission of the copyright owner. Further reproduction prohibited without permission.

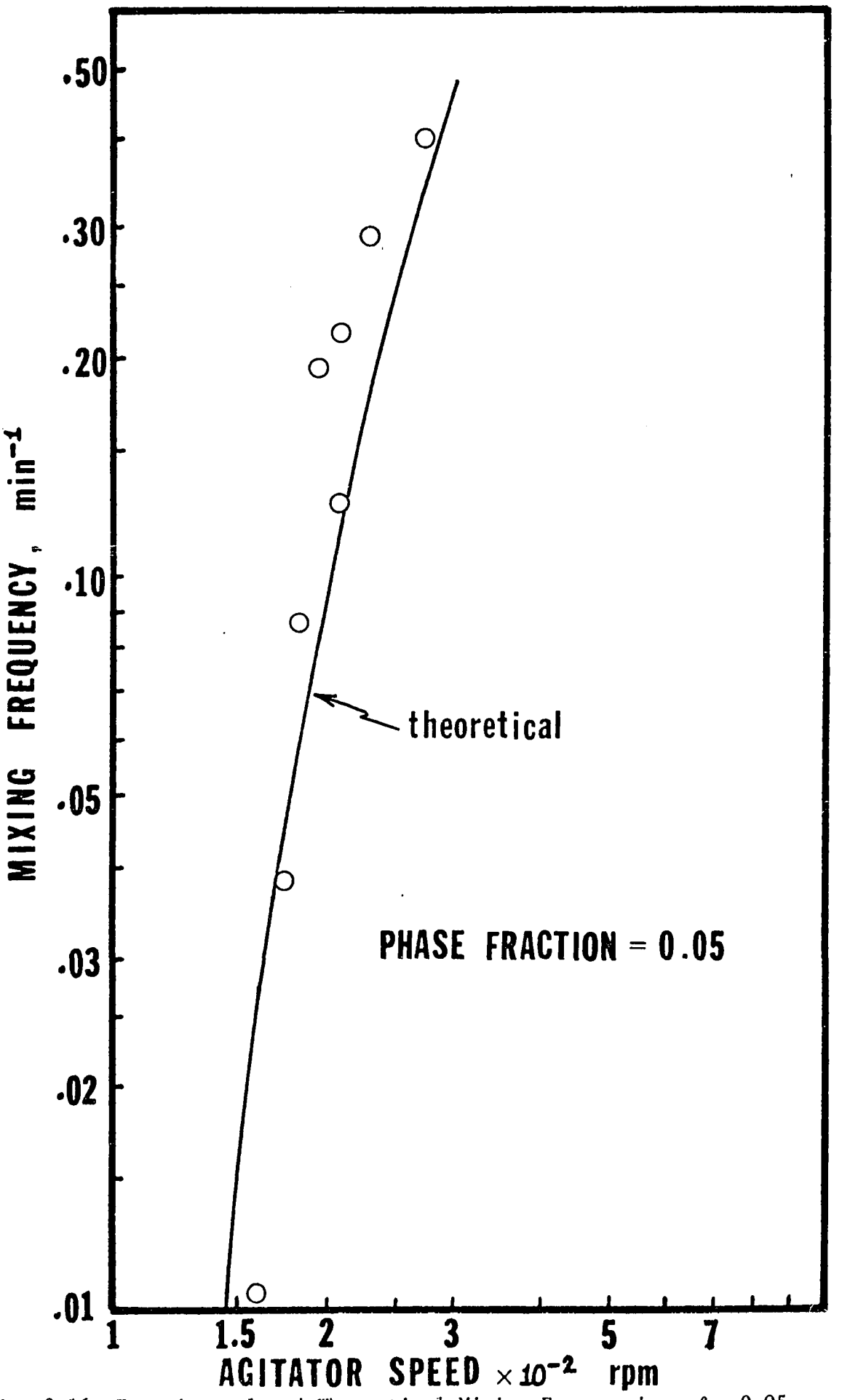

Fig. 9.16 Experimental and Theoretical Mixing Frequencies, $\theta = 0.05$

Reproduced with permission of the copyright owner. Further reproduction prohibited without permission.

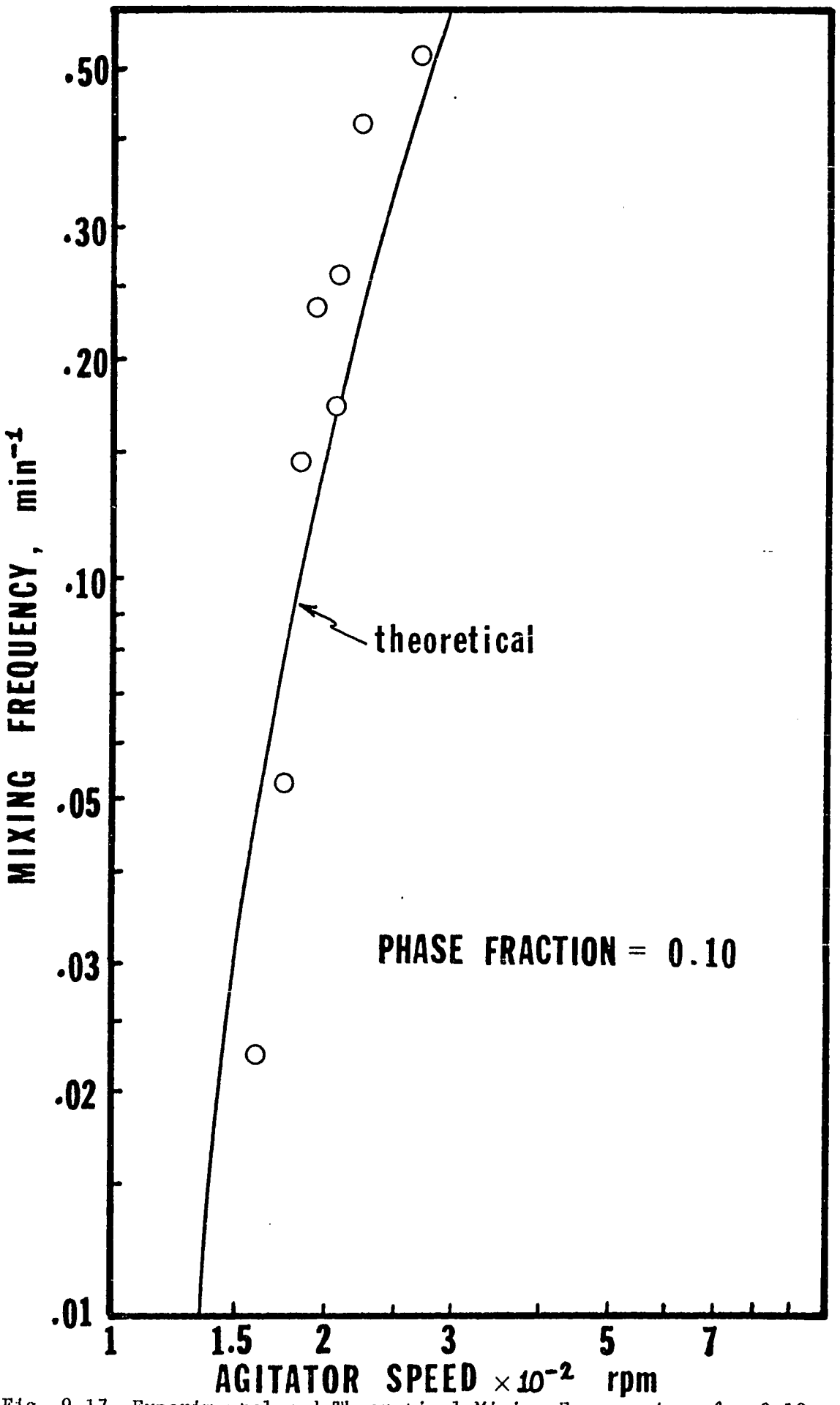

Fig. 9.17 Experimental and Theoretical Mixing Frequencies, θ = 0.10

Reproduced with permission of the copyright owner. Further reproduction prohibited without permission.

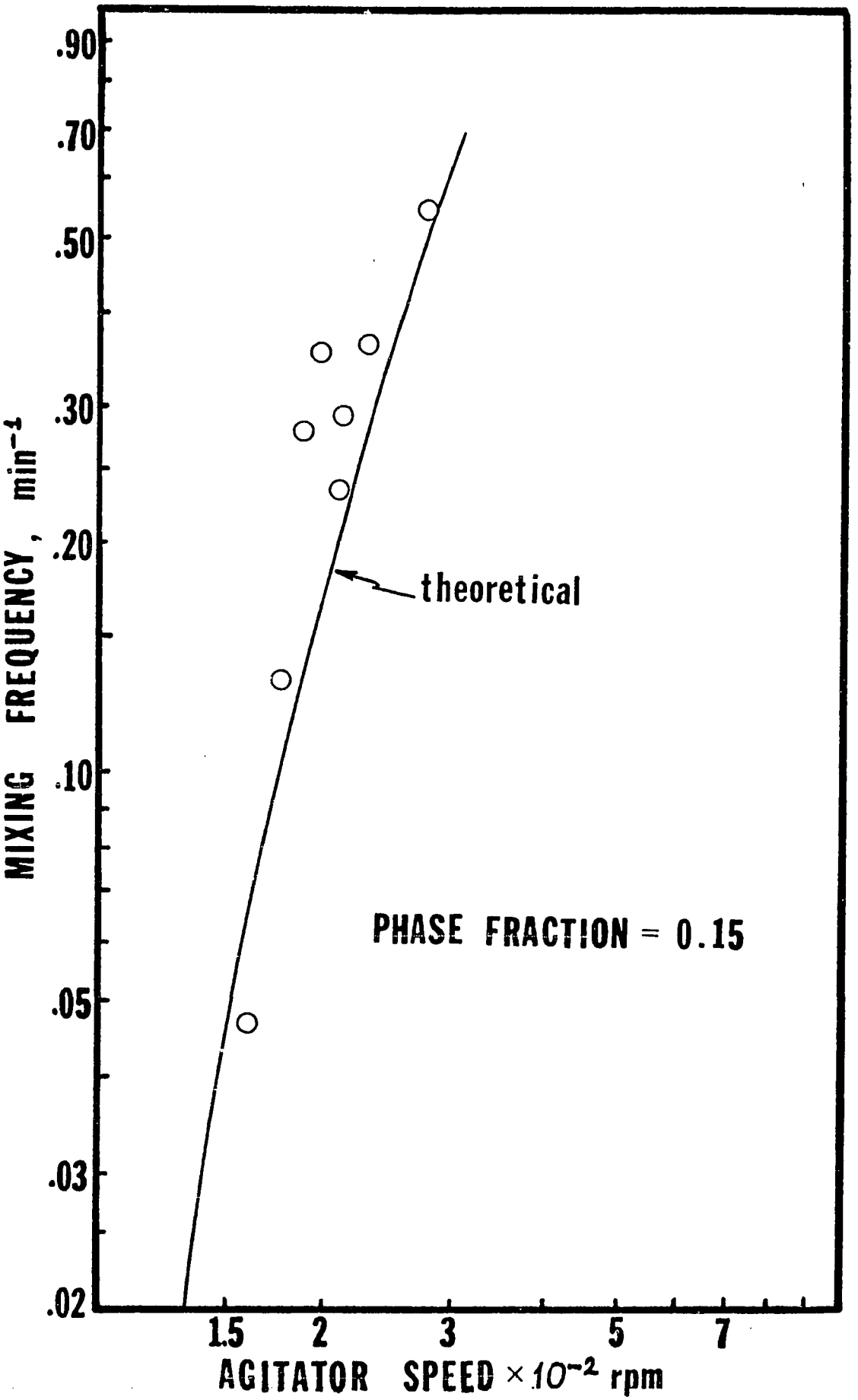

Fig. 9.18 Experimental and Theoretical Mixing Frequencies, $\theta = 0.15$

Reproduced with permission of the copyright owner. Further reproduction prohibited without permission.

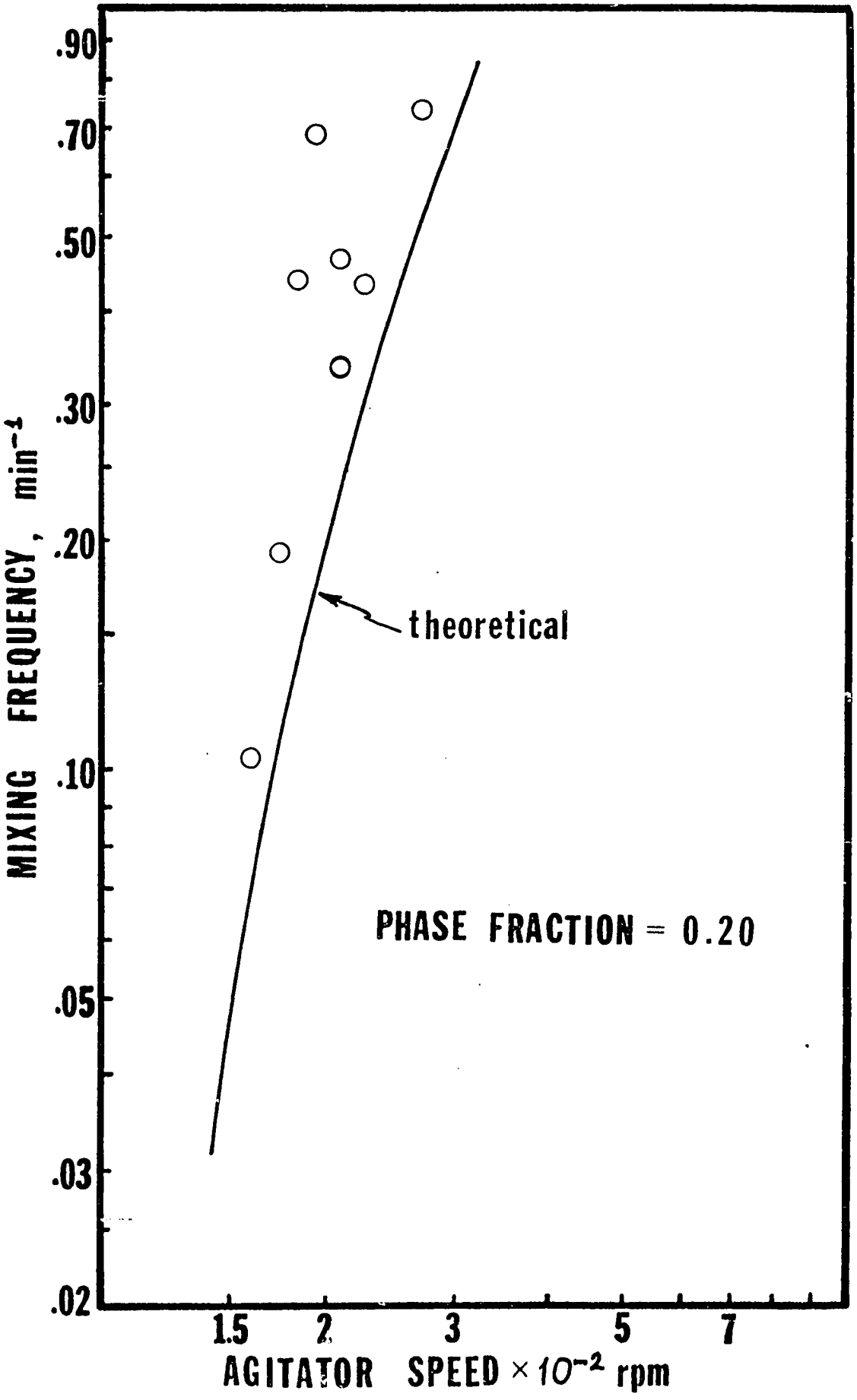

Fig. 9.19 Experimental and Theoretical Mixing Frequencies, $\theta = 0.20$

Reproduced with permission of the copyright owner. Further reproduction prohibited without permission.

9.4

$$h(v_1,v_2)\lambda(v_1,v_2) = \frac{0.625\times10^{-7}N(v_1^{1/3}+v_2^{1/3})^2}{1+5\theta}\exp\left\{-\frac{3.66\times10^{-4}N^3}{(1+5\theta)^3}\left(\frac{v_1^{1/3}v_2^{1/3}}{v_1^{1/3}+v_2^{1/3}}\right)^4\right\}$$

This function for $\theta = 0.05$, N = 160 rpm, and N = 278 rpm is plotted in figure 8.7 for two conditions.

9.3 Discussion of Results

The comparison of the experimental and mathematical results is shown in figures 9.2 - 9.19 is considered favorable. The theoretical Sauter-mean diameter agitator speed curves obtained for all phase fractions are almost the "best" curves through the experimental values (figures 9.12 - 9.15). The drop-size distribution curves also fit remarkably well, especially the cases at the lower phase fractions. At the higher phase fractions (only the 0.15 curves are shown here), the theoretical curves are more peaked than the experimental ones. The theoretical mixing frequencies shown in figures 9.16 - 9.19, although not displaying the extreme sensitivity to N as do the experimental values, are considered to be satisfactory.

The inclusion of "packing" parameters ($1 + \theta$, for the case of breakage and $1 + 5\theta$, for the case of coalescence) aided in the fitting of the high - θ experimental results. Although the theoretical basis for the introduction of a "packing" effect is reasonable (see Section 7.4(f)), the exact functional dependency is unknown. The $(1 + k_B\theta)$ and $(1 + k_c\theta)$ functions can be considered simply to be "resetting" functions which define the extent of turbulence-damping that is occurring at each dispersed phase concentration. Once defined they stay constant within each θ level and for varying

Reproduced with permission of the copyright owner. Further reproduction prohibited without permission.

agitator speeds. It is seen from equations 9.3 and 9.4 that the breakage frequency is affected to a much less extent than the coalescence frequency.

The good fits support a degree of validity of the derived theoretical models. This is especially true considering the several simplifying assumptions that were made, and considering the dramatic nature of the experimental results to be fit.

9.4 Comparison with Other Work

Groothius and Zuiderweg (15) carried out experiments in a continuous flow system similar to ours using a dispersed phase made up of a mixture of carbon tetrachloride and benzene with a density of about 1 gm/ml. Mixing frequency values for various power input were determined. The experimental conditions were θ = .08 and residence time, T, = 6 to 7 minutes. The best line through their results has a N^3 dependency.

Miller et. al. (32) performed batch mixing experiments in a similarly agitated vessel and a similar dispersed phase (iso-octane/carbon tetrachloride, made up to a density of 1 gm/ml). Although the data were not presented in their paper, they include the mixing frequency values at power input of 10 HP/1000 gal , and the slope of the best lines through their data. For each of four phase fractions (0.10 - 0.40) the dependency is $\propto N^3$.

These experimenters' results are presented in figure 9.20 along with the experimental and theoretical results of this work at θ = 0.10 and T = 19.6 minutes. All systems have dispersed phases whose density is 1 gm/ml. The part of the theoretical curve beyond

Reproduced with permission of the copyright owner. Further reproduction prohibited without permission.

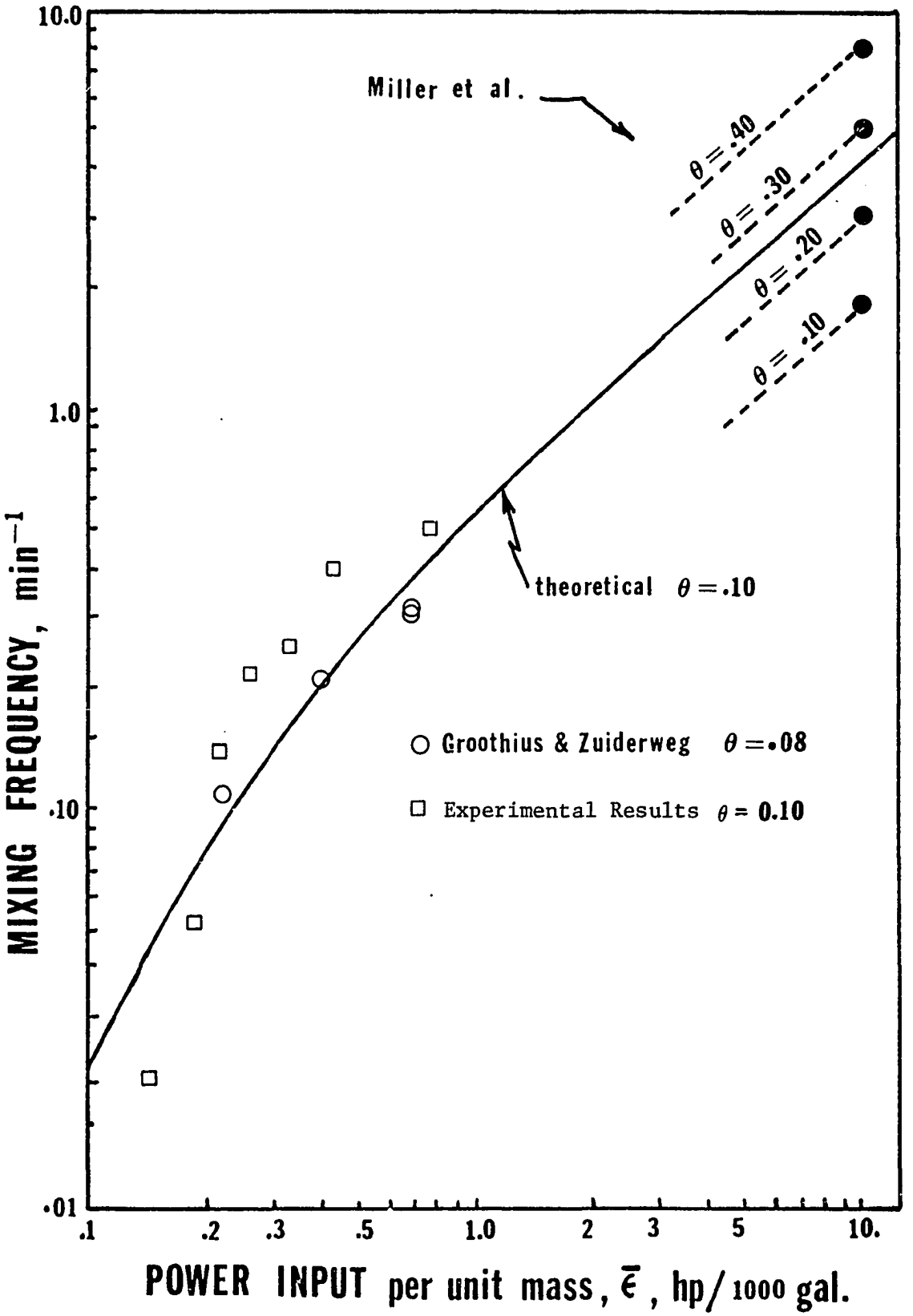

Fig. 9.20 Comparison of Mixing Frequencies with Other Work

Reproduced with permission of the copyright owner. Further reproduction prohibited without permission.

N = 278 rpm was obtained by carrying out a computer run at N = 500 rpm ($\bar{\varepsilon}$ = 4.43 HP/1000 gal). In this range the theoretical mixing frequency, ω_m, varies as N^3.

In view of the radically different techniques in all studies, the results are rather favorable.

Reproduced with permission of the copyright owner. Further reproduction prohibited without permission.

CHAPTER 10

SUMMARY

In this research, which is a continuation of the work started by Curl and Verhoff in 1964, the intention was to obtain a quantitative description of the mixing processes in a continuous flow, dispersed phase mixing vessel. The method for doing this involved (1) the experimental measurement of drop-size distributions and mixing rates for various conditions of agitator speed and dispersed phase fraction, and (2) the theoretical development of breakage and coalescence models which could be used in a mixing equation to generate drop-size distributions and mixing rates. The validity of these models was determined by the ability of the theoretical distributions and rates to explain and fit the experimental values.

The experimental information was obtained by a method, developed by Verhoff previously, which measured the bivariate drop volume-dye concentration distribution of the dispersed phase drops in the vessel. The 1.37 liter Rushton vessel was fed by two dispersed phase streams of drops of known size containing different concentrations of light-absorbing dye. The system was sampled at steady state by means of withdrawing a few hundred drops at one time, stabilizing them, and forcing them through a thin capillary upon which a photometer was focussed through a microscope. The photometer output consisted of a series of rectangular pulses which represent drop volume

Reproduced with permission of the copyright owner. Further reproduction prohibited without permission.

and concentration. These were digitized and analyzed on the computer.

The drop size - dye concentration distributions, based on 1000 - 3000 drops each, were determined in this way for a matrix of experiments in which agitator speed (160 - 278 rpm) and dispersed phase fraction (.025 - 0.20) were varied.

Because of the large sample size and the sophistication of the experimental technique, the results were found to be very reproducible. The drop-size distributions were found to be comparable to previously reported size dependence on agitator speed and phase fraction, the Sauter-mean diameter decreasing inversely with increasing agitator speed. The dispersed phase mixing rate, determined from the dye-concentration variance of the drops in the vessel, was found to vary dramatically in the agitator speed range studied. At the lower speeds where the mixing rates were small, a 10% increase in agitator speed resulted in a 300% increase in mixing frequency. At the higher agitator speeds the dependency was found to be more conventional, mixing frequency varying as N to the 3rd power.

The above results formed the basis for a theoretical modeling of the mixing processes. This involved the use of previously developed integro-differential equations, derived from conservation principles, which relate the distribution of drop sizes and overall mixing rates to the breakage and coalescence mechanisms. Initially very crude mixing models were used in conjunction with these mixing equations to generate distributions and mixing rates which were then compared to the experimental results. Gradually these models were changed and made more applicable on the basis of this comparison. Eventually mixing models were developed which not only could explain the experi-

Reproduced with permission of the copyright owner. Further reproduction prohibited without permission.

mental results but also were general enough to be compatible with the findings of other researchers.

The breakage model that was developed was based on the idea that a drop breaking in a turbulent field is analogous to a molecule decomposing in a thermal field. The drop is taken to be "activated" if the turbulent kinetic energy is sufficient to make up the difference in surface energy between the single drop and the smaller drops formed on break-up. Applying the theory of local isotropy and the transition-state theory, the number rate of breakage for n_d drops of size d was derived as:

$$\text{breakage rate} = k_2 \cdot N \cdot \left(\frac{D}{d}\right)^{2/3} \cdot n_d \cdot \exp\left\{- k_1 N_{we}^{-1} \left(\frac{D}{d}\right)^{5/3}\right\}$$

where D = impeller diameter, N_{we} is the Weber number and N is the agitator speed.

The coalescence model was derived, in part, by (1) extending the theoretical equations describing the approach of a deformable drop to a flat liquid-liquid surface to apply to two approaching liquid drops in a turbulent field, (2) taking the coalescence efficiency to be a function of the coalescence time and contact time during collision, and (3) taking the contact time to be distributed exponentially. The coalescence rate between n_1 and n_2 drops of size d_1 and d_2 was derived to be:

$$\text{coalescence rate} = k_4 \cdot N \cdot (d_1+d_2)^2 \cdot n_1 n_2 \cdot e^{-k_3 N^3 \cdot \left(\frac{d_1 \cdot d_2}{d_1+d_2}\right)^4}$$

Reproduced with permission of the copyright owner. Further reproduction prohibited without permission.

These models were used in the mixing equations and found to fit the results for the condition of low dispersed phase fraction. In order to fit the entire range of experimental results, the above equations were modified by accounting for the damping of turbulence at high droplet concentrations. The constants in the modified equations were adjusted by trial-and-error such that the drop size distributions and mixing rates, numerically generated, fit the experimental results. This comparison was favorable and indicated the general validity of the derived mixing models.

The mixing models can be used to explain the results of other research in batch systems, in particular, the $d \propto N^{-6/5}$ dependency for breakage in the absence of coalescence, and the $d \propto N^{-3/4}$ dependency and the concept of "turbulence-stabilized" dispersions for coalescence in the absence of breakage.

Reproduced with permission of the copyright owner. Further reproduction prohibited without permission.

APPENDICES

Reproduced with permission of the copyright owner. Further reproduction prohibited without permission.

APPENDIX I

DATA REDUCTION PROGRAM

(a) Description

The data from the experiments (the height and base of each rectangular pulse produced by a drop passing through the capillary) are available on computer cards. The program described here converts these values into real volumes by using input information of capillary volumetric flow rate, smallest drop size measured, and taping-speed ratios. Then all the various bivariate distributions and system statistics are calculated.

The computer program described in Appendix IX in Verhoff's thesis formed the basis for this program. Added onto his program are: (1) the calculation of a diameter-concentration distribution, and marginal diameter distribution, (2) the calculation of the concentration variance ratio, C_r, (3) the listing of the largest drops in the sample, (4) the listing of the highest and lowest concentration drops in an ordered sequence and (5) the filtering process described in the next Appendix.

This filtering process works as follows. Of the L drops in the sample, the NNN lowest concentration drops are ordered from the lowest concentration, CONCL upwards. These NNN drops are divided into KW intervals and the program searches for the interval containing

Reproduced with permission of the copyright owner. Further reproduction prohibited without permission.

the maximum volume density. The concentration at this interval is AVL2 (or AVLCW). Then the program searches for the concentration, AVL1, where the volume between CONCL and AVL2 equals the volume between AVL2 and AVL1. Once found, all the volume between CONCL and AVL1 (TOTLO) is put at AVL2. The equivalent procedure is carried out at the high concentration zone. If desired, the AVL2 and AVH2 values can be read in.

The program prints the following information:

(i) The maximum and minimum drop sizes and concentrations, the total volume in the sample, the average concentration, the first, second, third and cross moments of concentration and volume.

(ii) The bivariate distributions of (a) concentration-volume, (b) concentration-log volume, (c) concentration-volume (minus DPC fraction in upper range, and (d) concentration-diameter.

(iii) The marginal distributions of volume, log-volume, concentration and diameter.

(iv) A listing of the largest forty drops.

(v) An ordered list of the NNN lowest and highest concentration drops.

(vi) The statistics of v_{10}, v_{21}, d_{32}, and C_r.

(b) Use of Program and Cards

The experimental data are on computer cards in the format 2014, KONT (I), KONC (I), I = I, L where KONT is the drop "volume" and KONC is the drop "concentration" and L is the total number of

Reproduced with permission of the copyright owner. Further reproduction prohibited without permission.

drops. In order to get actual volumes and concentrations, the capillary volumetric flow rate, FRT, is needed and the minimum drop size, SDR is needed. These are given below in Table I. In addition AVL2, and AVH2 are given in the table. Let us consider the cards to be read in:

READ (5, 83) NEXP

READ (5, 200) NSS, FLOW, PHFR

READ (5, S) NBR, ... SDR

Here Choose

NBR = 30006, NSSB = 2000, NLEV = 85,

NOS = 1, NDIM = 10, NOO = 3, NORG = 1,

NMA = 20, BB = 4000, FAC = 8.0, FREQ = 15000.0

FRT and SDR are obtained from Table I

READ (5, 17) NSPDA ..... DRM

Here Choose

NSPDA = 1, NSTDA = 1, NDIP = 10, DPC = 0.04, DRM = 0.0

READ (5, 83) L

READ (5, 83) NNN

get L and NNN from Table I

READ (5, 83) KW

READ (5, 83) KZ

Choose KW = KZ = 40

READ (5, 83) NCONT

READ (5, 82) AA, BB

If the peak values AVL2 and AVH2 are to be set, read in AA = AVL2 and BB = AVH2 using the values in Table I or other values desired.

Reproduced with permission of the copyright owner. Further reproduction prohibited without permission.

Reproduced with permission of the copyright owner. Further reproduction prohibited without permission.

TABLE I

DATA REDUCTION PROGRAM PARAMETERS

	N = 160 θ = .05	N = 160 θ = .10	N = 160 θ = .15	N = 160 θ = .20	N = 174 θ = .05	N = 174 θ = .10	N = 174 θ = .15	N = 174 θ = .20
L	1828	3046	3155	1656	1265	1693	1781	979
NNN	800	1500	1000	300	500	400	300	200
FRT	2.550	3.540	4.970	4.970	1.260	1.260	1.260	1.790
SDR	0.0570	0.0790	0.110	0.110	0.0282	0.0282	0.0282	0.040
AVL2	260	257	253	252	292	283	288	287
ALH2	550	550	543	550	642	643	656	646

	N = 185 θ = .05	N = 185 θ = .10	N = 185 θ = .15	N = 185 θ = .20	N = 195 θ = .05	N = 195 θ = .10	N = 195 θ = .15	N = 195 θ = .20
L	2188	1507	2838	1735	2862	2871	3621	1880
NNN	500	300	400	200	300	200	400	100
FRT	1.26	1.26	1.79	1.79	1.26	1.79	1.79	2.63
SDR	.0282	.0282	.040	.040	.0282	0.04	0.04	0.0586
AVL2	305	302	277	274	297	278	270	275
ALH2	602	604	579	569	628	619	604	590

Reproduced with permission of the copyright owner. Further reproduction prohibited without permission.

TABLE I - Continued

	N = 210 θ = .05	N = 210 θ = .10	N = 210 θ = .15	N = 210 θ = .20	N = 210 θ = .05	N = 210 θ = .10	N = 210 θ = .15	N = 210 θ = .20
L	2042	3365	2020	2065	3073	3563	1816	1767
NNN	400	350	180	130	1000	700	400	200
FRT	0.925	1.29	1.29	1.79	0.925	1.29	1.29	1.79
SDR	0.0206	0.0288	0.0288	0.040	0.0206	0.0288	0.0288	0.04
AVL2	294	298	289	278	341	334	335	300
ALH2	667	654	648	635	645	625	622	583

	N = 227 θ = .05	N = 227 θ = .10	N = 227 θ = .15	N = 227 θ = .20	N = 278 θ = .05	N = 278 θ = .10	N = 278 θ = .15	N = 278 θ = .20
L	1952	3917	2520	2543	4089	2903	3528	4229
NNN	300	500	300	200	300	200	200	100
FRT	0.925	0.925	1.29	1.79	0.925	0.925	0.925	0.925
SDR	0.0206	0.0206	0.0288	0.040	0.0206	0.0206	0.0206	0.0206
AVL2	233	227	216	213	208	195	184	173
AVH2	563	580	573	558	592	588	577	565

N in rpm, SDR in mm^3 and FRT in mm^3/sec.

In this case, make NCONT = 0. If the computer is to search for AVL2 and AVH2 make NCONT = 1 and read in any values for AA and BB.

READ (5, 7) OPTP, ... OPTB

Here read in the following formats

(10F10.7)

(10F10.7 / 10F10.7)

(10F10.7)

(2014)

Follow all these read-in cards with the deck of data, making sure the top card, which is a MTS identification card, is removed.

List of Variables

All variables not included here are found in Verhoff's thesis pg. 159. The variables are listed in order of appearance.

SYMBOL	DESCRIPTION
NEXP	Experiment number
NSS	Agitator Speed, rpm
FLOW	Total volumetric flow into vessel, cc/min
PHFR	Dispersed phase fraction
L	Number of drops in sample
NBEG, NEND	Drop numbers range being considered, NBEG = 1, NEND = L, for all drops.
NNN	Number of drops to be sorted in upper and lower concentration zones.
KW, KZ	Number of intervals in upper and lower concentration zones.

Reproduced with permission of the copyright owner. Further reproduction prohibited without permission.

SYMBOL	DESCRIPTION
NCONT	0, read in AA and BB 1, AVLOW and AVHI calculated
AA, BB	Low and high concentration peak values read in.
TOTLO	Total volume in low concentration region between CONCL and AVL1.
TOTHI	Total volume in high concentration region between CONCM and AVH1.
LOW (I), LHIGH (I), AHI (I), LMOL (I)	Vectors used in the ordering of the low and high concentration regions and subsequent calculation of AVL2, AVH2, AVL1 and AVH1.
AVL2 = AVLOW	Minimum concentration peak value
AVH2 = AVHI	Maximum concentration peak value
AVL1	Low concentration where the volume between CONCM and AVHI equals the volume between AVHI and AVH1.
DIAM	Diameter
CDIAM	Concentration-diameter distribution
VDMAR	Marginal diameter distribution
VAR	Concentration variance ratio
SMD	Sauter-Mean diameter, d_{32}
VADS	Volume average drop size, v_{21}
ADS	Number average drop size, v_{10}
ACON	Average concentration $\bar{C}$

Reproduced with permission of the copyright owner. Further reproduction prohibited without permission.

```
      DIMENSION KONT(6000),LMOL(40)
       DIMENSION OTP(20),KONC(10000),CDIST(32,32),FCONC(2),CLDST(32,32)
       DIMENSION VMAR(30),VLMAR(30), CMAR(30),OPTM(20)
       DIMENSION CSDT(32,32),OPTA(20),OPTB(20)
      DIMENSION VOMAR(40),CDIAM(32,32)
      DIMENSION LOW(2000),LHIGH(2000),ALOW(100),AHI(100)
      DIMENSION F(50),FF(50),FFF(50)
  199 FORMAT('1',10X,'EXPERIMENT NUMBER IS ',1I5/)
  300 FORMAT('0',9X,'MKONT',10X,'DMAX',10X,'DMIN',10X,'DRM',9X,'CONCM',9
     1X,'CONCL'/)
  301 FORMAT('0',14X,'L',11X,'ADS',11X,'SMV',11X,'TMV',11X,'CVC',9X,'SMV
     2AC'/)
  302 FORMAT('0',11X,'NKSD',10X,'ACON',11X,'SMC',11X,'TMC',9X,'SMCAV',10
     3X,'STOT'/)
  303 FORMAT('0',25X,' CONCENTRATION-VOLUME DISTRIBUTION'/)
  304 FORMAT('0',25X,'CONCENTRATION-LOG VOLUME DISTRIBUTION'/)
  306 FORMAT('0',5X,'CONCENTRATION-VOLUME DISTRIBUTION MINUS ',1F10.4,1X
     4,'FRACTION IN UPPER RANGE'/)
  307 FORMAT('0',25X,'MARGINAL VOLUME DISTRIBUTION'/)
  308 FORMAT('0',25X,'MARGINAL LOG-VOLUME DISTRIBUTION'/)
  309 FORMAT('0',25X,'MARGINAL CONCENTRATION DISTRIBUTION'/)
  310 FORMAT('0',25X,'THE LARGEST 40 DROPS ARE'/)
  311 FORMAT('0',25X,'THE LOWEST CONCENTRATION DROPS ARE'/)
  312 FORMAT('0',25X,'THE HIGHEST CONCENTRATION DROPS ARE'/)
  313 FORMAT('0',10X,'THE STIRRING SPEED= ', 1I5/)
  314 FORMAT('0',10X,'THE TOTAL FLOW RATE = ',1F10.3/)
  315 FORMAT('0',10X,'THE PHASE FRACTION= ',1F10.3/)
  316 FORMAT(10X,4E14.6/)
  317 FORMAT('0',19X,'AVL1',10X,'AVH1',10X,'AVL2',10X,'AVH2'/)
  318 FORMAT('0',10X,'SAUTER-MEAN DIAMETER= ',1E14.6/)
  319 FORMAT('0',25X,'CONCENTRATION-DIAMETER DISTRIBUTION'/)
  320 FORMAT('0',25X,'MARGINAL DIAMETER DISTRIBUTION'/)
  321 FORMAT('0',25X,'VOLUME DIVISIONS'/)
  322 FORMAT('0',25X,'LOG-VOLUME DIVISIONS'/)
  323 FORMAT('0',25X,'DIAMETER DIVISIONS'/)
  324 FORMAT(10F10.6/11F10.6)
  325 FORMAT('0',10X,'NUMBER AVERAGE DROP VOLUME = ',1E14.6/)
  326 FORMAT('0',10X,'VOLUME AVERAGE DROP VOLUME = ',1E14.6/)
572    FORMAT(6I10,2E12.4)
571    FORMAT(25(1X,Z4))
   52 FORMAT(10I8/10I8/10I8/10I8)
17     FORMAT (3I10,2F10.4)
717    FORMAT(20I4)
   83 FORMAT(2I10)
7      FORMAT (20A4)
82     FORMAT(2F15.6)
87     FORMAT (1I15,5E14.6)
5      FORMAT  (8I5,5F8.4)
   88 FORMAT('0',11E10.4)
  100 FORMAT('0',1I15.1E14.6)
  200 FORMAT(1I10,3F10.3)
  702 FORMAT('0','FRACTION OF VOLUME IN UPPER CONC. ZONE = ',1E14.6/)
  703 FORMAT('0','FRACTION OF VOLUME IN LOWER CONC. ZONE = ',1E14.6/)
  704 FORMAT('0','CONCENTRATION VARIANCE RATIO,OUTPUT TO INPUT = ',1E14.
```

Reproduced with permission of the copyright owner. Further reproduction prohibited without permission.

```
     16/)
      READ(5,83)  NEXP
      READ(5,200) NSS,FLOW,PHFR
       READ(5,5) NBR,NSSB,NLEV,NOS,NDIM,NDO,NORG,NMA,BB,FRT,FAC,FREQ,SDR
       READ(5,17) NSPDA,NSTDA,NDIP,DPC,DRM
      READ(5,83) L
      READ(5,83) NNN
      READ(5,83) KW
      READ(5,83) KZ
      READ(5,83) NCONT
      READ(5,82) AA,BB
      READ(5,83) NBEG,NEND
       READ (5,7)  (OTP(I),I=1,20)
       READ(5,7) (OPTM(I),I=1,20)
       READ (5,7) (OPTA(I),I=1,20)
       READ (5,7)  (OPTB(I),I=1,20)
      READ(5,OPTB) (KONT(I),KONC(I),I=1,L)
      NDEL=NEND-NBEG+1
      DO 1 KSY=1,NDEL
      KONT(KSY)=KONT(NBEG+KSY-1)
      KONC(KSY)=KONC(NBEG+KSY-1)
    1 CONTINUE
      L=NDEL
       NSSBS=NSSB
       LT=0
       KOUNT=0
      JK=0
      TOTLO=0.0
      TOTHI=0.0
       MOLES=0
       MKONT=0
       NOG=0
       CONCM=0.0
       CONCL=10000.0
      DO 70 I=1,40
   70 LMOL(I)=0
      DO 71 I=1,NNN
      LOW(I)=1000
      LHIGH(I)=0
   71 CONTINUE
      DO 605 IJJ=1,KW
  605 AHI(IJJ)=0.0
      DO 607 IJJJ=1,KZ
  607 ALOW(IJJJ)=0.00
       NKSD=SDR*FREQ/(2.0*FRT*FAC*NOS)
       SOEK=FRT*FAC*NOS*2.0/FREQ
       STOT=0.0
       S1=0.0
       C1=0.0
       S2=0.0
       S1C1=0.0
       C2=0.0
       S3=0.0
       S2C1=0.0
       S1C2=0.0
```

Reproduced with permission of the copyright owner. Further reproduction prohibited without permission.

```
      C3=0.0
      TD=0.0
      DO 78 I=1,L
      D=(KONT(I))**0.6667
      TD=TD+D

      IF(KONT(I).LE.LMOL(1)) GO TO 91
       DO 72 I1=2,40
       IF (KONT(I).LT.LMOL(I1))  GO TO 77
      LP=I1
72     LMOL(I1-1)=LMOL(I1)
      I1=LP+1
77     LMOL(I1-1)=KONT(I)
 91  CONTINUE
      IF(KONC(I).GE.LOW(1)) GO TO 92
      DO 76 I2=2,NNN
      IF(KONC(I).GT.LOW(I2)) GO TO 79
      LPP=I2
 76   LOW(I2-1)=LOW(I2)
      I2=LPP+1
 79   LOW(I2-1)=KONC(I)
 92   CONTINUE
      IF(KONC(I).LE.LHIGH(1)) GO TO 400
      DO 74 I3=2,NNN
      IF(KONC(I).LT.LHIGH(I3)) GO TO 75
      LPPP=I3
 74   LHIGH(I3-1)=LHIGH(I3)
      I3=LPPP+1
 75   LHIGH(I3-1)=KONC(I)
400   CONTINUE
      IF(I.NE.L)  GO TO  670
      IF(NCONT.EQ.0) GO TO 800
      DIVL=(LOW(1)-LOW(NNN))/(KZ-0.001)
      DIVH=(LHIGH(NNN)-LHIGH(1))/(KW-0.001)
      DO 600 II=1,NNN
      LLOW=LOW(1)-LOW(II)
      LHI=LHIGH(NNN)-LHIGH(II)
      JLOW=LLOW/DIVL
      JHI=LHI/DIVH
      ALOW(JLOW+1)=ALOW(JLOW+1)+II
600   AHI(JHI+1)=AHI(JHI+1)+II
      MAXL=0
      MAXH=0
      DO 601 IJ=1,KW
      IF(AHI(IJ).LE.MAXH) GO TO 660
      MAXH=AHI(IJ)
      KHI=IJ
660   CONTINUE
601   CONTINUE
      DO 606 IJ=1,KZ
      IF(ALOW(IJ).LE.MAXL) GO TO 606
      MAXL=ALOW(IJ)
      KLOW=IJ
```

Reproduced with permission of the copyright owner. Further reproduction prohibited without permission.

```
606 CONTINUE
    AVLOW=LOW(1)-DIVI*KLOW
    AVHI=LHIGH(NNN)-DIVH*KHI
    GO TO 801
800 AVLOW=AA
    AVHI=BB
801 SUML=0.0
    SUMH=0.0
    NN=NNN/2
    DO 93 II=1,NNN
    KKLO=II
    SUML=SUML+LOW(NNN-II+1)
    AVL2=SUML/II

    IF(AVL2.GE.AVLOW) GO TO 602
 93 CONTINUE
602 CONTINUE
    DO 603 II=1,NNN
    KKHI=II
    SUMH=SUMH+LHIGH(NNN-II+1)
    AVH2=SUMH/II
    IF(AVH2.LE.AVHI) GO TO 604
603 CONTINUE
604 CONTINUE
670 CONTINUE
78   CONTINUE
    AVL1=LOW(NNN-KKLO+1)
    AVH1=LHIGH(NNN-KKHI+1)
    CONCM=AVH2
    CONCL=AVL2
    DO 65 I=1,L
    IF(KONC(I).GT.LOW(NNN-KKLO+1)) GO TO 700
    KONC(I)=AVL2
    TOTLO=TOTLO+KONT(I)
700 CONTINUE
    IF(KONC(I).LT.LHIGH(NNN-KKHI+1)) GO TO 701
    KONC(I)=AVH2
    TOTHI=TOTHI+KONT(I)
701 CONTINUE
     SOAD=KONT(I)*SOEK
     SOAD2=SOAD*SOAD
     SOAD3=SOAD2*SOAD
     CONC7=(KONC(I)-CONCL)/(CONCM-CONCL)
     COAD=SOAD*CONC7
     COAD2=COAD*CONC7
     STOT=STOT+SOAD
     S1=S1+SOAD2
     C1=C1+COAD
     S2=S2+SOAD3
     S1C1=S1C1+SOAD*COAD
     C2=C2+COAD2
```

Reproduced with permission of the copyright owner. Further reproduction prohibited without permission.

```
      S3=S3+SOAD3*SOAD
      S2C1=S2C1+SOAD2*COAD
      S1C2=S1C2+SOAD*COAD2
      C3=C3+COAD2*CONCZ
   65 CONTINUE
      MKONT=LMOL(40)
      SUM=0.0
      DO 53 IE=1,39
      I=41-IE
      SUM=SUM+LMOL(I)*SOEK/STOT
      IF(SUM.GT.DPC.AND.LMOL(I).NE.LMOL(I-1))  GO TO 54
53    CONTINUE
54    LMO=LMOL(I-1)
      IF(DRM.GT.0.0)  LMO=DRM/SOEK
      DO 21 I=1,NMA
      VMAR(I)=0.0
      VLMAR(I)=0.0
      VDMAR(I)=0.0
21    CMAR(I)=0.0
      KGR=NDIP
      IF (NDIM.GT.NDIP)  KGR=NDIM
      DO 85 I=1,KGR
      DO 85 J=1,KGR

      CDIST(I,J)=0.0
      CSDT(I,J)=0.0
      CLDST(I,J)=0.0
   85 CDIAM(I,J)=0.0
      DCM=(CONCM-CONCL)/(NDIP-0.001)
      DVM=(LMO-NKSD)/(NDIP-1.001)
      DC=(CONCM-CONCL)/(NDIM-0.0001)
      DV=(MKONT-NKSD)/(NDIM-0.001)
      DVV=(MKONT-NKSD)/(NMA-0.001)
      DCC=(CONCM-CONCL)/(NMA-0.001)
      BLOG=ALOG(MKONT+0.0001)
      SLOG=ALOG(NKSD+0.0001)
      DLV=(BLOG-SLOG)/(NDIM-0.0001)
      DLVV=(BLOG-SLOG)/(NMA-0.001)
      DIAMM=(6.0/3.1416*MKONT*SOEK)**0.333
      DIAML=(6.0/3.1416*NKSD*SOEK)**0.333
      DDD=(DIAMM-DIAML)/(NMA-0.001)
      DD=(DIAMM-DIAML)/(NDIM-0.001)
      KTOT=0
      DO 90  I=1,L,1
      DIAM=(6.0/3.1416*SOEK*KONT(I))**0.333
      DKOLT=DIAM-DIAML
      KOZT=KONT(I)
      KTOT=KTOT+KOZT
      CLOG=ALOG(KOZT+0.0001)-SLOG
      CONT=KONC(I)-CONCL
      KOLT=KOZT-NKSD
      JKK=CLOG/DLV
      JCC=CONT/DC
```

Reproduced with permission of the copyright owner. Further reproduction prohibited without permission.

```
      JNN=KOLT/DV
      JVV=KOLT/DVV
      JLV=CLOG/DLVV
      JCLC=CONT/DCC
      JKKK=KOLT/DVM
      JCCC=CONT/DCM
     JDD=DKOLT/DD
     JDDD=DKOLT/DDD
      IF(JKKK.GE.NDIP)  JKKK=NDIP-1
     VDMAR(JDDD+1)=VDMAR(JDDD+1)+KONT(I)
      VMAR(JVV+1)=VMAR(JVV+1)+KONT(I)
      VLMAR(JLV+1)=VLMAR(JLV+1)+KONT(I)
     CDIAM(JDD+1,JCC+1)=CDIAM(JDD+1,JCC+1)+KONT(I)
      CMAR(JCLC+1)=CMAR(JCLC+1)+KONT(I)
      CDIST(JKK+1,JCC+1)=CDIST(JKK+1,JCC+1)+KONT(I)
      CSDT(JKKK+1,JCCC+1)=CSDT(JKKK+1,JCCC+1)+KOZT
90  CLDST(JNN+1,JCC+1)=CLDST(JNN+1,JCC+1)+KONT(I)
      TVOL=KTOT
      DO 25 I=1,NMA
     VMAR(I)=VMAR(I)/TVOL/(DVV*SOEK)
     VLMAR(I)=(VLMAR(I)/TVOL)/DLVV
     VDMAR(I)=VDMAR(I)/TVOL/DDD
25     CMAR(I)=CMAR(I)/TVOL
      KGR=NDIP
      IF (NDIM.GT.NDIP)  KGR=NDIM
      DO 95 I=1,KGR
      DO 95 J=1,KGR
      CSDT(I,J)=CSDT(I,J)/TVOL
     CDIAM(I,J)=CDIAM(I,J)/TVOL
      CDIST(I,J)=CDIST(I,J)/TVOL
95  CLDST(I,J)=CLDST(I,J)/TVOL

      DMIN=(NKSD   )*SOEK
     F(1)=DMIN
     FF(1)=ALOG(DMIN)
     FFF(1)=DIAML
     NMAA=NMA+1
     DO 94 I=2,NMAA
     F(I)=F(I-1)+DVV*SOEK
     FF(I)=FF(I-1)+DLVV
94  FFF(I)=FFF(I-1)+DDD
     SMD=((6.0/3.1416)*SOEK)**0.333*TVOL/TD
     AVDV=STOT/L
      ADS=S1/STOT
      SMV=C2/STOT
      TMV=S3/STOT
      CVC=S1C1/STOT
      SMC=C2/STOT
      TMC=C3/STOT
      ACON=C1/STOT
      SMVAC=S2C1/STOT
      SMCAV=S1C2/STOT
      DMAX=MKONT*SOEK
      DRM=LMO*SOEK
     FRHI=TOTHI/TVOL
```

Reproduced with permission of the copyright owner. Further reproduction prohibited without permission.

```
      FRLO=TOTLO/TVOL
      VAR=(SMC-(ACON)**2)/(ACON*(1.00-ACON))
      WRITE(6,199) NEXP
      WRITE(6,313) NSS
      WRITE(6,314) FLOW
      WRITE(6,315) PHER
      WRITE(6,300)
       WRITE(6,87) MKONT,DMAX,DMIN,DRM,CONCM,CONCL
      WRITE(6,301)
       WRITE(6,87) L,ADS,SMV,TMV,CVC,SMVAC
      WRITE(6,302)
       WRITE(6,87) NKSD,ACON,SMC,TMC,SMCAV,STOT
      WRITE(6,303)
       WRITE (6,OTP) ((CLDST(I,J),J=1,NDIM),I=1,NDIM)
      WRITE(6,304)
       WRITE (6,OTP) ((CDIST(I,J),J=1,NDIM),I=1,NDIM)
      WRITE(6,306) DPC
       WRITE(6,OPTA)  ((CSOT(I,J),J=1,NDIP),I=1,NDIP)
      WRITE(6,319)
      WRITE(6,OTP) ((CDIAM(I,J),J=1,NDIM),I=1,NDIM)
      WRITE(6,307)
      WRITE(6,OPTM)      (VMAR(I),I=1,NMA)
      WRITE(6,308)
      WRITE(6,OPTM)      (VLMAR(I),I=1,NMA)
      WRITE(6,309)
      WRITE(6,OPTM)      (CMAR(I),I=1,NMA)
      WRITE(6,320)
      WRITE(6,OPTM)      (VDMAR(I),I=1,NMA)
      WRITE(6,310)
      WRITE(6,52) (LMOL(I),I=1,40)
      WRITE(6,311)
      WRITE(6,OPTR) (LOW(I),I=1,NNN)
      WRITE(6,312)
      WRITE(6,OPTR) (LHIGH(I),I=1,NNN)
      WRITE(6,317)
      WRITE(6,316) AVL1,AVH1,AVL2,AVH2
      WRITE(6,703) FRLO

      WRITE(6,702) FRHI
      WRITE(6,318)  SMD
      WRITE(6,326) ADS
      WRITE(6,325) AVDV
      WRITE(6,704) VAR
      WRITE(6,321)
      WRITE(6,324) (F(I),I=1,NMAA)
      WRITE(6,322)
      WRITE(6,324) (FF(I),I=1,NMAA)
      WRITE(6,323)
      WRITE(6,324) (FFF(I),I=1,NMAA)
      WRITE(6,100) LMO,SOFK
       END
```

Reproduced with permission of the copyright owner. Further reproduction prohibited without permission.

APPENDIX II

DETERMINATION OF CONCENTRATION VARIANCE

The estimate of the experimentally determined mixing frequency, ω , on the basis of equation 4.3, requires a knowledge of the concentration variance ratio, C_r, obtained from equation 4.1 and 4.2. The low and high concentrations of the feed are obtained from the average values of these concentrations in the vessel drops. For example, consider the "typical experiment" presented in Section 4.2, with N = 174 rpm and θ = 0.10 (the marginal number-concentration distribution for the upper and lower concentration zones are given in figure II. The numbers for concentration are those on the computer cards and represent the average concentration of the drops in question, and the density function represents the number of drops with a concentration between C_i and $C_i + \Delta C$. Now it is obvious that the high and low concentrations of feed are at the peak values of these high and low concentrations zones. For example the high concentration is at about 640 and the low concentration is at about 290. The fact that these concentrations are distributed is due to high frequency noise. Consider one of the "rectangular" pulses obtained as a drop passes through the capillary. In exaggerated schematic form it looks like:

Reproduced with permission of the copyright owner. Further reproduction prohibited without permission.

Reproduced with permission of the copyright owner. Further reproduction prohibited without permission.

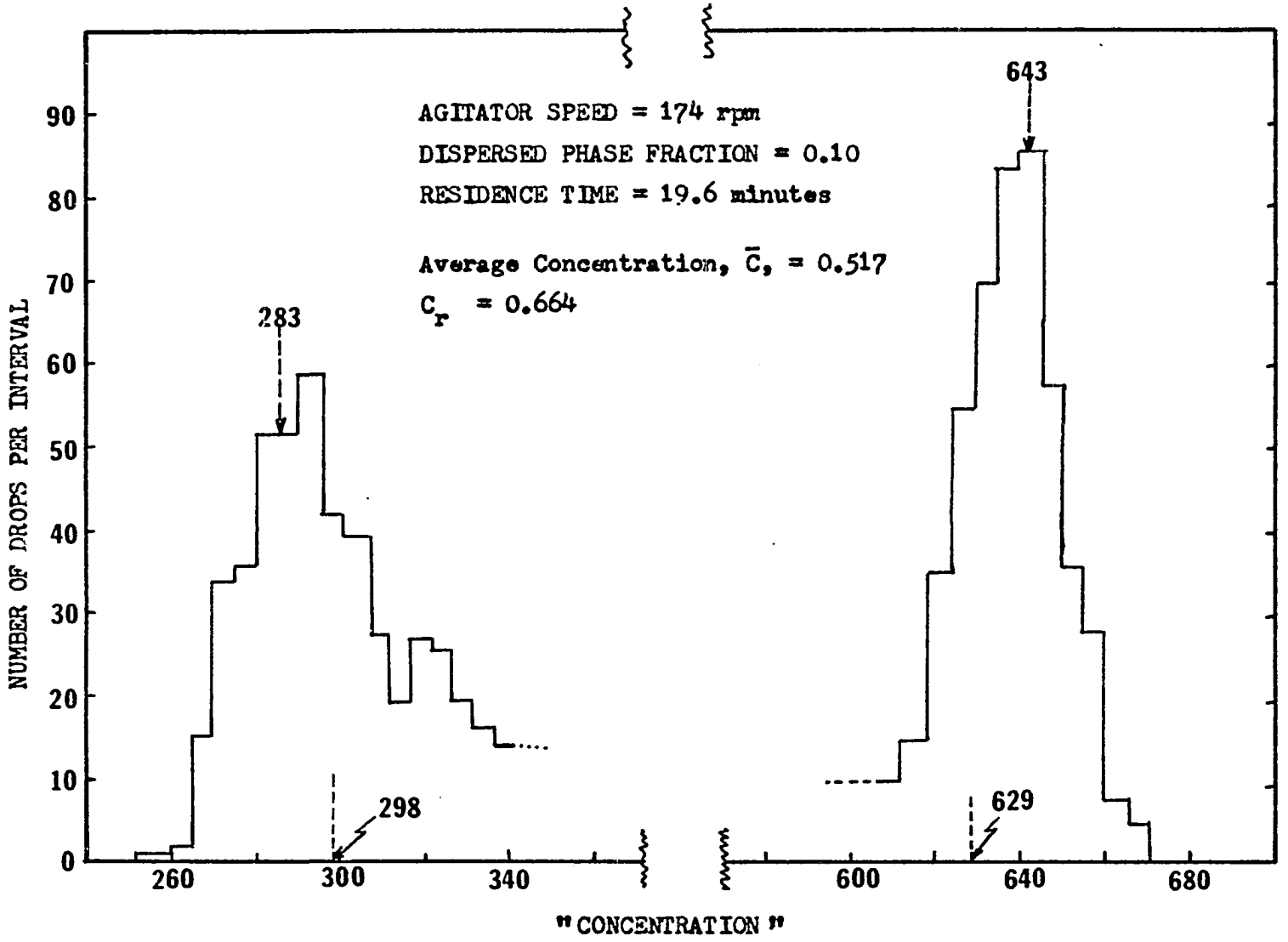

Fig. II Histograms for Lower and Upper Concentration Zones, N = 174 rpm, θ = 0.10

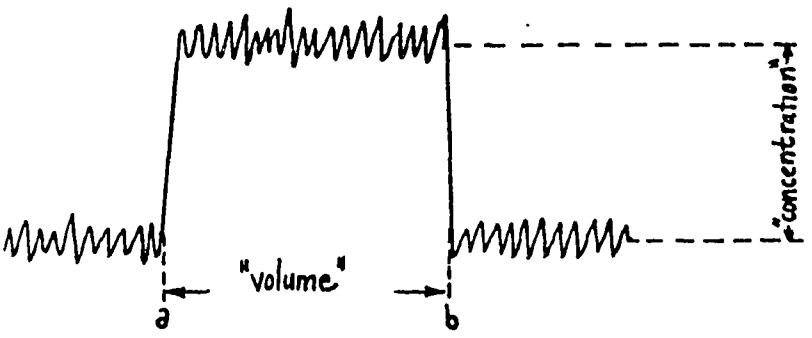

The dye concentration is obtained by averaging all the voltage signals between a and b. It is seen, whereas the concentration has an error associated with it, the volume is very well defined. This is one of the reasons that the marginal drop-size distributions were found to be more reproducible than the marginal concentration distributions. In any case, if no mixing were going on in the vessel, at N = 174 rpm and θ = 0.10, then all the drops would be distributed around $C_L \sim 290$ and $C_H \sim 640$ at shown in figure II. at this hypothetical no-mixing situation, the concentration variance ratio, C_r based on C_H = 640 and C_L = 290 would be greater than 1.0 (using equation 4.1 and 4.2). Clearly this is undesirable because we are interested in how C_r decreases from a value of 1.0 at no-mixing to lower values as mixing proceeds. To rectify this situation, two different techniques were carried out to "remove" this high frequency noise. The simplest technique was to take all the values distributed symmetrically about C_L and C_H and put them at these concentrations. Thus for no mixing the vessel drops would all have concentration at C_L or C_H and these would be delta functions on a density-concentration plot, the C_r value would be equal to 1.0 for no mixing. This was done by the computer program described in Appendix I. The programs orders all the concentration

Reproduced with permission of the copyright owner. Further reproduction prohibited without permission.

values and finds the C_L and C_H concentrations where the volume density is at a maximum. It assumes the distribution to be symmetrical and takes the volume of drops on either side of C_H or C_L to have concentrations of C_H and C_L respectively. For example, in figure II, for the high concentration zone, the peak (on a volume basis) was found to be at 643 and the volume between 629 and 643 was equal to the volume found between 643 and the highest concentration. For the low concentration zone the volume between the lowest concentration and 283 equalled the volume between 283 and 298. Note here that the peak volume obtained (283) on a volume basis is slightly different than that obtained on a number basis. It is seen that the error associated with these peaks is about (643-283) / (643-283) = 3.9% or (298-283) / (643-283) = 4.1%. These high and low concentration regions are less than 1/20 the values between 643 and 283. Thus the high and low concentration intervals shown in figure 4.4 contain the high and low concentration drops. This is essentially true for all the experiments. That is, the first and last 1/20 division in concentration contain the distributed high and low concentrations, C_H and C_L .

Another method of dealing with the high frequency noise was to assume it is distributed normally with zero-mean. Let us say we have the volume density values for N concentration intervals.

Let v_i be the actual volume fraction of the drops in the concentration-interval i, i = 1, ..., N.

Let v_i' be the observed volume fraction of the drops in the concentration-interval i - 1, ..., N.

For any drop c' = c + x where x is a random variable distributed as

Reproduced with permission of the copyright owner. Further reproduction prohibited without permission.

$n(x; 0, \sigma_x)$. Assume that the number of actual drops in each category is large.

Let a_{ij} be the expected volume fraction of actual drops in the interval i which is observed as occurring in interval j. Then:

$$v'_j = a_{1j} v_1 + a_{2j} v_2 \cdots\cdots a_{nj} v_n$$

Let $\bar{v}' = \text{col}(v'_1, \ldots\ldots, v'_n)$

$$\bar{v} = \text{col}(v_1, \ldots\ldots, v_n)$$

$$A = [a_{j,i}]$$

Then $$\bar{v}' = A \cdot \bar{v} \qquad (1)$$

We now need values for a_{ji}. Assume that the volume fraction is uniformly distributed over each interval. Let W be the width of the interval and X be the random variable denoting how far to the right of the L. H. border of the interval, the drop occurs, Then

$$\text{prob}\left\{X = x\right\} = \frac{1}{W} \quad \text{for all } i$$

Let Y be the random variable denoting the concentration error associated with observation process. Let:

$$n(y; o, \sigma_y) = \text{Prob}\left\{Y = y \mid o, \sigma_x\right\}$$

Reproduced with permission of the copyright owner. Further reproduction prohibited without permission.

$Z = X + Y$ where Z is the r. v. denoting the observed concentration. It can be shown that:

$$a_{ij} = \frac{1}{W} \int_c^W \left[N\{(W-x + (j-i)\ W\} - N\{ W-x + (j-i-1)\ W\} \right] dx$$

where N is the cumulative normal distribution.

$\bar{v}'$ can now be solved. The computer program for doing this is shown in the following page. In solving for the noise-free marginal concentration distribution, values of $\bar{v}_x$ were chosen from the data. This method of filtering the noise presented one major difficulty: if $\bar{v}_x$ was taken to be too high, some of the density values become negative. So $\bar{v}_x$ was always chosen such that these volume density never became negative. When this was done it was found that the C_r values calculated on the filtered and non-filtered basis were not very different. This was not surprising considering the small error associated with the measurement of concentration (3 - 5%). For this reason, the first technique was used without zero-mean noise filtering for all the cases presented in this thesis.

Reproduced with permission of the copyright owner. Further reproduction prohibited without permission.

LIST OF VARIABLES

SYMBOL	DESCRIPTION
A(I, J)	Matrix a_{ij}
SIG	σ_x zero mean standard deviation
CONCM	Maximum concentration
CONCL	Minimum concentration
V(I)	v_i
VV(I)	v_i'
N	Number of intervals
W	W
NDTR	Cumulative normal distribution, IBM "package" subroutine
MINR	Matrix inversion, IBM "package" subroutine
SUMV, SUMVV	Volume check; should both equal 1
VAR, ACON	C_r and $\overline{C}$ before filtering
VAR2, ACON2	C_r and $\overline{C}$ after filtering

Reproduced with permission of the copyright owner. Further reproduction prohibited without permission.

```
      READ(5,11) SIG,CONCM,CONCL
$RUN *FORTRAN SPUNCH=-OBJ
      DOUBLE PRECISION A,D,X,P,Q
      DIMENSION A(20,20),L(20),M(20),V(20),VV(20)
      READ(5,9) N,NN
      READ(5,11) (V(I),I=1,N)
      W=(CONCM-CONCL)/N
      H=W/NN
      DO 20 I=1,N
      DO 30 J=1,N
      NNN=NN+1
      Q=0.0
      DO 40 JJ=1,NNN
      X=(-(JJ-1.0)*W/NN-(I-J-1.0)*W)/SIG
      IF(J.EQ.N) X=1000.0
      CALL NORTR(X,P,D)
      RA=P
      X=(-(JJ-1.0)*W/NN-(I-J)*W)/SIG
      IF(J.EQ.1) X=-1000.0
      CALL NORTR(X,P,D)
      RB=P
      ALPHA=1.0
      IF(JJ.EQ.1) ALPHA=0.5
      IF(JJ.EQ.NNN) ALPHA=0.5
      Q=Q+ALPHA*(RA-RB)/W*H
   40 CONTINUE
      A(J,I)=Q
   30 CONTINUE
   20 CONTINUE
      WRITE(6,101) ((A(I,J),J=1,N),I=1,N)
      CALL MINV(A,N,D,L,M)
      WRITE(6,101) ((A(I,J),J=1,N),I=1,N)
      WRITE(6,101) D
      DO 50 J=1,N
      VNEW=0.0
      DO 60 I=1,N
      VNEW=VNEW+A(J,I)*V(I)
   60 CONTINUE
      VV(J)=VNEW
   50 CONTINUE
      WRITE(6,103) (V(I),I=1,N)
      WRITE(6,102)
      SUMVV=0.0
      SUMV=0.0
      SMC=0.0
      ACON=0.0
      SMC2=0.0
      ACON2=0.0
      DO 70 J=1,N
      SUMV=SUMV+V(J)
```

Reproduced with permission of the copyright owner. Further reproduction prohibited without permission.

```
      SUMVV=SUMVV+VV(J)
      CONC=CONCL+(J-0.5)*W
      CONZ=(CONC-CONCL)/(CONCM-CONCL)
      CONZ2=CONZ
      SMC=SMC+V(J)*CONZ*CONZ
      ACON=ACON+V(J)*CONZ
      SMC2=SMC2+VV(J)*CONZ2*CONZ2
      ACON2=ACON2+VV(J)*CONZ2
   70 CONTINUE
      VAR=(SMC-ACON**2)/(ACON-ACON**2)
      VAR2=(SMC2-ACON2**2)/(ACON2-ACON2**2)
      WRITE(6,104) SUMV,SUMVV
      WRITE(6,105) VAR,ACON
      WRITE(6,106) VAR2,ACON2
   11 FORMAT(5E10.3)
  101 FORMAT(10E10.3/10E10.3/)
  102 FORMAT('0','FILTERED VOLUME DISTRIBUTION'/)
  103 FORMAT(10E10.3)
  104 FORMAT('0','SUMV AND SUMVV= ',2E10.3/)
  105 FORMAT('0','VAR AND ACON= ',2E10.3/)
  106 FORMAT('0','VAR2 AND ACON2 =',2E10.3/)
```

Reproduced with permission of the copyright owner. Further reproduction prohibited without permission.

APPENDIX III

PROGRAM FOR SOLUTION OF MIXING EQUATION

The computer program described here for the solution of the mixing equation follows the numerical scheme of equation 5.17 - 5.26 in Chapter 5. The program can be used to calculate the case of breakage-alone or the full breakage and coalescence case. The description of how this program operates is given in Chapter 8.

LIST OF VARIABLES

SYMBOL	DESCRIPTION
PSS	Agitator speed, N, rpm
PHFR	Dispersed phase fraction,
PMAX	Largest drop size in vessel , mm^3
PMIN	Smallest drop size in vessel, mm^3
VT	Tank volume, mm^3
Q	Total flow rate, mm^3/ min
V ZERO	Input drop size, mm^3
N	Number of volume integration intervals
NN	Number of diameter intervals
KOK = 0	No print out for breakage-alone
KOK = 1	Print out for breakage-alone
KN	Number of iterations allowed

Reproduced with permission of the copyright owner. Further reproduction prohibited without permission.

SYMBOL	DESCRIPTION
KM = 1	Breakage-only
KM = 0	Breakage and Coalescence
KDAT = 1	Read in values for Y
= 0	Y values calculated from breakage alone
KPUN = 1	Punch out Y values
= 0	No punch
NERL	Number of Y's to be compared for convergence
AA, BB, CC, DE, FE, Z5, FSS GG, Z1, Z2, Z3, Z4, PF, EE	Breakage "constants" Coalescence "constants"
ERR	Convergence limit
CNU	ν
C	"a" in beta function
FF	f(v), escape frequency
PNA	Number flow rate into vessel, drops/min
H	Integration interval
CA	$a = (a' + 2 - \nu) / (\nu - 1)$
CGAM	Normalizing constant in beta function
VAR	Variance of beta function
SIG	Standard deviation in a(v), σ_o, eq. 8.7
V, VI, VL, VJJ	Volume
G (I)	g(v) breakage frequency
B (I)	$\beta (v/v_o)$
COAL (I, J)	$h(v,v') \cdot \lambda (v, v')$
Y (I)	nA (v), number
A (I)	vnA (v), volume
F	F (equation 5.24)

Reproduced with permission of the copyright owner. Further reproduction prohibited without permission.

SYMBOL	DESCRIPTION
ETA	ξ (equation 5.25)
BETA	$\beta(v/v')$
K	Number of iteration
WW (I)	(v) (equation 5.21)
QNUM	n, total number of drops in vessel
ADS	v_{10} mm^3
VADS	v_{21} mm^3
SMD	Sauter-mean diameter, d_{32}, mm
PHFR3	Readjusted phase fraction
DMAX	Largest drop in vessel, diameter, mm
DMIN	Smallest drop in vessel, diameter, mm
DD	Diameter interval
PD (I)	Diameter p. d. f.
VM	v_m, equation 5.31
PNCR	1/2 ω_n, number coalescence frequency
VCR	ω_v, volume coalescence frequency
MIXR	ω_m, mixing frequency

Reproduced with permission of the copyright owner. Further reproduction prohibited without permission.

```
      REAL MIXR,LIM
      DIMENSION Y(400),A(400),G(400),B(400),YY(400),W(400),D(400)
      DIMENSION WW(400),PD(40),BR(400)
      DIMENSION COAL(300,300)
   79 FORMAT('0','BETA DISTRIBUTION WITH C= ',1F10.3/)
   80 FORMAT(1F10.3)
   97 FORMAT('0','READJUSTED PHASE FRACTION,PHFR3= ',1F10.6/)
   98 FORMAT(2I10)
   99 FORMAT(1E20.6)
  100 FORMAT(2F10.3)
  101 FORMAT('0','BREAKAGE CONSTANTS,AA,BB,CC,DE,FE,FSS,Z5= ',7E11.4/)
  102 FORMAT(5I10)
  105 FORMAT(5F10.3)
  106 FORMAT('0','COALESCENCE EFFICIENCY,EQUAL SIZE DROPS'/)
  107 FORMAT('0','COALESCENCE EFFICIENCY,SMALL DROPS WITH OTHERS'/)
  108 FORMAT(1X,10E11.4)
  109 FORMAT(1X,3F10.6)
  110 FORMAT(1X,1E20.6)
  111 FORMAT(1I10)
  112 FORMAT(7F10.4)
  113 FORMAT(1F10.3)
  114 FORMAT(7F10.4)
  115 FORMAT(3I10)
  116 FORMAT('0','COALESCENCE CONSTANTS,EE,GG,Z1-Z4,PF,=',2E11.4,5F7.3/)
  200 FORMAT('0','PV VOLUME-VOLUME DENSITY DISTRIBUTION'/)
  201 FORMAT('0','AV NUMBER-VOLUME DENSITY DISTRIBUTION'/)
  202 FORMAT('0','BREAKAGE FREQUENCY FUNCTION,G(V)'/)
  203 FORMAT('0','PD VOLUME-DIAMETER DENSITY DISTRIBUTION'/)
  204 FORMAT('0','STIRRING SPEED,PSS= ',1F10.3/)
  205 FORMAT('0','PHASE FRACTION,PHFR= ',1F10.3/)
  209 FORMAT('0','AVERAGE NUMBER OF DROPS PER BREAKAGE,CNU= ',1F10.3/)
  212 FORMAT('0','MAX. AND MIN. DROP SIZE  ,PMAX &PMIN,= ',2F10.3/)
  213 FORMAT('0','NUMBER OF VOLUME & DIAMETER DIVISIONS, N & NN= ',2I5/)
  214 FORMAT('0','ESCAPE FREQUENCY,FF=Q/VT,= ',1F10.4/)
  215 FORMAT('0','TANK VOLUME,VT, & TOTAL FLOW INTO TANK,Q,= ',2E20.6/)
  216 FORMAT('0','IN.DROP VOL,VZERO,& NO. FLOW IN TANK,PNA= ',2E20.6/)
  217 FORMAT('0','AVERAGE DROP SIZE (WRT NUMBER),ADS,= ',1F10.6/)
  218 FORMAT('0','VOLUME-AVERAGE DROP SIZE,VADS,= ',1F10.6/)
  219 FORMAT('0','CALCULATED PHASE FRACTION IN TANK,PHFR2,= ',1F10.6/)
  220 FORMAT('0','SAUTER-MEAN DIAMETER,SMD,= ',1F10.6/)
  221 FORMAT('0','NUMBER OF DROPS IN TANK, ONUM,= ',1E20.6/)
  223 FORMAT('0','DMIN AND DMAX = ',2E20.6/)
  224 FORMAT('0','DIAMETER DIVISIONS'/)
  225 FORMAT('0','VOLUME DIVISIONS'/)
  226 FORMAT('0','BREAKAGE WITHOUT COALESCENCE'/)
  234 FORMAT('0','VOL. COALES.RATE,VCR,&NUM.COALES.RATE,PNCR= ',2E20.6/)
  250 FORMAT('0','VARIANCE OF GAMMA DIST..VAR =',1F10.6/)
  210 FORMAT('0','VARIANCE CONSTANT IN BREAKAGE DIST.,C= ',1F10.3/)
  222 FORMAT('0','NORMALIZING CONSTANT FOR BR. DIST., CGAM= ',1E20.6/)
  235 FORMAT('0','MIXING RATE,MIXR = ',1F20.6/)
  236 FORMAT('0','COALESCENCE FREQUENCY FROM DROP REGION DV'/)
  237 FORMAT(2E20.6,5F5.3)
  238 FORMAT(1E20.6)
```

Reproduced with permission of the copyright owner. Further reproduction prohibited without permission.

```
240 FORMAT(10E8.3)
260 FORMAT('0','ALLOWED ITERATIONS EXCEEDED'/)
300 FORMAT('0','BREAKAGE AND COALESCENCE'/)
400 FORMAT('0','DISTRIBUTION BEFORE LAST ITERATION'/)
    READ(5,100) PSS,PHFR
    READ(5,105) PMAX,PMIN,VT,Q,VZERO
    READ(5,102) N,NN,KOK,KN,KM

    READ(5,115) KDAT,KPUN,NERL
    READ(5,114) AA,BB,CC,DE,FE,FSS,Z5
    READ(5,102) NEXP,NEXP2,NBR
    READ(5,237) EE,GG,Z1,Z2,Z3,Z4,PF
    READ(5,238) ERR
    READ(5,100) CNU,C
    FF=Q/VT
    PNA=PHFR*Q/VZERO
    H=(PMAX-PMIN)/N
    CA=(C+2.0-CNU)/(CNU-1.0)
    CGAM=GAMMA(CA+C+2)/(GAMMA(CA+1)*GAMMA(C+1))
    VAR=GAMMA(CA+C+2)*GAMMA(CA+3)/(GAMMA(CA+C+4)*GAMMA(CA+1))-(1./CNU)
   1**2
    K=0
    VEL=(PSS/160.)/(1.0+Z5*PHFR)
    SIG=(PMAX-VZERO)/3.1
    FN=N
    DO 10 JL=1,N
    V=JL*PMAX/N
    VQ=JL/FN
    ENR=DE*(V**(-FE)*VEL**(-FSS))
    G(JL)=CC*VEL**AA*V**BB*EXP(-(ENR)**NEXP2)
    BR(JL)=CGAM*(VQ)**CA*(1.0-VQ)**C
    B(JL)=(0.3989/(1.0*SIG))*EXP(-(V-VZERO)**2/(2.0*(SIG)**2))
 10 CONTINUE
    PCU=(PSS/160.)**3
    PN=(PSS/160.0)**Z4
    PFK=(PF-PHFR)/PF
    PFK1=PFK**Z1
    PFK2=1.0/(PFK)**Z2
    IF(KM.EQ.1) GO TO 51
    DO 50 J=1,N
    DO 60 I=J,N
    VJ=J*PMAX/N
    VI=I*PMAX/N
    PV=VJ**0.333+VI**0.333
    PX=PV**Z3
    PY=(VI*VJ)**1.333/PV**4
    IF(NBR.EQ.1) PY=VJ**1.333
    QCOL=EXP(-(GG*PCU*PY*PFK1)**NEXP)
    COAL(I,J)=EE*PN*PX*PFK2*QCOL
    COAL(J,I)=COAL(I,J)
 60 CONTINUE
 50 CONTINUE
 51 CONTINUE
```

Reproduced with permission of the copyright owner. Further reproduction prohibited without permission.

```
      IF(KDAT.EQ.1) GO TO 450
      Y(N)=PNA*B(N)/(FF+G(N))
      A(N)=PMAX*Y(N)
      DO 1 J=2,N
      JJ=N-J+1
      F=PNA*B(JJ)/(FF+G(JJ))
      X=0.0
      JJJ=JJ+1
      DO 2 I=JJJ,N
      ETA=1.0/(FF+G(JJ))
      VI=I*PMAX/N
      VJJ=JJ*PMAX/N
      BETA=CGAM/VI*(VJJ/VI)**CA*(1.0-VJJ/VI)**C
      ALPHA=1.0
      IF(I.EQ.N) ALPHA=0.5

      PK=ETA*CNU*G(I)*BETA
      IF(J.EQ.2) GO TO 12
      X=X+ALPHA*H*PK*Y(I)
    2 CONTINUE
      GO TO 13
   12 Y(N-1)=H*PK*Y(N)+F
      A(N-1)=VJJ*Y(N-1)
      GO TO 1
   13 Y(JJ)=X+F
      A(JJ)=VJJ*Y(JJ)
    1 CONTINUE
      IF(KOK.NE.1) GO TO 600
      WRITE(6,226)
      IF(KOK.EQ.1) GO TO 500
  450 CONTINUE
       IF(KDAT.E  .1) READ(5,99)  ONUM
      IF(KDAT.EC     READ(5,240) (Y(I),I=1,N)
      DO 301 I=
      Y(I)=ONUM   ,I)
  301 CONTINUE
       IF(K.EQ.0) GO TO 600
      DO 31 I=1,NERL
      LIM=ERR*YY(I)
      DIFF=Y(I)-YY(I)
      IF(ABS(DIFF).GT.LIM) GO TO 600
   31 CONTINUE
      GO TO 900
  600 K=K+1
      WRITE(6,111) K
      IF(K.EQ.KN) GO TO 800
      DO 302 I=1,N
      YY(I)=Y(I)
  302 CONTINUE
      DO 23 J=1,N
      XX=0.0
      NJ=N-J+1
      DO 24 I=1,NJ
```

Reproduced with permission of the copyright owner. Further reproduction prohibited without permission.

```
      DELTA =1.0
      IF(I.EQ.NJ) DELTA=0.5
      XX=XX+DELTA*H*COAL(J,I)*Y(I)
   24 CONTINUE
      WW(J)=XX
   23 CONTINUE
      F=PNA*B(N)
      ETA=1.0/(FF+G(N)+WW(N))
      XY=0.0
      N2=N/2
      DO 25 I=1,N2
      RAMMA=1.0
      IF(I.EQ.N2) RAMMA=0.5
      XY=XY+RAMMA*H*COAL(N-I,I)*Y(N-I)*Y(I)
   25 CONTINUE
      Y(N)=(F+XY)*ETA
      N1=N-1
      DO 26 J=2,N1
      JJ=N-J+1
      F=PNA*B(JJ)
      XR=0.0
      JJJ=JJ+1
      DO 27 I=JJJ,N
      ETA=1.0/(FF+G(JJ)+WW(JJ))
      VI=I*PMAX/N
      VJJ=JJ*PMAX/N
      BETA=CGAM/VI*(VJJ/VI)**CA*(1.0-VJJ/VI)**C
      ALPHA=1.0
      IF(I.EQ.N) ALPHA=0.5
      XR=XR+ALPHA*H*CNU*G(I)*BETA*Y(I)
   27 CONTINUE
      XS=0.0
      JJ2=JJ/2
      DO 28 IS=1,JJ2
      SAMMA=1.0
      IF(IS.EQ.JJ2) SAMMA=0.5
      XS=XS+SAMMA*H*COAL(JJ-IS,IS)*Y(JJ-IS)*Y(IS)
   28 CONTINUE
      ETA=1.0/(FF+G(JJ)+WW(JJ))
      Y(JJ)=ETA*(F+XR+XS)
   26 CONTINUE
      XT=0.0
      DO 29 I=2,N
      VI=I*PMAX/N
      VJJ=PMAX/N
      BETA=CGAM/VI*(VJJ/VI)**CA*(1.0-VJJ/VI)**C
      ALPHA=1.0
      IF(I.EQ.N) ALPHA=0.5
      XT=XT+ALPHA*H*CNU*G(I)*BETA*Y(I)
   29 CONTINUE
      F=PNA*B(1)
      ETA=1.0/(FF+G(1)+WW(1))
```

Reproduced with permission of the copyright owner. Further reproduction prohibited without permission.

```
      Y(1)=(F+XT)*ETA
  800 CONTINUE
      IF(K.EQ.KN) WRITE(6,260)
  500 CONTINUE
      S1=0.0
      DO 35 IB=1,N
      VIB=IB*PMAX/N
      A(IB)=VIB*Y(IB)
       S1=S1+H*A(IB)
   35 CONTINUE
      PHER2=S1/VT
      A(N)=A(N)*PHER/PHER2
      Y(N)=Y(N)*PHER/PHER2
      QNUM=H/2.0*Y(N)
      S2=H/2.0*PMAX*A(N)
      S3=H/2.0*PMAX**(-1.0)*A(N)
      S4=H/2.0*PMAX**(-.333)*A(N)
      S5=H/2.0*A(N)
      NP=N-1
      DO3 IJ=1,NP
      Y(IJ)=Y(IJ)*PHER/PHER2
      A(IJ)=A(IJ)*PHER/PHER2
      S2=S2+H*IJ*PMAX/N*A(IJ)
      S3=S3+H*(IJ*PMAX/N)**(-1.)*A(IJ)
      S4=S4+H*(IJ*PMAX/N)**(-.333)*A(IJ)
      S5=S5+H*A(IJ)
      QNUM=QNUM+H*Y(IJ)
    3 CONTINUE
      ADS=VT*PHER/S3
      VADS=S2/(VT*PHER)
      SMD=(6*VT*PHER)/(3.1416**(.333)*6.0**(.6667)*S4)
      PHER3=S5/VT
      DO 14 JI=1,N
      Y(JI)=Y(JI)/QNUM
      A(JI)=A(JI)/(VT*PHER)
   14 CONTINUE
      DMAX=(6.0/3.1416*PMAX)**.333
      DMIN=(6.0/3.1416*PMAX/N)**.333
      DD=(DMAX-DMIN)/NN
      DO 15 ID=1,NN
      D(ID)=DMIN+(ID-1)*DD
      XJD=3.1416/6.0*D(ID)**3*N/PMAX
      JD=XJD
      PVOL=(A(JD+1)+A(JD))/2.0+(A(JD+1)-A(JD))*(XJD-JD)
   15 PD(ID)=PVOL*1.5708*(D(ID))**2
      IF(K.NE.0) WRITE(6,300)
      WRITE(6,200)
      WRITE(6,108) (A(I),I=1,N)
      WRITE(6,201)
      WRITE(6,108) (Y(I),I=1,N)
      WRITE(6,202)
```

Reproduced with permission of the copyright owner. Further reproduction prohibited without permission.

```
      WRITE(6,108)   (G(I),I=1,N)
      WRITE(6,79) C
      WRITE(6,108) (BR(I),I=1,N)
      WRITE(6,203)
      WRITE(6,108) (PD(I),I=1,NN)
      WRITE(6,225)
      DO 19 M=1,50
   19 W(M)=M*PMAX/N
      WRITE(6,108)   (W(I),I=1,50)
      WRITE(6,224)
      WRITE(6,108) (D(I),I=1,NN)
      WRITE(6,204) PSS
      WRITE(6,205) PHFR
      WRITE(6,209) CNU
      WRITE(6,210) C
      WRITE(6,222) CGAM
      WRITE(6,250) VAR
      WRITE(6,212) PMAX,PMIN
      WRITE(6,223) DMIN,DMAX
      WRITE(6,213) N,NN
      WRITE(6,214) FF
      WRITE(6,215) VT,Q
      WRITE(6,216) VZERO,PNA
      WRITE(6,217) ADS
      WRITE(6,218) VADS
      WRITE(6,220) SMD
      WRITE(6,219) PHFR2
      WRITE(6,97) PHFR3
      WRITE(6,221) QNUM
      WRITE(6,101) AA,BB,CC,DE,FE,FSS,Z5
      WRITE(6,116) EE,GG,Z1,Z2,Z3,Z4,PF
      IF(KM.EQ.1) GO TO 900
      IF(K.EQ.0) GO TO 450
      DO 34 IJ=1,2
      ZZ=0.0
      Z=0.0
      DO 32 J=2,N
      VJ=J*PMAX/N
      IF(IJ.EQ.2) VJ=1.0
      XZ=0.0

      X=0.0
      JD2=J/2
      DO 33 I=1,JD2
      VI=I*PMAX/N
      TAMMA=1.0
      IF(I.EQ.JD2) TAMMA=0.5
      X=X+VJ*TAMMA*H*COAL(J-I,I)*Y(J-I)*Y(I)
      IF(IJ.EQ.2) GO TO 33
      VM=VI*ALOG(VJ/VI)+(VJ-VI)*ALOG(VJ/(VJ-VI))
      XZ=XZ+VM*TAMMA*H*COAL(J-I,I)*Y(J-I)*Y(I)
   33 CONTINUE
```

Reproduced with permission of the copyright owner. Further reproduction prohibited without permission.

```
      ALPHA=1.0
      IF(J.EQ.N) ALPHA=0.5
      Z=Z+ALPHA*H*X
      ZZ=ZZ+ALPHA*H*X7
   32 CONTINUE
      IF(IJ.EQ.2) GO TO 34
      MIXR=(ZZ*(ONUM)**2/(PHER2*VT))/ALOG(2.0)
      VCR=Z*(ONUM)**2/(PHER2*VT)
   34 CONTINUE
      PNCR=Z*ONUM
      WRITE(6,234) VCR,PNCR
      WRITE(6,235) MIXR
      WRITE(6,106)
      WRITE(6,108)  (COAL(I,I),I=1,N)
      WRITE(6,107)
      WRITE(6,108) (COAL(1,I),I=1,N)
      WRITE(6,236)
      WRITE(6,108) (WW(I),I=1,N)
      IF(KPUN.EQ.1) WRITE(7,240)(Y(I),I=1,N)
      IF(K.EQ.KN) WRITE(6,400)
      IF(K.EQ.KN) WRITE(6,108) (YY(I),I=1,N)
      IF(K.EQ.KN) GO TO 900
      GO TO 450
  900 CONTINUE
      END
```

Reproduced with permission of the copyright owner. Further reproduction prohibited without permission.

APPENDIX IV

COMPARISON OF MIXING FREQUENCIES

The three mixing frequencies W_N, W_V, and W_M,* defined by equations 5.27 - 5.33 were calculated numerically in the program described in Appendix III. Only the W_M values are shown in the figures in Chapter 9. In Table V-1 these frequencies are presented for the entire N x θ matrix.

If all the coalescing drops are of equal size, then $W_N = W_V = W_M$. The fact that $W_N > W_V$ indicates that the coalescing drops are comprised of small drops more than large ones. The fact that $W_M < W_V$ indicates that drops of unequal size are coalescing with other.

It is seen in the table that the W_M/W_V ratio for all conditions are about the same. The $(d_1 d_2)/(d_1 + d_2)$ function in the coalescing efficiency is responsible for this.

It can be easily shown that the W_V/W_N ratio is equal to the ratio of the average drop size coalescing to the average drop size in the vessel (v_{10}, in both cases). It is seen that as N increases at a constant θ this ratio increases. The W_V/W_N ratio at $\theta = 0.05$ for N = 130 rpm (neither of these are in the table) are 0.470 and 0.755 respectively.

*$W_N = \omega_n$, $W_V = \omega_v$, $W_M = \omega_m$

Reproduced with permission of the copyright owner. Further reproduction prohibited without permission.

Reproduced with permission of the copyright owner. Further reproduction prohibited without permission.

TABLE IV-1

COMPARISON OF MIXING FREQUENCIES

Dispersed Phase Fraction	Mixing Frequency min^{-1}	Agitator Speed, rpm						
		160	174	185	195	210	227	278
0.05	W_N	0.0581	0.0864	0.117	0.145	0.199	0.268	0.570
	W_V	0.0340	0.0522	0.0740	0.0938	0.135	0.186	0.418
	W_M	0.0287	0.0446	0.0621	0.0804	0.116	0.160	0.356
0.10	W_N	0.0956	0.138	0.171	0.220	0.290	0.382	0.740
	W_V	0.0580	0.0852	0.113	0.142	0.196	0.261	0.535
	W_M	0.0496	0.0729	0.0958	0.122	0.168	0.223	0.452
0.15	W_N	0.126	0.176	0.224	0.270	0.354	0.460	0.864
	W_V	0.0790	0.111	0.146	0.178	0.232	0.313	0.615
	W_M	0.0674	0.0948	0.125	0.152	0.200	0.266	0.518
0.20	W_N	0.134	0.191	0.250	0.296	0.372	0.502	0.910
	W_V	0.0783	0.116	0.162	0.193	0.247	0.344	0.643
	W_M	0.0657	0.0980	0.137	0.164	0.208	0.291	0.537

APPENDIX V

SUGGESTIONS FOR FUTURE WORK

1. It is suggested, if this work is to be continued, that more sophisticated input drop generators be designed and constructed. If it were possible to produce input drop sizes that were of equal size and smaller than that which would break in the vessel, then it would be possible to test the coalescence mechanism, independently of the breakage process.

2. With these new drop generators it would be possible to study the breakage mechanism in the absence of coalescence. This could be done by feeding into the vessel drops that are too large to coalesce but small enough so that only one breakage is possible. The breakage distribution, $\beta(v/v')$ and $\nu(v)$ could thus be determined.

3. The models could be tested by carrying out a series of experiments in which residence time is varied. Again, these should be performed using the newly designed drop generators, because, presently, the input drop size is dependent on the flow rates.

4. The constants in the mixing models are functions of the system parameters, e.g.,

$$c_3 \propto \frac{\mu \rho_d}{\sigma^2}$$

It might be possible to check the validity of the models by using

Reproduced with permission of the copyright owner. Further reproduction prohibited without permission.

liquids in which μ , ρ , and σ are sufficiently different. c_3 could be changed proportionately. The breakage equation is in terms of Weber number (known for each system) and the c_2 and c_4 constants should be about the same for each system.

5. A series of batch experiments could be performed using the same system as the one used in this study. The mixing equation can be set up to describe transient behavior. Using the models and constants found in this work, the experimental results can be compared to the theoretically obtained distributions and mixing rates.

Reproduced with permission of the copyright owner. Further reproduction prohibited without permission.

BIBLIOGRAPHY

1. Allan, R. S., and Mason, S. G., "Particle Motions in Sheared Suspensions. XIV. Coalescence of Liquid Drops in Electric and Shear Fields," J. Colloid Sci., 17, 383 (1962).

2. Allen, R. S., Charles, G. E., and Mason, S. G., "The Approach of Gas Bubbles to a Gas-Liquid Interface," J. Coll. Sci., 16, 150 (1961).

3. Bagnold, R. A., "Experiments on a Gravity-Free Dispersion of Large Solid Spheres in a Newtonian Fluid Under Shear," Proc. Royal Soc. London, 225A, 49 (1954).

4. Bartok, W., and Mason, S. G., "Particle Motions in Sheared Suspensions. VIII. Singlets and Doublets of Fluid Spheres," J. Colloid Sci., 14, 13 (1959).

5. Batchelor, G. K., "The Theory of Homogeneous Turbulence," Cambridge University Press, England (1953).

6. Bradley, R. S., "The Cohesion Between Smoke Particles," Phil. Mag., 13, 853 (1932).

7. Calderbank, P. H., "The Interfacial Area in Gas-Liquid Contacting with Mechanical Agitation," Trans. Inst. Chem. Engrs, 36, 443 (1958).

8. Chappelear, D. C., "Models of a Liquid Drop Approaching an Interface," J. Colloid Sci., 16, 186 (1961).

9. Charles, G. E., and Mason, S. G., "The Coalescence of Liquid Drops with Flat Liquid/Liquid Interfaces," J. Colloid Sci., 15, 236 (1960).

10. Chen, H. T., and Middleman, S., "Drop Size Distribution in Agitated Liquid-Liquid Systems," A. I. Ch. E. Journal, 13, 989 (1967).

11. Curl, R. L., "Dispersed Phase Mixing: 1. Theory and Effects in Simple Reactors," A.I. Ch. E. Journal, 9, 175 (1963).

12. Cutter, L. A., "Flow and Turbulence in a Stirred Tank," A. I. Ch. E. Journal, 12, 35 (1966).

13. Davies, J. T., and Rideal, E. K., "Interfacial Phenomena," Chapter 8, Academic Press, New York, (1961).

Reproduced with permission of the copyright owner. Further reproduction prohibited without permission.

14. Fox, L., and Goodwin, E. T., "Non-Singular Linear Integral Functions," Phil. Trans. Royal Soc. of London, 245A, 501 (1952).

15. Groothius, H., and Zuiderweg, F. J., "Coalescence Rates in a Continuous-Flow Dispersed Phase System," Chem. Eng. Sci., 19, 63 (1964).

16. Hartland, S., "The Approach of a Rigid Sphere to a Deformable Liquid-Liquid Interface," J. Coll. Interfac. Sci., 26, 383 (1968).

17. Hartland, S., "The Coalescence of a Liquid Drop at a Liquid-Liquid Interface: Part I. Drop Shape," Trans. Inst. Chem. Eng., 45, T97 (1967): "Part II. Film Thickness," ibid., T102; "Part III. Film Rupture," ibid., T109; "Part V. The Effect of Surface Active Agent," ibid., 46, T275 (1968).

18. Hinze, J. O., "Fundamentals of the Hydrodynamic Mechanism of Splitting in Dispersion Processes," A. I. Ch. E. Journal, 1, 289 (1955).

19. Hinze, J. O., "Turbulence," Chapter 5, McGraw-Hill, (1959).

20. Howarth, W. J., "Coalescence of Drops in a Turbulent Flow Field," Chem. Eng. Sci., 19, 33 (1964).

21. Howarth, W. J., "Measurement of Coalescing Frequency in an Agitated Tank," A. I. Ch. E. Journal, 13, 1007 (1967).

22. Jeffreys, G. V., Davies, G. A., and Pitt, K., "Rate of Coalescence of the Dispersed Phase in a Laboratory Mixer Settler Unit: Part 1," A. I. Ch. E. Journal, 16, 823 (1970).

23. Jeffreys, G. V., Davies, G. A., and Pitt, K., "Part 2, The Analysis of Coalescence in a Continuous Mixer Settler System by a Differential Model," ibid., p. 827.

24. Kolmogoroff, A. N., Comp. Rend. Acad. Sci., URSS (Doklody), 30, 4 (1941).

25. Lawson, G. B., "Coalescence Processes," Chem. Proc. Eng., 48, 45 (1967).

26. Levich, V. G., "Physiochemical Hydrodynamics," Chapter 5, Prentice-Hall, (1962).

27. McAvoy, R. M., and Kintner, R. C., "Approach of Two Identical Rigid Spheres in a Liquid Field," J. Colloid Interfac. Sci., 20, 188 (1965).

28. MacKay, G. D. M., and Mason, S. G., "The Gravity Approach and Coalescence of Fluid Drops at Liquid Interfaces," Can. J. Chem. Eng., 41, 203 (1963).

Reproduced with permission of the copyright owner. Further reproduction prohibited without permission.

29. Madden, A. J., and Damerell, G. L., "Coalescence Frequencies in Agitated Liquid-Liquid Systems," A. I. Ch. E. Journal, 8, 233 (1962).

30. Manley, R. St. J., and Mason, S. G., "Particle Motions in Sheared Suspensions. II. Collisions of Uniform Spheres," J. Colloid Sci., 7, 354 (1952).

31. Manley, R. St. J., and Mason, S. G., "Particle Motion in Sheared Suspensions. III. Further Observations on Collisions of Spheres," Can. J. Chem., 33, 763 (1955).

32. Miller, R. S., Ralph J. L., Curl., R. L., and Towell, G. D., "Dispersed Phase Mixing: Measurements in Organic Dispersed Systems," A. I. Ch. E. Journal, 9, 196 (1963).

33. Murdoch, P. G., and Leng, D. E., "The Mathematical Formulation of Hydrodynamic Film Thinning and its Application to Colliding Drops Suspended in a Second Film - II," Chem. Eng. Sci., in press (1971).

34. Nielsen, L. E., Wall, R., and Adams, G., "Coalescence of Liquid Drops at Oil-Water Interfaces," J. Colloid Sci., 13, 441 (1958).

35. Princen, H. M., "Shape of a Fluid Drop at a Liquid-Liquid Interface," J. Colloid Sci., 18, 178 (1963).

36. Reynolds, O., Phil. Trans Roy. Soc. (London) A177, 157 (1886).

37. Rietema, K., "Segregation in Liquid-Liquid Dispersions and Its Effect on Chemical Reactions," Advance in Chemical Engineering, Vol. 5, Academic Press, New York (1964).

38. Rodger, W. A., Trice, V. G. Jr., and Rushton, J. H., "Effect of Fluid Motion on Interfacial Area of Dispersions," Chem. Eng. Prog. 52, 515 (1956).

39. Rumscheidt, F. D., and Mason, S. G., "Particle Motion in Sheared Suspensions: XII Deformation and Burst of Fluid Drops in Shear and Hyperbolic Flow," J. Coll. Sci., 16, 238 (1961).

40. Rushton, J. H., Costich, E. W., and Everett, H. J., "Power Characteristics of Mixing Impellers," Part I and II, Chem. Eng. Prog. 46, 395-476 (1950).

41. Sachs, J. P., and Rushton, J. H., "Discharge Flow from Turbine-Type Mixing Impellers," Chem. Eng. Prog., 50, 597 (1954).

42. Scheele, G. F., and Leng, D. E., "An Experimental Study of Factors Which Promote Coalescence of Two Colliding Drops Suspended in Water - I," Chem. Eng. Sci., in press (1971).

Reproduced with permission of the copyright owner. Further reproduction prohibited without permission.

43. Schuichi, A., "Flow Patterns of Liquids in Agitated Vessels," A. I. Ch. E. Journal, 4, 485 (1958).

44. Shinnar, R., "On the Behavior of Liquid Dispersions in Mixing Vessels," J. Fluid Mech., 10, 259 (1961).

45. Shinnar, R., and Church, J. M., "Statistical Theories of Turbulence in Predicting Particle Size in Agitated Dispersions," Ind. Eng. Chem., 52, 253 (1960).

46. Sleicher, C. A. Jr., "Maximum Stable Drop Size in Turbulent Flow," A. I. Ch. E. Journal, 8, 471 (1962).

47. Sprow, F. B., "Distribution of Drop Sizes Produced in Turbulent Liquid-Liquid Dispersion," Chem. Eng. Sci., 22, 435 (1967).

48. Sprow, F. B., "Drop Size Distributions in Strongly Coalescing Agitated Liquid-Liquid Systems," A. I. Ch. E. Journal, 13, 995 (1967).

49. Valentas, K. J., and Amundson, N. R., "An Analytical Study of Dispersed Phase Reactors," Report on NSF Project G19722, University of Minnesota, (1964).

50. Valentas, K. J., Bilous, O., and Amundson, N. R., "Analysis of Breakage in Dispersed Phase Systems," Ind. Eng. Chem. Fundam., 5, 271 (1966).

51. Valentas, K. J., and Amundson, N. R., "Breakage and Coalescence in Dispersed Phase Systems," ibid., 5, 533 (1966).

52. Verhoff, F. H., "A Study of the Bivariate Analysis of Dispersed Phase Mixing," Ph.D Thesis, University of Michigan, 1969.

53. Vermeulen, T., Williams, G. M., and Langois, G. E., Chem. Eng. Prog., 51, 85F (1955).

Reproduced with permission of the copyright owner. Further reproduction prohibited without permission.